Non-leptonic B Decays in QCD Factorization

Dissertation
zur Erlangung des Grades eines Doktors
der Naturwissenschaften

vorgelegt von
Dipl. Phys. Susanne Cornelia Kränkl

eingereicht bei der Naturwissenschaftlich-Technischen Fakultät
der Universität Siegen
Siegen 2015

Gutachter:

- Prof. Dr. Thomas Mannel
- Prof. Dr. Guido Bell

Datum der mündlichen Prüfung: 27.11.2015

Prüfer:

- Prof. Dr. Guido Bell
- Prof. Dr. Otfried Gühne
- Prof. Dr. Thomas Mannel (Vorsitz der Prüfungskommission)
- Prof. Dr. Markus Risse

Abstract

Non-leptonic B decays are with their rich phenomenology ideally suited to study the quark flavour sector of the Standard Model (SM) of particle physics. They have been measured extensively at collider experiments. On the theoretical side their description is complicated due the appearance of strong interactions ranging from short- to long-distance physics scales. QCD factorization (QCDF) is a model-independent framework that disentangles such short-distance and long-distance effects in the heavy-mass limit. It allows one to systematically calculate transition amplitudes to leading power in Λ_{QCD}/m_b in a perturbative expansion in the strong coupling. QCDF has already been successfully applied to non-leptonic two-body decays. In contrast, for non-leptonic three-body decays no genuine QCD-based description has been developed so far. In this work we consider two applications of QCDF.

First, we evaluate the perturbative vertex corrections to the colour-allowed tree topology of the decay $\bar{B}^0 \to D^+\pi^-$ to next-to-next-to leading order accuracy. The calculation is technically challenging and involves the reduction of several thousand scalar two-loop two-scale integrals to master integrals which have to be evaluated thereafter. For the reduction we apply the Laporta algorithm and for evaluating the master integrals we use common methods like differential equations and Mellin Barnes representations. In addition, we apply a novel approach to obtain analytical results for all master integrals in a canonical basis. As the decay $\bar{B}^0 \to D^+\pi^-$ is dominated by SM physics a comparison of theoretically calculated observables with experimental data allows us to estimate the size of the neglected power corrections that arise in QCDF due to the finite mass of the b quark.

In the second part of the thesis we apply QCDF to non-leptonic three-body decays such as $B^+ \to \pi^+\pi^-\pi^+$. As the kinematics of three-body decays is not fixed in contrast to two-body decays, the final-state particles populate a kinematic phase space (the Dalitz plot). We identify special kinematic configurations as regions in the Dalitz plot. Adopting the well-established factorization properties of non-leptonic two-body decays, we employ different descriptions in the central region and in the edges of the Dalitz plot. In contrast to the two-body case, this requires introducing generalized non-perturbative quantities such as $B \to \pi\pi$ form factor and two-pion distribution amplitudes. We evaluate the transition amplitudes in the different regions to leading power in Λ_{QCD}/m_b and to leading order in the strong coupling. Finally, we investigate the prospects of a matching of the descriptions in both regions for a physical value of the b-quark mass.

Zusammenfassung

Nicht-leptonische B Zerfälle besitzen ein breites Spektrum an phänomenologischen Observablen um den Quarkflavoursektor des Standardmodels (SM) der Teilchenphysik zu untersuchen. Deshalb wurden (und werden) diese Zerfälle an Beschleunigern sehr intensiv gemessen. Jedoch ist ihre theoretische Beschreibung aufgrund des Auftretens von starken Wechselwirkungen, die sich über physikalische Skalen von kurzer bis langer Reichweite erstrecken, sehr anspruchsvoll. Eine Modell-unabhängige Herangehensweise, um Effekte dieser sich über große Skalen erstreckenden Wechselwirkungen zu entkoppeln, stellt im Grenzfall einer unendlich schweren Masse des b Quarks die Methode der QCD Faktorisierung (QCDF) dar. QCDF ermöglicht eine systematische Berechnung der Übergangsamplituden zu führender Ordnung in $\Lambda_{\rm QCD}/m_b$ in einer perturbativen Entwicklung in der starken Kopplung. QCDF wurde schon erfolgreich auf nicht-leptonische Zweikörperzerfälle angewandt. Für nicht-leptonische Dreikörperzerfälle hingegen exisiert derzeit keine generische QCD basierte Beschreibung. In dieser Arbeit werden zwei Anwendungen von QCDF betrachtet.

Im ersten Teil werden zuerst die perturbativen Vertexkorrekturen zur farberlaubten Tree Topologie zum Zerfall $\bar{B}^0 \to D^+\pi^-$ zur zweiten Ordnung berechnet. Diese technisch anspruchsvolle Berechnung beinhalted das Reduzieren einiger Tausender skalarer Zweiloop-Integrale zu Masterintegralen, die im Anschluss berechnet werden müssen. Für die Reduzierung wird der Laporta Algorithmus verwendet. Die Berechnung der Masterintegrale kann unter Zuhilfenahme von allgemein gebräuchlich Methoden, wie die der Differentialgleichungen oder Mellin-Barnes-Darstellungen, durchgeführt werden. Zusätzlich werden die Masterintegrale mit einer neue Methode berechnet, durch die für alle Integrale analytische Ergebnisse in einer kanonischen Basis gefunden werden können. Im Zerfall $\bar{B}^0 \to D^+\pi^-$ sind keine dominanten Beiträge zu erwarten, die nicht vom SM beschrieben werden. Deshalb erlaubt dieser Zerfall durch einen Vergleich von theoretisch berechneten Observablen mit den experimentell gemessenen Größen eine Abschätzung der Größenordung der Korrekturen, welche in QCDF aufgrund der endlichen Masse des b Quarks enstehen.

Im zweiten Teil der Arbeit wird die Methode der QCDF auf nicht-leptonische Dreikörperzerfälle, insbesondere den Zerfall $B^+ \to \pi^+\pi^-\pi^+$, angewandt. Da im Gegensatz zu Zweikörperzerfällen die Kinematik von Dreikörperzerfällen nicht eindeutig bestimmt ist, besetzen die Mesonen im Endzustand einen kinematischen Phasenraum, der im Dalitz-Plot dargestellt werden kann. Die möglichen kinematischen Konfigurationen der Zerfallsprodukte

können in verschiedenen Regionen des Dalitz-Plots identifiziert werden. Unter der Verwendung der Faktorisierungseigenschaften von nicht-leptonischen Zweikörperproblemen können die zentrale Region und die Ränder im Dalitz Polt unterschiedlich beschrieben werden. Im Gegensatz zur Beschreibung von Zweikörperzerfällen ist es hierbei notwendig, generalisierte nicht-perturbative Größen einzuführen, wie die $B \to \pi\pi$ Formfaktoren und die Zwei-Pion-Verteilungsamplituden. Die Übergangsamplituden in den verschiedenen Regionen werden zur führenden Ordnung in $\Lambda_{\rm QCD}/m_b$ und in der starken Kopplung berechnet. Abschließend wird untersucht, ob ein Zusammenführen ("Matching") der Beschreibungen beider Regionen für eine physikalische Masse des b Quarks möglich ist.

Contents

Introduction **xi**

1. Exclusive Non-leptonic B Decays **1**
1.1. QCD Factorization 1
1.1.1. Factorization Formula for Two-body Decays 2
1.1.2. $B \to D\pi$ in QCDF 5
1.1.3. QCDF for Three-body Decays 8
1.2. Alternative Approaches 8
1.3. Effective Hamiltonian for Weak Decays 9

I. NNLO corrections to the decay $B \to D\pi$ **11**

2. Soft Collinear Effective Theory and Matching **13**
2.1. Introduction to SCET 13
2.1.1. Scaling of the Fields 14
2.1.2. Leading Power SCET Lagrangian 15
2.1.3. $B \to D\pi$ in SCET 17
2.2. Derivation of the Master Formula 19
2.2.1. Matching 19
2.2.2. Perturbative Contributions 23
2.2.3. Tree-level and One-loop 26
2.2.4. Two-loop 30

3. Simplification of the Two-loop Amplitudes **33**
3.1. Passarino-Veltman Decomposition 33
3.2. Scalar Integrals 35
3.3. Integration by Part Identities and Laporta Algorithm 37
3.4. Reduction of Dirac Matrices to Operators 39

4. Evaluation of the Master Integrals **41**
4.1. The Master Integrals . . . 41
4.2. Feynman Parameters and Hypergeometric Functions . . . 43
4.3. Mellin-Barnes Representation . . . 44
4.3.1. Numerical Evaluation with MB.m . . . 46
4.3.2. Automated Derivation of MB Representations with AMBRE.m . . . 47
4.4. Differential Equations . . . 48
4.4.1. Harmonic Polylogarithms and HPL.m . . . 48
4.4.2. Evaluation of the Integrals . . . 50
4.5. Differential Equations and Canonical Basis . . . 52
4.5.1. Goncharov Polylogarithms . . . 53
4.5.2. Canonical Basis . . . 54
4.5.3. Solving Differential Equations . . . 55
4.6. Checks . . . 56

5. Results and Phenomenological Applications **59**
5.1. Hard Scattering Kernels . . . 59
5.1.1. Renormalization Factors and Matching Coefficients . . . 59
5.1.2. Discussion of the Results for the Hard Kernels . . . 62
5.2. Perturbative Amplitude a_1 . . . 63
5.2.1. Hadronic Matrix Elements and Definition of a_1 . . . 64
5.2.2. Results and Dependence on Input Parameters . . . 66
5.3. Branching Ratios . . . 69
5.4. Factorization Tests . . . 71
5.4.1. Ratios of Non-leptonic Decay Rates . . . 71
5.4.2. Ratios of Non-leptonic and Semi-leptonic Decay Rates . . . 72
5.5. Summary and Discussion . . . 73

II. $B \to \pi\pi\pi$ in QCD factorization **75**

6. Three-body Decays from QCD **77**
6.1. Identifying Regions in the Dalitz Plot . . . 77
6.2. Factorization Formula . . . 79
6.3. Generalized Form Factors and Distribution Amplitudes . . . 82
6.3.1. Two-pion Distribution Amplitude . . . 82
6.3.2. Generalized Form Factor . . . 85
6.4. The Central Region of the Dalitz Plot . . . 86
6.4.1. Leading Order Feynman Diagrams . . . 86
6.4.2. Differential Decay Rate . . . 88
6.5. The Collinear Regions of the Dalitz Plot . . . 90
6.6. Reconstructing the Dalitz Plot . . . 92

7. Conclusion and Outlook **97**

A. Laporta Reduction of a Sample Feynman Diagram **103**

B. Reduction of the γ-matrix Algebra to Operators **109**
B.1. Part I: Simplification by a Mathematica Routine 109
B.2. Part II: Reduction to Known Operators 111
B.3. Examples for the Reduction 115

C. Results for the Master Integrals **119**

D. Examples of Evaluating Master Integrals **125**
D.1. Hypergeometric Functions: M_{15} 125
D.2. MB Representations: $M_{23}^{\leftrightarrow}$ and M_{18} 127
D.2.1. "Manual" Evaluation of $M_{23}^{\leftrightarrow}$ 127
D.2.2. Evaluation of M_{18} by Using AMBRE.m 129
D.3. Differential Equations: M_4 and M_5 130
D.4. Canonical Basis: M_6 and M_7 133

E. Useful Identities and Definitions for Evaluating Integrals **139**
E.1. Identities for Calculating Feynman Diagrams 139
E.2. Cauchy's Residue Theorem and Barnes Lemmas 140

F. Results for the Feynman Diagrams in the Central Region of the Dalitz Plot **143**

Bibliography **147**

Publications and Proceedings **159**

Acknowledgements **161**

Introduction

Over the last decades the Standard Model (SM) of particle physics has proven to be a successful theory describing the interactions between all particles known to date. The six quarks and leptons are grouped into three families such that the families are identical, except for a strong hierarchy in the quark and lepton masses with increasing family number. The SM covers the electromagnetic, strong and weak interactions, which are mediated by gauge bosons. The last missing ingredient to complete the particle content of the SM is the Higgs boson. Its interactions with the quarks and leptons are described by the Yukawa sector of the SM. By spontaneous symmetry breaking the Higgs field obtains a non-vanishing vacuum expectation value which couples to the fermions and the heavy gauge bosons and consequently gives masses to these particles. A Higgs boson was finally discovered in 2012 by the ATLAS [1] and CMS [2] experiment at the Large Hadron Collider (LHC). Its quantum numbers are compatible with the SM Higgs boson [3, 4]. Englert and Higgs who had proposed this particle as early as 1964 were awarded the Nobel prize in 2013.

However, there still remain open questions that cannot be answered within the SM, such as dark matter, dark energy or the observed baryon asymmetry in the universe. The latter is significantly larger than the baryon asymmetry calculated from the measured CP (charge conjugation and parity) asymmetry in weak decays. Another puzzle of the SM is the origin of the quark and lepton mass hierarchy. This concerns the flavour sector of the SM that describes the mixing of the quark and lepton flavours induced by weak interactions and the associated CP violation.

Flavour physics started to develop after the discovery of parity violation in weak decays in 1957 [5, 6], which gave a better understanding of weak interactions of the three quarks known at that time. In 1964 it was further discovered that the combined CP symmetry is not conserved either [7]. A possible theoretical explanation for this phenomenon was the existence of three additional quark flavours and hence, a third family[1]. The top quark was the last of the three quark to be discovered in 1995 at Fermilab [8]. The mixing of the six quarks is described by the Cabbibo-Kobayashi-Maskawa (CKM) matrix [9, 10]. In the SM it is a unitary 3×3 matrix. The values for the entries are not predicted by the SM but must

[1] There were also other indications for the existence of at least a fourth quark like for instance the discrepancy of the theoretical and experimental branching ratio for the decay $K_L \to \mu\mu$, which could be explained by the contribution of an additional quark flavour.

be extracted from a comparison of theoretically calculated observables with experimental data. A discovery of deviations from unitarity of the CKM matrix would be a clear sign of physics beyond the SM. The lepton flavour sector in the SM including neutrino masses[2] has a similar structure. Charged lepton flavour violation is predicted to be negligibly small and has not been observed yet.

Decays of heavy mesons, which are bound states of a light and a much heavier quark, are among the primary objects to study quark flavour in high-energy physics. They yield a broad spectrum of observables for investigating the CKM structure of the SM. In particular, we are interested in non-leptonic two-body and three-body decays of B mesons, which constitute a large portion of the branching fraction. They allow for CP studies including the extraction of the CKM angles α, β, γ [11–13]. In most cases three-body decays proceed dominantly via quasi-two-body final states as intermediate resonances, however, in some decay channels the contributions from the non-resonant three-particle states seems to be rather large [14]. The study of the interference pattern of the resonances in Dalitz plots also allows to infer information on the strong resonances, such as masses, widths and quantum numbers [15].

The searches for physics beyond the SM, also called "new physics", can be divided into two classes: On the one hand, there are the direct searches for new particles which may be produced on-shell in collider experiments; on the other hand, there are the indirect searches that look for the impact of new, heavy virtual particles on SM observables. For latter searches (precision) calculations of SM observables are essential to be sensitive to possible deviations when comparing to experimental data. In the last two decades non-leptonic two-body B decays have been studied extensively in e^+e^- collider experiments like CLEO, Babar and Belle. In addition, the LHCb experiment, which is located at the pp storage ring LHC, has started to collect data in 2010. Recently, also a sizable amount of observables from branching ratios and CP asymmetries from Dalitz plot analyses of several non-leptonic three-body B decay channels (cf. [16–20]) has become available, raising the interest in these decays, and more is expected to come in the next run of LHC [21] and from Belle II [22].

However, the theoretical description of this kind of decays is complicated due to the purely hadronic environment, entailing QCD effects from many widely separated scales. Non-leptonic two-body B decays have already been extensively studied in the literature. In a first approach, known as naive factorization, the hadronic matrix elements are expressed as products of a decay constant and a form factor, see e.g. [23]. At the present day, the two main approaches to these decays are flavour symmetries of the light quarks [24] and factorization frameworks such as perturbative QCD (pQCD) [25] and QCD factorization (QCDF) [26–28]. The latter is a model-independent framework that systematically disentangles perturbative from non-perturbative effects in the heavy-mass limit. It has proven successful in several applications [26, 27].

The theoretical description of non-leptonic three-body decays, on the other hand, is still in the stage of modeling. Common methods, reflecting the state of the art, are the isobar model [29, 30] and the K-matrix formalism [31]. In these approaches resonances are modeled, for example by Breit-Wigner distributions, and the non-resonant contributions are often

[2]The discovery of neutrino oscillations has shown that, in contrast to the SM prediction, neutrinos have small but non-vanishing masses. Nowadays, massive neutrinos are often considered as a trivial extension of the SM.

described by an empirical distribution in order to reproduce the full range of the phase space (cf. [32]). Flavour symmetry relations of three-body decays have been studied in order to obtain new constraints on SM parameters [33, 34]. Studies in a factorization framework have been performed. In [35–37] the matrix elements were factorized naively, but no attempt was made to discuss the breakdown of factorization in the regions of phase space where they are not expected to apply. In a recent work relying on pQCD [38] experimental values for branching ratios and CP violation could be reproduced [39]. However, if the conceptual issues of pQCD [40, 41] cannot be resolved, the predictive power of this approach is limited. In the future also the Miranda procedure could become interesting, which is a novel model-independent approach that directly accesses CP violation by significance analyses of density populations in the Dalitz plot [42, 43]. However, for a quantitative approach a QCD based description of the Dalitz distribution as well as the phase information on the amplitudes is indispensable.

In this work we consider two different applications of QCDF. In the first part we calculate the two-loop correction to the heavy-to-heavy decay $\bar{B}^0 \to D^+\pi^-$ in QCDF. In QCDF, next-to-leading order (NLO) corrections to both, heavy-to-heavy [27] and heavy-to-light [26, 44] transitions have been known since more than a decade. More recently, also next-to-next-to-leading order (NNLO) results for heavy-to-light decays have become available [45–48]. In the heavy-quark limit, the decay amplitude for $\bar{B}^0 \to D^+\pi^-$ is given by [27]

$$\langle D^+\pi^-|\mathcal{Q}_i|\bar{B}^0\rangle = \sum_j F_j^{B\to D}(m_\pi^2)\int_0^1 du\, T_{ij}(u)\Phi_\pi(u)\,, \tag{1}$$

where $\mathcal{Q}_i$ are the operators from the effective Hamiltonian that describe the underlying weak decay. The $F_j^{B\to D}$ form factors and the pion light-cone distribution amplitude (LCDA) $\Phi_\pi(u)$, with momentum fractions u and $1-u$ shared among the pion constituents, are the non-perturbative inputs. The hard-scattering kernels $T_{ij}(u)$ on the other hand can be evaluated in a perturbative expansion in the strong coupling. They give rise to a perturbative contribution a_1 which in naive factorization simply has the value $a_1 = 1$ [23]. QCDF predicts that for the set $\bar{B}^0 \to D^{(*)}L$ with $L = \{\pi, \rho, K\}$, a_1 only mildly depends on the light meson L which can be seen from the quasi-universality of a_1. As an example the results for a_1 to NLO accuracy are given below where light meson LCDA has been expanded in Gegenbauer moments up to the first moment α_1^L [27]

$$\begin{aligned} |a_1(\bar{B}^0 \to DL)| &= (1.055^{+0.019}_{-0.017}) - (0.013^{+0.011}_{-0.006})\alpha_1^L\,, \\ |a_1(\bar{B}^0 \to D^*L)| &= (1.054^{+0.018}_{-0.017}) - (0.015^{+0.013}_{-0.007})\alpha_1^L\,. \end{aligned} \tag{2}$$

In case of π and ρ we have $\alpha_1^{\pi(\rho)} = 0$ and for the kaon $|\alpha_1^K| < 1$ is assumed [27]. One finds a quasi-universal value $|a_1| \simeq 1.05$. For the decays $\bar{B}^0 \to D^{(*)}L$ with $L = \{\pi, K\}$, values for a_1 have been recently extracted from experimental data [49] and here, the favored central value is $|a_1| \simeq 0.95$, with errors in individual channels at the 10-20%-level.

Yet it is interesting to go beyond NLO in $B \to D\pi$ transitions: Since the contribution at NLO is colour suppressed and appears alongside small Wilson coefficients, the NNLO

corrections may be comparable in size[3]. We calculate these and check whether there still exits a quasi-universal value. Moreover, since there is neither a colour-suppressed tree amplitude nor penguin contributions, and spectator scattering and weak annihilation are power-suppressed [27], we have only the vertex kernels to the colour-allowed tree amplitude. A precise theory prediction of this single contribution, together with comparison to experimental data, might give a reliable estimate of the size of power corrections in QCDF.

The second part is concerned with a new application of QCDF. We outline a new method based on QCDF for the description of three-body and quasi-two-body decays. To set up the method we focus on the decay $B^+ \to \pi^+\pi^-\pi^+$. We start by identifying the different regions in the Dalitz plot, in which the well-established factorization properties of two-body decays apply to three-body decays. In the heavy-quark limit, we discuss how to compute the central region of the Dalitz plot as well as its edges. We will see that the methods and the theoretical inputs to be used are different in the different regions: While the center can be described in terms of regular from factors and pion distributions, the description at the edges requires introducing generalized versions of these hadronic matrix elements. As an application, we consider the $B^+ \to \rho^0\pi^+$ branching ratio by integrating the differential rate around the ρ resonance. Finally, we reconstruct the full Dalitz plot by matching the descriptions of these different regions.

This work is structured as follows: In Chap. 1 we give an introduction to the description of exclusive non-leptonic B decays. We present the basic concepts of QCDF and briefly discuss the application of QCDF for $B \to D\pi$ and for non-leptonic three-body decays. Moreover, we comment on the two main alternative approaches, flavour symmetries and pQCD. The further work is then divided into two parts which deal with two different applications of QCDF. The calculation of the two-loop correction to the decay $\bar{B}^0 \to D^+\pi^-$ in QCDF is topic of Part I. In Chap. 2 we give a brief introduction to Soft Collinear Effective Theory (SCET). Moreover, we derive a master formula for the hard scattering kernels by performing a matching from QCD to SCET. In Chap. 3 we present the calculational techniques for the two-loop Feynman diagrams that enter the master formula. They consist of the reduction of the two-loop integrals to master integrals by the Laporta algorithm and the reduction of the Dirac structures to a set of known operators. The evaluation of the two-loop two-scale master integrals is presented in Chap. 4. Here, we show several computation techniques including a new method which allows us to obtain the results for all master integrals analytically in a canonical basis. The result for the two-loop amplitude is presented and discussed in Chap. 5. Part II is discussed in Chap. 6, where we investigate the application of QCDF to the decay $B^+ \to \pi^+\pi^-\pi^+$. Adopting the factorization properties of non-leptonic two-body decays, we construct factorization formulae for the three-body transition amplitude in different regions of the Dalitz plot. We evaluate the amplitudes to leading order in the strong coupling and to leading power in the heavy-quark mass. In addition, we investigate a possible merging of the descriptions in these different regions and check the "goodness" of the matching for the physical value of the b-quark mass (compared to the heavy-mass limit). Finally we conclude with a summary and an outlook to future work in Chap. 7.

[3]Note, that this does not imply a breakdown of perturbation theory, as was already pointed out for two-loop corrections to the colour-suppressed tree-amplitude in $B \to \pi\pi$ decays in [47, 45, 46].

Chapter 1

Exclusive Non-leptonic B Decays

In this chapter we provide the basics for the two applications of QCD factorization (QCDF) which follow later in Part I and II of this thesis. We give a brief introduction to QCDF and present the factorization formula for non-leptonic two-body B decays, which disentangles perturbative from non-perturbative effects in the heavy-mass limit. Moreover, we review the decays $B \to D\pi$ in QCDF and briefly discuss the applicability of QCDF to non-leptonic three-body B decays. At the end of this chapter, we comment in short on alternative approaches and present the effective Hamiltonians that describe the underlying weak transitions for the decays $B \to D\pi$ and $B \to \pi\pi\pi$.

1.1. QCD Factorization

QCDF has been developed in 1999 by Beneke, Buchalla, Neubert and Sachrajda [26, 27]. They provided the first systematic description of non-leptonic two-body B decays by a neat merging of two theoretical approaches: factorization in hard exclusive processes for large momentum transfer [50, 51] on the one hand and the heavy quark expansion [52] on the other hand. We briefly explain the basic ideas in the following.

Weak decays of heavy mesons involve three fundamental scales: the weak scale M_W, the b quark mass m_b and the QCD scale $\Lambda_{\rm QCD} \sim 0.5$ GeV, where quarks and gluons hadronize. We remark that $M_W \gg m_b \gg \Lambda_{\rm QCD}$. QCD effects which vary over the range of these different scales complicate the evaluation of the decays. One has to get a handle on these effects in order to identify perturbative and nonperturbative contributions to the decay amplitude. We start by considering particles which are much heavier than the B-meson mass like the massive gauge bosons W and Z, and the top quark. Effects of these particles can be absorbed into short-distance coefficients C_i, which are referred to as the Wilson coefficients. The transition amplitude then takes the form

$$\mathcal{A}(B \to M_1 M_2) = \frac{G_F}{\sqrt{2}} \sum_i \lambda_i \, C_i(\mu) \langle M_1 M_2 | \mathcal{Q}_i | B \rangle(\mu) \,, \tag{1.1}$$

where G_F is the Fermi constant and λ_i are CKM parameters. The weak interaction is described by local four-fermion operators $\mathcal{Q}_i$. The scale μ is a specific scale, usually denoted as factorization or renormalization scale, which is sizably larger than $\Lambda_{\rm QCD}$. The Wilson coefficients contain the effects above μ and are therefore calculable as perturbative expansions in the strong coupling α_s. They can also be regarded as effective coupling constants which indicate the strength of the different contributions of the local operators. The matrix elements of the latter, in contrast, depend on the physics below the scales μ. Note that their scale dependence is such that it compensates the one of the Wilson coefficients, since the amplitude (1.1) is independent on the factorization scale.

At leading power in $1/M_W$, Eq. (1.1) is equivalent to the full SM amplitude with the only difference that the gauge bosons W and Z, and the top quark do not appear as dynamical degrees of freedom anymore. This corresponds to integrating out these heavy particles on the level of the Lagrangian and thus Eq. (1.1) can also be considered as the amplitude corresponding to an effective theory which for $\mu \gtrsim m_b$ has five dynamical (active) flavours. The Wilson coefficients are usually obtained by a matching of the full theory to the effective one at the weak scale. By applying the renormalization group equation they are then evolved down to an arbitrary scale $\mu \gg \Lambda_{\rm QCD}$ such that they are still accessible in perturbation theory. The matrix elements $\langle M_1 M_2|\mathcal{Q}_i|B\rangle$ on the other hand cannot be evaluated straightforwardly due to the appearance of strong interactions at scales of order $\Lambda_{\rm QCD}$. However, in QCDF they can be reduced to simpler objects. The factorization properties rely on the fact that the mass of the b quark is heavy compared to the typical hadronic scale. By choosing $\mu \sim \mathcal{O}(m_b)$ in Eq. (1.1)[1] the hadronic matrix elements do not depend on virtualities larger than m_b, which then can be seen as the hard scale of the process. Performing an expansion of the amplitude in powers of $\Lambda_{\rm QCD}/m_b$ a systematic separation of soft scales of $\mathcal{O}(\Lambda_{\rm QCD})$ and hard scales can be achieved by power counting. In the heavy-quark limit, i.e. for $m_b \to \infty$, perturbative and non-perturbative effects are disentangled and the matrix elements can be expressed in terms of hadronic functions and hard scattering kernels. The former are non-perturbative but universal objects (like form factors and meson distribution amplitudes) and can be obtained using other techniques (see Sec. 1.1.1). In contrast, the hard scattering kernels are process specific and contain the effects from short-distances. Thus, they only depend on the large scale m_b and are calculable in perturbation theory. At leading power in $\Lambda_{\rm QCD}/m_b$ and leading order in α_s QCDF reproduces naive factorization. Note that this is not necessarily the case for other factorization approaches (see e.g. Sec. 1.2).

QCDF has been successfully applied to many non-leptonic two-body B meson decays such as $B \to \pi\pi$, $B \to D\pi$ and $B \to K\pi$ [26, 27]. Below, we present the general factorization formula for these decays.

1.1.1. Factorization Formula for Two-body Decays

The leading Fock state of the B mesons consists of a b quark with mass m_b and a much lighter u or d quark[2]. In the heavy-quark limit almost the total momentum is carried by the

[1] The exact choice will be specified in Chap. 5.

[2] Note that assuming $SU(3)$ flavour symmetry, one could also take B_s mesons into consideration, which have a strange quark as light partner of the b quark. However, this is not of any concern for our applications.

heavy b quark while the light spectator quark has only a residual momentum of order $\Lambda_{\rm QCD}$. Thus, we approximate $m_b \simeq m_B$, where m_B is the mass of the B meson.

The factorization properties of the matrix elements $\langle M_1 M_2|\mathcal{Q}_i|B\rangle$ depend on the invariant masses m of the final states. A final state meson is taken to be light (compared to m_B) if $m \sim \mathcal{O}(\Lambda_{\rm QCD})$. On the other hand, a meson is considered as heavy if its mass scales with m_B in the heavy-quark limit, i.e. the ratio m/m_B remains fixed for $m_B \to \infty$. In this sense the B meson is heavy and mesons like the pion are light. A problem arises in the classification of D mesons, which consist of a charm quark and a light u or d quark. The mass m_c of the charm roughly scales as $\sqrt{m_B \Lambda_{\rm QCD}}$. Since we have the hierarchy of scales $\Lambda_{\rm QCD} \ll \sqrt{m_B \Lambda_{\rm QCD}} \ll m_B$, it is neither heavy nor light. In this work m_c and correspondingly D mesons are regarded as heavy. The case, in which m_c is treated as a light quark, can be adopted from $B \to \pi\pi$ decays [45–47].

In [27] factorization has been studied for the cases that both final state mesons are light and that one meson is heavy and the other one is light, which we call a heavy-light final state in the following. The corresponding factorization formulae in the heavy-quark limit read[3]

$$\begin{aligned}\langle M_1 M_2|\mathcal{Q}_i|B\rangle = &\sum_j F_j^{B\to M_1}(m_2^2)\int_0^1 du\, T_{ij}^I(u)\Phi_{M_2}(u) + (M_1 \leftrightarrow M_2)\\ &+ \int_0^1 d\xi\, du\, dv\, T_i^{II}(\xi,u,v)\Phi_B(\xi)\Phi_{M_1}(v)\Phi_{M_2}(u)\,, \end{aligned} \tag{1.2}$$

if M_1 and M_2 are both light,

$$\langle M_1 M_2|\mathcal{Q}_i|B\rangle = \sum_j F_j^{B\to M_1}(m_2^2)\int_0^1 du\, T_{ij}^I(u)\Phi_{M_2}(u)\,, \tag{1.3}$$

if M_1 is heavy and M_2 is light. Here $F_j^{B\to M_1}$ denotes the $B \to M_1$ form factors and v, u and ξ are the momentum fractions of the constituents of the mesons $M_{1,2}$ and B, respectively, which are described by the light-cone distribution amplitudes (LCDAs) $\Phi_{M_{1,2}}$ and Φ_B. The T_{ij}^I and T_i^{II} are the hard scattering kernels corresponding to the operators $\mathcal{Q}_i$. For a finite B-meson mass, Eqs. (1.2) and (1.3) receive corrections, which are suppressed by powers of $\Lambda_{\rm QCD}/m_B$.

The first (second) term in Eq. (1.2) describes the interactions where the spectator quark of the B meson goes to the meson M_1 (M_2). Hard interactions involving the spectator quark, in short "spectator interactions", cannot be reduced to $F^{B\to M}$ form factors and are collected in the last term in Eq. (1.2).

In the case of M_1 being heavy (cf. Eq. (1.3)) the contribution from the light meson receiving the spectator quark does not factorize anymore but fortunately is power suppressed. Also spectator interactions only arise beyond leading power. Last but not least, there are contributions to both final state configurations, in which the two final state mesons M_1 and M_2 emerge from the weakly annihilating constituents of the B meson. These as well are

[3]Note that we have suppressed the μ-dependence of the matrix elements in the notation.

power suppressed. We will discuss all these power corrections in more detail in Sec. 1.1.2 for the decays $B \to D\pi$. Note that an essential condition for factorization to apply is that the contributions from the endpoint regions $u \sim \Lambda_{\rm QCD}/m_B$ and $\bar{u} \sim \Lambda_{\rm QCD}/m_B$ in Eqs. (1.2) and (1.3) must also be power suppressed. Otherwise endpoint divergences arise, i.e. the convolution of the hard scattering kernels with the LCDAs will diverge at the integration borders. This is a sign that no clear separation of long-distance and short-distance physics has been performed. We will use this fact in the discussion of three-body decays in Part II of this thesis. Next, we identify the perturbative and non-perturbative contributions in Eqs. (1.2) and (1.3).

Non-perturbative Parameters

The scalar $B \to M$ form factors $F_+^{B\to M}(q^2)$ and $F_0^{B\to M}(q^2)$ are defined in the decomposition of the matrix elements $\langle M(p')|\bar{c}\,\Gamma\, b|\bar{B}(p)\rangle$, where $q = p - p'$ and p and p' are the momenta of the B meson and the meson M, respectively, and Γ is a Dirac matrix. For instance for a pesudoscalar meson P the decomposition of the matrix element with the vector current $\Gamma = \gamma^\mu$ reads [53]

$$\langle P(p')|\bar{c}\gamma^\mu b|\bar{B}(p)\rangle = F_+^{B\to P}(q^2)(p^\mu + p'^\mu) + \left[F_0^{B\to P}(q^2) - F_+^{B\to P}(q^2)\right]\frac{m_B^2 - m_P^2}{q^2}q^\mu\,. \quad (1.4)$$

It is convenient to consider physical form factors, which contain effects from soft and hard gluons and therefore do not correspond to purely non-perturbative objects. This allows one to obtain the form factors experimentally by comparison to semi-leptonic decay rates or, on theory side, from lattice QCD [54] and QCD sum rule [55] calculations. Working with the physical form factor will not spoil factorization when omitting the corresponding hard contributions from the hard scattering kernel.

The LCDAs Φ_M are non-perturbative quantities. For a light pesudoscalar meson P, like the pion, its leading-twist expression is defined as follows[4]

$$\langle P(q)|\bar{d}(y)_\alpha [y,x] u(x)_\beta|0\rangle|_{(x-y)^2=0} = \frac{if_P}{4}(\not{q}\gamma_5)_{\beta\alpha}\int_0^1 du\, e^{i(\bar{u}qx+uqy)}\Phi_P(u,\mu)\,, \quad (1.5)$$

where q is the momentum of the meson, f_P the P meson decay constant and we use the abbreviation $\bar{u} \equiv 1-u$. α, β are Dirac indices and μ is the renormalization scale of the non-local operator. The LCDA Φ_P is a colour singlet and is normalized to $\int_0^1 du\,\Phi_P(u,\mu) = 1$. Note that the Wilson line $[y,x]$ renders the operator gauge invariant. The LCDAs are universal objects that can be probed experimentally e.g. in $\gamma\gamma^* \to \pi$ processes in the case of the pion. A theoretical description is given by the Gegenbauer expansion (see Eq. (5.29)). The leading term of this expansion coincides with the asymptotic limit of the LCDAs, which are defined by taking the renormalization scale to infinity

$$\Phi_P(u,\mu) \overset{\mu\to\infty}{=} 6u\bar{u}\,. \quad (1.6)$$

[4]The subleading-twists are power suppressed.

For convenience we will use the definition of the leading-twist LCDA in momentum space and substitute

$$\bar{u}(uq)_{\alpha a}\Gamma(u\dots)_{\alpha\beta}\, v(\bar{u}q)_{\beta b} \longrightarrow \frac{if_P}{4N_c}\int_0^1 du\,\Phi_P(u,\mu)(\not{q}\gamma_5)_{\beta\alpha}\Gamma(u,\dots)_{\alpha a,\beta b}\,, \tag{1.7}$$

where a, b are colour indices and N_c denotes the number of colours (in our applications we have $N_c = 3$). The quark and the antiquark spinors with momenta uq and $\bar{u}q$, respectively, form the leading Fock states of the pseudoscalar meson. Note that for longitudinally polarized vector mesons V Eq. (1.7) modifies to [27]

$$\bar{u}(uq)_{\alpha a}\Gamma(u\dots)_{\alpha\beta}\, v(\bar{u}q)_{\beta b} \longrightarrow -\frac{if_V}{4N_c}\int_0^1 du\,\Phi_V(u,\mu)\not{q}_{\beta\alpha}\Gamma(u,\dots)_{\alpha a,\beta b}\,, \tag{1.8}$$

whereas the normalization and the asymptotic limit are the same as the one for the LCDAs of pesudoscalar mesons.

LCDAs for pseudoscalar heavy mesons like the B meson are defined in a similar expansion [27], but are less understood theoretically and experimentally (see e.g. [56]).

Perturbative Parameters

At leading power the infrared (IR) contributions of the amplitude match those of the form factors and the LCDAs. This means that the hard scattering kernels $T^{I,II}$ are IR finite and indeed only receive contributions from short-distances above the scale m_B. Considering that $\alpha_s(m_b) \simeq 0.22$ is still rather small, a perturbative expansion in the strong coupling at the scale $\mu = m_b$ is expected to be well-behaved. Thus, the kernels $T^{I,II}$ can be evaluated in a perturbative series

$$T = T^{(0)} + \alpha_s T^{(1)} + \alpha_s^2 T^{(2)} + O(\alpha_s^3)\,. \tag{1.9}$$

We shall remember that when using physical form factors the corresponding hard contributions have to be removed from the hard kernels as mentioned before.

In the following, we discuss the decays $B \to D\pi$ within the framework of QCDF.

1.1.2. $B \to D\pi$ in QCDF

We consider the following set of weak decays $B \to D\pi$ which at parton level are all described by a $b \to c\bar{u}d$ transition: $\bar{B}^0 \to D^+\pi^-$, $\bar{B}^0 \to D^0\pi^0$ and $B^- \to D^0\pi^-$. The corresponding decay amplitudes can be decomposed into the flavour topologies depicted in Fig. 1.1: (a) commonly is referred to as colour-allowed or tree topology, (b) as colour-suppressed topology, and (c) is denoted as weak annihilation topology. In the decay $\bar{B}^0 \to D^+\pi^-$ the pion can be directly created by the weak current or both final states can emerge from the weak annihilation of the two constituents of the $\bar{B}^0$ meson. Thus, $\bar{B}^0 \to D^+\pi^-$ receives contributions from the topologies (a) and (c). From similar considerations one finds that the flavour structure in the decay $B^- \to D^0\pi^-$ is given by the topologies (a) and (b), and in $\bar{B}^0 \to D^0\pi^0$ by (b) and (c).

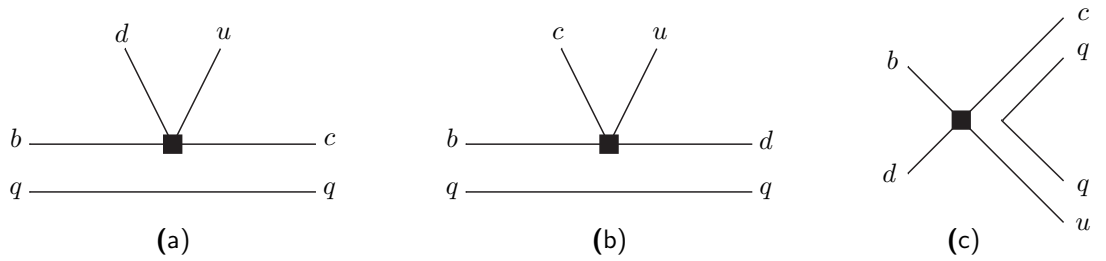

Figure 1.1. – The basic quark topologies (a), (b) and (c) show the flavour flows for $B \to D\pi$ decays with $q = u, d$. Quarks grouped together in pairs form mesons. The black squares denote the different effective vertices from the weak interaction. $\bar{B}^0 \to D^+\pi^-$ receives contributions from (a) and (c), $B^- \to D^0\pi^-$ from (a) and (b), and $\bar{B}^0 \to D^0\pi^0$ from (b) and (c).

QCDF for non-leptonic two-body B decays has been discussed in the previous section. The B meson in our case decays into a heavy D meson and a light pion. A consequence of the factorization properties for a heavy-light final state is that the tree topology can be factorized in the heavy-quark limit (cf. Eq. (1.3)), whereas perturbative and nonperturbative effects cannot be disentangled in the contributions from the colour-suppressed topology. This can be understood by a rather simple argument known as colour-transparency, which had been used to justify naive factorization.

Without loss of generality we consider the decay of the B meson in its rest frame where both final state particles decay back-to-back with large energies. The pion has a small invariant mass and therefore gets highly boosted, while the rather heavy D meson is less boosted. In the tree topology the pion is created by the weak current moving away from the interaction point with high velocity. Thus, in a first approximation it can be considered as colour singlet which cannot be resolved by soft gluons emitted from the heavy B and D mesons. Soft gluon interactions between the B and D mesons, on the other hand, do not cause a problem since they can be absorbed in the $F^{B\to D}$ form factor. Hence, the tree topology can be decomposed into a $F^{B\to D}$ form factor and a compound object describing the fast moving pion.

From the above considerations it is evident that factorization does not work for the colour-suppressed topology. This time the D meson emerges from the weak interaction. Since its velocity is small soft gluon exchanges with the B meson and the pion will occur making a clear separation of perturbative and nonperturbative effects impossible. It was shown that in the heavy-quark limit this contributions is power suppressed in comparison to the leading amplitude [27]. However, rather large deviations for the scaling occur for a finite b quark mass. Thus, QCDF is expected to be more accurate in the description of decays where the colour-suppressed topology does not arise, like e.g. in $\bar{B}^0 \to D^+\pi^-$.

Next, we consider the weak annihilation topology. The constituents of the B meson weakly annihilate to a $c\bar{u}$ ($c\bar{d}$) pair in the case of the $\bar{B}^0$ (B^-) meson. Two additional quarks which are needed to form the final state mesons emerge from a gluon in a quark-antiquark-pair ($\bar{q}q$) production. The hard part of this topology would contribute to the hard scattering kernel T^{II}, whereas the soft part would spoil factorization. However, in any case the weak annihilation topology is power suppressed compared to the leading amplitude [27].

The last category that remains to be discussed are the hard spectator interactions in the

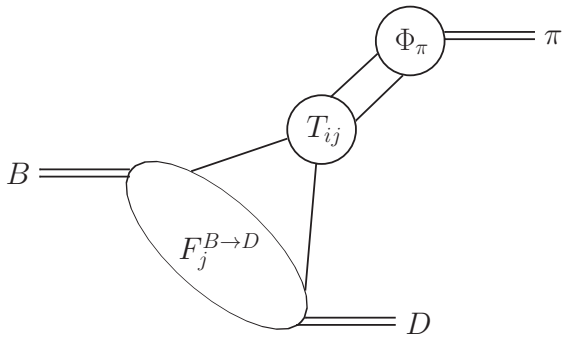

Figure 1.2. – Schematic visualization of the factorization formula for the decay $\bar{B}^0 \to D^+\pi^-$.

tree topology[5]. As already mentioned in the previous section, in the heavy-quark limit the heavy b quark carries almost the total momentum of the B meson, and the spectator quark has momentum of order $\Lambda_{\rm QCD}$ and is thus treated as soft. The same considerations apply for the heavy D meson and we assign the momentum fraction $\bar{v} \sim \Lambda_{\rm QCD}/m_B$ to its soft quark[6]. Due to momentum conservation it is forbidden that a soft quark emits a hard gluon without a significant change of momentum of order of m_B (the hard scale). Thus, after the hard interaction the spectator quark carries momentum of order m_B and is then absorbed into the D meson. The latter gets a contribution from the endpoint region of $\bar{v} \sim \mathcal{O}(1)$, meaning that the heavy c quark carries almost no momentum. This configuration is highly unlikely and one can show that it is power suppressed relative to the tree topology [27].

We summarize that the tree topology can be factorized in the heavy-quark limit and the colour-suppressed and the weak annihilation topology are power suppressed, as are interactions with the spectator quark. In the following, we focus on the decay $\bar{B}^0 \to D^+\pi^-$ which only receives contributions from vertex corrections of the tree topology at leading power. Moreover, the flavour structure of the tree topology does not allow for contributions of penguin operators which could provide a source of new physics in form of new heavy particles running in the loop. Thus, new physics effects are expected to be negligibly small and this decay is dominated by SM physics. By calculating the vertex corrections to NNLO accuracy one can estimate the size of the power corrections and provide a reasonable test of the framework of QCDF (see Sec. 5.5). In the heavy-quark limit the $\bar{B}^0 \to D^+\pi^-$ decay amplitude takes the form (cf. Eq. (1.3)

$$\langle D^+\pi^-|\mathcal{Q}_i|\bar{B}^0\rangle = \sum_j F_j^{B\to D}(m_\pi^2) \int_0^1 du\, T_{ij}^I(u)\Phi_\pi(u)\,, \tag{1.10}$$

where $F_j^{B\to D}$ are the $B \to D$ form factors and Φ_π is the pion LCDA. The T_{ij}^I are the hard scattering kernels corresponding to the local four-fermion operators $\mathcal{Q}_i$, which will be specified in Sec. 1.3. Eq. (1.10) does not contain spectator interactions. Thus, we will drop

[5]Note that in principle only the interactions between the constituents of the pion and the spectator quark have to be considered since the interactions involving the b and c quark are part of the physical form factor.

[6]From the view of power counting we take $m_D \simeq m_B$.

the index "I" in what follows and do not draw the spectator quark in the Feynman diagrams in Chap. 2. A graphical illustration of Eq. (1.10) is given in Fig. 1.2. Next, we briefly discuss the application of QCDF to non-leptonic three-body B decays.

1.1.3. QCDF for Three-body Decays

The factorization properties in QCDF depend on the final states, as we have seen in the case of non-leptonic two-body decays. Thus, we restrict ourselves to the analysis of B decays to three pesudoscalar light mesons in this thesis, to be specific to the decay $B^+ \to \pi^+\pi^-\pi^+$. Note that most of the discussion also applies to final states involving different final-state pions or even kaons, like e.g. $B \to K\pi\pi$ or $B \to KKK$.

In contrast to two-body decays the kinetic energy can be arbitrarily distributed among the three final-state mesons resulting in a kinematic phase space for three-body decays. In the different regions of the phase space factorization properties similar to two-body decays apply and the amplitude might be factorized into regular form factors and LCDAs. However, as non-leptonic three-body B decays proceed dominantly through intermediate quasi-two body states we expect resonances to appear in certain corners of the phase space[7]. In these regions the non-perturbative quantities in the factorized amplitude have to be generalized: beside $B \to \pi$ form factors and pion LCDAs, one encounters generalized $B \to \pi\pi$ form factors and two-pion light cone distribution amplitudes (2π-LCDAs), which in general cannot be factorized further. The $B \to \pi\pi$ form factor and the 2π-LCDA have been discussed in the literature (see e.g. [57–68]) and are still subject of current studies [69, 70].

We will apply QCDF to non-leptonic three-body B decays in Part II of this thesis and construct factorization formulae analogous to Eqs. (1.2) and (1.3). In the last part of this chapter we comment on alternative approaches and present the effective weak Hamiltonians that describe the decays $\bar{B}^0 \to D^+\pi^-$ and $B^+ \to \pi^+\pi^-\pi^+$.

1.2. Alternative Approaches

Besides QCDF, the most famous approaches to study non-leptonic two-body B decays are perturbative QCD and flavour symmetries, which we briefly describe below. Note that these frameworks have also been used in the study of non-leptonic three-body B decays.

Perturbative QCD

Perturbative QCD (pQCD) [71–73], also known as k_T factorization, is similar to QCDF at first glance. The amplitudes of two-body decays are expressed as convolutions of hard scattering kernels and meson wave functions. However, there are major differences: First, the separation of effects from different scales is not performed systematically by power counting as in QCDF, but long-distance effects are assumed to be suppressed by Sudakov form factors. Second, as a consequence of the Sudakov effects, the dynamics from hard gluon exchanges

[7] Their exact location and shape depends on the specific decay.

dominates and the meson wave functions are accessible in perturbation theory. Third, in contrast to QCDF, naive factorization is not recovered in any limit.

It should be mentioned that in [40] the authors have found sizable contributions from long-distance effects that were supposed to be Sudakov suppressed. Doubts about inconsistencies in pQCD have also been raised in [41].

Nevertheless, NLO corrections in pQCD have been available for some years (cf. [74, 75]). This framework has also been adopted to non-leptonic three-body decays [38, 39]. Here, the decay amplitudes are written in terms of hard scattering kernels and two-meson wave functions. NLO corrections are not yet available.

Flavour Symmetries

The approximate symmetries of the light quark flavours u, d and s can be used in order to relate observables from different decay amplitudes. SU(3) flavour symmetries of two-body decays have already been studied in the 80's [24, 76] and later analyses also concern isospin [77] and U-spin (see e.g. [78]). From the symmetry relations one can infer information on CP violation [79] and on the weak angles [80] and it is possible to probe new physics [81].

Recently, flavour symmetries have been used in combination with QCDF. For instance in [34] the study of $SU(3)$ and U-spin breaking effects in different decay channels was found to give a measure on the size of non-factorizable contributions to the decay amplitude. Moreover, symmetry relations of the light quarks have also been found for three-body decays [33, 34].

1.3. Effective Hamiltonian for Weak Decays

We have argued in Sec. 1.1, that the physics at the weak scale does not couple to the dynamics at the scale m_B since $M_W \gg m_B \gg \Lambda_{\rm QCD}$. Thus, effects of particles with masses at and above the electroweak scale can be absorbed into short-distance coefficients and we work in the effective five flavour theory where the top quark and the heavy bosons are integrated out. The decays $B \to D\pi$ and $B \to \pi\pi\pi$ proceed by the underlying weak transitions $b \to c\bar{u}d$ and $b \to q\bar{q}d$ with $q = u, d$, respectively. The $b \to q\bar{q}d$ transition is described by the weak effective Hamiltonian [82, 28]

$$\mathcal{H}_{\rm eff} = \frac{G_F}{\sqrt{2}} \sum_{p=u,c} \lambda_p \left(C_1 \mathcal{Q}_1^p + C_2 \mathcal{Q}_2^p + \sum_{i=3,\dots,6} C_i \mathcal{Q}_i \right) + \text{h.c.}\,, \tag{1.11}$$

whereas the weak effective Hamiltonian for the $b \to c\bar{u}d$ transition is more simple [82, 28]

$$\mathcal{H}_{\rm eff} = \frac{G_F}{\sqrt{2}} \lambda_p \left(C_1 \mathcal{Q}_1^p + C_2 \mathcal{Q}_2^p \right) + \text{h.c.}\,, \quad \text{with} \quad p = c\,. \tag{1.12}$$

Here and above, we have $\lambda_p = V_{pb} V_{pd}^*$ and $\lambda_t = -\lambda_u - \lambda_c$. The effective local four-fermion current-current operators in the Chetyrkin-Misiak-Münz (CMM) basis [83] read

$$\mathcal{Q}_1^p = \bar{p}\gamma^\mu(1-\gamma_5)T^A b \;\; \bar{d}\gamma_\mu(1-\gamma_5)T^A u\,, \tag{1.13}$$

$$\mathcal{Q}_2^p = \bar{p}\gamma^\mu(1-\gamma_5) b \;\; \bar{d}\gamma_\mu(1-\gamma_5) u\,, \tag{1.14}$$

where T^A are generators of the $SU(3)$ colour gauge group. $\mathcal{Q}_1^p$ is referred to as the colour octet operator and $\mathcal{Q}_2^p$ as the colour singlet operator. The use of the CMM basis allows a consistent treatment of γ_5 in the naive dimensional regularization scheme with anticommuting γ_5. The QCD penguin operators $Q_3, \ldots, Q_6$ are defined as follows[8]

$$\mathcal{Q}_3 = \bar{d}\gamma^\mu(1-\gamma_5)b \sum_{q=u,d,s,c,b} \bar{q}\gamma_\mu(1-\gamma_5)q\,, \tag{1.15}$$

$$\mathcal{Q}_4 = \bar{d}\gamma^\mu(1-\gamma_5)T^A b \sum_{q=u,d,s,c,b} \bar{q}\gamma_\mu(1-\gamma_5)T^A q\,, \tag{1.16}$$

$$\mathcal{Q}_5 = \bar{d}\gamma^\mu(1-\gamma_5)b \sum_{q=u,d,s,c,b} \bar{q}\gamma_\mu(1+\gamma_5)q\,, \tag{1.17}$$

$$\mathcal{Q}_6 = \bar{d}\gamma^\mu(1-\gamma_5)T^A b \sum_{q=u,d,s,c,b} \bar{q}\gamma_\mu(1+\gamma_5)T^A q\,. \tag{1.18}$$

Note that they do not arise in the description of $B \to D\pi$ decays as they do not involve flavour transitions in both currents. The values for the Wilson coefficients $C_1, \ldots C_6$ can be found in [28] up to NLO accuracy. For the calculation of the two-loop transition amplitude of the decay $\bar{B}^0 \to D^+\pi^-$ we further need the NNLO expressions for C_1 and C_2, which can be obtained from [84, 85]. Moreover, as we perform the evaluation in dimensional regularization, the operators Q_1^c and Q_2^c are supplemented by evanescent operators [84]

$$E_1^{(1)} = \left[\bar{c}\gamma^\mu\gamma^\nu\gamma^\rho(1-\gamma_5)T^A b\right]\left[\bar{u}\gamma_\mu\gamma_\nu\gamma_\rho(1-\gamma_5)T^A d\right] - 16Q_1^c\,, \tag{1.19}$$

$$E_2^{(1)} = \left[\bar{c}\gamma^\mu\gamma^\nu\gamma^\rho(1-\gamma_5)b\right]\left[\bar{u}\gamma_\mu\gamma_\nu\gamma_\rho(1-\gamma_5)d\right] - 16Q_2^c\,, \tag{1.20}$$

$$E_1^{(2)} = \left[\bar{c}\gamma^\mu\gamma^\nu\gamma^\rho\gamma^\sigma\gamma^\lambda(1-\gamma_5)T^A b\right]\left[\bar{u}\gamma_\mu\gamma_\nu\gamma_\rho\gamma_\sigma\gamma_\lambda(1-\gamma_5)T^A d\right] - 20E_1^{(1)} - 256Q_1^c\,, \tag{1.21}$$

$$E_1^{(2)} = \left[\bar{c}\gamma^\mu\gamma^\nu\gamma^\rho\gamma^\sigma\gamma^\lambda(1-\gamma_5)b\right]\left[\bar{u}\gamma_\mu\gamma_\nu\gamma_\rho\gamma_\sigma\gamma_\lambda(1-\gamma_5)d\right] - 20E_2^{(1)} - 256Q_2^c\,. \tag{1.22}$$

These are unphysical operators that vanish in $d = 4$ dimensions. However, they have to be taken under consideration, since they mix with the physical operators under renormalization. At two loops the set of operators given in Eqs. (1.13), (1.14) and (1.19)-(1.22) closes under renormalization and thus will be sufficient for our two-loop calculation.

Finally, we have provided the basic framework for the two applications of QCDF. In the next four chapters (Part I) we consider the first application, which is the calculation of the NNLO vertex corrections to the decay $\bar{B}^0 \to D^+\pi^-$ in QCDF. Then we apply QCDF to the decay $B^+ \to \pi^+\pi^-\pi^+$ in Chap. 6 (Part II).

[8] At leading order in α_s the only contributions to the decay $B \to \pi\pi\pi$ come from operators where the quark-antiquark pair is either $\bar{u}u$ or $\bar{d}d$.

Part I.

NNLO corrections to the decay $B \to D\pi$

Chapter 2

Soft Collinear Effective Theory and Matching

We provide a brief introduction to Soft Collinear Effective Theory (SCET) and present the leading power SCET Lagrangian for collinear and soft fields. Heavy quarks are described in the framework of Heavy Quark Effective Theory. Moreover, we present the kinematics of $\bar{B}^0 \to D^+\pi^-$ and briefly discuss this decay within SCET. In the last part of this chapter we derive a master formula for the hard scattering kernels, which enter the factorization formula Eq. (1.10), in terms of bare amplitudes and renormalization factors up to two-loop accuracy by performing a matching of QCD to SCET.

2.1. Introduction to SCET

Soft Collinear Effective Theory (SCET) was developed in the beginning of this century [86–88]. It provides a good description for physical processes involving jets of light hadrons, as well as hard exclusive decays of heavy mesons with at least one light but energetic meson in the final state. The effective theory is constructed in a systematic expansion in inverse powers of the large scale of the process (e.g. the jet energy or the final-state energy) and separates low-energy contributions from high-energy ones. This expansion is valid up to a certain momentum cut-off and correctly reproduces the infrared behaviour of the process. Effects of scales above this cut-off are absorbed into short-distance coefficients. Note that the systematic expansion in the large energy leads to a non-local theory. Hence, SCET is technically more challenging than QCD. For a good introduction to SCET see [89, 90].

We remark that in the description of exclusive non-leptonic B decays SCET is a tool to prove QCDF in the heavy-quark limit. Factorization in SCET manifests itself on the level of the Lagrangian and is therefore valid to any order in perturbation theory. In contrast, factorization in QCDF is based on the analysis of momentum regions in Feynman diagrams at a given order in perturbation theory.

In the following, we discuss the scaling of certain fields in terms of the expansion parameter

of the theory. Moreover, we present the leading power SCET Lagrangian, which is suitable to describe the decay $\bar{B}^0 \to D^+\pi^-$. Heavy Quark Effective Theory (HQET) [91] is a natural part of SCET and heavy quarks thus will be described in HQET.

2.1.1. Scaling of the Fields

Power counting is performed in the expansion parameter λ of the effective theory, which explicitly depends on the physical process. For B decays $\lambda \sim \Lambda_{\rm QCD}/E$, where $E \gg \Lambda_{\rm QCD}$ is a large scale (typically of order m_B) and $\Lambda_{\rm QCD}$ is the typical hadronic scale. Fields and single components of the momenta scale differently with the large scale. To see their explicit scaling behaviour, we define two light-like vectors n_+^μ and n_-^μ which obey

$$n_\pm^2 = 0\,, \qquad n_+ \cdot n_- = 2\,. \tag{2.1}$$

Furthermore, we introduce a time-like vector

$$v^\mu = \frac{1}{2}\,(n_+^\mu + n_-^\mu)\;, \qquad v^2 = 1\,, \tag{2.2}$$

which will be used later to describe the velocity of the B meson in its rest frame. Any four-vector p^μ can be decomposed in terms of light-cone coordinates according to

$$p^\mu = (n_+ \cdot p)\frac{n_-^\mu}{2} + (n_- \cdot p)\frac{n_+^\mu}{2} + p_\perp^\mu \equiv p_+^\mu + p_-^\mu + p_\perp^\mu\,, \tag{2.3}$$

where the index $\perp$ denotes the components perpendicular to n_+ and n_-. The scaling of the different light-cone components $p^\mu = (p_+^\mu, p_-^\mu, p_\perp^\mu)$ can be expressed in terms of the expansion parameter λ. For exclusive decays, such as $B \to D\pi$, the relevant degrees of freedom are collinear Fourier modes (corresponding to the scaling $p^\mu \sim (\lambda^2, 1, \lambda)$) to describe the partons of the light energetic final-state mesons, and soft modes (corresponding to the scaling $p^\mu \sim (\lambda, \lambda, \lambda)$) for the soft partons inside the heavy mesons[1]. To obtain the scaling behaviour of quark and gluon fields when restricted to collinear and soft modes, we first consider a spinor ψ_c in full QCD that describes massless quarks with collinear momentum and decompose it into two-component spinors

$$\psi_c = \xi(x) + \eta(x)\,, \tag{2.4}$$

where

$$\xi = P_+\psi_c = \frac{\not{n}_+\not{n}_-}{4}\psi_c\,, \qquad \eta = P_-\psi_c = \frac{\not{n}_-\not{n}_+}{4}\psi_c\,. \tag{2.5}$$

$P_\pm$ are projectors, i.e. $P_\pm^2 = P_\pm$ and $P_+ + P_- = 1$. The spinors (2.5) satisfy the conditions $\not{n}_+\xi = 0$ and $\not{n}_-\eta = 0$. Their scaling can be found by analyzing the two-point correlation function of collinear fields

$$\langle 0|T\{\bar{\psi}_{c,\alpha}(x), \psi_{c,\beta}(y)\}|0\rangle = \int \frac{d^4p}{(2\pi)^4}\,\frac{i\not{p}_{\alpha\beta}}{p^2 + i\epsilon}e^{-ip(x-y)}\,, \tag{2.6}$$

[1] The theory for the description of exclusive decays is commonly referred to as $\text{SCET}_{\rm II}$. Fields and momenta with a different scaling behaviour are used in the description of inclusive decays, where the corresponding theory is denotes as $\text{SCET}_{\rm I}$.

where α and β denote the Dirac indices. Since ψ_c only contain collinear Fourier modes the integration measure $d^4p = \frac{1}{2}dp_+dp_-dp_\perp^2$ scales as λ^4 and $p^\mu \sim (\lambda^2, 1, \lambda)$. Projecting on the two-component spinors one finds that $\xi \sim \lambda$ and $\eta \sim \lambda^2$. Hence, η is suppressed by a factor λ with respect to ξ. In a similar manner, the scalings of q_s, which is the full QCD quark field restricted to soft Fourier modes, and the soft and collinear gauge fields A_c^μ and A_s^μ can be obtained. One finds $q_s \sim \lambda^{3/2}$ and the gauge fields scale like their corresponding momenta, i.e. $A_c^\mu \sim (\lambda^2, 1, \lambda)$ and $A_s^\mu \sim (\lambda, \lambda, \lambda)$.

2.1.2. Leading Power SCET Lagrangian

The derivation of the SCET Lagrangian for collinear and soft quarks interacting with collinear and soft gluons is rather involved. Here, we only outline the most important steps towards the leading power Lagrangian. For details see e.g. [88, 89].

We consider the QCD Lagrangian for massless quarks and gluons which are restricted to soft and collinear momenta and decompose the full QCD spinor into a soft and a collinear component, and similarly the full QCD gluon field $A^\mu = A_c^\mu + A_s^\mu$

$$\begin{aligned}\mathcal{L}^{\text{QCD}} &= \bar{\psi} i \not{D} \psi - \frac{1}{4}(F^a)_{\mu\nu}(F^a)^{\mu\nu} \\ &= (\bar{q}_s + \bar{\psi}_c)(i\not{\partial} + g\not{A}_c + g\not{A}_s)(q_s + \psi_c) - \frac{1}{4}(F^a)_{\mu\nu}(F^a)^{\mu\nu}\,. \end{aligned} \tag{2.7}$$

First, we focus on the collinear sector of this Lagrangian, which is given by

$$\mathcal{L}_c^{\text{QCD}} = \bar{\psi}_c i \not{D}_c \psi_c + (F_c^a)_{\mu\nu}(F_c^a)^{\mu\nu}\,. \tag{2.8}$$

Here, $D_c^\mu = \partial^\mu - igA_c^\mu$ and $(F_c^a)^{\mu\nu} = \partial^\mu A_c^\nu - \partial^\nu A_c^\mu - ig\,[A_c^\mu, A_c^\nu]$ are the collinear covariant derivative and the collinear field strength tensor, respectively. We proceed by splitting the four-spinor ψ_c into a large ($\xi \sim \lambda$) and a small ($\eta \sim \lambda^2$) component and expand the Dirac matrix γ^μ in terms of light-cone coordinates. Using the relations $\not{n}_+\xi = \not{n}_-\eta = 0$ and $\bar{\xi}\not{D}_{c\perp}\xi = \bar{\eta}\not{D}_{c\perp}\eta = 0$[2] the Lagrangian becomes

$$\mathcal{L}_c^{\text{QCD}} = \bar{\xi}\, i(n_+ \cdot D_c)\frac{\not{n}_-}{2}\xi + \bar{\eta}\, i(n_- \cdot D_c)\frac{\not{n}_+}{2}\bar{\eta} + \bar{\eta} i \not{D}_{c\perp}\xi + \bar{\xi} i \not{D}_{c\perp}\eta + (F_c)_{\mu\nu}(F_c)^{\mu\nu}\,. \tag{2.9}$$

We further remove the small component η from the Lagrangian by solving the classical equations of motion $\delta\mathcal{L}_q^{\text{QCD}}/\delta\bar{\eta} = 0$ and $\delta\mathcal{L}_q^{\text{QCD}}/\delta\eta = 0$, which results then read

$$\eta = -\frac{\not{n}_-}{2}\frac{1}{in_- \cdot D_c} i\not{D}_{c\perp}\xi\,, \quad \bar{\eta} = -\bar{\xi}\not{D}_{c\perp}\frac{\not{n}_-}{2}\frac{1}{in_- \cdot \overleftarrow{D}_c}\,. \tag{2.10}$$

Inserting these expressions back into Eq. (2.9), one obtains after a few simplifications

$$\mathcal{L}_c = \bar{\xi}\,\frac{\not{n}_-}{2} i(n_+ \cdot D_c)\,\xi + \bar{\xi}\,\frac{\not{n}_-}{2} i\not{D}_{c\perp}\frac{1}{in_- \cdot D_c} i\not{D}_{c\perp}\xi + (F_c)_{\mu\nu}(F_c)^{\mu\nu}\,. \tag{2.11}$$

[2] This is consequence of $\{\not{n}_\pm, \not{D}_{c\perp}\} = 0$.

This Lagrangian is exact to all orders in λ and is equivalent to the QCD Lagrangian Eq. (2.8), but boosted to a reference frame where all fields are collinear[3]. Hence, a collinear sector in which the quark and gluon fields are restricted to collinear Fourier modes is equivalent to full QCD restricted to only soft momenta and then boosted. We will make use of this fact in the explicit calculation of the two-loop colour octet hard scattering kernels in Sec. 5.1.

Next, we consider the soft sector of Eq. (2.7). It is simply given by the Lagrangian

$$\mathcal{L}_s = \bar{q}_s i \not{D}_s q_s + (F_s)_{\mu\nu}(F_s)^{\mu\nu}\,, \tag{2.12}$$

where $D_s^\mu = \partial^\mu - igA_s^\mu$ and $(F_s^a)^{\mu\nu} = \partial^\mu A_s^\nu - \partial^\nu A_s^\mu - ig\,[A_s^\mu, A_s^\nu]$ are the soft covariant derivative and soft field strength tensor, respectively. It is exact to all orders in λ and thus, also the soft sector when restricted to soft fields is equivalent to full QCD restricted to soft momenta.

Finally, there are also interactions between the two sectors. Soft and collinear fields cannot couple directly as such interactions would result in highly off-shell momenta and therefore are absorbed in the short distance coefficients of the effective theory. However, there is an additional long-distance mode which scales like $p^\mu \sim (\lambda^2, \lambda, \lambda^{3/2})$ and is commonly referred to as soft-collinear or "messenger" mode. Although such fields do not appear as external legs they need to be included in the effective theory, since they can interact separately with the soft and collinear fields without changing their scaling properties. The soft-collinear sector is described by the soft-collinear Lagrangian $\mathcal{L}_{sc}$. Its derivation proceeds analogously to the collinear sector, splitting the soft-collinear spinor q_{sc} into a large ($\sim \lambda^2$) and a small ($\sim \lambda^{5/2}$) component and removing the small component from the Lagrangian. The result has a similar structure as $\mathcal{L}_c$. Since the explicit form of $\mathcal{L}_{sc}$ is not relevant for this work we refrain from specifying it and refer to [89] for a definition. The leading power interaction term consists of collinear and soft quarks and gluon fields coupling to a soft-collinear gauge field A_{sc}. It has to be expanded in λ for obtaining a Lagrangian with a single and homogeneous scaling behaviour. To this point, we have omitted the dependence on position and considered all fields as local. We do not go into further details here as they are not relevant for this work, but just mention that in interactions with collinear and soft fields the light-cone components of $A_{sc}(x)$ scale differently. At leading power one finds $A_{sc}(x) = A_{sc}(x_-) + \mathcal{O}(\lambda)$ in collinear interactions[4]. The soft-collinear gauge field has to be evaluated at the position $x_-^\mu = (x\cdot n_-)n_+^\mu/2$, whereas all collinear fields remain at the position x. Similar, in interaction with soft fields $A_{sc}(x) = A_{sc}(x_+) + \mathcal{O}(\lambda)$ is the leading component. Hence, the requirement of a homogeneous scaling leads to the non-local nature of SCET. The final leading power interaction term reads

$$\mathcal{L}^{(0)}_{\text{int,s,c}} = \bar{q}_s(x)\frac{\not{n}_+}{2}\, g\not{n}_- \cdot A_{sc}(x_+)q_s(x) + \bar{\xi}(x)\frac{\not{n}_-}{2}\, g\not{n}_+ \cdot A_{sc}(x_-)\xi(x) + \text{pure gluon terms}\,. \tag{2.13}$$

So far, we have only considered the massless case. Particles with masses of order Λ_{QCD} can be included in above considerations by adding suitable mass terms. In contrast, effects

[3]Note that the factor $n_- \cdot D_c$ in the denominator only becomes meaningful after introducing Wilson lines in SCET.

[4]This expansion is also referred to as multipole expansion.

of heavy quarks, which cannot be described by collinear and soft fields since their mass m is much larger than $\Lambda_{\rm QCD}$, are described by the HQET Lagrangian [91] and short distance coefficients. Taken into account that interactions of heavy quarks with collinear fields only arise at subleading power, as they put the quark highly off-shell, the HQET Lagrangian reads

$$\mathcal{L}_{\rm HQET} = \bar{h}_v(iv\cdot D_s)h_v + O\left(1/m\right) . \tag{2.14}$$

The field h_v describes a heavy quark moving with velocity v and satisfies $\not{v}h_v = h_v$. It scales like a soft quark field and the leading power interaction to soft-collinear fields takes the form $\mathcal{L}^{(0)}_{\rm int,HQET} = \bar{h}_v(x)\frac{\not{n}_+\cdot v}{2} g n_-\cdot A_{sc}(x_+)h_v(x)$.

Putting all pieces together, the leading power SCET Lagrangian reads

$$\mathcal{L}_{\rm SCET} = \mathcal{L}_c + \mathcal{L}_s + \mathcal{L}_{sc} + \mathcal{L}_{\rm HQET} + \mathcal{L}^{(0)}_{\rm int,s,c} + \mathcal{L}^{(0)}_{\rm int,HQET} . \tag{2.15}$$

Note that for processes which involve two different heavy quarks a second heavy-quark Lagrangian and a corresponding interaction term to the soft-collinear gluon field can be added. It turns out, however, that by performing suitable field redefinitions the leading power interaction terms vanish. To see this, we first consider the heavy-quark Lagrangian $\mathcal{L}_{\rm HQET}$ and introduce Wilson lines in HQET. They arise from the fact that attachments of soft gluons to a heavy quark are not power-suppressed. These interactions therefore need to be resummed and as a result we obtain a Wilson line $S_v(x) = \mathrm{P}\exp(ig\int_{-\infty}^0 ds\, v\cdot A_s(x+vs))$, where P is the path-ordered exponential. The Wilson line has the properties $S_v^\dagger S_v = S_v S_v^\dagger = 1$ and (more importantly) $S_v^\dagger iv\cdot D_s S_v = iv\cdot\partial$. By a suitable field redefinition $h_v(x) = S_v(x)h_v^{(0)}(x)$ we find that at leading power $\mathcal{L}_{\rm HQET}$ transforms to the free-particle heavy-quark Lagrangian $\mathcal{L}_{\rm HQET} = h_v^{(0)} iv\cdot\partial h_v^{(0)} + O\left(1/m\right)$. The soft gluons do not couple to the "sterile" fields $h_v^{(0)}$ anymore but only interact with the Wilson lines. Whereas this decoupling affects for instance the normalization of heavy-to-heavy form factors at zero recoil in HQET [92, 93], one finds that suitable field redefinitions of the soft and collinear fields, which involve soft-collinear Wilson lines, remove the leading power interactions between these fields [88]. Hence, at leading power all interaction terms in Eq. (2.15) can be dropped. This decoupling of soft and collinear interactions results in factorization of many physical processes at leading power provided that external operators do not reintroduce soft-collinear fields. In contrast, the existence of these interactions at subleading power usually implies a breakdown of factorization. Next, we present the kinematics of $\bar{B}^0 \to D^+\pi^-$ and briefly discuss this decay within SCET.

2.1.3. $B \to D\pi$ in SCET

The decay $\bar{B}^0 \to D^+\pi^-$ is mediated at parton level by the process $b\to c\bar{u}d$. The kinematics of the latter are shown in the tree-level Feynman diagram depicted in Fig. 2.1. All external momenta are taken to be incoming here and throughout the rest of this work. The b and the c quark are considered to be massive, while we treat the light d and u quark as massless. q_4 and q_3 denote the momenta of the b and the c quark, respectively, which fulfill the on-shell

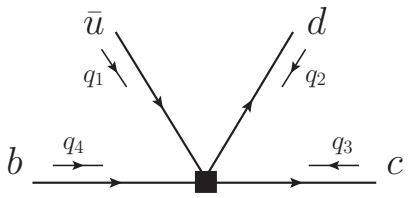

Figure 2.1. – The tree-level Feynman diagram for the $b \to c\bar{u}d$ transition in full (five flavour) QCD: the black square represents the vertex of the effective weak interaction. q_4 and q_3 are the momenta of the quark lines with masses m_b and m_c, respectively. $q_1 + q_2 = q$ where q is the momentum of the pion. All momenta are taken to be incoming.

constraints $q_{4,3}^2 = m_{b,c}^2$. The constituents of the pion share the momentum q with $q_1 = uq$ and $q_2 = (1-u)q \equiv \bar{u}q$, with $u \in [0,1]$ being the momentum fraction of the quarks inside the pion entering Eq. (1.10) in a convolution of the hard scattering kernel and the pion LCDA. The pion has a small invariant mass $q^2 \sim \Lambda_{\rm QCD}^2$. Note that for practical purpose we can set $q^2 = 0$ in the calculation of the QCD Feynman diagrams.

We choose a reference frame such that the heavy b quark within the B meson moves with velocity $q_b = m_b v + k$, where k is a residual momentum of order $\Lambda_{\rm QCD}$ and v is the velocity of the B meson[5]. The b quark can then be described by the HQET Lagrangian Eq. (2.14). In the B meson rest frame the pion and the D meson travel back-to-back, carrying an energy $E = m_B/2$ each. The invariant mass of the pion is of order $\Lambda_{\rm QCD}^2$ and we define the expansion parameter $\lambda = \Lambda_{\rm QCD}/E$. We further choose a reference frame such that the fast pion moves in the light-cone direction n_+ and assign a collinear momentum $q^\mu \sim (\lambda^2, 1, \lambda)$ to it. The leading Fock states of the pion can be described by the collinear Lagrangian Eq. (2.11). As they nearly move in the same direction we describe them by the same type of collinear SCET field χ, which satisfies the equations of motion $\not{n}_+\chi = 0$ and $\bar{\chi}\not{n}_+ = 0$. In the derivation of the factorization formula Eq. (1.10) the charm quark and consequently the D meson were assumed to be heavy. Hence, we approximate the D meson by another heavy meson moving with velocity v'. We can then describe the charm quark with momentum $q_c = m_c v' + k'$, where k' is another residual momentum, by the HQET Lagrangian Eq. (2.14) with the substitution $v \to v'$. Since $m_c/m_b \sim O(1)$ we find that $v \cdot v' \sim O(1)$.

The tree-level operators for the corresponding heavy-to-heavy transition have been worked out in [88]. For the calculation of the two-loop Feynman diagrams shown in Figs. 2.4 and 2.5 the basis has to be extended to include evanescent operators, which have been defined in [47] for heavy-to-light transitions, and operators with a different chirality, to take into account the non-vanishing mass of the charm quark. The complete basis is presented in the next section in Eqs. (2.18)-(2.23).

Moreover, it was shown in [88] that in the leading power $\bar{B}^0 \to D^+\pi^-$ transition soft and collinear interactions decouple to all orders in perturbation theory. The leading power decay amplitude can be described by a $B \to D$ form factor and a pion LCDA, reproducing the QCD factorization formula (1.10) in the large energy limit[6]. Hence, at a certain scale called,

[5] In the explicit calculation of the Feynman diagrams we use on-shell momenta and set $k^\mu = 0$.

[6] This is not a complete proof of factorization, as it is not shown that the convolution integrals $\int du\, T(u)\Phi(u)$ exist to all orders in perturbation theory.

the matching scale (which lies below the momentum cut-off upon which the effective theory is valid), the decay amplitudes in QCDF and SCET are equivalent in the heavy-quark limit[7] and we can perform a matching of QCD onto SCET. From this a master formula for the hard scattering kernels can be extracted. This is the topic of the next section.

2.2. Derivation of the Master Formula

We have seen in Chap. 1.1 that the hard scattering kernel can be calculated perturbatively in an expansion in the strong coupling α_s. For convenience we modify Eq. (1.9) and take out an explicit factor $1/(4\pi)$ for each loop. The hard scattering kernel for the colour octet and colour singlet operators is then given by an expansion of the form

$$T = T^{(0)} + \frac{\alpha_s}{4\pi} T^{(1)} + \left(\frac{\alpha_s}{4\pi}\right)^2 T^{(2)} + \mathcal{O}(\alpha_s^3)\,. \tag{2.16}$$

Here, we derive the expressions for $T^{(0,1,2)}$ in terms of bare amplitudes and renormalization factors by performing a matching of QCD to SCET. The reasons for this matching are twofold: First, the degrees of freedom of the decay are naturally described within SCET. Second, in the matching many "factorizable" Feynman diagrams cancel (see Sec. 2.2.2 for the proper definition of the diagrams).

2.2.1. Matching

The QCD amplitude for the $b \to c\bar{u}d$ transition, which underlies the decay $\bar{B}^0 \to D^+\pi^-$ at parton level, is described by the weak effective Hamiltonian given in Sec. 1.3. The contributing operators are the QCD current-current operators $\mathcal{Q}_1^c$ and $\mathcal{Q}_2^c$ (see Eqs. (1.13) and (1.14)). We will omit the superscript "c" on these operators throughout Part I of this thesis. At the matching scale, the amplitudes in full QCD and in SCET are made equal by adjusting the corresponding hard coefficients. The renormalized matrix elements of the QCD operators $\mathcal{Q}_i$ can then be expressed as a linear combination of a suitable basis of SCET operators at leading power[8]

$$\langle \mathcal{Q}_i \rangle = \sum_a \left[H_{ia} \langle \mathcal{O}_a \rangle + H'_{ia} \langle \mathcal{O}'_a \rangle \right] . \tag{2.17}$$

Here, H_{ia} and H'_{ia} are the matching coefficients, which by construction are finite in ϵ. The basis of SCET operators is given by

$$\mathcal{O}_1 = \bar{\chi} \frac{\not{n}_-}{2} (1-\gamma_5) \chi \;\; \bar{h}_{v'} \not{n}_+ (1-\gamma_5) h_v \,, \tag{2.18}$$

$$\mathcal{O}_2 = \bar{\chi} \frac{\not{n}_-}{2} (1-\gamma_5) \gamma_\perp^\alpha \gamma_\perp^\beta \chi \;\; \bar{h}_{v'} \not{n}_+ (1-\gamma_5) \gamma_{\perp,\beta} \gamma_{\perp,\alpha} h_v \,, \tag{2.19}$$

$$\mathcal{O}_3 = \bar{\chi} \frac{\not{n}_-}{2} (1-\gamma_5) \gamma_\perp^\alpha \gamma_\perp^\beta \gamma_\perp^\gamma \gamma_\perp^\delta \chi \;\; \bar{h}_{v'} \not{n}_+ (1-\gamma_5) \gamma_{\perp,\delta} \gamma_{\perp,\gamma} \gamma_{\perp,\beta} \gamma_{\perp,\alpha} h_v \tag{2.20}$$

[7] Note that even though the hard fluctuations of the heavy b quark are integrated out, the energy E is still of the order m_B.

[8] We use the same convention as in [47].

and

$$\mathcal{O}_1' = \bar{\chi}\frac{\not{n}_-}{2}(1-\gamma_5)\chi\ \ \bar{h}_{v'}\not{n}_+(1+\gamma_5)h_v\,, \tag{2.21}$$

$$\mathcal{O}_2' = \bar{\chi}\frac{\not{n}_-}{2}(1-\gamma_5)\gamma_\perp^\alpha\gamma_\perp^\beta\chi\ \ \bar{h}_{v'}\not{n}_+(1+\gamma_5)\gamma_{\perp,\alpha}\gamma_{\perp,\beta}h_v\,, \tag{2.22}$$

$$\mathcal{O}_3' = \bar{\chi}\frac{\not{n}_-}{2}(1-\gamma_5)\gamma_\perp^\alpha\gamma_\perp^\beta\gamma_\perp^\gamma\gamma_\perp^\delta\chi\ \ \bar{h}_{v'}\not{n}_+(1+\gamma_5)\gamma_{\perp,\alpha}\gamma_{\perp,\beta}\gamma_{\perp,\gamma}\gamma_{\perp,\delta}h_v\,. \tag{2.23}$$

For simplicity the Wilson lines in the operators (2.18)-(2.23) have been suppressed. Since the latter are non-local on the light-cone[9], the full notation would be $\bar{\chi}(tn_-)[\dots]\chi(0)$. Therefore, the coefficients H_{ia} are also functions of the variable t and Eq. (2.17) must be interpreted as a convolution product. The operators Eqs. (2.18)-(2.23) are all colour singlets. In that way we have already take into account that the contributions of the colour octet operators vanish when projected onto the pion, which is a colour singlet state. Moreover, all operators with index $a > 1$ are evanescent, i.e. they vanish in $d = 4$. Note that the evanescence of these operators can be shown by reducing them to the 16 bilinear covariants in $d = 4$ dimensions. For technical details on the operators see [91, 94].

Eq. (2.17) is the matching relation from full (five flavour) QCD to SCET with three active light flavours. Thus, $\langle\mathcal{Q}_i\rangle$ can be evaluated in a perturbative expansion in terms of both, the matching coefficients and SCET operators on the one hand and the QCD amplitudes on the other hand. We work in dimensional regularization and evaluate the one- and two-loop amplitudes in the on-shell subtraction scheme. The renormalization of the strong coupling is performed in the $\overline{\text{MS}}$ scheme. We first consider the expansion of $\langle\mathcal{Q}_i\rangle$ in terms of QCD amplitudes in the following.

QCD Side

The expression for the renormalized matrix elements of the operators $\mathcal{Q}_i$ (1.13) and (1.14) up to the two-loop accuracy reads

$$\begin{aligned}\langle\mathcal{Q}_i\rangle = \Big\{&A_{ia}^{(0)} + \frac{\alpha_s}{4\pi}\Big[A_{ia}^{(1)} + Z_{ext}^{(1)}A_{ia}^{(0)} + Z_{ij}^{(1)}A_{ja}^{(0)}\Big]\\
&+\Big(\frac{\alpha_s}{4\pi}\Big)^2\Big[A_{ia}^{(2)} + Z_{ij}^{(1)}A_{ja}^{(1)} + Z_{ij}^{(2)}A_{ja}^{(0)} + Z_{ext}^{(1)}A_{ia}^{(1)} + Z_{ext}^{(2)}A_{ia}^{(0)} + Z_{ext}^{(1)}Z_{ij}^{(1)}A_{ja}^{(0)}\\
&+(-i)\delta m_b^{(1)}A_{ia}^{*(1)} + (-i)\delta m_c^{(1)}A_{ia}^{**(1)} + Z_\alpha^{(1)}A_{ia}^{(1)}\Big] + \mathcal{O}\big(\alpha_s^3\big)\Big\}\langle\mathcal{O}_a\rangle^{(0)}\\
&+(A\leftrightarrow A')\langle\mathcal{O}_a'\rangle^{(0)}\,.\end{aligned} \tag{2.24}$$

Here, a sum over a is understood with $a = 1, 2, 3$ and α_s is the $\overline{\text{MS}}$ strong coupling constant with five light flavours. The index i denotes the physical operators only (e.g. $i = 1, 2$) whereas j includes also evanescent operators (i.e. $j = 1, \dots, 6$) (see Sec. 1.3 for the definition of the evanescent operators). The $A^{(l)}$ are the bare l-loop on-shell amplitudes (the corresponding Feynman diagrams up to two loops are given in Sec. 2.2.2). $A^{*(1)}$ ($A^{**(1)}$)

[9] The non-locality is a result of the momentum distribution of the quarks forming the leading Fock states of the pion LCDA.

is the one-loop bare amplitude with a b (c) quark mass insertion on the heavy b (c) line. The primed amplitudes are defined analogously. Z, Z_{ext} and Z_α are renormalization factors from operator renormalization, self-energy renormalization of all external legs and coupling renormalization, respectively. They are defined in a perturbative expansion

$$Z = 1 + \sum_{k=1}^{\infty} \frac{\alpha_s^k}{(4\pi)^k} Z^{(k)} \,. \tag{2.25}$$

Their explicit one-loop expressions are given in Sec. 5.1. The renormalization is performed such that matrix elements of evanescent operators vanish also beyond tree level. However, evanescent operators cannot be neglected right from the beginning as they yield physical contributions as intermediate states in the products $Z_{ij}^{(1)} A_{ja}^{(0,1)}$ and $Z_{ij}^{(2)} A_{ja}^{(0)}$. Note that we have already substituted the SCET operators $\mathcal{O}_a$ and $\mathcal{O}'_a$ in Eq. (2.24), since at tree-level their matrix elements are equivalent to the corresponding QCD operators, which are given by the operators in Eqs. (2.18)-(2.23), except that all fields are QCD fields.

SCET Side

Similar to the QCD case, we can write down the expression for the renormalized matrix elements of the SCET operators Eqs. (2.18)-(2.20). We find

$$\begin{aligned}\langle \mathcal{O}_a \rangle = \Big\{ \delta_{ab} &+ \frac{\hat{\alpha}_s}{4\pi} \Big[M_{ab}^{(1)} + Y_{ext}^{(1)} \delta_{ab} + Y_{ab}^{(1)} \Big] \\ &+ \left(\frac{\hat{\alpha}_s}{4\pi} \right)^2 \Big[M_{ab}^{(2)} + Y_{ext}^{(1)} M_{ab}^{(1)} + Y_{ac}^{(1)} M_{cb}^{(1)} + \hat{Z}_\alpha^{(1)} M_{ab}^{(1)} + Y_{ext}^{(2)} \delta_{ab} \\ &+ Y_{ext}^{(1)} Y_{ab}^{(1)} + Y_{ab}^{(2)} \Big] + \mathcal{O}\big(\hat{\alpha}_s^3\big) \Big\} \langle \mathcal{O}_b \rangle^{(0)} \,,\end{aligned} \tag{2.26}$$

where $a = 1, 2, 3$ and a sum over $b = 1, 2, 3$ is understood. $\hat{\alpha}_s$ is the strong coupling constant in the $\overline{\text{MS}}$ scheme for three light flavours and $M^{(l)}$ are the bare l-loop SCET amplitudes. $Y_{ext}^{(l)}$, $Y^{(l)}$ and $\hat{Z}_\alpha^{(l)}$ are the l-loop wave-function, operator and coupling renormalization constants, respectively. They are defined in a perturbative expansion analogous to Eq. (2.25) except that the strong coupling has only three light flavours. Note that there are no mass counter term insertions with the b and c quarks, since the latter are treated as heavy quarks and thus do not appear as dynamical fields anymore. The expression for the primed operators Eqs. (2.21)-(2.23) is given by substituting $M \to M'$ and $\mathcal{O} \to \mathcal{O}'$ in Eq. (2.26).

Eq. (2.26) can be simplified by a large amount. In dimensional regularization the on-shell renormalization constants Y_{ext} are equal to unity and the bare on-shell amplitudes are zero, since they contain only scaleless integrals, which vanish in dimensional regularization. We thus arrive at the following simplified expression of Eq. (2.26)

$$\langle \mathcal{O}_a \rangle = \left\{ \delta_{ab} + \frac{\hat{\alpha}_s}{4\pi} Y_{ab}^{(1)} + \left(\frac{\hat{\alpha}_s}{4\pi} \right)^2 Y_{ab}^{(2)} + \mathcal{O}\left(\hat{\alpha}_s^3\right) \right\} \langle \mathcal{O}_b \rangle^{(0)} \,, \tag{2.27}$$

which for the primed operators takes a similar form. The $Y^{(1,2)}$ can be obtained from Eq. (2.26) by using another regulator than dimensional regularization for handling the IR

divergences. We remark that since we will evaluate the one- and two-loop amplitudes in the on-shell subtraction scheme, the quantities $H^{(l)}$, $A^{(l)}$ and the hard scattering kernels $T^{(l)}$, to be defined later, depend on the momentum fraction u of the pion (as do the corresponding primed quantities). Whenever they appear along a renormalization factor $Y^{(l)}$ such as $Y^{(1)}_{ac} H^{(1)}_{cb}$ we must keep in mind that these expressions must be interpreted as a convolution product $\int_0^1 du'\, Y^{(1)}_{ac}(u,u') H^{(1)}_{cb}(u')$.

Hard Scattering Kernels

For relating the matching coefficients H and H' in Eq. (2.17) to the hard scattering kernels we follow [47] and introduce two QCD operators $\mathcal{Q}^{(\prime)\mathrm{QCD}} = [\bar{q}\frac{\not{n}_-}{2}(1-\gamma_5)q][\bar{c}\not{n}_+(1\mp\gamma_5)b]$. The renormalized operators are then made equivalent to the renormalized SCET operators O_1 and O_1' by adjusting the corresponding hard coefficients. For the renormalized light-to-light current we make the ansatz

$$\left[\bar{q}\frac{\not{n}_-}{2}(1-\gamma_5)q\right] = C_{\bar{q}q}\left[\bar{\chi}\frac{\not{n}_-}{2}(1-\gamma_5)\chi\right]. \tag{2.28}$$

The matching coefficient $C_{\bar{q}q}$ is expressed as perturbative expansion in the five flavour coupling (see Eq. (2.44) for the conversion of the three flavour to the five flavour coupling). It receives a correction at $\mathcal{O}(\alpha_s^2)$ only, i.e. $C^{(1)}_{\bar{q}q} = 0$, since at one loop only scaleless integrals contribute. The heavy-to-heavy currents with different chiralities mix in the matching. Thus, we make the ansatz

$$\left[\bar{c}\not{n}_+(1-\gamma_5)b\right] = C^{\mathrm{LL}}_{FF}\left[\bar{h}_{v'}\not{n}_+(1-\gamma_5)h_v\right] + C^{\mathrm{LR}}_{FF}\left[\bar{h}_{v'}\not{n}_+(1+\gamma_5)h_v\right], \tag{2.29}$$

$$\left[\bar{c}\not{n}_+(1+\gamma_5)b\right] = C^{\mathrm{RL}}_{FF}\left[\bar{h}_{v'}\not{n}_+(1-\gamma_5)h_v\right] + C^{\mathrm{RR}}_{FF}\left[\bar{h}_{v'}\not{n}_+(1+\gamma_5)h_v\right]. \tag{2.30}$$

The matching coefficients C_{FF} are also given in an expansion in the five flavour coupling. For the diagonal coefficients we have $C^{\mathrm{LL,RR}}_{FF} = 1+\mathcal{O}(\alpha_s)$. In contrast, the non-diagonal matching coefficients that induce the chirality mixing only arise beyond tree level, i.e. $C^{\mathrm{LR,LR}}_{FF} = \mathcal{O}(\alpha_s)$. The explicit one-loop expressions for the heavy-to-heavy coefficients are give in Sec. 5.1. One finds at this order

$$\left(C^{\mathrm{LL}}_{FF}\right)^{(1)} = \left(C^{\mathrm{RR}}_{FF}\right)^{(1)} \equiv C^{\mathrm{D}(1)}_{FF}, \tag{2.31}$$

$$\left(C^{\mathrm{LR}}_{FF}\right)^{(1)} = \left(C^{\mathrm{RL}}_{FF}\right)^{(1)} \equiv C^{\mathrm{ND}(1)}_{FF}. \tag{2.32}$$

Finally, we obtain

$$\mathcal{Q}^{\mathrm{QCD}} = \left[\bar{q}\frac{\not{n}_-}{2}(1-\gamma_5)q\right]\left[\bar{c}\not{n}_+(1-\gamma_5)b\right] = C_{\bar{q}q}C^{\mathrm{LL}}_{FF}\mathcal{O}_1 + C_{\bar{q}q}C^{\mathrm{LR}}_{FF}\mathcal{O}_1', \tag{2.33}$$

$$\mathcal{Q}'^{\mathrm{QCD}} = \left[\bar{q}\frac{\not{n}_-}{2}(1-\gamma_5)q\right]\left[\bar{c}\not{n}_+(1+\gamma_5)b\right] = C_{\bar{q}q}C^{\mathrm{RL}}_{FF}\mathcal{O}_1 + C_{\bar{q}q}C^{\mathrm{RR}}_{FF}\mathcal{O}_1'. \tag{2.34}$$

By construction $\mathcal{Q}^{\mathrm{QCD}}$ and $\mathcal{Q}'^{\mathrm{QCD}}$ factorize into a light-to-light and a heavy-to-heavy current and the matrix element of these operators is the product of a light-cone distribution amplitude and the full QCD form factor with the corresponding helicity structure[10].

We now consider the two hard scattering kernels $\hat{T}_i$ and $\hat{T}'_i$ that are defined in following expression

$$\langle \mathcal{Q}_i \rangle = \hat{T}_i \langle \mathcal{Q}^{\mathrm{QCD}} \rangle + \hat{T}'_i \langle \mathcal{Q}'^{\mathrm{QCD}} \rangle + \sum_{a>1} \left[H_{ia} \langle \mathcal{O}_a \rangle + H'_{ia} \langle \mathcal{O}'_a \rangle \right] . \tag{2.35}$$

Comparing Eqs. (2.17) and (2.35) $\hat{T}_i$ and $\hat{T}'_i$ can then be related to the matching coefficients as follows

$$\begin{pmatrix} \hat{T}_i \\ \hat{T}'_i \end{pmatrix} = \begin{pmatrix} C_{\bar{q}q} C_{FF}^{\mathrm{LL}} & C_{\bar{q}q} C_{FF}^{\mathrm{RL}} \\ C_{\bar{q}q} C_{FF}^{\mathrm{LR}} & C_{\bar{q}q} C_{FF}^{\mathrm{RR}} \end{pmatrix}^{-1} \begin{pmatrix} H_{i1} \\ H'_{i1} \end{pmatrix} . \tag{2.36}$$

Plugging in the matching coefficients as expansions in the five flavour coupling α_s, the matrix can be inverted and we obtain the following expressions for the one- and two-loop hard scattering kernels

$$\begin{aligned}
\hat{T}_i = {} & H_{i1}^{(0)} + \frac{\alpha_s}{4\pi} \left[H_{i1}^{(1)} - C_{FF}^{\mathrm{D}(1)} H_{i1}^{(0)} - C_{FF}^{\mathrm{ND}(1)} H_{i1}^{\prime(0)} \right] \\
& + \left(\frac{\alpha_s}{4\pi} \right)^2 \Big[\left(C_{FF}^{\mathrm{D}(1)} \right)^2 H_{i1}^{(0)} + \left(C_{FF}^{\mathrm{ND}(1)} \right)^2 H_{i1}^{(0)} - C_{FF}^{\mathrm{LL}(2)} H_{i1}^{(0)} - C_{\bar{q}q}^{(2)} H_{i1}^{(0)} - C_{FF}^{\mathrm{D}(1)} H_{i1}^{(1)} \\
& \quad + H_{i1}^{(2)} - C_{FF}^{\mathrm{LR}(2)} H_{i1}^{\prime(0)} + 2 C_{FF}^{\mathrm{D}(1)} C_{FF}^{\mathrm{ND}(1)} H_{i1}^{\prime(0)} - C_{FF}^{\mathrm{ND}(1)} H_{i1}^{\prime(1)} \Big] + \mathcal{O}(\alpha_s^3) , \qquad (2.37) \\
\hat{T}'_i = {} & H_{i1}^{\prime(0)} + \frac{\alpha_s}{4\pi} \left[H_{i1}^{\prime(1)} - C_{FF}^{\mathrm{D}(1)} H_{i1}^{\prime(0)} - C_{FF}^{\mathrm{ND}(1)} H_{i1}^{(0)} \right] \\
& + \left(\frac{\alpha_s}{4\pi} \right)^2 \Big[- C_{FF}^{\mathrm{ND}(1)} H_{i1}^{(0)} - C_{FF}^{\mathrm{D}(1)} H_{i1}^{\prime(0)} + H_{i1}^{\prime(1)} + 2 C_{FF}^{\mathrm{D}(1)} C_{FF}^{\mathrm{ND}(1)} H_{i1}^{(0)} - C_{FF}^{\mathrm{RL}(2)} H_{i1}^{(0)} \\
& \quad - C_{FF}^{\mathrm{ND}(1)} H_{i1}^{(1)} + \left(C_{FF}^{\mathrm{D}(1)} \right)^2 H_{i1}^{\prime(0)} + \left(C_{FF}^{\mathrm{ND}(1)} \right)^2 H_{i1}^{\prime(0)} - C_{\bar{q}q}^{(2)} H_{i1}^{\prime(0)} - C_{FF}^{\mathrm{RR}(2)} H_{i1}^{\prime(0)} \\
& \quad - C_{FF}^{\mathrm{D}(1)} H_{i1}^{\prime(1)} + H_{i1}^{\prime(2)} \Big] + \mathcal{O}(\alpha_s^3) . \qquad (2.38)
\end{aligned}$$

Before deriving the explicit expressions for $T_{1,2}$ in terms of bare amplitudes and renormalization factors up to two-loop accuracy, we present the Feynman diagrams that contribute to the bare QCD amplitudes $A^{(l)}$ and $A'^{(l)}$ in Eq. (2.24).

2.2.2. Perturbative Contributions

We present the QCD Feynman diagrams that contribute to the amplitudes $A^{(l)}$ and $A'^{(l)}$ up to two-loop accuracy. In the following we will only consider $A^{(l)}$, but the same considerations apply for the primed amplitudes.

[10] Using Eqs. (2.1), (B.21) and (B.24) one can show that the identity $\left[\bar{q}\gamma^\mu(1 \mp \gamma_5)q\right]\left[\bar{c}\,\gamma_\mu(1-\gamma_5)b\right] = \left[\bar{q}\frac{\not{n}_-}{2}(1 \mp \gamma_5)q\right]\left[\bar{c}\,\not{n}_+(1-\gamma_5)b\right]$ holds at leading power.

Figure 2.2. – "Factorizable" one-loop diagrams contributing to $A^{(1)f}$. The first diagram is part of $A^{(1)fh}$ and the second one contributes to $A^{(1)fl}$.

Figure 2.3. – "Non-factorizable" vertex corrections contributing to $A^{(1)nf}$.

For performing the matching it is convenient to split the amplitudes into a "factorizable" (f) and a "non-factorizable" (nf) part

$$A^{(l)} = A^{(l)f} + A^{(l)nf} \,. \tag{2.39}$$

All Feynman diagrams where the heavy-to-heavy current factorizes from the light-to-light current are collected in $A^{(l)f}$. The contributions, where both currents are connected by a hard gluon exchange are part of $A^{(l)nf}$. Note that we have adopted the notation from [27] and have used quotation marks in order to distinguish from the factorizable and non-factorizable contributions to the decay amplitude Eq. (1.1). We further divide the "factorizable" amplitude as follows

$$A^{(l)f} = A^{(l)fh} + A^{(l)fl} + A^{(l)fhl} \,. \tag{2.40}$$

Here, $A^{(1)fh}$ and $A^{(1)lf}$ contain all Feynman diagrams where the hard gluon is exchanged only between the two heavy or the two light quarks, respectively. All Feynman diagrams with hard gluon interactions between the two heavy quarks *and* between the two light quarks are described by $A^{(l)fhl}$[11] The corresponding one- and two-loop Feynman diagrams are presented below.

Tree-level and One-loop

The tree-level bare amplitude $A^{(0)}$ is given by the single Feynman diagram depicted in Fig. 2.1. In the following we omit the arrows and the inscriptions on the fermion lines.

The set of Feynman diagrams describing the one-loop bare amplitude $A^{(1)}$ is shown in Figs. 2.2 and 2.3. The diagrams in Fig. 2.2 belong to the "factorizable" amplitude $A^{(1)f}$. The first (second) diagram is the single contribution to $A^{(1)fh}$ $(A^{(1)fl})$. In Fig. 2.3 we find the "non-factorizable" vertex corrections which constitute $A^{(1)nf}$.

[11]The only contribution to $A^{(l)fhl}$ up to two-loop accuracy is the last diagram shown in Fig. 2.6.

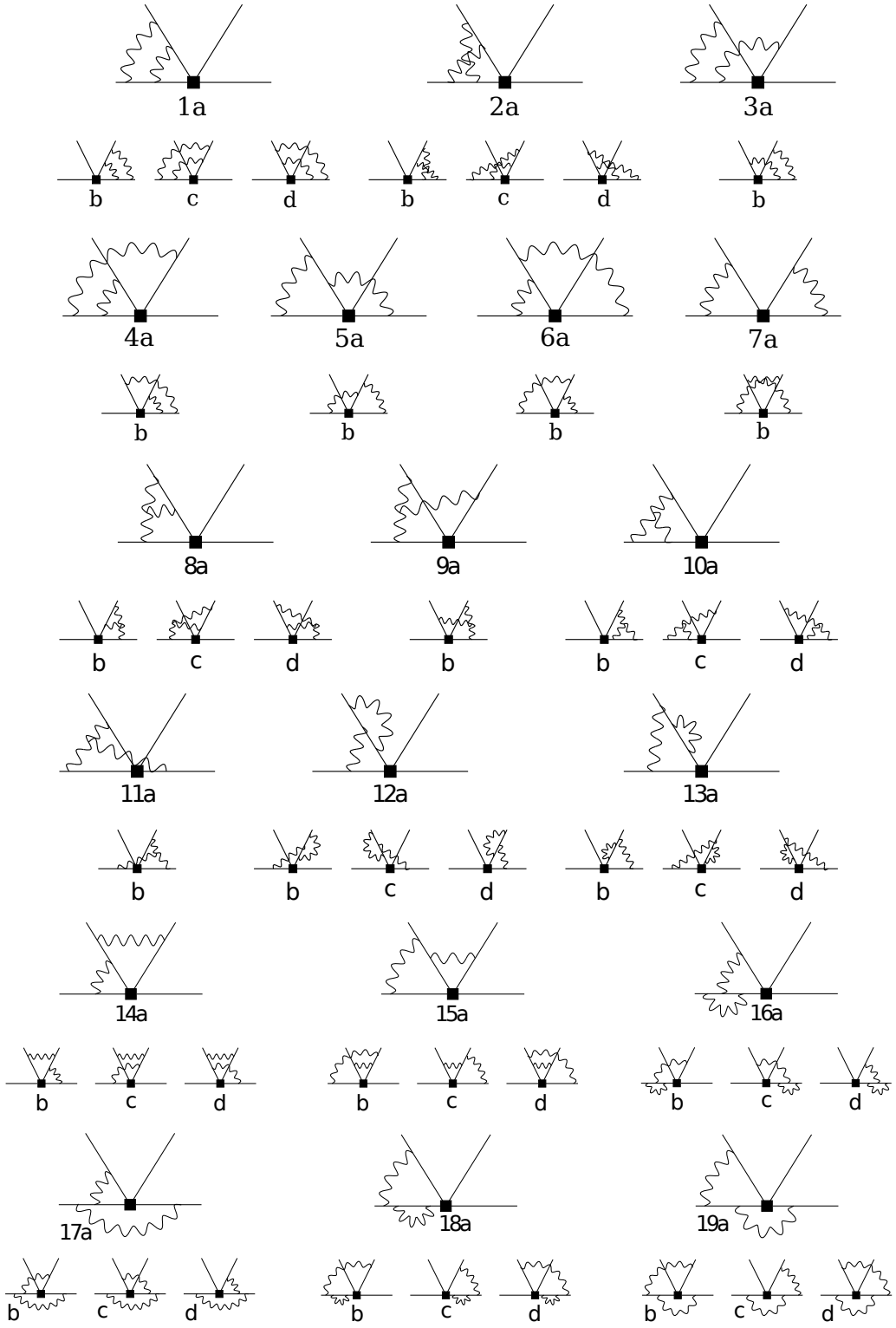

Figure 2.4. – First part of the two-loop Feynman diagrams contributing to $A^{(2)nf}$ (pictures adopted from [27]). The curly lines denote gluon propagators.

Figure 2.5. – Second part of the two-loop Feynman diagrams contributing to $A^{(2)nf}$. Gluons, massless u, d, s quarks and the massive charm and bottom run in the fermion loop.

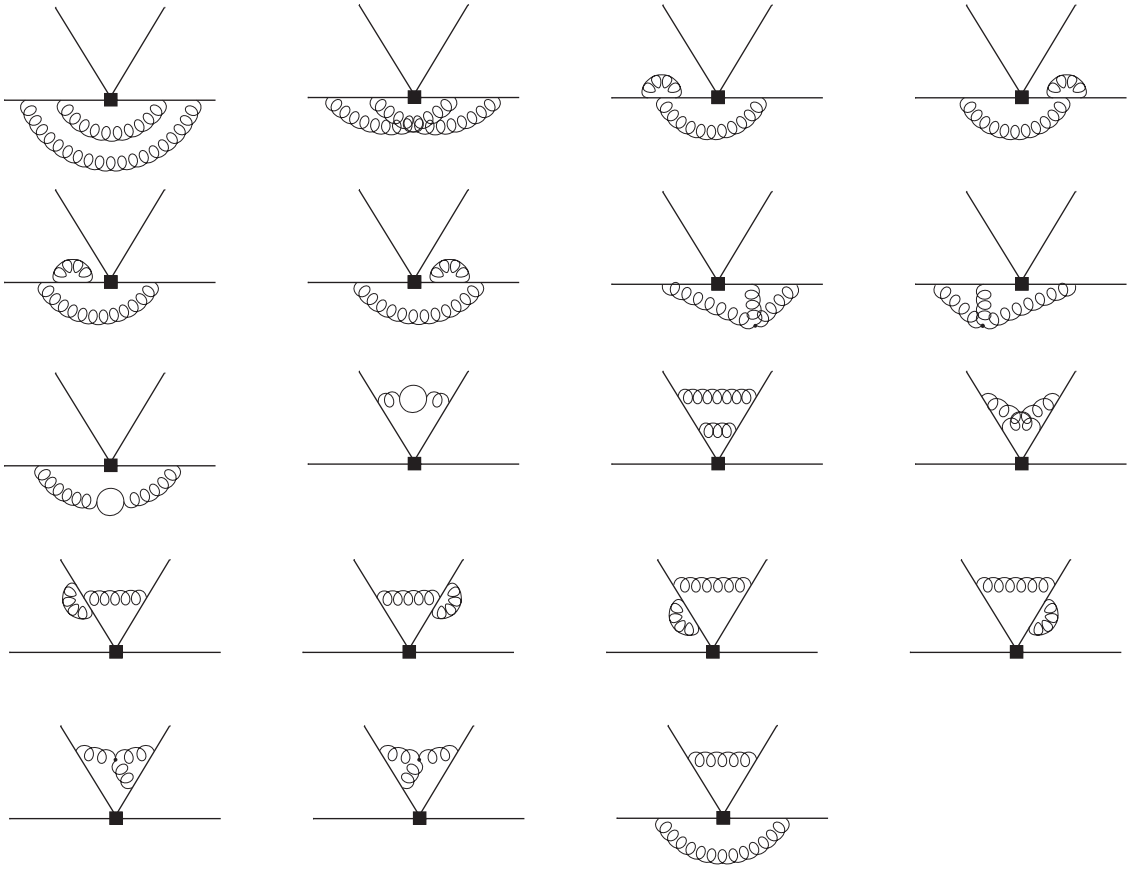

Figure 2.6. – The "factorizable" two-loop diagrams which constitute to $A^{(2)f}$: Gluons and the quarks u, d, s, c, and b run in the fermion loop.

Two-loop

The "non-factorizable" bare amplitude $A^{(2)nf}$ consists of the 66 diagrams depicted in Figs. 2.4 and 2.5. The "factorizable" two-loop diagrams contributing to the bare amplitude are shown in Fig. 2.6. We proceed with the derivation of the tree-level and one-loop matching relations.

2.2.3. Tree-level and One-loop

For performing the matching we have to compensate for the difference in dynamical flavours on the QCD and on the SCET side. Therefore, we convert the three flavour coupling constant to the five flavour one as described in the following[12].

[12]Note that the calculation follows similar lines, if instead one converts the five flavour to the three flavour coupling.

The relation between the five flavour (α_s) and the four flavour ($\alpha_s^{(4)}$) coupling constants can be expressed as

$$\alpha_s = \xi_{45}\alpha_s^{(4)}\,. \tag{2.41}$$

Here, ξ_{45} is four-to-five flavour conversion factor which can be written as an expansion in the five flavour coupling

$$\xi_{45} = 1 + \alpha_s\xi_{45}^{(1)} + \mathcal{O}\big(\alpha_s^2\big)\,. \tag{2.42}$$

Inserting this in Eq. (2.41) one obtains

$$\alpha_s^{(4)} = \alpha_s - \xi_{45}^{(1)}\alpha_s^2 + \mathcal{O}(\alpha_s^3)\,. \tag{2.43}$$

Analogously, one can derive a relation between the four flavour and the three flavour coupling, which is denoted by $\hat{\alpha}_s$, with the four-to-three flavour conversion factor ξ_{34}. The final expression for converting the three flavour to the five flavour coupling constant is given by

$$\hat{\alpha}_s = \alpha_s + \left(-\xi_{34}^{(1)} - \xi_{45}^{(1)}\right)\alpha_s^2 + \mathcal{O}(\alpha_s^3)\,. \tag{2.44}$$

At tree level the matching relations Eqs. (2.33) and (2.34) for the QCD and SCET currents are simply given by

$$\langle\mathcal{Q}^{\rm QCD}\rangle^{(0)} = \langle\mathcal{O}_1\rangle^{(0)}\,, \tag{2.45}$$

$$\langle\mathcal{Q}'^{\rm QCD}\rangle^{(0)} = \langle\mathcal{O}'_1\rangle^{(0)}\,. \tag{2.46}$$

Comparing Eqs. (2.17) and (2.24) we obtain $H_{i1}^{(0)} = A_{i1}^{(0)}$ and $H_{i1}^{\prime(0)} = A_{i1}^{\prime(0)}$. However, the contribution of $A_{i1}^{\prime(0)}$ and hence $H_{i1}^{\prime(0)}$ vanishes since at tree level, the QCD operators $\mathcal{Q}_i$ cannot mix with $\mathcal{O}'_1$, which has a different Dirac structure. The tree-level matrix element of the colour octet operator $\mathcal{Q}_1$ is zero when projected onto the singlet operator $\mathcal{O}_1$, i.e. $H_{11}^{(0)} = A_{11}^{(0)} = 0$. From Eq. (2.36) we further obtain $\hat{T}_2^{(0)} = H_{21}^{(0)}$ and $\hat{T}_2^{\prime(0)} = H_{21}^{\prime(0)}$. With $A_{21}^{(0)} = H_{21}^{(0)} = 1$, the result for the tree-level hard scattering kernels is given by

$$\hat{T}_1^{(0)} = 0\,, \qquad \hat{T}_1^{\prime(0)} = 0\,, \tag{2.47}$$

$$\hat{T}_2^{(0)} = 1\,, \qquad \hat{T}_2^{\prime(0)} = 0\,. \tag{2.48}$$

Hence, the tree-level hard scattering kernel is independent of the momentum fraction u of the pion. In the factorization formula (1.10) the integration over u simply yields the pion decay constant f_π, which is multiplied by a $B \to D$ form factor. We find that at leading order in α_s and at leading power in $\Lambda_{\rm QCD}/m_B$ the factorization formula (1.10) reproduces the result of the naive factorization, as anticipated in Sec. 1.1.

Next, we derive the expressions for the one-loop hard scattering kernels. At this order $\hat{\alpha}_s = \alpha_s$ (see Eq. (2.44)) and hence there do not appear conversion factors ξ_{45} and ξ_{34} in the one-loop matching. The one-loop expression for the QCD amplitude can be extracted from Eq. (2.24)

$$\langle\mathcal{Q}_i\rangle^{(1)} = \Big[A_{ia}^{(1)} + Z_{ext}^{(1)}A_{ia}^{(0)} + Z_{ij}^{(1)}A_{ja}^{(0)}\Big]\,\langle\mathcal{O}_a\rangle^{(0)} + (A \leftrightarrow A')\langle\mathcal{O}'_a\rangle^{(0)}\,. \tag{2.49}$$

From the matching relation Eq. (2.17) we also find

$$\langle \mathcal{Q}_i \rangle^{(1)} = H_{ib}^{(1)} \langle \mathcal{O}_b \rangle^{(0)} + H_{ic}^{(0)} \langle \mathcal{O}_c \rangle^{(1)} + (H \leftrightarrow H', \mathcal{O} \leftrightarrow O') \,. \tag{2.50}$$

The one-loop matrix element of the SCET operators can be obtained from Eq. (2.27)

$$\langle \mathcal{O}_c \rangle^{(1)} = Y_{cb}^{(1)} \langle \mathcal{O}_b \rangle^{(0)} \,, \qquad \langle \mathcal{O}'_c \rangle^{(1)} = Y_{cb}^{(1)} \langle \mathcal{O}'_b \rangle^{(0)} \,, \tag{2.51}$$

and we arrive at

$$\langle \mathcal{Q}_i \rangle^{(1)} = H_{ib}^{(1)} \langle \mathcal{O}_b \rangle^{(0)} + H_{ic}^{(0)} Y_{cb}^{(1)} \langle \mathcal{O}_b \rangle^{(0)} + (H \leftrightarrow H', \mathcal{O} \leftrightarrow O') \,. \tag{2.52}$$

We remark that only $b = 1, 1'$ contribute since the tree-level matrix elements of the evanescent operators vanish in $d = 4$ dimensions.

First, we consider the matrix element of the colour singlet operator $\mathcal{Q}_2$. At this point it is convenient to bring the corresponding hard scattering kernels $\hat{T}_2$ and $\hat{T}'_2$ into play. Their one-loop expressions can be extracted from Eqs. (2.37) and (2.38). For the colour singlet kernel they read

$$\hat{T}_2^{(1)} = H_{21}^{(1)} - C_{FF}^{\mathrm{D}(1)} \,, \qquad \hat{T}_2'^{(1)} = H_{21}'^{(1)} - C_{FF}^{\mathrm{ND}(1)} \,, \tag{2.53}$$

and Eq. (2.52) takes the form (with $H_{2c}'^{(0)} = 0$)

$$\langle \mathcal{Q}_2 \rangle^{(1)} = \left[\hat{T}_2^{(1)} + C_{FF}^{\mathrm{D}(1)} + Y_{11}^{(1)} \right] \langle \mathcal{O}_1 \rangle^{(0)} + \left[\hat{T}_2'^{(1)} + C_{FF}^{\mathrm{ND}(1)} \right] \langle \mathcal{O}'_1 \rangle^{(0)} \,. \tag{2.54}$$

Next, we consider the operator $\mathcal{Q}^{\mathrm{QCD}}$ which has the same colour structure as $\mathcal{Q}_2$. Its one-loop matrix element can be extracted from the matching relation Eq. (2.33)

$$\langle \mathcal{Q}^{\mathrm{QCD}} \rangle^{(1)} = \left[C_{FF}^{\mathrm{D}(1)} + Y_{11}^{(1)} \right] \langle \mathcal{O}_1 \rangle^{(0)} + C_{FF}^{\mathrm{ND}(1)} \langle \mathcal{O}'_1 \rangle^{(0)} \,, \tag{2.55}$$

where we have used Eq. (2.51) and $C_{FF}^{\mathrm{LR,LR}} = \mathcal{O}(\alpha_s)$. On the other hand, $\langle \mathcal{Q}^{\mathrm{QCD}} \rangle^{(1)}$ can be expressed in terms of QCD amplitudes. By definition $\mathcal{Q}^{\mathrm{QCD}}$ factorizes into a heavy-to-heavy and a light-to-light current and thus its one-loop matrix element reads

$$\begin{aligned} \langle \mathcal{Q}^{\mathrm{QCD}} \rangle^{(1)} = &\left[A_{21}^{(1)fh} + \left(Z_{hh}^{(1)} + Z_{ext}^{(1)fh} \right) A_{21}^{(0)} + A_{21}^{(1)fl} + \left(Z_{BL}^{(1)} + Z_{ext}^{(1)fl} \right) A_{21}^{(0)} \right] \langle \mathcal{O}_1 \rangle^{(0)} \\ &+ (A \leftrightarrow A') \langle \mathcal{O}'_1 \rangle^{(0)} \,. \end{aligned} \tag{2.56}$$

Here, Z_{hh} is the renormalization constant for the heavy-to-heavy QCD current and Z_{BL} is the well known ERBL kernel for massless quarks which are separated by a light-like distance [50, 51]. Note that the heavy-to-heavy vector and axial vector currents are conserved and thus $Z_{hh} A_{21} = 1$ to all orders in perturbation theory. The one-loop ERBL kernel vanishes when convoluted with the on-shell amplitude $A_{21}^{(0)}$, which is just a constant. The amplitudes $A^{(1)fh}$ and $A^{(1)fl}$ with $A^{(1)fh} + A^{(1)fl} = A^{(1)f}$ are defined in Fig. 2.2. The wave function renormalization constant for the heavy-to-heavy (light-to-light) current $Z_{ext}^{(1)fh}$ ($Z_{ext}^{(1)fl}$) by definition factorizes for all loops

$$Z_{ext}^{(l)} = Z_{ext}^{(l)fh} + Z_{ext}^{(l)fl} \,. \tag{2.57}$$

The simplified version of Eq. (2.56) then reads

$$\langle \mathcal{Q}^{\mathrm{QCD}} \rangle^{(1)} = \left[A_{21}^{(1)f} + Z_{ext}^{(1)} A_{21}^{(0)} \right] \langle \mathcal{O}_1 \rangle^{(0)} + (A \leftrightarrow A') \langle \mathcal{O}_1' \rangle^{(0)} \,. \tag{2.58}$$

We remark that the corresponding expression for the one-loop matrix element of the primed operator $\mathcal{Q}'^{\mathrm{QCD}}$ is not independent of Eq. (2.58) and thus does not yield any new information. By equating Eqs. (2.55) and (2.58), we can extract an expression each for $C_{FF}^{\mathrm{D}(1)}$ and $C_{FF}^{\mathrm{ND}(1)}$ in terms of bare QCD amplitudes and renormalization factors, which can be substituted in Eq. (2.54). In a comparison of the coefficients proportional $\mathcal{O}_1$ in Eqs. (2.54) and (2.49) the "factorizable" contribution $A^{(1)f}$ cancels on each side of the equation and we obtain the simple result for the hard kernel

$$\hat{T}_2^{(1)} = A_{21}^{(1)nf} + Z_{2j}^{(1)} A_{j1}^{(0)} \,. \tag{2.59}$$

The amplitude $A_{21}^{(1)nf}$ vanishes when projected onto the singlet operator $\mathcal{O}_1$. Moreover, $A_{j1}^{(0)} = 0$ for $j \neq 2$ and $Z_{22}^{(1)} = 0$, which can be seen in the explicit expression of $Z^{(1)}$ given in Eq. (5.2). Thus, $\hat{T}_2^{(1)}$ is equal to zero. Similar considerations can be applied for the primed one-loop kernel and we find that $\hat{T}_2'^{(1)}$ vanishes as well. Hence, at one-loop the colour singlet hard scattering kernels vanishes.

Let us in the following consider the contribution of the colour octet operator $\mathcal{Q}_1$. The one-loop expressions for $\hat{T}_1$ and $\hat{T}_1'$ can be obtained from Eqs. (2.37) and (2.38) and read

$$\hat{T}_1^{(1)} = H_{11}^{(1)} \,, \qquad \hat{T}_1'^{(1)} = H_{11}'^{(1)} \,. \tag{2.60}$$

Eq. (2.52) then simplifies to (considering that $H_{1c}^{(0)} = H_{1c}'^{(0)} = 0$)

$$\langle \mathcal{Q}_1 \rangle^{(1)} = \hat{T}_1^{(1)} \langle \mathcal{O}_1 \rangle^{(0)} + (\hat{T}_1')^{(1)} \langle \mathcal{O}_1' \rangle^{(0)} \,. \tag{2.61}$$

Comparing this expression with Eq. (2.49) we find (with $A_{11}^{(0)} = A_{11}'^{(0)} = 0$)

$$\hat{T}_1^{(1)} = A_{11}^{(1)} + Z_{1j}^{(1)} A_{j1}^{(0)} \,, \qquad \hat{T}_1'^{(1)} = A_{11}'^{(1)} + Z_{1j}^{(1)} A_{j1}'^{(0)} \,. \tag{2.62}$$

The diagrams contributing to the "factorizable" amplitudes $A^{(1)f}$ and $A'^{(1)f}$ are shown in Fig. 2.2. The first diagram vanishes for the insertion of the $\mathcal{Q}_1$ when projected onto the singlet SCET operator. The second diagram does not contribute either, since it is a scaleless diagram and thus vanishes in dimensional regularization. Hence, only the "non-factorizable" diagrams shown in Fig. 2.3 survive. The final results for the one-loop hard scattering kernels then read

$$\hat{T}_1^{(1)} = \left[A_{11}^{(1)nf} + Z_{1j}^{(1)} A_{j1}^{(0)} \right] , \qquad \hat{T}_1'^{(1)} = \left[A_{11}'^{(1)nf} + Z_{1j}^{(1)} A_{j1}'^{(0)} \right] , \tag{2.63}$$

$$\hat{T}_2^{(1)} = 0 \,, \qquad \hat{T}_2'^{(1)} = 0 \,. \tag{2.64}$$

We shall remember that in the convolution of $Z^{(1)}$ with the tree-level QCD amplitudes evanescent operators appear.

2.2.4. Two-loop

At two-loop accuracy we obtain a contribution from the conversion of the three-flavour to the five-flavour coupling (2.44). Whereas Eq. (2.24) remains the same, namely

$$\begin{aligned}\langle\mathcal{Q}_i\rangle^{(2)} = \Big[&A_{ia}^{(2)} + Z_{ij}^{(1)}A_{ja}^{(1)} + Z_{ij}^{(2)}A_{ja}^{(0)} + Z_{ext}^{(1)}A_{ia}^{(1)} + Z_{ext}^{(2)}A_{ia}^{(0)} + Z_{ext}^{(1)}Z_{ij}^{(1)}A_{ja}^{(0)} \\ &+ (-i)\delta m_b^{(1)}A_{ia}^{*(1)} + (-i)\delta m_c^{(1)}A_{ia}^{**(1)} + Z_\alpha^{(1)}A_{ia}^{(1)}\Big]\langle\mathcal{O}_a\rangle^{(0)} \\ &+ (A \leftrightarrow A')\langle\mathcal{O}'_a\rangle^{(0)}\,, \end{aligned} \tag{2.65}$$

the two-loop the SCET matrix element in Eq. (2.27) acquires an additional contribution

$$\langle\mathcal{O}_a\rangle^{(2)} = \left[Y_{ab}^{(2)} - \left(\xi_{34}^{(1)} + \xi_{45}^{(1)}\right)Y_{ab}^{(1)}\right]\langle\mathcal{O}_b\rangle^{(0)}\,. \tag{2.66}$$

A similar modification applies to the matrix elements of the primed operators. Next, we write down an expression for $\mathcal{Q}_i$ from the matching relation Eq. (2.17)

$$\begin{aligned}\langle\mathcal{Q}_i\rangle^{(2)} = &\left\{H_{ia}^{(2)} + H_{i1}^{(1)}Y_{1a}^{(1)} + \sum_{b\neq 1}H_{ib}^{(1)}Y_{ba}^{(1)} + H_{ib}^{(0)}\left[Y_{ba}^{(2)} - \left(\xi_{34}^{(1)} + \xi_{45}^{(1)}\right)Y_{ba}^{(1)}\right]\right\}\langle O_a\rangle^{(0)} \\ &+ (H \leftrightarrow H')\langle\mathcal{O}'_a\rangle^{(0)} \end{aligned} \tag{2.67}$$

In the following, we focus on the contribution of the colour singlet operator. From Eqs. (2.37) and (2.38) we obtain the two-loop expressions for the hard kernels

$$\hat{T}_2^{(2)} = H_{21}^{(2)} - C_{FF}^{\mathrm{LL}(2)} - C_{\bar{q}q}^{(2)}\,, \tag{2.68}$$

$$\hat{T}_2^{\prime(2)} = H_{21}^{\prime(2)} - C_{FF}^{\mathrm{RL}(2)}\,. \tag{2.69}$$

Here, we have made use of Eq. (2.53) and the fact that the one-loop colour singlet kernels $T_2^{(1)}$ and $T_2^{\prime(1)}$ are zero. From these equations we can extract expressions for $H_{21}^{(2)}$ and $H_{21}^{\prime(2)}$ and substitute them in Eq. (2.67), which then reads

$$\begin{aligned}\langle\mathcal{Q}_2\rangle^{(2)} = &\left\{\hat{T}_2^{(2)} + C_{\bar{q}q}^{(2)} + C_{FF}^{\mathrm{LL}(2)} + Y_{11}^{(2)} - \left(\xi_{34}^{(1)} + \xi_{45}^{(1)}\right)Y_{11}^{(1)} + H_{21}^{(1)}Y_{11}^{(1)} + \sum_{b\neq 1}H_{2b}^{(1)}Y_{b1}^{(1)}\right\}\langle\mathcal{O}_1\rangle^{(0)} \\ &+ \left\{\hat{T}_2^{\prime(2)} + C_{FF}^{\mathrm{RL}(2)} + H_{21}^{\prime(1)}Y_{11}^{(1)} + \sum_{b\neq 1}(H'_{2b})^{(1)}Y_{b1}^{(1)}\right\}\langle\mathcal{O}'_1\rangle^{(0)}\,. \end{aligned} \tag{2.70}$$

Next, we consider the two-loop matrix element of $\mathcal{Q}^{\mathrm{QCD}}$, which in terms of QCD amplitudes is given by

$$\begin{aligned}\langle\mathcal{Q}^{\mathrm{QCD}}\rangle^{(2)} = \Big\{&A_{21}^{(2)f} + \left(Z_{hh}^{(1)} + Z_{BL}^{(1)} + Z_{ext}^{(1)}\right)A_{21}^{(1)f} + \left(Z_{hh}^{(2)} + Z_{BL}^{(2)} + Z_{ext}^{(2)}\right)A_{21}^{(0)} \\ &+ Z_{hh}^{(1)}Z_{BL}^{(1)}A_{21}^{(0)} + Z_{ext}^{(1)}\left(Z_{hh}^{(1)} + Z_{BL}^{(1)}\right)A_{21}^{(0)} + Z_\alpha^{(1)}A_{21}^{(1)f} \\ &+ (-i)\delta m_b^{(1)}A_{21}^{*(1)f} + (-i)\delta m_c^{(1)}A_{21}^{**(1)f}\Big\}\langle\mathcal{O}_1\rangle^{(0)} \\ &+ (A \leftrightarrow A')\langle\mathcal{O}'_1\rangle^{(0)}\,. \end{aligned} \tag{2.71}$$

This expression can be simplified considering that $Z_{hh}^{(2,1)} A_{21}^{(0)}$ and $Z_{hh}^{(1)} A_{21}^{(1)(f)}$ vanish, as the heavy-to-heavy current is conserved. Moreover, the convolution of the ERBL kernel with an expression which is a constant in u yields zero. Hence, $Z_{BL}^{(2,1)} A_{21}^{(0)} = 0$ as well as $Z_{BL}^{(1)} A_{21}^{(1)f}$ (Two diagrams contribute to $A_{21}^{(1)f}$ (see Fig. 2.2), the first is a constant with respect to u and second is a scaleless integral vanishing in dimensional regularization). Eq. (2.71) then takes the form

$$\begin{aligned}\langle \mathcal{Q}^{\mathrm{QCD}} \rangle^{(2)} = \Big\{ & A_{21}^{(2)f} + Z_{ext}^{(1)} A_{21}^{(1)f} + Z_{ext}^{(2)} A_{21}^{(0)} + Z_{\alpha}^{(1)} A_{21}^{(1)f} \\ & + (-i)\delta m_b^{(1)} A_{21}^{*(1)f} + (-i)\delta m_c^{(1)} A_{21}^{**(1)f} \Big\} \langle \mathcal{O}_1 \rangle^{(0)} \\ & + (A \leftrightarrow A') \langle \mathcal{O}_1' \rangle^{(0)} \end{aligned} \tag{2.72}$$

On the other hand, $\langle \mathcal{Q}^{\mathrm{QCD}} \rangle^{(2)}$ can be obtained from the relation (2.33)

$$\begin{aligned}\langle \mathcal{Q}^{\mathrm{QCD}} \rangle^{(2)} = & \left\{ C_{\bar{q}q}^{(2)} + C_{FF}^{\mathrm{LL}(2)} + C_{FF}^{\mathrm{D}(1)} Y_{11}^{(1)} + Y_{11}^{(2)} - \left(\xi_{34}^{(1)} + \xi_{45}^{(1)} \right) Y_{11}^{(1)} \right\} \langle \mathcal{O}_1 \rangle^{(0)} \\ & + \left\{ C_{FF}^{\mathrm{LR}(2)} + C_{FF}^{\mathrm{ND}(1)} Y_{11}^{(1)} \right\} \langle \mathcal{O}_1' \rangle^{(0)} . \end{aligned} \tag{2.73}$$

By equating Eqs. (2.72) and (2.73) we can extract an expression for $C_{\bar{q}q}^{(2)}$ and substitute in Eq. (2.70). A comparison of the coefficients proportional to $\langle \mathcal{O}_1 \rangle^{(0)}$ in Eqs. (2.70) and (2.65) then yields

$$\begin{aligned}\hat{T}_2^{(2)} = & A_{21}^{(2)} - A_{21}^{(2)f} + Z_{ext}^{(1)} \left(A_{21}^{(1)} - A_{21}^{(1)f} \right) + Z_{\alpha}^{(1)} \left(A_{21}^{(1)} - A_{21}^{(1)f} \right) + Z_{2j}^{(1)} A_{j1}^{(1)} + Z_{2j}^{(2)} A_{j1}^{(0)} \\ & + (-i)\delta m_b^{(1)} \left(A_{21}^{*(1)} - A_{21}^{*(1)f} \right) + (-i)\delta m_c^{(1)} \left(A_{21}^{**(1)} - A_{21}^{**(1)f} \right) + Z_{ext}^{(1)} Z_{2j}^{(1)} A_{j1}^{(0)} \\ & - Y_{11}^{(1)} \left(-C_{FF}^{\mathrm{D}(1)} + H_{21}^{(1)} \right) - \sum_{b \neq 1} H_{2b}^{(1)} Y_{b1}^{(1)} . \end{aligned} \tag{2.74}$$

We find that the "factorizable" one-loop amplitudes cancel and the one-loop "non-factorizable" amplitudes with and without mass insertion are zero. Moreover, the last three terms vanish since either $A_{j1}^{(0)}$ or $Z_{2j}^{(1)}$ is zero and $\hat{T}_2^{(1)} = -C_{FF}^{\mathrm{D}(1)} + H_{21}^{(1)} = 0$, as well as $H_{2b}^{(1)} = 0$ with $b > 1$, which can be seen by an explicit calculation. Finally, we arrive at the simple result

$$\hat{T}_2^{(2)} = \left(A_{21}^{(2)nf} + Z_{2j}^{(1)} A_{j1}^{(1)} + Z_{2j}^{(2)} A_{j1}^{(0)} \right) . \tag{2.75}$$

The derivation for $\hat{T}_2^{\prime(2)}$ follows the same lines. But instead of Eqs. (2.71) and (2.73) we use the corresponding equations for the primed operator $\mathcal{Q}^{\prime \mathrm{QCD}}$ to extract an expression for $C_{FF}^{\mathrm{RL}(2)}$. The final result has the same form as $\hat{T}_2^{(2)}$ and is given by Eq. (2.75) replacing $A \leftrightarrow A'$.

At last, we derive the two-loop contribution of the colour octet operator. From Eqs. (2.37) and (2.38) we obtain an expression for two-loop hard scattering kernels

$$\hat{T}_1^{(2)} = -C_{FF}^{\mathrm{D}(1)} H_{11}^{(1)} - C_{FF}^{\mathrm{ND}(1)} H_{11}^{\prime(1)} + H_{11}^{(2)} , \tag{2.76}$$

$$\hat{T}_1^{\prime(2)} = -C_{FF}^{\mathrm{ND}(1)} H_{11}^{(1)} - C_{FF}^{\mathrm{D}(1)} H_{11}^{\prime(1)} + H_{11}^{\prime(2)} . \tag{2.77}$$

From these we extract $H_{11}^{(2)}$ and $H_{11}^{\prime(2)}$ and insert them into Eq. (2.67), which using Eq. (2.60), takes the form

$$\begin{aligned}\langle\mathcal{Q}_1\rangle^{(2)} = &\left\{\hat{T}_1^{(2)} + \hat{T}_1^{(1)}\left(C_{FF}^{\mathrm{D}(1)} + Y_{11}^{(1)}\right) + \hat{T}_1^{\prime(1)} C_{FF}^{\mathrm{ND}(1)} + \sum_{b\neq 1} H_{1b}^{(1)} Y_{b1}^{(1)}\right\}\langle\mathcal{O}_1\rangle^{(0)} \\ &+ \left\{\hat{T}_2^{\prime(2)} + \hat{T}_1^{\prime(1)}\left(C_{FF}^{\mathrm{D}(1)} + Y_{11}^{(1)}\right) + \hat{T}_1^{(1)} C_{FF}^{\mathrm{ND}(1)} + \sum_{b\neq 1} H_{1b}^{\prime(1)} Y_{b1}^{(1)}\right\}\langle\mathcal{O}_1^{\prime}\rangle^{(0)} . \end{aligned} \tag{2.78}$$

A comparison of this equation with Eq. (2.65) yields

$$\begin{aligned}\hat{T}_1^{(2)} = &A_{11}^{(2)} + Z_{1j}^{(1)} A_{j1}^{(1)} + Z_{1j}^{(2)} A_{j1}^{(0)} + (-i)\delta m_b^{(1)} A_{11}^{*(1)} + (-i)\delta m_c^{(1)} A_{11}^{**(1)} + Z_{\alpha}^{(1)} A_{11}^{(1)} \\ &+ Z_{ext}^{(1)} A_{11}^{(1)} + Z_{ext}^{(1)} Z_{1j}^{(1)} A_{j1}^{(0)} - \left(C_{FF}^{\mathrm{D}(1)} + Y_{11}^{(1)}\right)\hat{T}_1^{(1)} - C_{FF}^{\mathrm{ND}(1)}\hat{T}_1^{(1)} - \sum_{b\neq 1} H_{1b}^{(1)} Y_{b1}^{(1)} . \end{aligned} \tag{2.79}$$

For the colour singlet operator, all one-loop "factorizable" amplitudes with and without mass insertion are zero (see discussion for the one-loop kernels). Moreover, the "factorizable" two-loop amplitudes $A_{11}^{(2)f}$ (see Fig. 2.6) are zero, since the corresponding diagrams are either scaleless and vanish in dimensional regularization or they do not yield a contribution to the colour singlet SCET operator. With $Z_{1j}^{(1)} A_{j1}^{(0)} = \hat{T}_1^{(1)} - A_{11}^{(1)nf}$ (Eq. (2.64)) we obtain the following expression for the two-loop octet hard scattering kernel

$$\begin{aligned}\hat{T}_1^{(2)} = &A_{11}^{(2)nf} + Z_{1j}^{(1)} A_{j1}^{(1)} + Z_{1j}^{(2)} A_{j1}^{(0)} + Z_{\alpha}^{(1)} A_{11}^{(1)nf} + (-i)\delta m_b^{(1)} A_{11}^{*(1)nf} + (-i)\delta m_c^{(1)} A_{11}^{**(1)nf} \\ &- \hat{T}_1^{(1)}\left[C_{FF}^{\mathrm{D}(1)} + Y_{11}^{(1)} - Z_{ext}^{(1)}\right] - C_{FF}^{\mathrm{ND}(1)}\hat{T}_1^{\prime(1)} - \sum_{b\neq 1} H_{1b}^{(1)} Y_{b1}^{(1)} . \end{aligned} \tag{2.80}$$

The quantities $Y_{b1}^{(1)}$ and $H_{1b}^{(1)}$ are explained in more detail in Sec. 5.1. Similarly, one can derive the expression for the primed kernel $\hat{T}_1^{\prime(2)}$. The result is given by Eq. (2.80) with the replacement ($A \leftrightarrow A'$, $H \leftrightarrow H'$, $T \leftrightarrow T'$).

We remark that Eqs. (2.75) and (2.80) have a structure similar to the corresponding expressions for the two-loop hard scattering kernels for the decay $B \to \pi\pi$, which are given in Eq. (24) in [47][13]. The main differences are the additional mass counter term in Eq. (2.80), which arises from the massive charm quark, and the off-diagonal element $C_{FF}^{\mathrm{ND}(1)}\hat{T}_1^{\prime(1)}$, which is a result of the mixing of the heavy-to-heavy currents with different chiralities.

Since the two-loop amplitudes $A^{(2)nf}$ in Eqs. (2.75) and (2.80) are technically the most challenging contributions to the hard kernels, we proceed with their evaluation in the next two chapters. The renormalization factors and matching coefficients will be discussed in Sec. 5.1, as well as the results for the hard scattering kernels.

[13]Note that for the colour singlet kernel Eq. (24) in [47] reduces to Eq. (2.75).

Chapter 3

Simplification of the Two-loop Amplitudes

In this chapter, we present the calculational techniques and tools that we use for the evaluation of the two-loop two-scale Feynman integrals shown in Figs. 2.4 and 2.5. First, all tensor integrals are decomposed into scalar ones and tensorial structures by applying the Passarino-Veltman decomposition. The subsequent calculation is then divided into two parts: the evaluation of the scalar integrals on the one hand and on the other hand the reduction of the strings of Dirac γ-matrices which are contracted with the tensorial structures to a set of known operators.

We use the Laporta algorithm which is based on integration by part identities to reduce the large number of integrals to a set of a few rather simple ones, the master integrals. The evaluation of the latter is topic of Chap. 4. Finally, we briefly comment on the reduction of the γ-matrices to the operator basis given in Eqs. (2.18)-(2.23).

3.1. Passarino-Veltman Decomposition

Most of the techniques that we use for the evaluation of the two-loop two-scale Feynman integrals have been worked out for scalar integrals. Therefore, we first reduce all tensorial integrals to scalar ones. A well-known procedure for performing this reduction is the Passarino-Veltman (PV) decomposition [95] which will be explained below[1].

In QCD, by definition, all tensor integrals stemming from multi-loop Feynman integrals are Lorentz invariant quantities. One may easily check that the two-loop integrals shown in Figs. 2.4 and 2.5 carry at most four Lorentz indices. For simplicity we consider in the following an integral with m internal loops and two Lorentz indices (μ, ν) that depends on two external independent on-shell momenta q_1 and q_2

$$I^{\mu\nu}(q_1, q_2) = \int d^d k_1 \dots d^d k_m \frac{k_i^\mu k_j^\nu}{E_1^{a_1} \dots E_n^{a_n}} \,. \tag{3.1}$$

[1]In the amplitude, there also appear scalar integrals that will not change during this decomposition.

Here, $k_{i,j}$ are the loop momenta and the indices i, j run from 1 to m. The a_l are positive integers and the E_l denote the denominators of the Feynman propagators (or just propagators for short). The explicit expression for the propagators is given by $E_l = p_l^2 - m_l^2 + i\eta$, where p_l is the off-shell momentum flowing in the internal line l and m_l is the mass of the corresponding line ($p_l^2 \neq m_l^2$). The p_l can be expressed as linear combinations of q_1, q_2 and the loop momenta k_i. The small imaginary part $i\eta$, $\eta > 0$, indicates the location of the poles of the propagator in the complex plane. For compactness of notation we will omit the $i\eta$ description in the following. In the final results displayed in this chapter we anyway find that $i\eta$ can be safely dropped.

We further assume that the integral (3.1) is symmetric in μ and ν. After integrating over all loop momenta, the result only depends on the external momenta q_1 and q_2 as well as the initial Lorentz structure. Hence, we construct the following ansatz for the decomposition

$$I^{\mu\nu}(q_1, q_2) = q_1^\mu q_1^\nu C_1 + q_1^\mu q_2^\nu C_2 + q_2^\mu q_1^\nu C_3 + q_2^\mu q_2^\nu C_4 + g^{\mu\nu} C_5 \,. \tag{3.2}$$

The C_k are linear combinations of scalar loop integrals and only depend on the Lorentz invariant combinations of the external momenta ($q_1^2 = m_1^2, q_2^2 = m_2^2, q_1 \cdot q_2$). All information about the Lorentz structure of $I^{\mu\nu}(q_1, q_2)$ is now contained in the four-vectors $q_r^\mu q_{r'}^\nu$ and the symmetric tensor $g^{\mu\nu}$. The explicit form of the scalar loop integrals will be addressed in the next section. Multiplying Eq. (3.2) by $q_r^\mu q_{r'}^\nu$ and $g^{\mu\nu}$, respectively, the tensor integral on the left hand side reduces to a scalar integral, denoted by $I_1, \ldots, I_5$ for the five different equations. We obtain a set of five independent equations that suffices to determine the five unknown coefficients C_{1-5} in terms of the scalar integrals $I_1, \ldots, I_5$.

As an example we consider the decomposition of the one-loop integral

$$I^{\mu\nu}(p) = \int \frac{d^d k}{(2\pi)^d} \frac{k^\mu k^\nu}{[(p-k)^2 - m^2]\, k^2} \,, \tag{3.3}$$

where k is the loop momentum and p the on-shell external momentum with $p^2 = m^2$. For this integral the ansatz (3.2) simplifies to

$$I^{\mu\nu}(p) = p^\mu p^\nu C_1(m^2) + g^{\mu\nu} C_2(m^2) \,. \tag{3.4}$$

Multiplying Eq. (3.4) by $p_\mu p_\nu$ and $g_{\mu\nu}$, respectively, we obtain two equations

$$\int \frac{d^d k}{(2\pi)^d} \frac{(k\cdot p)(k\cdot p)}{[(p-k)^2 - m^2]\, k^2} \equiv I_1 = \left(p^2\right)^2 C_1(m^2) + p^2 C_2(m^2) \,, \tag{3.5}$$

$$\int \frac{d^d k}{(2\pi)^d} \frac{(k\cdot k)}{[(p-k)^2 - m^2]\, k^2} \equiv I_2 = p^2 C_1(m^2) + d\, C_2(m^2) \,, \tag{3.6}$$

from which we can extract the coefficients

$$C_1(m^2) = \frac{d}{(d-1)m^4}\, I_1 - \frac{1}{(d-1)m^2}\, I_2 \,, \tag{3.7}$$

$$C_2(m^2) = -\frac{1}{(d-1)m^2}\, I_1 + \frac{1}{(d-1)}\, I_2 \,. \tag{3.8}$$

Note that Eq. (3.2) is only based on Lorentz invariance and thus this general ansatz is independent of the number of loop momenta and propagators. Moreover, it can easily be extended to integrals with a different Lorentz structure and an arbitrary number of external momenta.

3.2. Scalar Integrals

The scalar loop integrals that appear as linear combinations in the coefficients C_k in Eq. (3.2) are formally given by expressions of the form

$$\int d^d k_1 \dots d^d k_m \frac{K}{E_1^{a_1} \dots E_n^{a_n}} \,. \tag{3.9}$$

Here, K consists of products of the various possible combinations of the scalar products $(k_i \cdot k_j)$ and $(q_r \cdot k_j)$ (or it simply is 1). For later purpose it is convenient to express the products in terms of the propagators E_l. Using the on-shell conditions $q_r^2 = m_r^2$ we can rewrite $(k_i \cdot k_j)$ and $(q_r \cdot k_j)$ and as follows

$$k_i \cdot k_j = \frac{1}{2}\left[(k_i + k_j + \tilde{p})^2\right] - \frac{1}{2}\left[k_i^2 + k_j^2 + \tilde{p}^2 + 2k_i\tilde{p} + 2k_j\tilde{p}\right] \,, \tag{3.10}$$

$$q_r \cdot k_j = \frac{1}{2}\left[(q_r + k_j + \tilde{p})^2 - m_r^2\right] - \frac{1}{2}\left[k_j^2 + \tilde{p}^2 + 2q_r\tilde{p} + 2k_j\tilde{p}\right] \,. \tag{3.11}$$

Here, $\tilde{p}$ is a linear combination of external and loop momenta chosen such that the first bracket of the right hand side of each equation exactly matches one of the propagators E_l. By successively applying replacements similar to Eqs. (3.10) and (3.11) one may be able to express all scalar products which appear in K in terms of the propagators. However, if the number of possible scalar products of a given Feynman integral exceeds the number n of propagators, not all scalar products can be reduced to propagators. We write these irreducible scalar products in form of new "propagators" which appear in the numerator only. Thus, formally they look like propagators raised by a negative power. Hence, after expressing all scalar products in terms of propagators Eq. (3.9) takes the form

$$\int d^d k_1 \dots d^d k_m \frac{1}{E_1^{\tilde{a}_1} \dots E_s^{\tilde{a}_s}} \,, \quad s \geq n \,. \tag{3.12}$$

Here, the E_l with $n < l \leq s$ arise from the irreducible scalar products and thus the corresponding powers $\tilde{a}_l$ are negative integers. The $\tilde{a}_l$ with $l \leq n$ are equal to the original powers a_l in Eq. (3.9) or reduced by integers, if they were canceled by a corresponding expression resulting from some scalar products.

As an example we consider the integrals I_1 and I_2 defined in Eqs. (3.5) and (3.6) and reduce all scalar products which appear in the numerator to the corresponding propagators. Using

$$p \cdot k = -\frac{1}{2}\left[(p-k)^2 - m^2\right] + \frac{1}{2}k^2 \,, \tag{3.13}$$

we can rewrite I_1 and I_2 as follows

$$\begin{aligned} I_1 &= \int \frac{d^dk}{(2\pi)^d} \frac{(k\cdot p)(k\cdot p)}{[(p-k)^2-m^2]\,k^2} \\ &= \int \frac{d^dk}{(2\pi)^d} \frac{\left(-\frac{1}{2}\left[(p-k)^2-m^2\right]+\frac{1}{2}\left[k^2\right]\right)\left(-\frac{1}{2}\left[(p-k)^2-m^2\right]+\frac{1}{2}k^2\right)}{[(p-k)^2-m^2]\,[k^2]} \\ &= \frac{1}{4}\int \frac{d^dk}{(2\pi)^d} \frac{[(p-k)^2-m^2]}{[k^2]} + \frac{1}{4}\int \frac{d^dk}{(2\pi)^d} \frac{[k^2]}{[(p-k)^2-m^2]} \\ &\equiv \frac{1}{4}\int \frac{d^dk}{(2\pi)^d} \frac{1}{E_1^{-1}E_2^1} + \frac{1}{4}\int \frac{d^dk}{(2\pi)^d} \frac{1}{E_1^1E_2^{-1}}\,, \end{aligned} \tag{3.14}$$

$$\begin{aligned} I_2 &= \int \frac{d^dk}{(2\pi)^d} \frac{(k\cdot k)}{[(p-k)^2-m^2]\,[k^2]} = \int \frac{d^dk}{(2\pi)^d} \frac{1}{[(p-k)^2-m^2]} \\ &\equiv \int \frac{d^dk}{(2\pi)^d} \frac{1}{E_1^1E_2^0}\,, \end{aligned} \tag{3.15}$$

with $E_1 = [(p-k)^2-m^2]$ and $E_2 = [k^2]$. It is not necessary to introduce further propagators since the scalar products (here $k\cdot p$ and k^2) can be completely reduced to E_1 and E_2. The results for the integrals I_1 and I_2 can be easily obtained. I_1 receives contributions from two integrals. The one with the denominator $E_1^{-1}E_2^1$ is a scaleless integral and therefore vanishes in dimensional regularization. With (E.1)-(E.3) we obtain

$$I_1 = \frac{d}{4}\,\frac{i}{(4\pi)^{d/2}}\Gamma(-\tfrac{d}{2})\frac{1}{(m^2)^{-\frac{d}{2}}}\,. \tag{3.16}$$

The integral I_2 is a tadpole (one-propagator integral) and can be evaluated by using Eqs. (E.1) and (E.3)

$$I_2 = -\frac{i}{(4\pi)^{d/2}}\Gamma(1-\tfrac{d}{2})\frac{1}{(m^2)^{1-\frac{d}{2}}}\,. \tag{3.17}$$

Finally, let us introduce the terms topology and subtopology. Therefore, we consider a set of integrals

$$F(a_1,\ldots,a_s) \equiv \int d^dk_1\ldots d^dk_m \frac{1}{E_1^{a_1}\ldots E_n^{a_n}E_{n+1}^{a_n+1}\ldots E_s^{a_s}}\,, \quad s\geq n\,, \tag{3.18}$$

which completely determines all scalar integrals of a particular Feynman diagram. Here, the E_l with $n<l\leq s$ are a result of the irreducible scalar products[2]. The topology of this set is characterized by the integrals where all powers a_l ($l\leq n$) take arbitrary positive values. All integrals where some of the a_l ($l\leq n$) are zero or negative integers, are subtopologies of this topology. For instance the integral given in Eq. (3.3) formally belongs to the topology

$$F(a_1,a_2) = \int \frac{d^dk}{(2\pi)^d}\,\frac{1}{[(p-k)^2-m^2]^{a_1}}\frac{1}{[k^2]^{a_2}}\,, \quad a_1,a_2>0\,. \tag{3.19}$$

[2]We shall remember that by construction all a_l with $n<l\leq s$ are negative integers or zero.

However, we find that it only recieves contributions proportional to integrals I_1 and I_2, which obviously can be expressed in terms of $F(1,-1)$ and $F(1,0)$

$$I_1 = \frac{1}{4}F(1,-1)\,, \tag{3.20}$$

$$I_2 = F(1,0)\,, \tag{3.21}$$

and hence are subtoplogies of (3.19).

3.3. Integration by Part Identities and Laporta Algorithm

In the previous section we have shown that all tensor loop-integrals can be reduced to scalar integrals of the form (3.12) (or equivalently (3.18)). Thus, we are left with the evaluation of these integrals. Their number is process dependent and in the case at hand exceeds a few thousands. Therefore a straightforward calculation is not advisable. The Laporta algorithm [96, 97] is a powerful tool to reduce this large amount of integrals to a limited number of linear combinations of rather simple integrals, the master integrals, by exploiting integration by part identities (IBPs) [98]. They follow from the vanishing of the surface terms for dimensionally regularized integrals [99][3]

$$\underbrace{\int \frac{d^dk_1\ldots d^dk_m}{(2\pi)^{d\,m}}\frac{\partial}{\partial k_i^\mu}\left(\ell^\mu\frac{1}{E_1^{a_1}\ldots E_s^{a_s}}\right)=0}_{\equiv\,\mathrm{IBP}(k_i,\ell)}\,. \tag{3.22}$$

Here, ℓ is q_r or k_j. By performing the derivatives $\partial/\partial k_i$ for the various ℓ one obtains a set of linear equations for the different integrals, the IBPs. The number of independent IBPs is given by

$$\mathcal{N}_{\mathrm{IBP}} = m(m+N_r)\,, \tag{3.23}$$

where N_r is the number of the independent external momenta. Reducing all scalar products to the propagators, the IBPs (3.22) can be written as follows

$$\sum_k c_k F(a_1+b_{k,1},\ldots,a_s+b_{k,s}) = 0\,. \tag{3.24}$$

Here, the b_k are integers and the coefficients c_k are polynomials in the invariants of the problem (for our two-loop integrals these are the momentum fraction u of the pion, the ratio

[3] For the evaluation of our two-loop Feynman integrals, it is more convenient to use the modified IBPs

$$\int \frac{d^dk_1\ldots d^dk_m}{(2\pi)^{d\,m}}\frac{\partial}{\partial k_i^\mu}\left(p_l^\mu\frac{1}{E_1^{a_1}\ldots E_s^{a_s}}\right)=0\,.$$

with $E_l = p_l^2 - m_l^2$. This will simplify the explicit reduction of the numerators to the propagators.

of the quark masses $z_c = m_c^2/m_b^2$ and the dimension d). For the topology (3.19) of our previous example there exist $1 \times (1+1) = 2$ independent IBPs, which read

$$\int \frac{d^dk}{(2\pi)^d} \frac{\partial}{\partial k^\mu} \left(p^\mu \frac{1}{E_1^{a_1} E_2^{a_2}} \right) = 0\,, \tag{3.25}$$

$$\int \frac{d^dk}{(2\pi)^d} \frac{\partial}{\partial k^\mu} \left(k^\mu \frac{1}{E_1^{a_1} E_2^{a_2}} \right) = 0\,. \tag{3.26}$$

Explicitly performing the derivative and reducing the scalar products to the propagators using Eq. (3.13) the identities takes the form

$$\begin{aligned} &2a_1 m^2 F(a_1+1, a_2) + (a_1 - a_2) F(a_1, a_2) \\ &-a_1 F(a_1+1, a_2-1) + a_2 F(a_1-1, a_2+1) = 0\,. \end{aligned} \tag{3.27}$$

$$(d - a_1 - 2a_2) F(a_1, a_2) - a_1 F(a_1+1, a_2-1) = 0\,. \tag{3.28}$$

The IBPs form a homogeneous system of linear equations. The unknowns are the integrals $F(a_1, \ldots a_s)$. As not all IBPs are linearly independent, the system of equations is underdetermined [97] and there exist integrals that cannot be evaluated from this system. These are referred to as the master integrals.

Let us go back to our previous example. We have seen that the integrals I_1 and I_2 can be expressed in terms of the two integrals $F(1,-1)$ and $F(1,0)$ (cf. Eqs. (3.20) and (3.21)). Now, let us evaluate I_1 and I_2 using a different subset $\{F(1,-1),\, F(2,-1)\}$. The integral I_1 remains as before but applying Eq. (3.28) with $(a_1, a_2) = (1, 0)$ we find that I_2 can be expressed as follows

$$I_2 = \frac{1}{(d-1)} F(2,-1)\,. \tag{3.29}$$

For consistency let us check whether this result coincides with the one given in Eq. (3.17). $F(2,-1)$ can be evaluated by using Eqs. (E.1)-(E.3)

$$F(2,-1) = (1-d) \frac{i}{(4\pi)^{\frac{d}{2}}} \Gamma(1 - \tfrac{d}{2}) \frac{1}{(m^2)^{1-\frac{d}{2}}}\,. \tag{3.30}$$

We indeed find that the explicit results fulfill the relation $F(2,-1) = (d-1)F(1,0)$. Thus, both sets $\{F(1,-1),\, F(1,0)\}$ and $\{F(1,-1),\, F(2,-1)\}$ allow us to determine I_1 and I_2. Such irreducible integrals are referred to as the master integrals. We are free to choose either set as basis. In this simple example the integrals in both sets are easy to calculate.

The Laporta algorithm has been constructed such that all scalar integrals of a given topology can be expressed in terms of master integrals by solving the corresponding system of IBPs[4]. The procedure goes as follows. First, all IBPs from the topology and all subtologies of the unknown integral of interest are generated. As the number of relations grows faster than the number of unknown integrals in this system of linear equations the latter becomes over-constrained [97]. By successively extracting integrals from certain relations and substituting them into the remaining ones one can find an expression of the integral of interest in terms of the master integrals. For a detailed description of the algorithm see [97]. We only remark here that for the procedure to be applicable in practice one has to introduce an ordering for the extractions of the integrals. Any ordering leads to the same solution, however there are huge differences in the evaluation time. Moreover, the explicit form of the master integrals can change for different choices of ordering and the master integrals are not unique as already demonstrated in the previous example. It is convenient to find a set (basis) with rather simple master integrals since their evaluation will be less complicated. Moreover, we will see in Sec. 4.5 that a suitable choice of the basis has advantages.

The Laporta algorithm has been implemented in several computer programs. To the present day there exist three public versions AIR [100] (Maple), FIRE [101, 102] (Mathematica, C^{++}) and Reduze [103] (C^{++}), as well as a few private implementations. For the reduction of the set of two-loop diagrams depicted in Figs. 2.4 and 2.5 to master integrals we used FIRE. It can be run in the pure Laporta mode, that is the reduction to master integrals is performed by applying the Laporta algorithm only, or can be combined with other features. We have applied it in combination with s-bases [104–106], which is another algorithmic approach to solve IBPs. It is implemented in the Mathematica package SBases.m and reduces the evaluation time by a large amount. For more information on the implementation of the Laporta algorithm and of the s-bases approach we refer to [101]. As an explicit example the reduction of diagram 14a) in Fig. 2.4 is given in App. A.

After completing the reduction of the set of Feynman diagrams in Figs. 2.4 and 2.5, we have found 23 unknown master integrals. Their evaluation will be the topic of the next chapter.

3.4. Reduction of Dirac Matrices to Operators

We finally consider the tensorial structures from the PV decomposition (cf. Sec. (3.1)) involving the momenta $q_1, \ldots, q_4$ and the symmetric tensor $g^{\mu\nu}$. In the further calculation they are contracted with the Dirac γ-matrices that arise due to the fermion propagators and the gluon-fermion vertices. The resulting γ-structures are reduced to the operator basis given in Eqs. (2.18)-(2.23)[5]. We perform the reduction in Mathematica by using simple algebraic transformations like the Dirac algebra, on-shell conditions and applying the equations of

[4]The number of master integrals grows rapidly with the number of loops and legs of the corresponding Feynman diagram [97]. If the corresponding system of IBPs becomes too large a solution by applying the Laporta algorithm may not work in practice.

[5]In fact, we reduce the γ-structures to the QCD equivalent of Eqs. (2.18)-(2.23), meaning the fields are still defined in full QCD. The explicit matching onto the SCET operators is performed in Sec. 2.2.

motions for the spinors and finally decompose the Dirac matrices into their light-cone components. The calculation is rather lengthy but not complicated and is briefly described in App. B.

Using the above methods we are able to express the amplitudes $A^{(0)}$, $A^{(1)}$ and $A^{(2)nf}$ as products of the operators Eqs. (2.18)-(2.23), the master integrals and some coefficients, which are functions of the invariants of the problem. These amplitudes then enter the master formulae for the two-loop hard scattering kernels $T_{1,2}^{(2)}$ given in Eqs. (2.75) and (2.80). The results for the latter are discussed in Chap. 5. In the next chapter, we present the evaluation of the master integrals.

Chapter 4

Evaluation of the Master Integrals

We present the calculation of the 23 not yet known two-loop two-scale master integrals, that we have found after the Laporta reduction in Sec. 3.3. The results for the integrals which are simply products of one-loop integrals can be expressed analytically in terms of hypergeometric functions. We employ differential equations to find analytical expressions for genuine two-loop master integrals that only depend on one scale, in the case at hand on the ratio of the heavy-quark masses $z_c = m_c^2/m_b^2$. The master integrals with three or four external legs and involving both scales are expressed in terms of Mellin-Barnes representations. Therefore their result is "semi-analytical", since for reasons explained later we perform the integrations over the Mellin-Barnes parameters only numerically. In addition, we present a new method developed by Henn [107] which is based on solving differential equations in a canonical basis. We apply it to obtain analytical results in terms of iterated integrals, also for our two-scale master integrals. At the end of this chapter, we briefly comment on the preformed cross-checks in order to validate our results.

4.1. The Master Integrals

The calculation of the set of two-loop amplitudes $A^{(2)nf}$ depicted in Figs. 2.4 and 2.5 yield several master integrals. Many of those are already known from several $B \to \pi\pi$ calculations [45–47], but we find the 23 diagrams depicted in Fig. (4.1) yet to be unknown. The notation of the diagrams is as follows: The double (curly) line represents a propagator with mass m_b (m_c) and the dashed line denotes a massless one. The dot on a line indicates a squared propagator. $q_1 = uq, q_2 = \bar{u}q, q_3$ and q_4 are the incoming external momenta. Due to the linear dependence of the momenta $q_1 + q_2 = q = -q_3 - q_4$ the kinematics is completely determined by two of the on-shell conditions and one additional kinematic invariant, for instance

$$q_4^2 = m_b^2\,, \quad q_3^2 = m_c^2\,, \quad q_3 \cdot q_4 = -\frac{1}{2}(m_b^2 + m_c^2)\,. \tag{4.1}$$

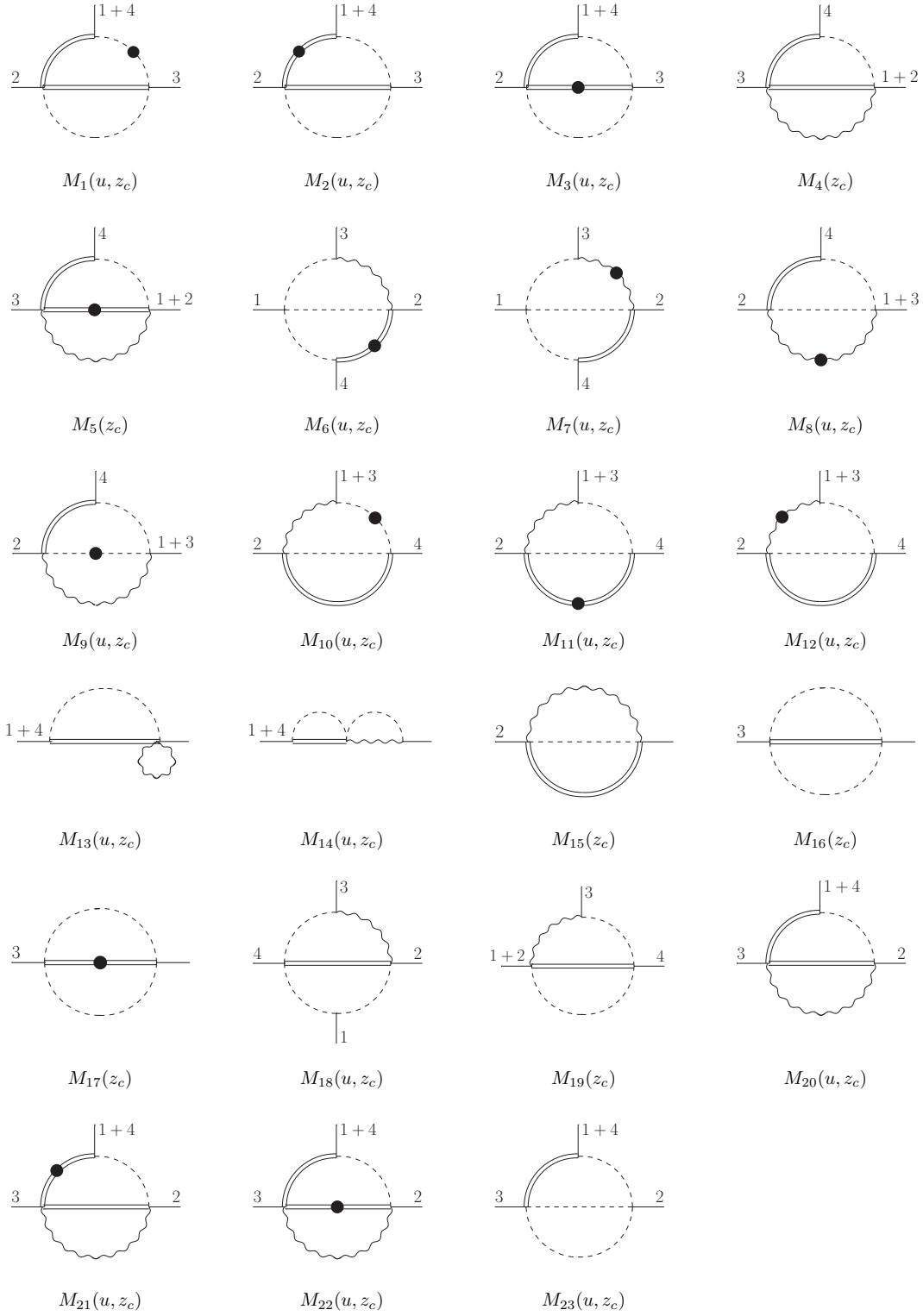

Figure 4.1. – Set of master integrals obtained in the calculation of the two-loop Feynman diagrams; $1-4$ denote the incoming external momenta $q_1, \ldots, q_4$. The double/curly/dashed line represents a propagator with mass $m_b/m_c/0$. A dot on a line indicates a squared propagator.

In the derivation of the factorization formula (1.10) the charm quark was assumed to be heavy. Hence, the ratio m_c/m_b remains fixed in the heavy-quark limit and the master integrals depend on two scales: the momentum fraction u of the quarks inside the light meson and the ratio of the heavy-quark masses $z_c = m_c^2/m_b^2$. The exeptions are $M_{4,5,15,16,17,19}$, which only depend on z_c.

In the amplitude the master integrals in Fig. (4.1) also appear in the following variations: the $m_b \leftrightarrow m_c$ flipped integrals, the $u \leftrightarrow \bar{u}$ flipped ones, and both flipped at the same time. In addition to the set from Fig. (4.1) we calculate the mass-flipped master integrals, denoted by $M^{\leftrightarrow}$, since some contain additional imaginary parts. A $u \leftrightarrow \bar{u}$ interchange does not yield any additional imaginary part and thus, can be performed straightforwardly. We work in dimensional regularization with $d = 4 - 2\epsilon$ dimensions and calculate all master integrals as expansions in ϵ. The Feynman diagrams contributing to the bare two-loop amplitude $A^{(2)nf}$ that enters the hard scattering kernels (2.75) and (2.80) contain up to $1/\epsilon^4$ poles stemming from infrared and ultraviolet regions. Thus, we investigate the factors multiplying the master integrals in the amplitude for possible divergences in ϵ and then calculate the master integrals up to the required order.

Below, we present four calculational techniques for the master integrals. The results for the integrals evaluated by the first three approaches are given in App. C.

4.2. Feynman Parameters and Hypergeometric Functions

There are simple integrals like e.g. the one-loop factorizable ones M_{13} and M_{14} that can be evaluated by text book knowledge. By introducing Feynman parameters (cf. Eq. (E.6)) and performing a suitable shift of the integration variables the integration over the loop momenta can be carried out applying Eqs. (E.2)-(E.4). The remaining integrations over the Feynman parameters can be performed analytically e.g. by matching the definition of the beta function (see Eq. (E.7)) and/or the hypergeometric function [108]

$$
\begin{aligned}
&{}_JF_{J-1}(A_1,\ldots,A_J;B_1,\ldots,B_{J-1};z) = \\
&\left[\Pi_{i=1}^{J-1}\frac{\Gamma(B_i)}{\Gamma(A_i)\Gamma(B_i-A_i)}\right]\int_0^1 dt_1\ldots dt_{J-1}\frac{\Pi_{k=1}^{J-1}t_k^{A_k-1}(1-t_k)^{B_k-A_k-1}}{(1-zt_1\ldots t_{J-1})^{A_J}}\,.
\end{aligned}
\tag{4.2}
$$

For $J = 2$ the expression simplifies to

$$
{}_2F_1(A_1,A_2,B;z) = \frac{\Gamma(B)}{\Gamma(A_1)\Gamma(B-A_1)}\int_0^1 dt\,\frac{t^{A_1-1}(1-t)^{B-A_1-1}}{(1-t\,z)^{A_2}}\,. \tag{4.3}
$$

Since we work in $d = 4 - 2\epsilon$ dimensions, at least one of the parameters A_1, A_2 or B will depend on ϵ. This is clear considering that by applying Eqs. (E.2)-(E.4) we introduce a dependence on d in the exponent of the denominator which then will enter some of the coefficients A_1, A_2 and B. The hypergeometric function can be expanded analytically in ϵ by using the Mathematica package HypExp.m [109].

Note that for more complicated Feynman diagrams it is often not possible to perform the integrations over the Feynman parameters straightforwardly or to express the result in terms of beta or hypergeometric functions. In those cases introducing Mellin-Barnes integrations may help, which we describe in the next section.

We have applied the above procedure to calculate the master integrals M_{13-15}. As an example the evaluation of M_{15} is presented in App. D.1.

4.3. Mellin-Barnes Representation

A method for evaluating more complicated multi-loop multi-scale master integrals makes use of Mellin-Barnes (MB) representations. We have previously mentioned that a straightforward evaluation of master integrals by introducing Feynman parameters (see Sec. 4.2) can fail when it comes to performing the integrations over the Feynman parameters. MB representations can allow one to carry out those integrations analytically, at the cost of introducing additional integrations in the complex plane. The latter can be evaluated numerically by using the Mathematica routine MB.m [110], and even analytically, but to do so quite some effort is required. However in our case, the structure of the lowest coefficients in the ϵ-expansion usually is simple and thus, the ϵ-pole terms can often be extracted analytically by applying Cauchy's theorem. This feature represents one of the main powers of MB representations.

The idea of exploiting Mellin transformations as a tool for Feynman integrals goes back to the 70's [111] and was then also employed to calculate individual Feynman integrals [112, 113]. A first systematic evaluation followed by Smirnov [114] and Tausk [115] in the end of the 90's. We will explain the method below, a detailed description can also be found in [116].

By using MB representations one can expresses a sum of two variables in terms of products raised by a complex parameter z

$$\frac{1}{(A+B)^\sigma} = \frac{B^{-\sigma}}{2\pi i\,\Gamma(\sigma)} \int_{c-i\infty}^{c+i\infty} dz\, A^z B^{-z} \Gamma(-z)\Gamma(\sigma+z)\,. \tag{4.4}$$

Here A, B and σ are some (possibly complex) variables and Γ is the Gamma function. The integration contour is parallel to the imaginary axis with negative c with $0 < |c| < \mathrm{Re}(\sigma)$. The integration over the complex parameter z is often referred to as Barnes integration and z as Barnes parameter. The poles of $\Gamma(\cdots \mp z)$ go to the right/left and thus, are called right/left poles in the following.

The integration in the complex plane can be performed by applying Cauchy's theorem. We will demonstrate this for a concrete choice $\sigma = \epsilon - i\alpha$, $\epsilon > 0$ and $\alpha > 0$. If A and B are analytic functions, the poles of the integrand lie in the complex plane as shown in Fig. 4.2. The contour is chosen such that it separates right and left poles, a possible choice C_1 is shown in Fig. 4.2. The integral can be evaluated by applying Cauchy's theorem closing the contour in a huge semi-circle to the right or to the left and summing up all poles in the enclosed region[1]. For $d = 4 - 2\epsilon$ the integration contour lies within $-\epsilon < \mathrm{Re}(z) < 0$. In the limit $\epsilon \to 0$ the first left pole at $z = -\epsilon + i/2$ hits the contour C_1. In this case, the

[1]Note the minus sign when closing to the right.

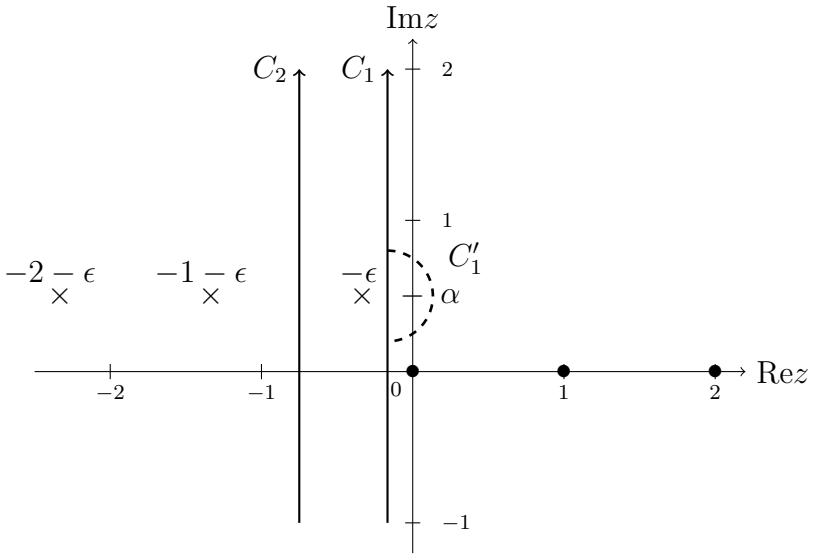

Figure 4.2. – The poles of the function (4.4) with $\sigma = \epsilon - i\alpha$, $\epsilon > 0$ are shown in the complex z plane with three possible contours C_1, C_1' and C_2. $\times$ denote the left and $\bullet$ the right poles.

contour can be deformed around the pole at $z = i/2$, as long as the new contour does not encounter any singularity. A possible choice is C_1' in Fig. 4.2. We now consider the case where all poles lie on the real axis (this corresponds to the limit $\alpha \to 0$). For $\epsilon \to 0$ the first left pole at $z = -\epsilon$ and the first right poles at $z = 0$ merge, which makes above mentioned deformation impossible. Still working in d dimensions we circumvent this problem by shifting the integration contour such that the pole at $z = -\epsilon$ lies to the right of it, e.g. C_2 in Fig. 4.2. The integral along the shifted contour can safely be expanded in ϵ and then can be evaluated by closing the contour to the right. We compensate for the change of the nature of the pole at $z = -\epsilon$ by adding the residue at this point. Note that in general, the procedure of shifting contours, performing the limit $\epsilon \to 0$ and taking the residues extracts the pole terms in ϵ of a master integral in an algorithmic manner.

From the discussion above we summarize that when evaluating Barnes integrations the location of the integration contour in the complex plane is very important. We have to keep track of it in order not to miss or double count poles and it must be chosen such that is does not hit any of the latter.

Next, we demonstrate that MB representations allow one to perform the integrations over the Feynman parameters analytically. Consider a simple example with one Feynman parameter x

$$\int_0^1 dx \, \frac{x^a (1-x)^b}{(xA + yB)^\sigma} f(y) \,, \tag{4.5}$$

where A, B are variables and $f(y)$ is an arbitrary function. We apply Eq. (4.4) and obtain the following result

$$\frac{(yB)^{-\sigma}}{2\pi i\,\Gamma(\sigma)} f(y) \int_{c-i\infty}^{c+i\infty} dz\, A^z (yB)^{-z} \Gamma(-z)\Gamma(z+\sigma) \int_0^1 dx\, x^{a+z}(1-x)^b\,. \tag{4.6}$$

The integration over x yields the beta function. The integration over the Barnes parameter z can be performed by applying Cauchy's residue theorem, but the calculation is quite involved and not very illuminating. For a simpler example where the integrations over the Barnes parameters can be carried out more easily see Eq. (E.8) in the appendix. In that way, by introducing a sufficient number of new Barnes integrations, all Feynman integrations can be traded for MB integrations. For simple MB integrals, which usually appear in the pole terms of our master integrals, the integrations over the Barnes parameters can be carried out analytically by applying the residue theorem as described above.

A generalization of the MB representation to a sum of arbitrary many variables in terms of products can be derived by induction and is given by the following expression [116]

$$\begin{aligned}\frac{1}{(A_1+\cdots+A_n)^\lambda} = \frac{1}{\Gamma(\lambda)\,(2\pi i)^{(n-1)}} \int_{-i\infty}^{i\infty} \cdots \int_{-i\infty}^{i\infty} dz_2 \ldots dz_n \prod_{i=2}^{n} A_i^{z_i} \\ \times A_1^{-\lambda-z_2-\cdots-z_n} \Gamma(\lambda+z_2+\cdots+z_n) \prod_{i=2}^{n} \Gamma(-z_i)\,.\end{aligned} \tag{4.7}$$

The dimensionality of a MB representation for an integral is defined as the number of Barnes integrations. Note that there is no unique MB representation for an integral, however it is convenient to search for a low dimensional representation. Next, we briefly explain the numerical evaluation by the Mathematica routine MB.m.

4.3.1. Numerical Evaluation with MB.m

The Mathematica package MB.m is designed to solve Barnes integrations numerically by Monte Carlo integration. Consider a given MB representation for an arbitrary integral. In this representation all singularities in ϵ are contained in Gamma and polygamma functions, defined in Eq. (E.2), since these are the only functions that are analyzed by the routine for possible divergences. MB.m proceeds as follows. First a suitable integration contour is found that does not hit any pole and separates left from right poles. Then, the analytic continuation $\epsilon \to 0$ is performed. MB.m also gives the real part of all Barnes parameters that fix the integration contours along the imaginary axis. Finally, the Barnes integrations can be performed numerically specifying the desired accuracy of the calculation. The result is presented as an expansion in ϵ along with the corresponding errors.

Note that usually the numerical integration is more complex for a higher dimensional representation. Hence, in general the accuracy of the evaluation decreases and the runtime increases with the number of dimensions.

4.3.2. Automated Derivation of MB Representations with AMBRE.m

AMBRE.m is a Mathematica routine that automatically constructs a MB representation for a given planar integral [117]. Consider a scalar L-loop Feynman integral with N internal lines

$$G(m_1^2,\ldots,m_N^2,P) = \frac{1}{(i\pi^{d/2})^L}\int d^dk_1\ldots d^dk_L \frac{1}{(q_1^2-m_1^2)^{\nu_1}\ldots(q_N^2-m_N^2)^{\nu_N}}\,, \tag{4.8}$$

where $P=(p_1,\ldots,p_r)$ are the r independent external momenta, q_i are linear combinations of P and the loop momenta k_i, m_i are masses, and $\nu_i > 0$ some arbitrary integers. First, AMBRE.m replaces the momentum integrals by Feynman integrals

$$\begin{aligned} G(m_1^2,\ldots,m_N^2,P) = (-1)^{N_\nu}\frac{\Gamma(N_\nu-\frac{d}{2}L)}{\Gamma(\nu_1)\ldots\Gamma(\nu_N)}\int_0^1\prod_{j=1}^N dx_j\, x_j^{\nu_j-1}\delta\left(1-\sum_{i=1}^N x_i\right) \\ \times\frac{U(x)^{N_\nu-d(L+1)/2}}{F(x)^{N_\nu-dL/2}} \end{aligned} \tag{4.9}$$

with $N_\nu=\sum_{i=1}^N\nu_i$. The functions $U(x)$ and $F(x)$ can be derived from

$$\mathcal{N} = \sum_{i=1}^N x_i(q_i^2-m_i^2) \equiv k_l M_{ll'}k_{l'} - 2k_lQ_l + J\,, \tag{4.10}$$

where $M_{ll'}=\sum_{i=1}^N\alpha_{il'}x_i\alpha_{il}$, $Q_l=\sum_{i=1}^N\alpha_{il}P_ix_i$ and $J=\sum_{i=1}^N(P_i^2-m_i^2)x_i$. One finds them to be polynomials in x_i and they are formally given by the expressions

$$U(x) = \det(M)\,, \tag{4.11}$$

$$F(x) = -\det(M)\;J + Q_l\tilde{M}_{ll'}Q_{l'} - i\eta\,, \tag{4.12}$$

where $\tilde{M}=\det(M)\;M^{-1}$ and η marks the location of the pole of the combined Feynman propagators in the complex plane.

Next, a sufficient number of MB representations is introduced such that the integrations over the Feynman parameters can be performed analytically. Note that the sequence of replacing the momentum integrals by Feynman integrals and later by MB integrations is done for each momentum separately. The integration over the two loop momenta is performed one after another. The choice of which comes first, influences the MB representation but not the final result. For more details see [117].

AMBRE.m is not optimized to construct the lowest dimensional MB representation but rather finds some representation and often, an integral is expressed as a sum of different dimensional representations. In many cases it is possible to reduce the dimensionality by applying the residue theorem or by using the first or second Barnes lemma or modified versions of the latter (see App. E.2). Indeed, there are reasons for aiming at a lower dimensional representation: The extraction of the pole terms is much simpler and the numerical precision of the result obtained with MB.m decreases with the number of Barnes integrations

while the runtime increases. Moreover, MB.m fails to evaluate representations that contain a highly oscillating factor, if the convergence of the result is too slow. Such oscillating factors can arise from kinematic thresholds of the integral. Sometimes, they can be removed by performing some of the Barnes integrations analytically.

We have evaluated the master integrals $M_{1-3,6-12,16-18,20-23}$ applying this method. In App. (D.2) we present the calculation of $M_{23}^{\leftrightarrow}$ by "manually" introducing MB representations and of M_{18} by using Ambre as an example.

4.4. Differential Equations

A very powerful method for evaluating master integrals analytically is based on differential equations. In 1990, Kotikov was the first to show that by differentiating an unknown scalar integral with respect to one of the propagator masses one could evaluate the master integral by solving the resulting differential equation [118]. He was able to produce results for 2- and 3-point functions. Based on this idea Remiddi [119] proposed to use IBP identities for obtaining a linear system of first order differential equations for the master integrals in one of the kinematic invariants of the process. Finally, this method was fully developed and extended to multi-leg and multi-loop graphs by Remiddi and Gehrmann [120–122] and has already been applied in the calculation of various processes[2].

The differential equations can be solved by variation of constants. The boundary conditions to obtain the integration constants correspond to pseudo thresholds of the kinematic invariants and finding the boundary conditions can be a tedious task. Fortunately, for the master integrals that we have calculated by this method simple conditions could be found. The differential equations are Laurent-expanded about a certain value of the spacetime dimension, usually $d = 4$, up to the required order and then solved iteratively order by order in the expansion parameter, here $\epsilon = (4 - d)/2$. The result can be expressed in a basis of iterated integrals, the harmonic polylogarithms (HPLs) [124]. Using the Mathematica package HPL.m [125, 126] the HPLs are rather easy to handle and allow for an efficient calculation. Before we describe the method of differential equations in detail we present the definition of the HPLs and provide a short description of the most important relations.

4.4.1. Harmonic Polylogarithms and HPL.m

The harmonic polylogarithms (HPLs) [124] are a generalization of the ordinary polylogarithms [127] and the Nielson polylogarithms [128]. They are defined by the following recursive relation

$$H_{a_1,\ldots,a_n}(x) = \int_0^x dt\, f_{a_1}(t) H_{a_2,\ldots,a_n}(t)\,, \tag{4.13}$$

[2] A good description of this method can be reviewed in [123], where the authors also provide a copious list of references for applications.

where $\vec{a} = (a_1, \ldots, a_n)$ and each a_i can be 0 or ± 1. The functions

$$f_1(t) = \frac{1}{1-t}\,, \qquad f_0(t) = \frac{1}{t}\,, \qquad f_{-1}(t) = \frac{1}{1+t} \tag{4.14}$$

are called weight functions and correspondingly n is called the weight of the HPL. For integrals with trailing zeros the recursive relation (4.13) does not hold, but diverges. In order to handle HPLs in such cases, one defines

$$H_{\vec{0}_n}(x) = \frac{1}{n!}\log^n(x)\,. \tag{4.15}$$

We find the following relations between HPLs and ordinary logarithms

$$H_1(x) = \int_0^x dt\, f_1(t) = \int_0^x dt\, \frac{1}{1-t} = -\log(1-x)\,, \tag{4.16}$$

$$H_0(x) = \log(x), \tag{4.17}$$

$$H_{-1}(x) = \int_0^x dt\, f_{-1}(t) = \int_0^x dt\, \frac{1}{1+t} = \log(1+x)\,. \tag{4.18}$$

The HPLs obey a Hopf algebra and hence, the products of two HPLs with weight n and m can be written as a linear combination of HPLs with weight $n+m$. The product of two HPLs with vectors $\vec{a} = (a_1, \ldots, a_n)$ and $\vec{b} = (b_1, \ldots, b_m)$ is given by the following expression

$$H_{\vec{a}}(x) H_{\vec{b}}(x) = \sum_{\vec{c}} H_{\vec{c}}(x)\,, \tag{4.19}$$

where the sum runs over all vectors $\vec{c}$ of length $n+m$ containing the elements of $\vec{a}$ and $\vec{b}$ such that the ordering of all a_i's and b_i's separately is conserved. For examples see Eqs. (4.20) and (4.21) below. Note that some of the HPLs might diverge for $x = 0$ and $x = 1$. HPLs with n trailing zeros contain as leading logarithmic divergence $\log^n(x)$, which can be extracted explicitly by applying the product algebra (4.19) recursively. E.g. the logarithmic divergence of $H_{a_1,a_2,0}(x)$ can be extracted from the following equation

$$H_{a_1,a_2}(x) H_0(x) = H_{a_1,a_2,0}(x) + H_{a_1,0,a_2}(x) + H_{0,a_1,a_2}(x)\,. \tag{4.20}$$

Similarly, HPLs with n 1's to the left result in leading logarithmic divergences $\log^n(1-x)$ and we can extract the logarithmic divergence of e.g. $H_{1,a_1,a_2}(x)$ from the following relation

$$H_{a_1,a_2}(x) H_1(x) = H_{1,a_1,a_2}(x) + H_{a_1,1,a_2}(x) + H_{a_1,a_2,1}(x)\,. \tag{4.21}$$

For practical applications it is also convenient to define the "plus" and "minus" weights

$$f_+(x) = f_1(x) + f_{-1}(x) = \frac{2}{1-x^2}\,, \tag{4.22}$$

$$f_-(x) = f_1(x) - f_{-1}(x) = \frac{2x}{1-x^2}\,. \tag{4.23}$$

The product algebra, the derivative and integration properties, series expansion, numerical evaluation and many more features of HPLs have been implemented in the Mathematica package HPL.m [125, 126].

4.4.2. Evaluation of the Integrals

The method of employing differential equations proposed by Gehrmann and Remiddi works well for master integrals that depend on one scale. Hence, we apply it to obtain analytic results for some master integrals in Fig. 4.1 that only depend on the scale z_c and whose result is hard to obtain by using the standard text book techniques:

$$M_{4,5} \quad \text{and} \quad M_{19}\,. \tag{4.24}$$

Their evaluation will be explained below.

The master integrals of the set (4.24) depend on the ratio of the heavy-quark masses $z_c = m_c^2/m_b^2$ and on the expansion parameter $\epsilon = (4-d)/2$. Moreover, they are functions of the kinematic invariants (4.1)

$$M(z_c, \epsilon) \equiv M(q_3^2, q_3 \cdot q_4, q_4^2, z_c, \epsilon)\,. \tag{4.25}$$

The total derivative of M with respect to z_c is then given by

$$\frac{dM(z_c,\epsilon)}{dz_c} = \frac{\partial M}{\partial z_c} + \frac{\partial M}{\partial q_3^2}\frac{dq_3^2}{dz_c} + \frac{\partial M}{\partial (q_3\cdot q_4)}\frac{d(q_3\cdot q_4)}{dz_c} + \frac{\partial M}{\partial q_4^2}\frac{dq_4^2}{dz_c}\,. \tag{4.26}$$

$\partial M/\partial z_c$ can be easily computed whereas the partial derivatives of M with respect to the kinematics on the r.h.s of Eq. (4.26) can be obtained from [123]

$$\sum_{a=1}^{N}\left(p_{j,\mu}\cdot\frac{\partial s_a}{\partial p_{k,\mu}}\right)\frac{\partial M(\mathbf{s})}{\partial s_a} = p_{j,\mu}\frac{\partial M(\mathbf{s})}{\partial p_{k,\mu}}\,, \tag{4.27}$$

where $\mathbf{s} = \{\mathbf{s_1}, \ldots, \mathbf{s_N}\}$ is the set of N kinematic invariants formed by the momenta $p_{k,\mu}$, $p_{j,\mu}$. In our case $\mathbf{s} = \{q_3^2, q_3\cdot q_4, q_4^2\}$ and $p_{k,\mu} = \{q_{3,\mu}, q_{4,\mu}\}$. One obtains

$$2q_3^2\frac{\partial M}{\partial q_3^2} + (q_3\cdot q_4)\frac{\partial M}{\partial (q_3\cdot q_4)} = q_{3,\mu}\frac{\partial M}{\partial q_{3,\mu}}\,, \tag{4.28}$$

$$q_3^2\frac{\partial M}{\partial (q_3\cdot q_4)} + 2(q_3\cdot q_4)\frac{\partial M}{\partial q_4^2} = q_{3,\mu}\frac{\partial M}{\partial q_{4,\mu}}\,, \tag{4.29}$$

$$2(q_3\cdot q_4)\frac{\partial M}{\partial q_3^2} + q_4^2\frac{\partial M}{\partial (q_3\cdot q_4)} = q_{4,\mu}\frac{\partial M}{\partial q_{3,\mu}}\,, \tag{4.30}$$

$$(q_3\cdot q_4)\frac{\partial M}{\partial (q_3\cdot q_4)} + 2q_4^2\frac{\partial M}{\partial q_4^2} = q_{4,\mu}\frac{\partial M}{\partial q_{4,\mu}}\,. \tag{4.31}$$

The derivatives with respect to the four-momenta on the r.h.s can be carried out explicitly and yields linear combinations of M and several integrals belonging to subtopologies of M. Substituting the expressions for the derivatives with respect to the invariants in Eq. (4.26) and considering that $dq_4^2/dz_c = 0$ we obtain

$$\frac{dM}{dz_c} = \frac{\partial M}{\partial z_c} - \frac{1}{1-z_c}\left(q_{3,\mu}\frac{\partial M}{\partial q_{3,\mu}} + q_{4,\mu}\frac{\partial M}{\partial q_{3,\mu}}\right)\,. \tag{4.32}$$

This is a general differential equation valid for master integrals of the form $M(z_c, \epsilon)$. Applying the Laporta algorithm all integrals appearing on the r.h.s. of Eq. (4.32) can be expressed in terms of M and in terms of master integrals of the considered topology having a lower number of lines than M. Here, the master integrals of the subtopologies are either known or very easy to calculate and thus we assume them to be known. Note that Eqs. (4.28)-(4.31) are not independent of each other, i.e. $\partial M/\partial q_3^2$ can be either determined from Eqs. (4.28) and (4.30) or from Eqs. (4.29) and (4.31). Each way will lead to the same result which provides a check for this part of the calculation.

Inserting the results for all partial derivatives in Eq. (4.32) one obtains a differential equation of the form

$$\frac{dM(z_c,\epsilon)}{dz_c} = \sum_l A_l(z_c,\epsilon) S_l(z_c,\epsilon) + D(z_c,\epsilon) M(z_c,\epsilon)\,, \tag{4.33}$$

where the A_l and D are known functions depending on z_c and ϵ, and S_l, which also depend on z_c and ϵ, are the known masters with fewer lines[3] belonging to the same topology as M. There might exist cases where $D = 0$, however we did not come across them. One can simplify Eq. (4.33) by multiplying it by the exponential $\exp(-\mathcal{D})$, where $\mathcal{D}(z_c,\epsilon) \equiv \int_{z_{c_0}}^{z_c} dz_c' D(z_c',\epsilon)$ and z_{c_0} is an arbitrary lower integration bound. Using the following trick

$$\left(\frac{dM}{dz_c} - M\frac{d\mathcal{D}}{dz_c}\right)\exp\left[-\mathcal{D}\right] = \frac{d}{dz_c}\big(M\exp\left[-\mathcal{D}\right]\big)\,, \tag{4.34}$$

we arrive at

$$\frac{d}{dz_c}\big(M(z_c,\epsilon)\exp\left[-\mathcal{D}(z_c,\epsilon)\right]\big) = \sum_l A_l(z_c,\epsilon) S_l(z_c,\epsilon)\,\exp\left[-\mathcal{D}(z_c,\epsilon)\right]\,. \tag{4.35}$$

The r.h.s. of Eq. (4.35) is a function of z_c and ϵ and can be evaluated explicitly. Performing in Eq. (4.35) the integration over z_c order by order in ϵ and afterwards multiplying both sides by $\exp(\mathcal{D})$ one obtains the following expression

$$M(z_c,\epsilon) = \big(f(z_c,\epsilon) + \mathcal{C}\big)\exp\left[\mathcal{D}(z_c,\epsilon)\right]\,, \tag{4.36}$$

where f is the integral of the r.h.s. of Eq. (4.35) and $\mathcal{C}$ is an integration constant. The latter still needs to be determined using boundary conditions. It is known that the master integrals are analytic functions of z_c for all $z_c > 0$[4]. Observation shows that for each master integral of the set (4.24) there exists a value $z_c > 0$ for which the exponential $\exp(\mathcal{D})$ and thus the master integral given by Eq. (4.36) diverges[5]. Let us denote it by $z_{c,bound}$. For all masters

[3] If there are more master integrals in one topology there might also appear integrals with the same number of lines as M. In the case at hand we find that M_4 and M_5 lead to a system of coupled equations. Its solution is presented in App. (D.3).

[4] Note that the master integrals can have infrared divergences for $z_c = 0$ ($z_c = 0$ implies $m_c = 0$).

[5] The divergence in $\mathcal{D}$ will be logarithmic so that together with the exponential we just face a simple pole and not an essential singularity.

in the set (4.24) we have found $z_{c,bound} = 1$. This artificial divergence can be removed by a proper choice of the integration constant $\mathcal{C}$ such that

$$M(z_c, \epsilon) = \big(f(z_c, \epsilon) - f(z_{c,bound}, \epsilon)\big) \exp\left[\mathcal{D}(z_c, \epsilon)\right] \tag{4.37}$$

is finite for all $z_c > 0$[6] . Finally, we obtain a result of the master integral M as a series in ϵ expression with some analytic coefficients $B_i(z_c)$

$$M(z_c, \epsilon) = \frac{B_{-4}(z_c)}{\epsilon^4} + \frac{B_{-3}(z_c)}{\epsilon^3} + \frac{B_{-2}(z_c)}{\epsilon^2} + \frac{B_{-1}(z_c)}{\epsilon} + B_0(z_c) + B_1(z_c)\epsilon + \dots . \tag{4.38}$$

Some of the B_i may be zero and the expansion may just start with a double or single pole in ϵ. For M_4 and M_{19} we have found that the expansion starts with a double pole in ϵ, whereas M_5 is finite.

In App. (D.3) we present the evaluation of the master integrals M_4 and M_5 as an example. As mentioned before there arises an additional complication since in constructing the differential equation for M_4 one finds that it couples to M_5 and vice versa.

4.5. Differential Equations and Canonical Basis

Recently, the method of employing differential equations for obtaining master integrals has been further developed by Henn [107]. As discussed in Sec. 3.3 the basis of master integrals is not unique. Henn discovered that in a suitable basis – denoted as canonical basis – the differential equations can be cast into a form that factorizes the dependences on the kinematic variables from that on the number of space-times dimensions d. The solution can be expressed in terms of iterated integrals, which in our case are the Goncharov polylogarithms [129]. This method was recently applied to a number of problems for loop [130–138, 48] and phase-space [139, 140] integrals. A great advantage of this approach is that, in comparison to the previous techniques, we obtain analytic results, also for the master integrals depending on both scales u and z_c. Moreover, in the basis of iterated integrals the convolution of the hard scattering kernel with the pion LCDA simplifies to a large extent.

To the present day, the construction of the canonical basis is mostly based on experience and experimentation rather than on a systematic procedure, although developments in this direction have recently become available [141–144]. In the future it would be most desirable to have a general algorithm for finding a canonical basis for arbitrary numbers of loops, legs, scales, and even space-time dimensions. Each calculation of master integrals by this new approach provides an important contribution towards finding a general algorithm for constructing the canonical basis. Before describing the method we present the definitions of the Goncharov polylogarithms, which is the class of iterated integrals that appear in the solution of our master integrals.

[6] With the exception of course that there still appear divergences as poles in ϵ.

4.5.1. Goncharov Polylogarithms

The Goncharov polylogarithms [129] are a generalization of HPLs to arbitrary weights. They are defined in a similar recursive relation (cf. Sec. 4.4.1)

$$G_{a_1\ldots,a_n}(x) = \int_0^x \frac{dt}{t-a_1}\, G_{a_2\ldots,a_n}(t)\,, \tag{4.39}$$

but the a_i can now take arbitrary values. Eq. (4.39) does not hold for trailing zeros and in analogy to Eq. (4.15) we define

$$G_{\vec{0}_n}(x) = \frac{1}{n!}\log^n(x)\,. \tag{4.40}$$

The concept of weight will become important in the discussion of the canonical basis. Note that due to Eq. (4.40) $\log^k(x)$ is assigned a weight k.

The relations between the weight one Goncharov polylogarithms and ordinary logarithms read as follows

$$G_1(x) = \log(1-x)\,, \tag{4.41}$$
$$G_0(x) = \log(x), \tag{4.42}$$
$$G_{-1}(x) = \log(1+x)\,. \tag{4.43}$$

Moreover, we find a connection to the Riemann zeta function

$$G_{0,\ldots,0,1}(1) = -\zeta(k) \tag{4.44}$$

with $k-1$ zeros and $k>1$. $\zeta(k)\sim\pi^k$ for k even, and thus, we assign a weight k to both, $\zeta(k)$ and π^k.

For $a_n\neq 0$ the Goncharov polylogarithms can be rescaled by an arbitrary variable $y\neq 0$

$$G_{a_1,\ldots,a_n}(x) = G_{ya_1,\ldots,ya_n}(yx)\,. \tag{4.45}$$

Note, that it is most convenient to choose u as the argument of the Goncharov polylogarithm whenever there is a dependence on this scale, bearing in mind that this choice simplifies a subsequent convolution with the pion LCDA, which in a Gegenbauer expansion (cf. Eq. (5.29)) is a u-dependent polynomial.

The definitions of the Goncharov polylogarithms (4.39) and of the HPLs (4.13) are closely related. For Goncharov polylogarithms with weights ±1 and 0 we find the correlation

$$H_{\vec{a}_n}(x) = G_{\vec{a}_n}(x)(-1)^{\sum_i \delta_{1,a_i}}\,. \tag{4.46}$$

Converting the Goncharov polylogarithms to HPLs, one may use the features implemented in the Mathematica package HPL.m, like the product algebra and the extraction of logarithmic divergences (cf. Sec. 4.4.1). In addition, the C^{++} routine GiNaC [145] allows one to numerically evaluate Goncharov polylogarithms for arbitrary weights.

4.5.2. Canonical Basis

For defining the canonical basis, we first need to define the term "pure function". Consider a specific power in the ϵ-expansion of a master integral, the associated function is called uniform, if each summand has the same weight. Moreover, a uniform function is defined as pure, if its derivative with respect to any one of its arguments again yields a uniform function whose weight is lowered by one unit.

Now, let us consider a system of differential equations in the kinematic variables x_i for master integrals in an arbitrary basis

$$\frac{d}{dx_i}\vec{M}(x_j,\epsilon) = B_i(x_j,\epsilon)\vec{M}(x_j,\epsilon)\,. \tag{4.47}$$

$\vec{M}(x_j,\epsilon)$ denote the N master integrals and $B_i(x_j,\epsilon)$ are $N\times N$ matrices. Note that Eq. (4.47) is the analogue of Eq. (4.33) from the previous approach with a single variable $x_i = z_c$ and for $N = 1$. In the canonical basis, the differential equation is cast into the form [107]

$$\frac{d}{dx_i}\vec{C}(x_j,\epsilon) = \epsilon\, A_i(x_j)\vec{C}(x_j,\epsilon)\,, \tag{4.48}$$

where $\vec{C}(x_j,\epsilon)$ are the new N master integrals. The matrix coefficients $A_i(x_j)$ are now independent on ϵ, in contrast to the ones in Eq. (4.47), which explicitly depend on ϵ.

It turns out that the functions A_i are the coefficients of the gradient of a function $\tilde{A}$, i.e. $d\tilde{A}/dx_i = A_i$. Eq. (4.48) then takes the form

$$\frac{d}{dx_i}\vec{C}(x_j,\epsilon) = \epsilon\left(\frac{d}{dx_i}\,\tilde{A}(x_j)\right)\vec{C}(x_j,\epsilon)\,. \tag{4.49}$$

By construction, $\tilde{A}$ contains all information about the differential equations with respect to the different kinematic variables. Hence, $\tilde{A}$ together with the boundary conditions, which are specific in each case, completely determines the master integrals.

The master integrals in such a basis have in turn several pleasant features: First, the solution decouples order-by-order in the ϵ-expansion. Second, it is given by pure functions to all orders in ϵ. Consequently assigning a weight -1 to each power of the expansion parameter ϵ and multiplying each master integral by an appropriate power of ϵ renders the total weight of the master integral zero to all orders. Third, the solution can be expressed in terms of iterated integrals. If the coefficients $A_i(x_j)$ are rational functions of the x_j, the Goncharov polylogarithms discussed above represent a suitable class of iterated integrals to describe the master integrals. We will refer to a basis that obeys Eq. (4.49) as a *canonical basis*.

In the absence of an algorithm for the systematic construction of the canonical basis, we obtain a canonical basis by searching for pure linear combinations of master integrals in a "traditional" basis that consists of undotted and singly-dotted integrals, and compute them up to terms that involve functions of weight two. This method is based on trial and error, but has proven to be successful. As only disadvantage, an analytic representation of the master integrals in this other basis up to weight two has to be known from other sources,

like for instance from MB representations. An illustration of this procedure can be found in App. (D.4) where the calculation of a set of master integrals in the canonical basis is presented as an example. Next, we consider the differential equations in the invariants.

4.5.3. Solving Differential Equations

In the case at hand, the master integrals depend on the two scales z_c and u. The differential equation with respect to z_c can be derived analogous to the previous section and is given by Eq. (4.32). The one for u is simple and we find

$$\frac{dC_i}{dz_c} = \frac{\partial C_i}{\partial z_c} - \frac{1}{1-z_c}\left(q_{3,\mu}\frac{\partial C_i}{\partial q_{3,\mu}} + q_{4,\mu}\frac{\partial C_i}{\partial q_{3,\mu}}\right), \tag{4.50}$$

$$\frac{dC_i}{du} = \frac{\partial C_i}{\partial u}. \tag{4.51}$$

For our master integrals in the canonical basis the explicit expressions for Eqs. (4.50) and (4.51) factorize in ϵ and take the form

$$\frac{dC_i}{dz_c} = \epsilon\left(a_i(u,z_c)\,C_i + \sum_{j\neq i} a_j(u,z_c)\,C_j\right), \tag{4.52}$$

$$\frac{dC_i}{du} = \epsilon\left(b_i(u,z_c)\,C_i + \sum_{j\neq i} b_j(u,z_c)\,C_j\right), \tag{4.53}$$

where the $a_{i,j}$ and $b_{i,j}$ are rational functions and C_j are master integrals with equal or lower lines than C_i. We calculate the master integrals in the canonical basis successively, starting with the lowest line integrals. Thus, we assume all lower line master integrals to be known and take the lowest order in ϵ coefficients of the master integrals with equal lines from elsewhere, i.e. from MB representations[7].

In order to obtain an analytic expression for the master integral $C_i(u,z_c)$ in terms of iterated integrals we first consider the differential equation (4.51) and integrate it in u

$$\int_{u_0}^{u} du'\,\frac{dC_i(u',z_c)}{du'} = C_i(u,z_c) - C_i(u_0,z_c)\,, \tag{4.54}$$

where $u_0 \in [0,1]$ is an arbitrary lower limit. The integrand on the l.h.s. which given by Eq. (4.53) can be integrated over and the master integral $C_i(u,z_c)$ is determined except for the function $C_i(u_0,z_c)$. The latter can be extracted from the differential equation (4.50) evaluated at $u=u_0$ and integrated in z_c over an interval $0 \leq z_{c_0} < z_c \leq 1$:

$$\int_{z_{c_0}}^{z_c} dz_c'\,\frac{dC_i(u,z_c')}{dz_c'}\bigg|_{u=u_0} = C_i(u_0,z_c) - C_i(u_0,z_{c_0})\,. \tag{4.55}$$

[7] If there are more master integrals in a topology the corresponding differential equations decouple order-by-order in ϵ, as it can be seen from Eqs. (4.52) and (4.53), and thus can be solved.

The integrand on the l.h.s. given by Eq. (4.52) is known and thus the integration can be performed. The constant $C_i(u_0, z_{c_0})$ can be matched to the analytical result of the master integral at the point $u = u_0$ and $z_c = z_{c_0}$ obtained e.g. from MB representations.

Similar to the previous approach described in Sec. 4.4, the differential equations are solved iteratively order by order in ϵ. Note, that it is useful to find boundary conditions for which the master integrals vanish or take a simple expression. This might simplify the calculation to a large extent.

We find that in the differential equations of the 23 master integrals in Fig. 4.1 there appear in addition 14 lower line master integrals, which are known from previous calculations but also have to be converted to the canonical basis in order to close the system of differential equations. Thus, we need to calculate in total 37 integrals. The full set including results can be found in [C] [8].

We have evaluated $M_{8,9}$, $M_{8,9}^{\leftrightarrow}$ and M_{15} in the canonical basis using the steps outlined in Eqs. (4.54) and (4.55). These integrals correspond to the master integrals $C_{3,\ldots,7}$ in the canonical basis (see App. D.4 for the definition of the C_i) and we have found that they all vanish in a certain kinematic point. However, there are master integrals such as $C_{1,2}$, which correspond to $M_{6,7}$, for which we have only obtained non-vanishing boundary conditions and more importantly, for which we find Goncharov polylogarithms with non-trivial dependence on z_c in the weights in differential equation with respect to z_c (see Eq. (4.55)). Thus, this differential equation cannot straightforwardly be integrated by using the definition (4.39) but a suitable algorithm for the integration needs to be constructed. This is in principle possible and we use it in Sec. 5.1.2 to reexpress such Goncharov polylogiarhms in terms of HPLs. Instead one can follow another option which is to discard the differential equation with respect to z_c and obtain the function $C(u_0, z_c)$ from MB representations, as it was done in [C]. In App. D.4, the details of the calculation of $M_{6,7}$, $M_{8,9}$, $M_{8,9}^{\leftrightarrow}$ and M_{15} in the canonical basis are presented.

4.6. Checks

For numerical cross-checks we have evaluated the master integrals for twelve points in the $z_c - u$ plane. We have found that the results obtained in different MB representations agree to order 10^{-6} for the highest ϵ-coefficients. The agreement is even better for the pole terms and the integrals with different analytic representations in terms of HPLs or hypergeometric functions. However, for the integrals M_{20-22} and their mass-flipped counterparts, both obtained in a MB representation, the Monte-Carlo integration implemented in MB.m has failed due to highly oscillating integrands. In this case, we have relied on the numerical results of the sector decomposition method implemented in SecDec [146].

The master integrals in the canonical basis were evaluated in GiNaC, yielding an agreement to the previous results obtained in the former basis at the level of $5 \cdot 10^{-10}$. The only exceptions are C_{28-30} (see [C] for the definition) which correspond to the master integrals M_{20-22}. Their agreement is at the level of $8 \cdot 10^{-7}$ for the highest ϵ-coefficient, and $6 \cdot 10^{-4}$ for

[8] Note that in [C] two additional integrals are included which are the master integrals stemming from massive quarks in the gluon self energy correction.

the corresponding mass-flipped counter parts. For the lower coefficients in the ϵ-expansion, the agreement is several orders of magnitude better. We remark that having calculated the numerics in two different integral bases constitutes a non-trivial check.

In the further calculation, we will use the analytic expressions for the master integrals obtained in the canonical basis.

Chapter 5

Results and Phenomenological Applications

In this chapter, we present the renormalization factors and matching coefficients that enter the master formulae for the hard scattering kernels and briefly discuss the result for the latter. We calculate the perturbative contributions a_1 for the set of decays $\bar{B}^0 \to D^{(*)}L$ with $L = \pi, \rho$ and study the dependence on input parameters and on the factorization scale. Moreover, we evaluate the corresponding branching decay rates and confront the results with experimental data. In addition, we test how well the transition amplitude is described by Eq. (1.10) in the heavy-quark limit by comparing of ratios of non-leptonic decay rates on the one hand and ratios of non-leptonic and semi-leptonic decay rates on the other hand. We finish this chapter with a brief discussion of our results.

5.1. Hard Scattering Kernels

We have derived expressions for the one- and two-loop hard scattering kernels in terms of bare amplitudes, renormalization factors and matching coefficients in Sec. 2.2 . They are given in Eqs. (2.63), (2.64), (2.75) and (2.80) (and the corresponding expressions for the primed kernels). In the following, we give the explicit expressions for the renormalization factors and matching coefficients that enter these formulae and briefly discuss the results of the hard kernels.

5.1.1. Renormalization Factors and Matching Coefficients

The renormalization of the strong coupling is performed in the $\overline{\text{MS}}$ scheme. The corresponding renormalization factor Z_α can be found in [147] and reads

$$Z_\alpha = 1 - \frac{\alpha_s}{4\pi}\frac{1}{\epsilon}\left(\frac{11C_A}{3} - \frac{4n_f T_f}{3}\right) + \mathcal{O}(\alpha_s^2)\,. \tag{5.1}$$

Here, $n_f = 5$ is the total number of active quark flavours, and $C_A = 3$ and $T_f = 1/2$. The operator renormalization factors Z_{ij} of the operators Q_j have been calculated up to two-loop

accuracy in the $\overline{\text{MS}}$ scheme [148, 84]. The explicit one- and two-loop expressions are given by

$$Z^{(1)} = \frac{1}{\epsilon}\begin{pmatrix} -2 & \frac{4}{3} & \frac{5}{12} & \frac{2}{9} & 0 & 0 \\ 6 & 0 & 1 & 0 & 0 & 0 \end{pmatrix}, \tag{5.2}$$

$$\begin{aligned} Z^{(2)} = {} & \frac{1}{\epsilon^2}\begin{pmatrix} 17-\frac{4n_fT_f}{3} & \frac{2}{9}(4n_fT_f-39) & \frac{5}{18}(n_fT_f-15) & \frac{1}{54}(8n_fT_f-93) & \frac{19}{96} & \frac{5}{108} \\ 4n_fT_f-39 & 4 & \frac{2n_fT_f}{3}-\frac{31}{4} & 0 & \frac{5}{24} & \frac{1}{9} \end{pmatrix} \\ & + \frac{1}{\epsilon}\begin{pmatrix} \frac{8n_fT_f}{9}+\frac{79}{12} & \frac{20n_fT_f}{27}-\frac{205}{18} & \frac{1531}{288}-\frac{5n_fT_f}{108} & -\frac{2n_fT_f}{81}-\frac{1}{72} & \frac{1}{384} & -\frac{35}{864} \\ \frac{10n_fT_f}{3}+\frac{83}{4} & 3 & \frac{119}{16}-\frac{n_fT_f}{9} & \frac{8}{9} & -\frac{35}{192} & -\frac{7}{72} \end{pmatrix}. \end{aligned} \tag{5.3}$$

The row index of these matrices corresponds to $(\mathcal{Q}_1, \mathcal{Q}_2, E_1^{(1)}, E_2^{(1)}, E_1^{(2)}, E_2^{(2)})$ (see Sec. 1.3 for the definitions of the evanescent operators) and the column index to $(\mathcal{Q}_1, \mathcal{Q}_2)$. In contrast, the renormalization of the mass and the wave-function is performed in the on-shell scheme. The one-loop expression for the mass renormalization factor Z_{m_q} can be found in [147] and reads

$$Z_{m_q} = 1 - \frac{\alpha_s}{4\pi}\frac{C_F(2\epsilon-3)\Gamma(1-\epsilon)\Gamma(\epsilon)S_\Gamma}{(2\epsilon-1)}\big(m_q^2\big)^{-\epsilon} + \mathcal{O}(\alpha_s^2), \quad q = b, c. \tag{5.4}$$

Here, S_Γ is defined in Eq. (C.2) and $C_F = 4/3$. The wave-function renormalization factor Z_{ext} is given by the product of the on-shell field renormalization factors $Z_b^{1/2}$ and $Z_c^{1/2}$ which relate the bare quark field q_0 ($q = b, c$) to the renormalized field q via $q_0 = Z_q^{1/2} q$. To the one-loop accuracy Z_q coincides with Z_{m_q} [147]. Hence, the explicit expression for the wave-function renormalization factor is given by the following expression

$$Z_{\text{ext}} = 1 - \frac{\alpha_s}{4\pi}\frac{C_F(2\epsilon-3)\Gamma(1-\epsilon)\Gamma(\epsilon)S_\Gamma(1+z_c^{-\epsilon})}{2(2\epsilon-1)}\big(m_b^2\big)^{-\epsilon} + \mathcal{O}(\alpha_s^2). \tag{5.5}$$

In Eq. (2.80) we further encounter the SCET operator renormalization factor Y_{11}. If Y_{11} appears alongside a u-dependent function like $T_1^{(1)}$ we shall remember that this expression must be interpreted as convolution product, i.e. $T_1^{(1)} Y_{11}^{(1)} = \int_0^1 du'\, T_1^{(1)}(u') Y_{11}^{(1)}(u', u)$. By construction Y_{11} "factorizes"and hence can be split into the following two parts

$$Y_{11}(u', u) = Z_{Jh}\delta(u - u') + Z_{BL}(u', u). \tag{5.6}$$

Here, Z_{Jh} and Z_{BL} are the renormalization factors for the HQET heavy-to-heavy and the SCET light-to-light currents, respectively. Since one collinear sector in SCET is equivalent to full QCD – when restricted to soft fields and then boosted (see Sec. 2.1.2) – the renormalization constant Z_{BL} coincides with the ERBL kernel in QCD [50, 51]. We take Z_{BL} from [149]

$$\begin{aligned} Z_{BL}(v, w) = \delta(v-w) - \frac{\alpha_s}{4\pi}\frac{2C_F}{\epsilon}\Big\{ & \frac{1}{w\bar{w}}\left[v\bar{w}\,\frac{\Theta(w-v)}{w-v} + w\bar{v}\,\frac{\Theta(v-w)}{v-w}\right]_+ - \frac{1}{2}\delta(v-w) \\ & + \Delta\left[\frac{v}{w}\Theta(w-v) + \frac{\bar{v}}{\bar{w}}\Theta(v-w)\right]\Big\} + \mathcal{O}(\alpha_s^2). \end{aligned} \tag{5.7}$$

Here, $\Delta = 1$ for pseudoscalar and longitudinally polarized vector mesons and $\Delta = 0$ for transversally polarized vector mesons. The plus-distribution for symmetric kernels f is defined as follows

$$\int dw\,[f(v,w)]_+\,g(w) = \int dw f(v,w)(g(w)-g(v))\,. \tag{5.8}$$

The renormalization factor Z_{Jh} can be obtained in a matching of the heavy-to-heavy QCD current $\bar{c}\,\not{n}_+(1-\gamma_5)b$ to the HQET current $\bar{h}_{v'}\not{n}_+(1-\gamma_5)h_v$. Note that in this process also the matching coefficients C_{FF} can be determined. Since we treat the charm quark as heavy, it scales as of the order of the heavy-quark mass and we perform the matching at a scale of $\mathcal{O}(m_b)$. Beyond tree-level the QCD current mixes with the chirality flipped HQET current $\bar{h}_{v'}\not{n}_+(1+\gamma_5)h_v$. Hence, we make the following ansatz for the renormalized currents

$$\bar{c}\,\not{n}_+(1-\gamma_5)b = C_{FF}^{\mathrm{LL}}\left[\bar{h}_{v'}\not{n}_+(1-\gamma_5)h_v\right] + C_{FF}^{\mathrm{LR}}\left[\bar{h}_{v'}\not{n}_+(1+\gamma_5)h_v\right]\,, \tag{5.9}$$

$$\bar{c}\,\not{n}_+(1+\gamma_5)b = C_{FF}^{\mathrm{RL}}\left[\bar{h}_{v'}\not{n}_+(1-\gamma_5)h_v\right] + C_{FF}^{\mathrm{RR}}\left[\bar{h}_{v'}\not{n}_+(1+\gamma_5)h_v\right]\,, \tag{5.10}$$

where the different C_{FF} are the matching coefficients. We evaluate the latter in expansions of the strong coupling with five light flavours. The diagonal coefficients are given by $C_{FF}^{\mathrm{LL}} = C_{FF}^{\mathrm{RR}} = 1 + \mathcal{O}(\alpha_s)$, whereas the non-diagonal coefficients arise beyond tree-level only, i.e. $C_{FF}^{\mathrm{RL}} = C_{FF}^{\mathrm{RL}} = \mathcal{O}(\alpha_s)$. In order to obtain the explicit one-loop expressions, and in addition $Z_{Jh}^{(1)}$, we evaluate both sides of Eqs. (5.9) and (5.10) to one-loop accuracy. The renormalized matrix element of the QCD currents takes the form

$$\begin{aligned}\langle\bar{c}\,\not{n}_+(1\mp\gamma_5)b\rangle^{(1)} = &\left[\left(Z_{\mathrm{ext}}^{(1)} + Z_{hh}^{(1)}\right)A^{\mathrm{LL,RR}(0)} + A^{\mathrm{LL,RR}(1)}\right]\langle\bar{c}\,\not{n}_+(1\mp\gamma_5)b\rangle^{(0)} \\ &+ A^{\mathrm{LR,RL}(1)}\langle\bar{c}\,\not{n}_+(1\pm\gamma_5)b\rangle^{(0)}\,.\end{aligned} \tag{5.11}$$

Here, the $A^{(0,1)}$ are the bare tree-level/one-loop on-shell amplitudes. An explicit calculation yields

$$\begin{aligned}\langle\bar{c}\,\not{n}_+(1\mp\gamma_5)b\rangle^{(1)} = &\left[\left(\frac{1}{\epsilon}+L\right)C_F\left(\frac{(z_c+1)\log(z_c)}{z_c-1}-2\right) + C_F\frac{(z_c+1)\log^2(z_c)}{2-2z_c}\right. \\ &\left. + C_F\frac{(5z_c+1)\log(z_c)}{2(z_c-1)} - 4\right]\langle\bar{c}\,\not{n}_+(1\mp\gamma_5)b\rangle^{(0)} \\ &+ \left(C_F\frac{\sqrt{z_c}\log(z_c)}{z_c-1}\right)\langle\bar{c}\,\not{n}_+(1\pm\gamma_5)b\rangle^{(0)}\,.\end{aligned} \tag{5.12}$$

The one-loop matrix element of the HQET currents is given by[1]

$$\langle\bar{h}_{v'}\,\not{n}_+(1\mp\gamma_5)\bar{h}_v\rangle^{(1)} = \left[\left(Y_{\mathrm{ext}}^{(1)} + Z_{Jh}^{(1)}\right)M^{\mathrm{L,R}(0)} + M^{\mathrm{L,R}(1)}\right]\langle\bar{h}_{v'}\,\not{n}_+(1\mp\gamma_5)\bar{h}_v\rangle^{(0)}\,. \tag{5.13}$$

The SCET on-shell amplitudes $M^{\mathrm{L,R}(1)}$ and the on-shell wave-function renormalization factor $Y_{\mathrm{ext}}^{(1)}$ receive only contributions from scaleless integrals and therefore vanishes in dimensional

[1] We shall remember that at the one-loop accuracy the coupling constants with five and three light flavours coincide (see Sec. 2.2).

regularization, whereas the tree-level amplitudes $M^{\mathrm{L,R}(0)}$ are equal to unity. Thus, the only surviving contribution comes from $Z_{Jh}^{(1)}$. Comparing Eqs. (5.12) and (5.13) we can identify $Z_{Jh}^{(1)}$ as the pole term in ϵ, that is

$$Z_{Jh}^{(1)} = \frac{C_F}{\epsilon}\left(\frac{(z_c+1)\log(z_c)}{z_c-1} - 2\right), \tag{5.14}$$

which correctly reproduces the IR behaviour of QCD in the effective theory. The C_{FF} on the other hand are given by the coefficients in Eq. (5.12), which are finite in ϵ. We find that the explicit one-loop results each for the diagonal and off-diagonal expressions coincide, which is not surprising as Eqs. (5.9) and (5.10) are symmetric under interchanging $P_L \leftrightarrow P_R$. Introducing the notations $C_{FF}^{\mathrm{D}(1)} \equiv C_{FF}^{\mathrm{LL}(1)} = C_{FF}^{\mathrm{RR}(1)}$ and $C_{FF}^{\mathrm{ND}(1)} \equiv C_{FF}^{\mathrm{LR}(1)} = C_{FF}^{\mathrm{RL}(1)}$ the expressions read

$$C_{FF}^{\mathrm{D}(1)} = C_F\left[L\left(\frac{(z_c+1)\log(z_c)}{z_c-1} - 2\right) + \frac{(z_c+1)\log^2(z_c)}{2-2z_c} + \frac{(5z_c+1)\log(z_c)}{2(z_c-1)} - 4\right], \tag{5.15}$$

$$C_{FF}^{\mathrm{ND}(1)} = C_F\left(\frac{\sqrt{z_c}\log(z_c)}{z_c-1}\right). \tag{5.16}$$

As last contribution the sum $\sum_{b\neq 1} H_{1b}^{(1)} Y_{b1}^{(1)}$ in Eq. (2.80) needs to be further specified. Considering Eqs. (2.49) and (2.52) we find that only $H_{1b}^{(1)}$ with $b = 2$ yields a non-vanishing contribution which, comparing the coefficients proportional to O_2, is given by $H_{12}^{(1)} = A_{12}^{(1)} + Z_{\mathrm{ext}}^{(1)} A_{12}^{(0)} + Z_{1j}^{(1)} A_{j2}^{(0)}$. The tree-level amplitude $A_{12}^{(0)}$ is zero and the factorizable diagrams $A_{12}^{f(1)}$ vanish as well (see Sec. 2.2.3). Hence, $H_{12}^{(1)} = A_{12}^{(1)nf} + Z_{1j}^{(1)} A_{j2}^{(0)}$. The derivation for the corresponding primed contribution follows the same lines and we obtain a similar expression. The operator renormalization factor $Y_{21}^{(1)}$ has already been used in the NNLO calculation of the vertex corrections to the decay $B \to \pi\pi$ and is given in [45] in Eq. (45). Its explicit expression reads

$$Y_{21}^{(1)}(u',u) = 16\, C_F\left(\frac{u'\Theta(u-u')}{u} + \frac{(1-u')\Theta(u'-u)}{1-u}\right). \tag{5.17}$$

With this we have specified all renormalization factors and matching coefficients that enter the master formulae for the hard scattering kernels.

5.1.2. Discussion of the Results for the Hard Kernels

We find that our expressions for the one-loop kernels agree with the results given in Eqs. (89) and (90) in [27]. For performing this comparison one has to take into account that the one-loop result given in Eq. (90) was calculated in the "traditional basis" given in Eq. (V.1) in [82] (cf. [150]). The converted results are equal up to higher order corrections. The explicit results for the two-loop hard scattering kernels are not presented here as they are rather lengthy and not very illuminating. Instead we comment on some interesting features of

the master formulae (2.75) and (2.80). Analogous considerations apply to the corresponding formulae for the primed kernels.

As mentioned in Sec. 1.1.1 the hard scattering kernels must be free of IR divergences. The UV divergences are removed by considering renormalized amplitudes. Even though most of the individual terms in Eqs. (2.75) and (2.80) contain divergences, the total expressions are free of poles in ϵ. For calcuating the hard scattering kernels we use the master integrals in the canonical basis, which are written in terms of Goncharov polylogarithms. As we apply a numerically routine for evaluating the latter (see Sec. 4.5) we obtain only a numerical result for the kernels. We find that for $T_1^{(2)}$ all poles cancel, for the $1/\epsilon$ poles at the level of 2×10^{-5} for 12 different points in the u-z_c plain. The pole cancellation for the higher poles is much better as well as the pole cancellation of the colour singlet kernels, which is at the level of 3×10^{-7}. We remark that after the convolution of the hard scattering kernels with the LCDAs we can express the result in terms of harmonic polylogarithms, which can be easily simplified in Mathematica (see Sec. 4.4.1). We find that the poles then cancel analytically. Note that the master formula (2.75) for the two-loop colour singlet kernel is simpler than the one of the colour octet kernel. The reason is that the one-loop kernel $T_2^{(1)}$ as well as other one-loop colour singlet amplitudes are zero due to their colour factors. Hence, already $A_{21}^{(2)nf}$ is free of IR divergences, i.e. the $1/\epsilon^4$ and $1/\epsilon^3$ poles cancel in the sum, and performing the UV renormalization is sufficient for obtaining an in ϵ finite result.

Finally, we remark that after performing the convolution of the hard scattering kernels with the pion LCDA we reproduce the result for the vertex correction to the colour-allowed topology of the decay $B\to\pi\pi$ given in Eq. (48) in [47] in the limit $m_c\to0$. Next, we present and discuss the results for the perturbative amplitude a_1.

5.2. Perturbative Amplitude a_1

The perturbative amplitude a_1 is defined as the convolution of hard scattering kernels and the light meson (here the pion) LCDA multiplied by Wilson coefficients. As the hard kernels only contain the short distance physics above scales $\mu\geq m_b$ (see Sec. 1.1.1), they are independent of the explicit final-state mesons. Therefore, we can use the result for the hard scattering kernels to calculate the NNLO vertex corrections to the transition amplitudes for the set of decays $\bar{B}^0\to D^{(*)}L$ with $L=\pi,\rho$, whose weak transitions all are mediated by the operators $\mathcal{Q}_1$ and $\mathcal{Q}_2$. Note that our calculation only applies for longitudinally polarized vector mesons in the $\bar{B}^0\to D^{*+}\rho^-$ transition amplitude (see Eq. (5.7)). However, the contribution from transversally polarized vector mesons was found to be small [27] and thus can be neglected (see also Sec. 5.3). In the following, we define the hadronic quantities and identify the perturbative contribution a_1 in the transition amplitude Eq. (1.1). Then, we present the results for a_1 up to NNLO accuracy and analyse their dependence on the input parameters and on the factorization scale.

5.2.1. Hadronic Matrix Elements and Definition of a_1

For the decays $\bar{B}^0 \to D^{(*)}L$ the transition amplitude Eq. (1.1) reads

$$\mathcal{A}(\bar{B}^0 \to D^{(*)}L) = \frac{G_F}{\sqrt{2}} \sum_i V_{ud}^* V_{cd}\, C_i(\mu) \langle D^{(*)}L|\mathcal{Q}_i|\bar{B}^0\rangle\,. \tag{5.18}$$

The factorized hadronic matrix element is given by Eq. (2.35) which in $d = 4$ dimensions reduces to

$$\langle D^{(*)}L|\mathcal{Q}_i|\bar{B}^0\rangle = \hat{T}_i \langle D^{(*)}L|\mathcal{Q}^{\text{QCD}}|\bar{B}^0\rangle + \hat{T}_i' \langle D^{(*)}L|\mathcal{Q}'^{\text{QCD}}|\bar{B}^0\rangle\,. \tag{5.19}$$

We shall remember that at leading power $\mathcal{Q}^{(\prime)}_{\text{QCD}}$ factorizes in the product of a LCDA and the full QCD form factor and thus, Eq. (5.19) takes the form

$$\begin{aligned}\langle D^{(*)}L|\mathcal{Q}_i|\bar{B}^0\rangle = {}& \langle L|\bar{d}\,\gamma^\mu(1-\gamma_5)u|0\rangle \langle D^{(*)}|\bar{c}\,\gamma_\mu(1-\gamma_5)b|\bar{B}^0\rangle \int du\, \hat{T}_i(u)\Phi_L(u) \\ & + \langle L|\bar{d}\,\gamma^\mu(1-\gamma_5)u|0\rangle \langle D^{(*)}|\bar{c}\,\gamma_\mu(1+\gamma_5)b|\bar{B}^0\rangle \int du\, \hat{T}_i'(u)\Phi_L(u)\,. \end{aligned}\tag{5.20}$$

Note that in this expression all hadronic matrix elements are *local*. A comparison of Eq. (5.20) with Eqs. (1.7) and (1.8) yields the following relations for the local matrix elements

$$\langle \pi(q)|\bar{d}\,\gamma^\mu(1-\gamma_5)u|0\rangle = i f_\pi q^\mu\,, \tag{5.21}$$

$$\langle \rho(q)|\bar{d}\,\gamma^\mu(1-\gamma_5)u|0\rangle = -i f_\rho m_\rho \eta^{*\mu}\,, \tag{5.22}$$

where η is the polarization vector and m_ρ the mass of the ρ meson. For a longitudinally polarized ρ meson we have $\eta^\mu = q^\mu/{m_\rho}^2$. The decomposition of the $B \to D$ vector form factor is given in Eq. (1.4), whereas the axial form factor vanishes due to parity. The form factors for transitions involving the D^* can be found in [53] and read

$$\langle D^*(p',\epsilon^*)|\bar{c}\gamma^\mu\gamma_5 b|\bar{B}_0(p)\rangle = \frac{2iV(q^2)}{m_B + m_{D^*}} \epsilon^{\mu\nu\rho\sigma} \epsilon^*_\nu p'_\rho p_\sigma\,, \tag{5.23}$$

$$\begin{aligned}\langle D^*(p',\epsilon^*)|\bar{c}\gamma^\mu\gamma_5 b|\bar{B}_0(p)\rangle = {}& 2m_{D^*} A_0(q^2) \frac{\epsilon^*\cdot q}{q^2} q^\mu + (m_B + m_{D^*}) A_1(q^2) \left(\epsilon^{*\mu} - \frac{\epsilon^*\cdot q}{q^2} q^\mu\right) \\ & - A_2(q^2) \frac{\epsilon^*\cdot q}{m_B + m_{D^*}} \left(p^\mu + p'^\mu - \frac{m_B^2 - m_{D^*}^2}{q^2} q^\mu\right)\,. \end{aligned}\tag{5.24}$$

Here, ϵ is the polarization vector and m_{D^*} the mass of the D^*, and $q = p - p'$. The A_i and V are scalar form factors. Note that the $B \to D^*$ vector form factor vanishes when contracted with the matrix elements given in Eq. (5.21) and in Eq. (5.22) in the case of a longitudinally polarized ρ meson. Hence, neglecting the contribution from transversally polarized vector mesons we define a_1 as follows

$$\mathcal{A}(\bar{B}^0 \to DL) = \frac{G_F}{\sqrt{2}} \sum_i V_{ud}^* V_{cd}\, a_1(DL)\, \langle L|\bar{d}\,\gamma^\mu(1-\gamma_5)u|0\rangle \langle D|\bar{c}\,\gamma_\mu b|\bar{B}^0\rangle\,, \tag{5.25}$$

$$\mathcal{A}(\bar{B}^0 \to D^*L) = -\frac{G_F}{\sqrt{2}} \sum_i V_{ud}^* V_{cd}\, a_1(D^*L)\, \langle L|\bar{d}\,\gamma^\mu(1-\gamma_5)u|0\rangle \langle D^*|\bar{c}\,\gamma_\mu\gamma_5 b|\bar{B}^0\rangle\,, \tag{5.26}$$

[2] In general η is a linear combination of p and p' but in the limit $q^2 \to 0$ can be approximated by $\eta = q^\mu/m_\rho$.

with

$$a_1(DL)(\mu) = \sum_{i=1,2} C_i(\mu) \int_0^1 du\ [T_i(u,\mu) + T_i'(u,\mu)]\, \Phi_L(u,\mu)\,, \tag{5.27}$$

$$a_1(D^*L)(\mu) = \sum_{i=1,2} C_i(\mu) \int_0^1 du\ [T_i(u,\mu) - T_i'(u,\mu)]\, \Phi_L(u,\mu)\,. \tag{5.28}$$

Here, we have made explicit the dependence on the factorization scale μ. We take the values for the Wilson coefficients at the weak scale and evolve them down to a scale of order of the b-quark mass. The RG evolution can be found in [84, 85]. We take the running of the strong coupling from [151] to NNLO accuracy, also in the evolution of the LO and NLO Wilson coefficients. The light meson LCDAs are expanded in a basis of Gegenbauer polynomials $C_k^{3/2}(x)$ with Gegenbauer moments α_k^L

$$\Phi_L(u,\mu) = 6u(1-u)\left(1 + \sum_{k=1}^{\infty} \alpha_k^L(\mu) C_k^{3/2}(2u-1)\right). \tag{5.29}$$

Following [27] we assume that the leading-twist LCDA is close to its asymptotic form given in Eq. (1.6) and truncate the expansion at the second moment. The first two Gegenbauer polynomials read $C_1^{3/2}(x) = 3x$ and $C_2^{3/2}(x) = \frac{3}{2}(5x^2-1)$. The Gegenbauer moments are eigenfunctions of the one-loop renormalized ERBL-kernel. Hence, to leading-logarithmic (LL) accuracy they are multiplicatively renormalizable [152]

$$\alpha_n^L(\mu^2) = \left(\frac{\alpha_s(\mu^2)}{\alpha_s(\mu_0^2)}\right)^{\gamma_n^{(0)}/(2\beta_0)} \alpha_n^L(\mu_0^2)\,, \tag{5.30}$$

with $\beta_0 = (11C_A - 2\,n_f)/3$ and leading order anomalous dimension

$$\gamma_n^{(0)} = 8C_F\left(\sum_{k=1}^{n+1}\frac{1}{k} - \frac{3}{4} - \frac{1}{2(n+1)(n+2)}\right). \tag{5.31}$$

The next-to-leading logarithmic (NLL) evolution has been derived in [152–154]. Here, we use the result presented in [155], which has the form

$$\alpha_n^L(\mu^2) = \alpha_n^L(\mu_0^2) E_n^{\rm NLL} + \frac{\alpha_s(\mu^2)}{4\pi}\sum_{k=0}^{n-2}\alpha_k(\mu_0^2) E_k^{\rm NLL} d_{nk}^{(1)}\,, \tag{5.32}$$

with

$$E_n^{\rm NLL} = \left(\frac{\alpha_s(\mu^2)}{\alpha_s(\mu_0^2)}\right)^{\gamma_n^{(0)}/(2\beta_0)} \left[1 + \frac{\beta_0\gamma_n^{(1)} - \beta_1\gamma_n^{(0)}}{8\pi\beta_0^2}\left(\alpha_s(\mu^2) - \alpha_s(\mu_0^2)\right)\right]. \tag{5.33}$$

For the evolution of the lowest moments $n = 0, 1, 2$ we use

$$\gamma_0^{(1)} = 1, \quad \gamma_1^{(1)} = \frac{23488}{243} - \frac{512 n_f}{81}\,, \quad \gamma_2^{(1)} = \frac{34450}{243} - \frac{830 n_f}{81}\,, \tag{5.34}$$

Parameter	Value/Range	Parameter	Value/Range
$\alpha_s(m_Z)$	0.1185 ± 0.006	m_t	173.21 ± 0.87
$\Lambda^{(5)}_{\overline{\rm MS}}$(NNLO)	0.2143	m_b	4.78 ± 0.06
$\Lambda^{(3)}_{\overline{\rm MS}}$(NLO)	0.3957	m_c	1.67 ± 0.07
M_W	80.385 ± 0.015	$\alpha_2^\pi(1\,\text{GeV})$	0.29 ± 0.08 [156, 157]
M_Z	91.1876 ± 0.0021	$\alpha_2^{\|\rho}(1\,\text{GeV})$	0.17 ± 0.07 [157]

Table 5.1. – Dimensionful quantities are given in units of GeV. If not otherwise stated the values are taken from the Particle Data Group [158]. The given masses are the pole masses. $\alpha_2^{\|\rho}$ is the second Gegenbauer moment of the longitudinally polarized ρ meson.

and

$$d_{20}^{(1)} = \frac{7}{30}(5C_F - \beta_0)\frac{\gamma_2^{(0)}}{\gamma_2^{(0)} - 2\beta_0}\left[1 - \left(\frac{\alpha_s(\mu^2)}{\alpha_s(\mu_0^2)}\right)^{-1+\gamma_2^{(0)}/(2\beta_0)}\right]. \tag{5.35}$$

The Gegenbauer moments usually are obtained from lattice or sum rule calculations at scales around 1-2 GeV and are then evolved to scales $\mu \sim m_b$. For the evolution we consider the running of the strong coupling with $n_f = 3$ light flavours. Note that in the case of the pion and the ρ meson the first moment $\alpha_1^{\pi,\rho}$ vanishes in the isospin symmetry limit.

Next, we calculate the perturbative amplitude a_1 and study the impact of varying the input parameters and the factorization scale.

5.2.2. Results and Dependence on Input Parameters

We evaluate the perturbative amplitudes $a_1(D^{(*)}L)$ for the set of parameters given in Tab. 5.1 up to NNLO accuracy. The top mass enters the running of the Wilson coefficient only at NNLO and we find that changes of the mass in the range of $172\,\text{GeV} < m_t < 175\,\text{GeV}$ do not have any affect on our result within the considered accuracy. The same applies for varying M_W, M_Z and the second Gegenbauer moments within the given uncertainties. In the evolution of the Gegenbauer moments we take the NLO strong coupling with $n_f = 3$ light flavours. Note that a change to the coupling constant with $n_f = 4$ light flavours has a negligibly small impact on a_1. Moreover, we find that dependence on $z_c = m_c^2/m_b^2$ is given by a smooth function and changes of z_c in the range of $0.10 \leq z_c \leq 0.15$ affect a_1 only at the per mill level. The z_c-dependence for the decays $\bar{B}^0 \to D^{(*)}\pi$ is visualized in Fig. 5.1 where we have plotted the real and imaginary parts of $a_1^{\rm NLO}$ and $a_1^{\rm NNLO}$ as a function of z_c. Note that the z_c-dependence of the decays $\bar{B}^0 \to D^{(*)}\pi$ shows a similar behaviour. Although we do not expect any significant changes, it would be interesting to investigate the z_c-dependence when choosing a different scheme than the on-shell scheme for the renormalization of the quark masses; for instance choosing the $\overline{\rm MS}$ scheme. This is beyond the scope of this thesis but will be analyzed in a forthcoming publication [E].

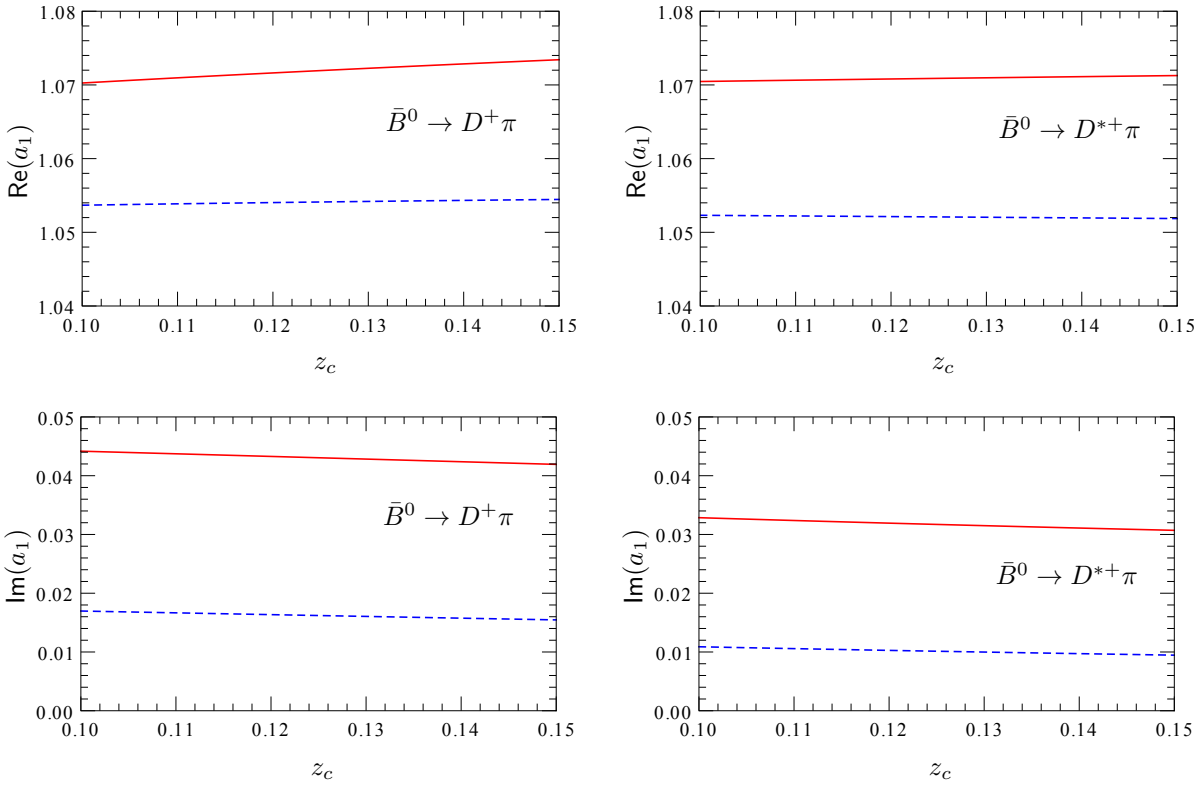

Figure 5.1. – z_c-dependence of the a_1 varying z_c in the range of physical values $0.10 < z_c < 0.15$. The upper panels show the values for real parts of $a_1(D\pi)$ (left) and $a_1(D^*\pi)$ (right), whereas the size of the imaginary parts are given in the lower panels, left for $a_1(D\pi)$ and right for $a_1(D^*\pi)$. The dashed/solid lines represent the NLO/NNLO results.

The largest uncertainty of a_1 comes from varying the factorization scale μ (see Eq. (1.1)) within $m_b/2 \leq \mu \leq 2m_b$. The μ-dependence is visualized in Fig. 5.2 for the decays $\bar{B}^0 \to D^{(*)}\pi$. We find that for the real parts the LO and NLO results have a large scale dependence, which gets significantly reduced in the NNLO results. This behaviour cannot be observed in the scale dependence of the imaginary parts. However, this is not surprising as the imaginary parts only arise at NLO. Hence, the NNLO results are in fact the first correction and we do not expect the scale dependence to be sizably reduced at this order. Note that the plots for the decays $\bar{B}^0 \to D^{(*)}\rho$ show a similar behaviour. Taking the specific value $\mu = m_b$ for the calculation of the central values we then obtain the following results for the perturbative amplitude a_1: At LO the values for the four different amplitudes coincide, are real and read

$$a_1^{\text{LO}}(D^{(*)}L) = 1.025 \pm 0.024\,. \tag{5.36}$$

The NLO results as functions of the second Gegenbauer moment are given by

$$a_1^{\text{NLO}}(DL) = (1.054^{+0.021}_{-0.018} + 0.016i^{+0.013i}_{-0.007i}) + (0.002^{+0.002}_{-0.001} - 0.001i^{+0.001i}_{-0.001i})\alpha_2^L\,, \tag{5.37}$$

$$a_1^{\text{NLO}}(D^*L) = (1.052^{+0.019}_{-0.017} + 0.010i^{+0.008i}_{-0.005i}) + (0.000^{+0.000}_{-0.000} - 0.001i^{+0.001i}_{-0.001i})\alpha_2^L\,. \tag{5.38}$$

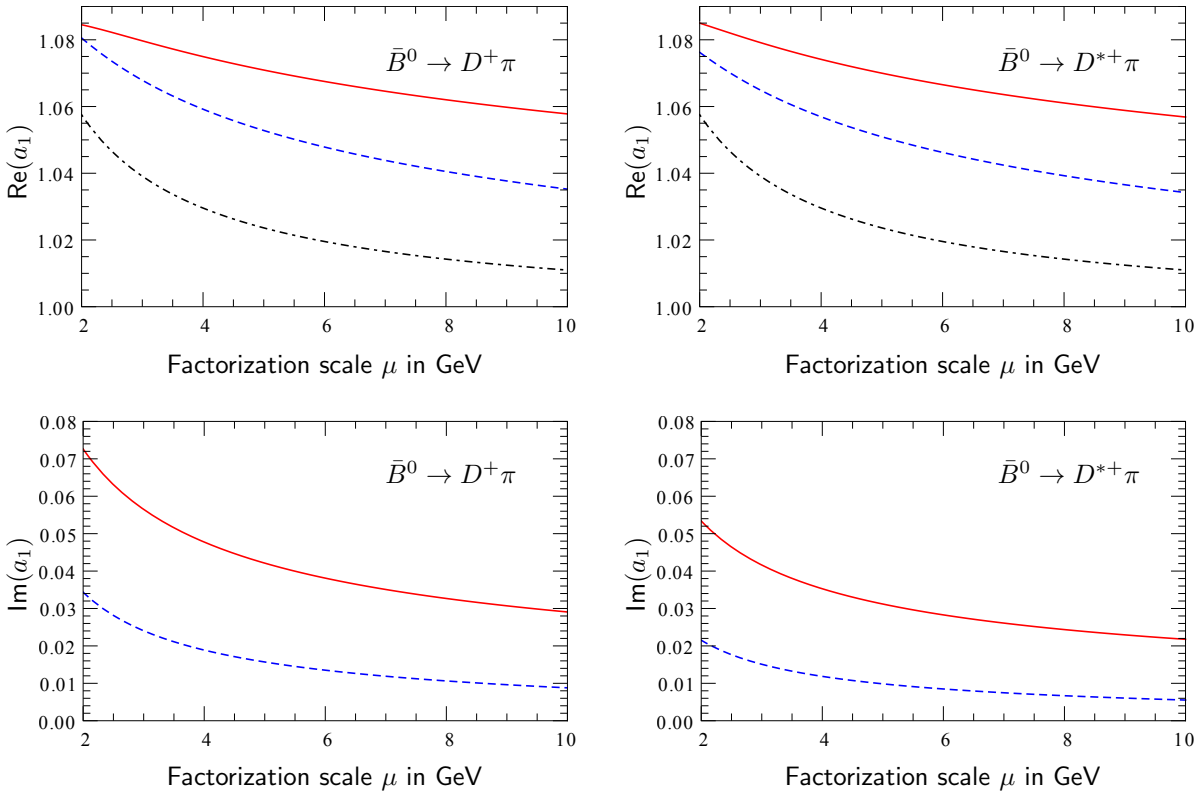

Figure 5.2. – Factorization scale-dependence of the a_1 in the range of $2 \leq \mu \leq 10$. In the upper panels the real parts of $a_1(D\pi)$ (left) and $a_1(D^*\pi)$ (right) are shown. The dependence of the imaginary parts of $a_1(D\pi)$and $a_1(D^*\pi)$ on μ is given in the left and right lower panels, respectively. The dashed-dotted/dashed/solid lines represent the LO/NLO/NNLO results. Note that the imaginary parts just starts at NLO.

We remark that these numbers have been calculated with updated values of input parameters in comparison to the NLO values given in Tab. (4) in [27]. However, even though using the input parameters provided in [27] we find a small discrepancy at the per mill level for the central values. This difference arises due to the neglected higher order corrections that are different since both calculations have been performed using different operator bases (see Sec. 5.1.2). At NNLO we obtain the following values

$$a_1^{\text{NNLO}}(DL) = (1.071^{+0.011}_{-0.013} + 0.044i^{+0.022i}_{-0.014i}) + (0.003^{+0.003}_{-0.002} - 0.007i^{+0.002i}_{-0.003i})\alpha_2^L\,, \tag{5.39}$$

$$a_1^{\text{NNLO}}(D^*L) = (1.071^{+0.012}_{-0.013} + 0.033i^{+0.017i}_{-0.010i}) + (0.000^{+0.001}_{-0.000} - 0.009i^{+0.003i}_{-0.004i})\alpha_2^L\,. \tag{5.40}$$

We find that in comparison to the NLO results the central NNLO values are increased by about 2%, whereas the imaginary parts obtain a correction which is even larger than the NLO imaginary parts themselves. Moreover, the uncertainties in real parts get reduced by approximately 30%, the uncertainties of the imaginary parts on the other hand are still sizable. The central values for real and imaginary parts of the LO/NLO/NNLO amplitude $a_1(\bar{B}^0 \to D^+\pi^-)$ are shown in Fig. 5.3 including the corresponding uncertainties. We find that the number of the real and imaginary part of the central values increases with the

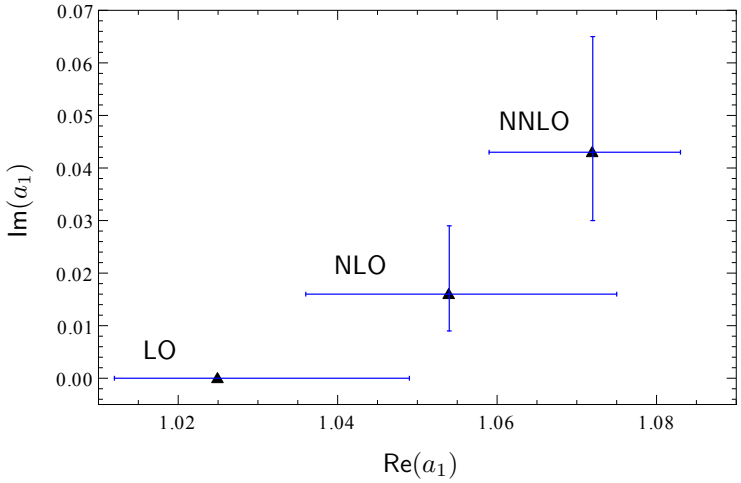

Figure 5.3. – The real and imaginary part of the LO/NLO/NNLO corrections are plotted for the decay $\bar{B}^0 \to D^+\pi^-$ including error bars that show the corresponding uncertainties. Note that the LO result has no imaginary part.

considered order in the perturbative expansion. Within the uncertainties the NLO and NNLO reals parts are in good agreement, whereas there is only a small overlap of the NLO and NNLO imaginary parts. Finally, we remark that within the given uncertainties the NNLO corrections agree and point towards a quasi-universal perturbative contribution of the vertex corrections to the decays $\bar{B}^0 \to D^{(*)}L$ in the framework of QCDF.

In the subsequent calculation of the branching ratios we will use the following results for $a_1^{\rm NNLO}$ that include the values for the Gegenbauer moments given in Tab. 5.1

$$a_1^{\rm NNLO}(D\pi) = 1.072^{+0.011}_{-0.013} + 0.043i^{+0.022i}_{-0.013i}\,, \tag{5.41}$$
$$a_1^{\rm NNLO}(D\rho) = 1.072^{+0.011}_{-0.013} + 0.044i^{+0.022i}_{-0.014i}\,, \tag{5.42}$$
$$a_1^{\rm NNLO}(D^*\pi) = 1.071^{+0.012}_{-0.013} + 0.032i^{+0.016i}_{-0.010i}\,, \tag{5.43}$$
$$a_1^{\rm NNLO}(D^*\rho) = 1.071^{+0.012}_{-0.013} + 0.032i^{+0.016i}_{-0.010i}\,. \tag{5.44}$$

5.3. Branching Ratios

We evaluate the branching ratios (BRs) for the decays $\bar{B}^0 \to D^{*+}L^-$ and compare the result with the experimentally measured ones. They are related to the decay rates Γ by $\mathrm{BR}(\bar{B}^0 \to D^{*+}L^-) = \tau_{\bar{B}^0}/\hbar\, \Gamma(\bar{B}^0 \to D^{*+}L^-)$, where $\tau_{\bar{B}^0}$ is the $\bar{B}^0$ meson life time. The expression for the rates are given by [27]

$$\Gamma(\bar{B}^0 \to D^+\pi^-) = \frac{G_F^2(m_B^2 - m_D^2)^2|\vec{q}|_{D\pi}}{16\pi m_B}|V_{ud}^*V_{cb}|^2\,|a_1(D\pi)|^2 f_\pi^2 F_0^2(m_\pi^2)\,, \tag{5.45}$$
$$\Gamma(\bar{B}^0 \to D^{*+}\pi^-) = \frac{G_F^2|\vec{q}|^3_{D^*\pi}}{4\pi}|V_{ud}^*V_{cb}|^2\,|a_1(D^*\pi)|^2 f_\pi^2 A_0^2(m_\pi^2)\,, \tag{5.46}$$

Parameter	Value/Range	Parameter	Value/Range
m_{π^+}	0.13957	ρ_D^2	1.185 ± 0.054 [14]
m_ρ	0.77526	$\rho_{D^*}^2$	1.207 ± 0.026 [14]
m_{D^+}	1.869, 61	$\eta_{EW}\mathcal{G}(1)\lvert V_{cb}\rvert$	$(42.65 \pm 1.53) \times 10^{-3}$ [14]
$m_{D^{*+}}$	2.01026	$\eta_{EW}\mathcal{F}(1)\lvert V_{cb}\rvert$	$(35.81 \pm 0.45) \times 10^{-3}$ [14]
$m_{\bar{B}^0}$	5.27958	$R_0(1)$	1.151 ± 0.023 [162, 14]
$\lvert V_{ud}\rvert$	0.974	$R_1(1)$	1.406 ± 0.033 [14]
f_π	0.131	$R_2(1)$	0.853 ± 0.020 [14]
f_ρ	0.216	$\tau_{\bar{B}^0}$	1.519 ps

Table 5.2. – Dimensionful quantities are given in units of 1 GeV except the life time of the B meson. If not otherwise stated the values are taken from the Particle Data Group [158].

$$\Gamma(\bar{B}^0 \to D^+\rho^-) = \frac{G_F^2 |\vec{q}|_{D\rho}^3}{4\pi} |V_{ud}^* V_{cb}|^2 \, |a_1(D\rho)|^2 f_\rho^2 F_+^2(m_\rho^2)\,, \tag{5.47}$$

$$\Gamma(\bar{B}^0 \to D^{*+}\rho^-) = \frac{G_F^2 |\vec{q}|_{D^*\rho}}{16\pi m_B^2} |V_{ud}^* V_{cb}|^2 \, (|H_0|^2 + |H_+|^2 + |H_-|^2)\,, \tag{5.48}$$

where $|\vec{q}|_{HL} = \frac{1}{2m_B}\sqrt{(m_B^2 - m_H^2 - m_L^2)^2 - 4m_H^2 m_L^2}$ is the three-momentum of the H and L mesons and $H_{0,\pm}$ are helicity amplitudes corresponding to the polarization of the vector meson. Both $|\vec{q}|_{HL}$ and $H_{0,\pm}$ are defined in the B meson rest frame. The explicit expression for H_0 reads

$$H_0 = \frac{a_1(D^*\rho) f_\rho}{2m_D^*} \left[(m_B^2 - m_{D^*}^2 - m_\rho^2)(m_B + m_{D^*}) A_1(m_\rho^2) - \frac{4m_B^2 |\vec{q}|_{D^*\rho}^2}{m_B + m_{D^*}} A_2(m_\rho^2) \right]. \tag{5.49}$$

The amplitudes $H_\pm$ are contributions from transversally polarized ρ mesons. They are suppressed with respect to H_0 with $H_\pm/H_0 = \mathcal{O}(m_\rho/m_B)$ and we therefore neglect them in our analysis. For the scalar form factors $F_{0,+}$ and $A_{0,1,2}$ we take the parametrization given in [159–161] and describe them by normalization factors and a slope function ρ, which are $\eta_{EW}\mathcal{G}(1)$ ($\eta_{EW}\mathcal{F}(1)$), $R_1(1)$ ($R_{0,2}(1)$) and ρ_D (ρ_{D^*}) in the case of the $B \to D(D^*)$ transition[3]. For performing the error analyses we neglect any correlations between these parameters but rather perform a conservative error estimate. The uncertainties taking into account these correlations are expected to be smaller and will be included in a forthcoming analysis [E].

We evaluate the BRs for the specific input parameters given in Tab. 5.2. The meson masses, the B-meson life time and $|V_{ud}|$ are well known and their uncertainties are below the accuracy of our result. We do not use any specific value for $|V_{cb}|$ but rather take values for the combinations $\eta_{EW}\mathcal{G}(1)|V_{cb}|$ and $\eta_{EW}\mathcal{F}(1)|V_{cb}|$, which have been determined from

[3]The one-parameter functions that describe the form factors include only short-distance and $1/m_b$ corrections to the heavy-quark limit. Thus, to obtain a full NNLO result for the BRs the order α_s^2, α_s/m_b and $1/m_b^2$ should be includes as well, which have not yet been worked out. The uncertainties arising due to these corrections are not accounted for in the uncertainties of the slope and the normalization.

Decay	LO	NLO	NNLO	Experiment
$\mathrm{BR}(\bar{B}^0 \to D^+\pi^-)$	$3.63^{+0.42}_{-0.38}$	$3.84^{+0.43}_{-0.41}$	$3.97^{+0.43}_{-0.41}$	2.68 ± 0.13
$\mathrm{BR}(\bar{B}^0 \to D^{*+}\pi^-)$	$3.19^{+0.24}_{-0.20}$	$3.36^{+0.25}_{-0.22}$	$3.49^{+0.22}_{-0.21}$	2.76 ± 0.13
$\mathrm{BR}(\bar{B}^0 \to D^+\rho^-)$	$9.50^{+1.06}_{-0.96}$	$10.06^{+1.07}_{-1.05}$	$10.41^{+1.08}_{-1.06}$	7.8 ± 1.3
$\mathrm{BR}(\bar{B}^0 \to D^{*+}\rho^-)$	$8.45^{+0.56}_{-0.45}$	$8.91^{+0.53}_{-0.50}$	$9.23^{+0.48}_{-0.49}$	6.8 ± 0.9

Table 5.3. – BRs for the decays $\bar{B}^0 \to D^{(*+)}L^-$ in units of 10^{-3}. The experimental values are taken from [158].

exclusive semi-leptonic decays. The results for the BRs up to NNLO accuracy are given in Tab. 5.3. We find that the BRs rise from LO to NNLO which is due to the increasing of the perturbative amplitude a_1 with higher order in the perturbative expansion. The calculated observables are about $20 - 30\%$ larger than experimental BRs and show a tension at the level of 2-3 σ. We will comment on this in Sec. 5.5. Next, we test the framework of QCDF by comparing non-leptonic and semi-leptonic decay rates.

5.4. Factorization Tests

We have seen in the end of Sec. 5.2 that the calculated NNLO amplitudes a_1 for the decays $\bar{B}^0 \to D^{*+}L^-$ are quasi-universal. In the following, we investigate whether also experimental data points towards a quasi-universal value a_1 in these decay channels. We follow [27] and probe the quasi-universality of a_1 by taking ratios of non-leptonic and semi-leptonic decay rates.

5.4.1. Ratios of Non-leptonic Decay Rates

We consider the following ratios of non-leptonic decay rates

$$\frac{\Gamma(\bar{B}^0 \to D^+\pi^-)}{\Gamma(\bar{B}^0 \to D^{*+}\pi^-)} = \frac{(m_B^2 - m_D^2)^2 |\vec{q}|_{D\pi}}{4m_B^2 |\vec{q}|^3_{D^*\pi}} \left(\frac{F_0(m_\pi^2)}{A_0(m_\pi^2)}\right)^2 \frac{|a_1(D\pi)|^2}{|a_1(D^*\pi)|^2}\,, \tag{5.50}$$

$$\frac{\Gamma(\bar{B}^0 \to D^+\rho^-)}{\Gamma(\bar{B}^0 \to D^+\pi^-)} = \frac{4m_B^2 |\vec{q}|^3_{D\rho}}{(m_B^2 - m_D^2)^2 |\vec{q}|_{D\pi}} \frac{f_\rho^2}{f_\pi^2} \left(\frac{F_+(m_\rho^2)}{F_0(m_\pi^2)}\right)^2 \frac{|a_1(D\rho)|^2}{|a_1(D\pi)|^2}\,. \tag{5.51}$$

For their evaluation we use the values for the BRs give in Tab. 5.3 taking into account that the B-meson life time drops out in the ratios. The results are presented in Tab. 5.4. We find that the LO/NLO/NNLO and experimental values are in good agreement within the given uncertainties. Moreover, taking the values for the experimental decay rates as input Eqs. (5.50) and (5.51) directly probe the experimentally determined ratios of different a_1. The ratio of $\Gamma(\bar{B}^0 \to D^+\pi^-)$ and $\Gamma(\bar{B}^0 \to D^{*+}\pi^-)$ is sensitive to the differences in a_1 given in Eqs. (5.39) and (5.40). In contrast, the ratio of $\Gamma(\bar{B}^0 \to D^+\pi^-)$ and $\Gamma(\bar{B}^0 \to D^+\rho^-)$ is sensitive to difference in the LCDAs of the pion and the ρ meson which only enters at the

Decay	LO	NLO	NNLO	Experiment
$\Gamma(\bar{B}^0 \to D^+\pi^-)/\Gamma(\bar{B}^0 \to D^{*+}\pi^-)$	$1.14^{+0.22}_{-0.19}$	$1.14^{+0.22}_{-0.19}$	$1.14^{+0.20}_{-0.18}$	$0.97^{+0.10}_{-0.09}$
$\Gamma(\bar{B}^0 \to D^+\rho^-)/\Gamma(\bar{B}^0 \to D^+\pi^-)$	$2.62^{+0.63}_{-0.51}$	$2.62^{+0.63}_{-0.51}$	$2.62^{+0.61}_{-0.49}$	$2.93^{+0.66}_{-0.60}$

Table 5.4. – Ratios of non-leptonic decay rates.

second Gegenbauer moment and is therefore expected to be small. We obtain the following results

$$\frac{|a_1(D\pi)|}{|a_1(D^*\pi)|}\frac{F_0(m_\pi^2)}{A_0(m_\pi^2)} = 0.95^{+0.05}_{-0.04}\,, \tag{5.52}$$

$$\frac{|a_1(D\rho)|}{|a_1(D\pi)|}\frac{F_+(m_\rho^2)}{F_0(m_\pi^2)} = 1.09 \pm 0.12\,. \tag{5.53}$$

Considering that the ratio of the form factors $F_+(m_\pi^2)$ ($F_+(m_\rho^2)$) and $A_0(m_\pi^2)$ ($F_0(m_\pi^2)$) numerically deviate from one only at the percentage level, we find no evidence for deviations from naive factorization within the given errors. Next, we consider ratios of non-leptonic and semi-leptonic decay rates.

5.4.2. Ratios of Non-leptonic and Semi-leptonic Decay Rates

Ratios of non-leptonic decay rates and the corresponding differential rates of semi-leptonic decays evaluated at the same momentum transfer $q^2 = m_L^2$ provide another possibility to test factorization as they directly probe the magnitude of the perturbative amplitude a_1 [163]. They are given by the following expression [164]

$$R_L^{(*)} = \frac{\Gamma(\bar{B}^0 \to D^{(*)}L^-)}{d\Gamma(\bar{B}^0 \to D^{(*)}l^-\bar{\nu})/dq^2|_{q^2=m_L^2}} = 6\pi^2|V_{ud}|^2 f_L^2 |a_1(D^{(*)}L)|^2 X_P\,. \tag{5.54}$$

The right hand side of this equation is true assuming that factorization holds and X_P deviates from 1 below the precent level. The experimental decay rates are obtained from the branching ratios given in Tab. 5.3. In order to obtain the differential rates at $q^2 = m_L^2$ we take the parametrization for the form factors given in [159] in terms of a normalization and a slope function. The form factors are written in the variable $\omega = v_B \cdot v_{D^{(*)}} = (m_B^2 + m_{D^{(*)}}^2 - q^2)/(2m_B m_{D^{(*)}})$, where v_B and $v_{D^{(*)}}$ are the four-velocities of the B and $D^{(*)}$ meson, respectively, and can be related to q^2 via the transformation

$$\frac{d\Gamma}{dq^2} = \frac{1}{2m_B m_{D^{(*)}}}\frac{d\Gamma}{d\omega}\,. \tag{5.55}$$

For the slope functions and the normalizations including $|V_{cd}|$ we use the input values given in Tab. 5.2 in the previous section.

The preliminary results for $R_L^{(*)}$ and $|a_1(D^{(*)+}L^-)|$ are presented in Tab. 5.5. We find that the experimentally determined values for the magnitude of a_1 lie below 1, the value for naive

Decay	$R_L^{(*)}$	$\lvert a_1\rvert$
$\bar{B}^0 \to D^+\pi^-$	$0.75^{+0.09}_{-0.08}$	0.88 ± 0.05
$\bar{B}^0 \to D^{*+}\pi^-$	0.89 ± 0.06	0.96 ± 0.02
$\bar{B}^0 \to D^+\rho^-$	$2.26^{+0.45}_{-0.44}$	$0.91^{+0.08}_{-0.09}$
$\bar{B}^0 \to D^{*+}\rho^-$	1.96 ± 0.27	0.86 ± 0.06

Table 5.5. – Preliminary results for the non-leptonic to semi-leptonic ratios $R_L^{(*)}$ and for the experimentally extracted values for $|a_1(D^{(*)+}L^-)|$.

factorization, favoring a central value $|a_1| \simeq 0.94$, which we obtain as the mean of the central values of Tab. 5.5. Moreover, the experimentally predicted amplitudes a_1 show a tension of 4-5 σ compared to the NNLO absolute value $|a_1^{\text{NNLO}}(D^{(*)+}L^-)| = 1.07 \pm 0.01$, except for $|a_1(D^+\rho^-)|$ which has rather large uncertainties. We note, however, at this point that these results are still preliminary. The values given in Tab. 5.5 will be updated in a forthcoming publication [E]. We summarize and discuss our results in the next section.

5.5. Summary and Discussion

We have evaluated the NNLO vertex corrections to the colour-allowed tree-topology of the decays $\bar{B}^0 \to D^{(*)+}L^-$ with L being π or ρ. The final result is given by a perturbative contribution a_1, which in naive factorization has the value 1. We find that our NNLO results for a_1, given in Eqs. (5.39) and (5.40), are close to one but have a small non-zero imaginary part. In comparison to the NLO results, which have been calculated in [27], the real parts have increased by 2%, whereas the imaginary parts obtain a contribution which is even larger than the NLO imaginary parts themselves. Moreover, a_1 only mildly depends on the ratio of the heavy-quark masses $z_c = m_c^2/m_b^2$ and variations of z_c within its physical ranges affect the result only at the per mill level. Changes in the second Gegenbauer moments within the given uncertainties do not have any impact on a_1 within the considered accuracy. The dependence on the factorization scale on the other hand yields the largest uncertainties. Nevertheless, for the real parts we find a significant reduction of the scale dependence compared to the NLO result. This reduction does not occur in the imaginary parts, which is expected as the latter only arise at NLO. In [27] it was further pointed out that to NLO accuracy there is a quasi-universal perturbative correction a_1 for the decays $\bar{B}^0 \to D^{*+}L^-$ in the framework of QCDF. Our results confirm the quasi-universality of a_1 to NNLO accuracy with a value $|a_1| \simeq 1.07 \pm 0.01$.

We have evaluated the BRs to NNLO accuracy and find a 2-3 σ tension compared to the experimental BRs, whose central values are about $20 - 30\%$ smaller. This tension had not been observed in an earlier analysis by Beneke et al [27] in 2000 using NLO BRs (the experimental and NLO BRs can be found in [27] in Tab. 5). Since then, the form factors have improved and increased at around 10% and the uncertainties of the experimental BRs have decreased significantly in most of the decay channels. In addition, the NNLO values of a_1 are slightly increased compared to the NLO values.

Moreover, we have analyzed whether data favors a quasi-universal value of a_1 in the decay channels $\bar{B}^0 \to D^{*+}L^-$ by considering ratios of non-leptonic and semi-leptonic decay rates. The ratios of different a_1 extracted from non-leptonic rates turn out to be compatible with naive factorization. The preliminary values for a_1 that we obtain from ratios of non-leptonic to semi-leptonic decay rates on the other hand favor a central value $|a_1| \simeq 0.94$, with errors in the individual channels at the 2-10%-level. These two results agree with an analysis performed in 2011 by Fleischer at al [49], which use the same data for the BRs and similar input parameters. From the ratios of non-leptonic to semi-leptonic decay rates they had extracted a central value $|a_1| \simeq 0.95$ for the decays $\bar{B}^0 \to D^{(*)}\pi$ and $\bar{B}^0 \to D^{(*)}K$. The corresponding errors in individual channels are at the 10-20%-level.

As mentioned in Sec. 1.1.2 our results for the perturbative NNLO amplitude and the factorization tests provide a better understanding of power corrections to the factorization formula (1.10). The 2-3 σ tension in the experimental and theoretical BRs indeed gives an indication towards non-negligible power corrections, together with the experimentally extracted favoured central value $|a_1| \simeq 0.94$, which is smaller than the central NNLO value $|a_1| \simeq 1.07$. Given the uncertainties of the BRs and a_1 (see above) the power corrections could be 10-20% in size, which coincides with a numerically estimated value of $\Lambda_{\rm QCD}/m_b$. Moreover, as data points towards a quasi-universality of a_1 and all central values for the NNLO BRs are about $20 - 30\%$ larger than the experimental BRs one could suspect a common mechanism that pushes the power correction in the same direction. This would also be supported by the good agreement of the experimental and theoretical values for the ratios of the non-leptonic decay rates. Additional contributions of similar-sized power corrections could cancel in the ratios.

We remark that still it remains to be clarified to what significance the deviations for the experimentally extracted and the NNLO value for a_1 occur. Moreover, for an interpretation of tensions one should take into account that the HFAG results for the normalizations and form factors given in Tab. 5.2 are global averages of several experimental measurements. The single measurements have different central values and mostly larger uncertainties. In addition, a small uncertainty also arises since the one-parameter functions that describe the form factors are only known to order α_s and $1/m_b$.

Part II.

$\mathrm{B} \to \boldsymbol{\pi\pi\pi}$ in QCD factorization

Chapter 6

Three-body Decays from QCD

We investigate the prospects of a QCD-factorization study for the decay $B^+ \to \pi^+\pi^-\pi^+$. Therefore, we identify different regions in the Dalitz plot where the final-state particles have special kinematic configurations. We claim that these regions can be treated in QCDF with appropriate non-perturbative input, which includes generalized form factors and generalized distribution amplitudes. We construct corresponding factorization formulae and give the definitions for the $B \to \pi\pi$ form factor and the two-pion distribution amplitudes. We calculate the three-body amplitude in the central region of the Dalitz plot and analyse it in the limit when moving towards the edges. Moreover, we evaluate the amplitude in the edge and integrate the corresponding differential decay rate in a window around the ρ resonance for a rough estimate of the branching ratios. Finally, we discuss how both descriptions merge to describe the full Dalitz plot, and what we can expect for a physical value of the b-quark mass.

The main results of this chapter are published in [D]. We further remark that the main ideas developed here have been discussed qualitatively by M. Beneke [165] and I. Stewart [166].

6.1. Identifying Regions in the Dalitz Plot

We consider the decay $B^+ \to \pi^+\pi^-\pi^+$, and define the external momenta as

$$B^+(p) \to \pi^+(k_1)\ \pi^-(k_2)\ \pi^+(k_3) \quad \text{with} \quad p = k_1 + k_2 + k_3\ . \tag{6.1}$$

We set the pion masses to zero in the kinematics and thus have

$$p^2 = m_B^2\,, \quad k_i^2 = 0 \quad \text{for} \quad i = 1,2,3\,, \tag{6.2}$$

where m_B is the mass of the B meson. The invariant masses of each pair of particles, normalized to m_B^2, are given by

$$s_{ij} \equiv \frac{2k_i \cdot k_j}{m_B^2} \quad (i \neq j)\,. \tag{6.3}$$

Due to momentum conservation they fulfill the following kinematic constraints

$$s_{12} + s_{13} + s_{23} = 1 \quad \text{and} \quad 0 \leq s_{ij} \leq 1\,. \tag{6.4}$$

The center-of-mass energies $E_i^{\rm CM}$ of any one pion can be expressed in terms of these invariants, and read $E_1^{\rm CM} = m_B(1 - s_{23})/2$, $E_2^{\rm CM} = m_B(1 - s_{13})/2$ and $E_3^{\rm CM} = m_B(1 - s_{12})/2$. Eq. (6.4) fixes one of the invariant masses, e.g. s_{13}, whereas the remaining two are free parameters. The differential decay rate of the three-body decay (6.1) in terms of those two invariants is given by [167]

$$d\Gamma = \frac{1}{32\,(2\pi)^3} m_B |\mathcal{A}|^2 ds_{12} ds_{23}\,, \tag{6.5}$$

where $\mathcal{A} = \mathcal{A}(s_{12}, s_{23})$ is the transition amplitude. A scatter plot $d\Gamma/(ds_{12}ds_{23})$ is known as a Dalitz plot[1]. In the case of massless final-state particles the physical kinematical region in the $s_{12} - s_{23}$ plane is given by a triangle. If $|\mathcal{A}|^2$ is constant the Dalitz plot is uniformly populated, otherwise structures arise due to dynamical effects. Resonances of intermediate two-body states appear as bands, which exhibit a characteristic shape that depends on the type of the resonance (scalar, vector or tensor) [170]. The regions of overlapping resonances yield information on strong and weak phase differences which allow for a study of CP violation [171].

In the case at hand, we encounter two identical particles in the final state and the invariants s_{12} and s_{23} are not distinguishable anymore. Hence, we label the two π^+ according to their CM energies. Choosing $E_1^{\rm CM} < E_3^{\rm CM}$ we find that $s_{12} < s_{23}$ and adopt the notation $s_{12} \equiv s_{+-}^{\rm low}$, $s_{23} \equiv s_{+-}^{\rm high}$ and $s_{13} \equiv s_{++}$. The physical kinematical region in the plane of the invariants $s_{+-}^{\rm low}$ and $s_{+-}^{\rm high}$ shown in Fig. 6.1 is then given by a triangle, where the region with $s_{+-}^{\rm high} < s_{+-}^{\rm low}$ is unpopulated by definition.

We distinguish three regions in the Dalitz plot where the final-state particles have special kinematical configurations:

I. "Mercedes Star" Configuration: This configuration occurs in the central region of the Dalitz plot, where all the invariant masses are roughly the same and of $\mathcal{O}(m_B)$

$$\textbf{Region I}: \quad s_{++} \sim s_{+-}^{\rm low} \sim s_{+-}^{\rm high} \sim 1/3\,, \tag{6.6}$$

corresponding to the kinematical situation where all three pions have a large energy in the B-meson rest frame and none of the pions moves collinearly to any other.

II. Collinear Decay Products: This corresponds to regions of the Dalitz plot where one invariant mass is small and the other two are large. The kinematic configuration is such that two pions are collinear, generating a small invariant mass recoiling against the third pion. In our case there are two such regions:

$$\textbf{Region IIa}: \quad s_{++} \sim 0\,, \quad s_{+-}^{\rm low} \sim s_{+-}^{\rm high} \sim 1/2\,, \tag{6.7}$$

[1]This visualization method goes back to Dalitz [168] who employed it for the study of the $\theta - \tau$ puzzle in 1953 and shortly afterwards was extended to a relativistic formulation by Fabri [169]. The latter version is commonly used in the current applications of Dalitz plot analyses.

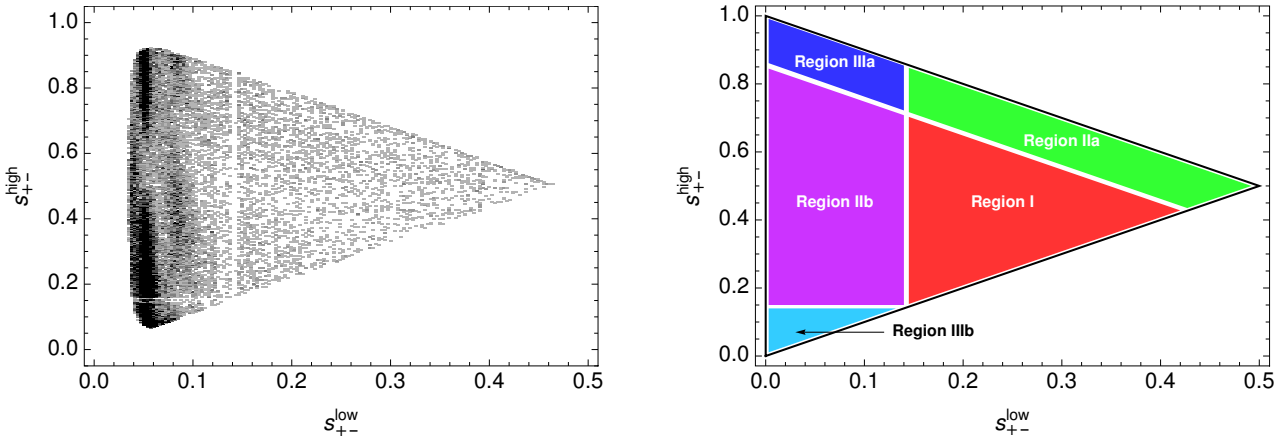

Figure 6.1. – Left: Dalitz plot distribution for $B^+ \to \pi^+\pi^-\pi^+$ from [19]. Right: Dalitz plot divided into the different regions with special kinematical configurations: I - Mercedes Star configuration, IIa,IIb - Two collinear pions, IIIa,b - One soft pion.

which is the region where the two π^+ move collinearly, recoiling against the π^-, and

$$\textbf{Region IIb :} \quad s_{+-}^{\rm low} \sim 0\,, \quad s_{++} \sim s_{+-}^{\rm high} \sim 1/2\,, \tag{6.8}$$

where the π^- and one π^+ move collinearly, recoiling against the second π^+.

III. One Soft Decay Product: The regions of the Dalitz plot where two invariant masses are small and one is large correspond to kinematical configurations where one pion is soft and the other two are fast and back-to-back. In our case there are two such regions:

$$\textbf{Region IIIa :} \quad s_{++} \sim s_{+-}^{\rm low} \sim 0\,, \quad s_{+-}^{\rm high} \sim 1\,, \tag{6.9}$$

which is the region where one π^+ is soft, and

$$\textbf{Region IIIb :} \quad s_{+-}^{\rm high} \sim s_{+-}^{\rm low} \sim 0\,, \quad s_{++} \sim 1\,, \tag{6.10}$$

where the π^- is soft.

The different regions are shown in the right-hand panel in Fig. 6.1. Next, we discuss the factorization properties that are expected to apply in the different regions.

6.2. Factorization Formula

We have briefly discussed the factorization properties of three-body decays in Sec. 1.1.3, which depend on the invariant masses of the final-state mesons. In the cases at hand at least one particle, which we denote by π^k in the following, has[2] $E_k^{\rm CM} = \mathcal{O}(m_B)$. We take π^k as the fastest particle in the following. The other two particles constitute a system, or a "compound

[2]As $m_B/\sqrt{3} \gg \Lambda_{\rm QCD}$ where $\Lambda_{\rm QCD}$ is the typical hadronic scale we adopt the power counting $m_B/\sqrt{3} \sim \mathcal{O}(m_B)$.

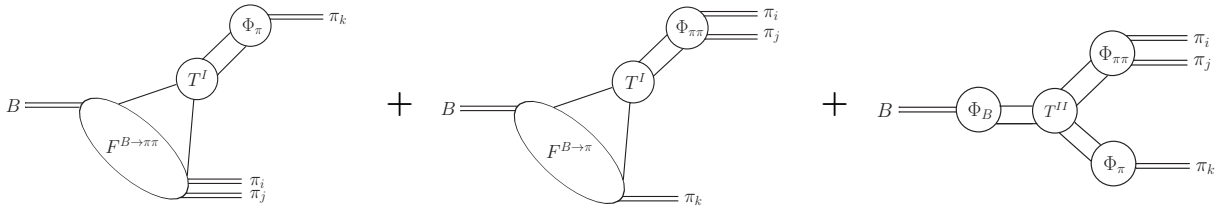

Figure 6.2. – Factorization formula in the edges (Regions II and III)

object", with invariant mass $s_{ij}\, m_B^2$ with $i, j \neq k$, moving in the direction opposite to π^k with large energy but not necessarily large momentum. With $s_{ij} = 1 - 2E_k^{\rm CM}/m_B$ one finds $0 < s_{ij} < 1/3$. From the point of view of power counting this compound object can be light ($s_{ij} \sim \Lambda_{\rm QCD}^2/m_B^2$), or heavy ($s_{ij} \sim 1$), or anything in between. We describe the $(\pi^i\pi^j)$ sub-system in terms of generalized form factors or generalized distribution amplitudes. Depending on the size of s_{ij} we adopt the factorization formulae of two-body decays (see Sec. 1.1.1) to describe the three-body decay amplitude in the heavy-quark limit. The regions II and III are part of the "edge" of the Dalitz plot, where $s_{ij} \ll 1$. This is where the physics of rescattering and resonance formation in the $(\pi^i\pi^j)$ sub-system is mostly contained. The central region of the Dalitz plot (Region I) on the other hand is expected to be dominated by standard QCD factorization. We start by considering the decay amplitude at the edges (Region II and III).

Factorization in the Edges (Regions II and III)

If s_{ij} is small, the three-body decay resembles a two-body decay into two light hadrons, the only difference being that one of the final light hadrons is replaced by the (light) system $(\pi^i\pi^j)$. The QCD-factorization ansatz takes then the following form (cf. Eq. (1.2))

$$\begin{aligned}\langle\pi^i\pi^j\pi^k|\mathcal{Q}_a|B\rangle_{s_{ij}\ll 1} &= T_a^I \otimes F^{B\to\pi^k} \otimes \Phi_{\pi^i\pi^j} + T_a^I \otimes F^{B\to\pi^i\pi^j} \otimes \Phi_{\pi^k} \\ &+ T_a^{II} \otimes \Phi_B \otimes \Phi_{\pi^k} \otimes \Phi_{\pi^i\pi^j}\ . \end{aligned} \tag{6.11}$$

Here $F^{B\to\pi\pi}$ and $\Phi_{\pi\pi}$ denote generalized $B \to \pi\pi$ form factor and the two-pion light-cone distribution amplitude (2π-LCDA) to be defined more precisely in Sec. 6.3. The expressions for the $F^{B\to\pi}$ vector form factor and the single-pion LCDA Φ_π are given in Sec. 1.1.1, and the hard scattering kernels T^I and T^{II} are perturbatively calculable in an expansion in the strong coupling α_s (cf. Eq. (1.9)). The operators $\mathcal{Q}_a$ are defined in Sec. 1.3. A schematic illustration of the factorization formula is given in Fig. 6.2.

The region $s_{ij} \ll 1$ of the Dalitz plot corresponds either to the kinematic configuration II or III in Sec. 6.1. However, in the limit where one pion is soft and the other two decay back-to-back (Region III) the 2π-LCDA reduces to a single-pion LCDA [60]. To what extent this configuration is included in Eq. (6.11) needs to be investigated in more detail. As this exceeds the scope of this thesis we will not consider Region III any longer.

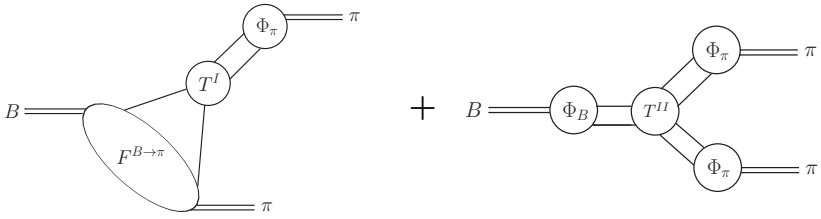

Figure 6.3. – Factorization of the $F^{B\to\pi\pi}$ form factor for a large invariant mass.

Factorization at the Center (Region I)

In the center of the Dalitz plot, where s_{ij} is large[3], the three-body decay resembles a two-body decay to one heavy and one light meson, e.g. $B \to D\pi$. If the spectator quark goes to either π^i or π^j, then the factorization theorem for a two-body decay to one heavy and one light meson Eq. (1.3) can be applied directly to the case at hand, resulting in a convolution of a generalized form factor $F^{B\to\pi\pi}(s_{ij})$ and a regular LCDA Φ_π. In addition, at large s_{ij} the $F^{B\to\pi\pi}$ form factor factorizes further[4]

$$F^{B\to\pi\pi}|_{s_{ij}\sim 1/3} \;=\; T^I \otimes F^{B\to\pi} \otimes \Phi_\pi + T^{II} \otimes \Phi_B \otimes \Phi_\pi \otimes \Phi_\pi \;. \tag{6.12}$$

This factorization is visualized schematically in Fig. 6.3. The situation in which the spectator goes to π^k is more subtle. We know that the corresponding $B \to D\pi$ analogue does not factorize. This is because the D meson sits at rest interfering with the $B \to \pi$ transition, and the idea of color transparency does not apply, as it was discussed in detail in Sec. 1.1.2. Therefore in the resonant contributions $B \to H[\to \pi^i\pi^j]\pi^k$ where H represents the heavy meson the description of the H resonance within the generalized LCDA $\Phi_{\pi\pi}(s_{ij})$ cannot be argued on the basis of present factorization theorems. One may now wonder if such decays pose a difficult background to $B \to \pi\pi\pi$. However, since the D meson in our example decays weakly, it is a very narrow resonance in the $(\pi\pi)$ invariant mass distribution of the $B \to \pi\pi\pi$ decay. Thus it can be described separately with good precision, or even directly removed from the measurement without introducing large systematic effects.

A different situation arises in the case in which H is a genuine QCD resonance, decaying strongly into $\pi^i\pi^j$. The masses m_R of these resonances however do not scale with the heavy B-meson mass and hence the width of the Region II scales as m_R/m_B, showing the dominance of Region I in the infinite mass limit. Therefore (in the heavy-mass limit) the decay $B \to \pi^i\pi^j\pi^k$ at large $s_{ij} \sim 1/3$ is purely non-resonant, and involves two fast light mesons π^i, π^j flying away with large invariant mass. The $(\pi^i\pi^j)$ system can then be described in terms of Φ_{π^i} and Φ_{π^j}, which factorize from the $F^{B\to\pi^k}$ form factor. This picture can be related to the perturbative limit of 2π-LCDAs, where $\Phi_{\pi_i\pi_j} \sim \Phi_{\pi_i} \otimes \Phi_{\pi_j}$ [172].

In addition, there are non-factorizable contributions to $B \to [\pi^i\pi^j]\pi^k$, which are power suppressed for $s_{ij} \ll 1$, but are of leading power for $s_{ij} \sim 1/3$. However, when $s_{ij} \sim 1/3$

[3]We recall that, by construction, $s_{ij} < 1/3$.

[4]In the calculation of the amplitude in the central region (see Sec. 6.4) we have shown that factorization applies for the leading order form factor in an expansion in the strong coupling α_s. The next-to-leading order proof is in preparation [70].

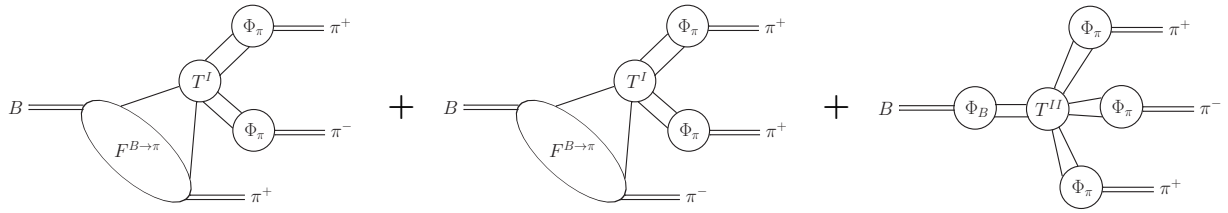

Figure 6.4. – Factorization formula in the center (Region I)

these contributions are perturbative and thus further factorize (see Sec. 6.6 for more details). All in all, for large s_{ij} the factorization formula reads:

$$\begin{aligned}\langle\pi^+\pi^-\pi^+|\mathcal{O}_i|B\rangle_{s_{ij}\sim 1/3} &= T^I\otimes F^{B\to\pi^+}\otimes\Phi_{\pi^-}\otimes\Phi_{\pi^+}+T^I\otimes F^{B\to\pi^-}\otimes\Phi_{\pi^+}\otimes\Phi_{\pi^+}\\ &+ T^{II}\otimes\Phi_B\otimes\Phi_{\pi^+}\otimes\Phi_{\pi^-}\otimes\Phi_{\pi^+}\ .\end{aligned}\tag{6.13}$$

A graphic visualization is given in Fig. 6.4.

The factorization formulae Eqs. (6.11) and (6.13) yield the transition amplitudes for certain regions in the Dalitz plot. We will evaluate these to leading order in the strong coupling in the sections 6.4 and 6.5. Next, we give the definitions for the generalized form factors and distributions amplitudes.

6.3. Generalized Form Factors and Distribution Amplitudes

Generalized form factors and distribution amplitudes have been studied in the literature, the former in the context of semi-leptonic B decays [57], and the latter in connection with two-meson electroproduction [59] or semi-leptonic τ decays [58] (see also [60–68]). Here, we present the definitions that we use in the evaluation of the transition amplitude to leading order in m_B and in the strong coupling α_s in Sec. 6.5.

6.3.1. Two-pion Distribution Amplitude

To leading twist, the 2π-LCDA for a $(\pi^+\pi^-)$ system is formally given by the non-local matrix element [59, 60, 62]

$$S^q_{\alpha\beta}(z,k_1,k_2)=\frac{k_{12}^+}{4\pi}\int dx^- e^{-iz(k_{12}^+x^-)/2}\langle\pi^+(k_1)\pi^-(k_2)|\bar q_\beta(x)[x,0]q_\alpha(0)|0\rangle_{x^+=x_\perp=0}\,,\tag{6.14}$$

where α, β are Dirac indices, $q=u,d$, and $[x,0]$ is a Wilson line. We take $k_{12}=k_1+k_2$ and define two light-like vectors $n_\pm^\mu=(1,0,0,\pm1)$, which obey $n_\pm^2=0$ and $n_+n_-=2$, such that

$$k_{12}^\mu=\frac{k_{12}^+}{2}n_+^\mu+\frac{k_{12}^-}{2}n_-^\mu\quad\text{and}\quad x^\mu=\frac{x^+}{2}n_+^\mu+\frac{x^-}{2}n_-^\mu+x_\perp^\mu\ .\tag{6.15}$$

Moreover, in the limit $k_{12}^2 \to 0$ one has $k_{12}^- \to 0$. The variable z is the fraction of the momentum k_{12} carried by the quark q. Note that due to isospin and charge conservation the operator $\bar{q}_\beta q_\alpha$ cannot create two equally-charged pions and hence the leading-twist distribution amplitude for the $(\pi^+\pi^+)$-system is zero.

The Lorentz decomposition of the matrices $S^q_{\alpha\beta}$ consistent with parity invariance, keeping only terms that contribute at lowest twist, is given by[5]

$$S^q_{\alpha\beta} = \frac{1}{4}\Phi^q_\parallel(z,\zeta,k_{12}^2)\,\not{k}_{12} + \Phi^q_\perp(z,\zeta,k_{12}^2)\,\sigma_{\mu\nu}k_1^\mu k_2^\nu \;, \tag{6.16}$$

which defines the vector ($\Phi_\parallel$) and tensor ($\Phi_\perp$) 2π-LCDAs. The variable $\zeta = k_1^+/k_{12}^+$ is the light-cone momentum fraction of the π^+. In terms of invariants, we have

$$k_{12}^2 = m_B^2\, s_{12} \;, \qquad \zeta = \frac{s_{13}}{1-s_{12}} \;. \tag{6.17}$$

Isosinglet ($\Phi^{\mathbf{0}} \equiv \frac{1}{2}[\Phi^{\mathbf{u}} + \Phi^{\mathbf{d}}]$) and isovector ($\Phi^{\mathbf{1}} \equiv \frac{1}{2}[\Phi^{\mathbf{u}} - \Phi^{\mathbf{d}}]$) 2π-LCDAs have been discussed in the literature (e.g. Refs [60, 62]). The $I = 1$ 2π-LCDAs are normalized as [60]

$$\int dz\, \Phi^{\mathbf{1}}_\parallel(z,\zeta,s) \;=\; (2\zeta-1)F_\pi(s) \;, \tag{6.18}$$

where $F_\pi(s)$ is the vector time-like form factor of the pion. The latter satisfies the normalization $F_\pi(0) = 1$. Isospin and C-parity invariance imply that the corresponding integral is zero for the isosinglet component [60]

$$\int dz\, \Phi_\parallel(z,\zeta,s) \;=\; 0\,. \tag{6.19}$$

We do not display the relations for the tensor distribution $\Phi_\perp$ here, as they do not contribute to leading order in α_s.

The renormalization group equation (RGE) for the 2π-LCDAs is given at leading order in α_s by the ERBL evolution equation [173, 50]. Hence, the z-dependence of the 2π-LCDAs can be expanded in Gegenbauer polynomials $C_n^{3/2}$. The ζ-dependence is additionally expanded in Legendre polynomials P_ℓ and one obtains

$$\Phi^{\mathbf{0}}_\parallel(z,\zeta,s;\mu) = 6z(1-z)\sum_{\substack{n=1\\ \text{odd}}}^{\infty}\sum_{\substack{\ell=0\\ \text{even}}}^{n+1} B_{n\ell}(s,\mu)C_n^{3/2}(2z-1)P_\ell(2\zeta-1)\,, \tag{6.20}$$

$$\Phi^{\mathbf{1}}_\parallel(z,\zeta,s;\mu) = 6z(1-z)\sum_{\substack{n=0\\ \text{even}}}^{\infty}\sum_{\substack{\ell=1\\ \text{odd}}}^{n+1} B_{n\ell}(s,\mu)C_n^{3/2}(2z-1)P_\ell(2\zeta-1)\,, \tag{6.21}$$

where we have made explicit the dependence on the renormalization scale μ. The normalization conditions lead to $B_{01}(s) = F_\pi(s)$. In the case of the isovector 2π-LCDA the coefficients

[5] This definition of $\Phi_\parallel$ agrees with reference [60] (up to the isospin decomposition). However the definition for $\Phi_\perp$ differs from that in [60] by an overall factor, which we do not address here because to the order considered $\Phi_\perp$ will not appear in the amplitude.

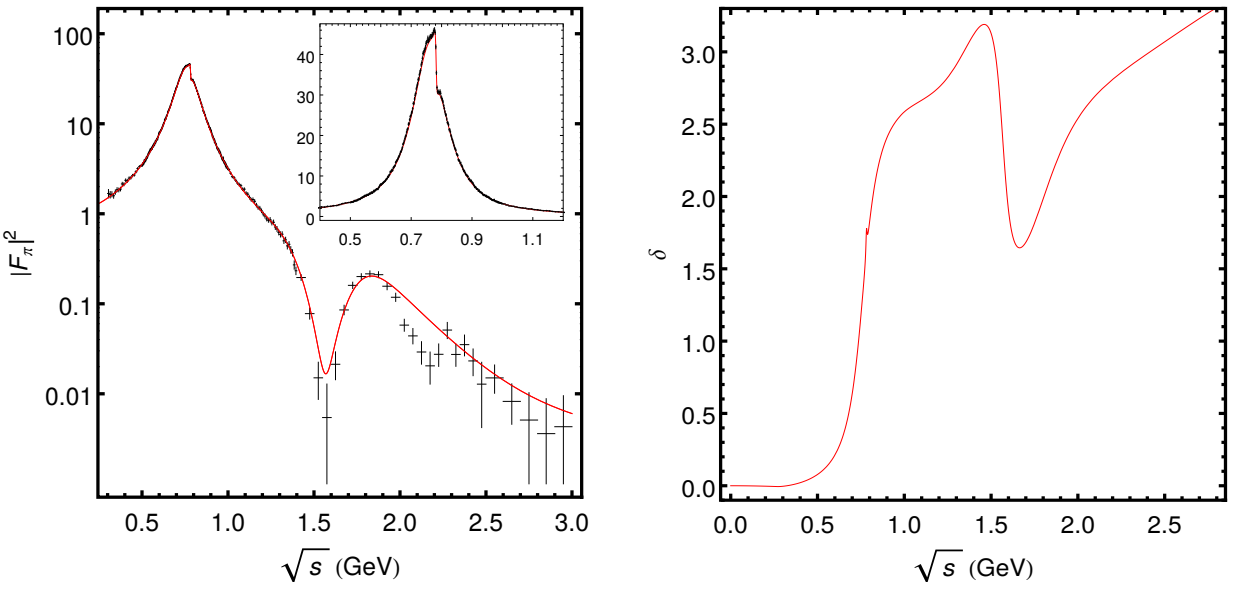

Figure 6.5. – Pion form factor $F_\pi(s) = |F_\pi| e^{i\delta}$ in the time-like region [174, 175].

$B_{n\ell}$ are multiplicatively renormalizable to leading order and the RGE is the same as for the single-pion LCDA (see Eq. (5.30) in Sec. 5.2.1). The asymptotic form of the isovector 2π-LCDAs is then given by

$$\Phi_\parallel^{\mathbf{1}}(z,\zeta,s;\mu) \overset{\mu\to\infty}{\longrightarrow} 6z(1-z)(2\zeta-1)F_\pi(s)\,. \tag{6.22}$$

The case of the isoscalar 2π-LCDA is more complicated since it mixes with gluon 2π-LCDAs. As a consequence, $\Phi_\parallel^{\mathbf{0}}$ in the asymptotic limit is described by coefficients which belong to the Belinfante-improved energy-momentum tensor defined in [61]. In order to see how these coefficients reduce to known form factors, a deeper analysis is required which would exceed the scope of this thesis. Thus, we disregard the isoscalar 2π-LCDAs in the numerical analysis later. We will find that this does not affect the final conclusions in Sec. 6.6.

We will see in Sec. 6.5 that at leading order the hard kernel $T(z)$ with which $\Phi(z,\zeta,s)$ is convoluted in the $B \to \pi\pi\pi$ amplitude does not depend on the momentum fraction z, so the amplitude depends only on the local form factor $F_\pi(s)$, just as the leading contribution in $B \to \pi\pi$ depends only on f_π. The vector form factor $F_\pi(s)$ in the time-like region ($s > 0$) can be obtained from measurements of the process $e^+e^- \to \pi^+\pi^-(\gamma)$ [174][6] – see Fig. 6.5. We employ here the fit parametrization of [175], which is consistent with general principles of QCD at low energies, and covers the energy range of interest, including the relevant resonances in that range. The particular choice of parametrization is not very important for the absolute value $|F_\pi(s)|$, where a good fit to the data is enough (see Fig. 6.5), but it is important for the phase, where data is not so precise. A thorough analysis of the phase of $F_\pi(s)$ and its impact in $B \to \pi\pi\pi$ is beyond the scope of this thesis, but it becomes a crucial issue as soon as one attempts to describe CP asymmetries. We leave this for future work.

[6] For simplicity we use only the latest Babar data, but see also Refs. [176–180, 66, 181].

6.3.2. Generalized Form Factor

The second nonperturbative input is the $B \to \pi\pi$ form factor, which has been discussed already in the context of $B \to \pi\pi\ell\nu$ decays in [57]. We consider the generic form factor

$$F_{\alpha\beta}(k_1, k_2, k_3) \equiv \langle \pi^+(k_1)\pi^-(k_2)|\, \bar{b}_\beta\, u_\alpha |B^+(p)\rangle\,, \tag{6.23}$$

where α, β are Dirac indices. The most general Lorentz decomposition consistent with parity invariance is given in terms of four independent form factors

$$F = F_t \frac{1}{4\sqrt{k_3^2}} \not{k}_3 \gamma_5 + F_2\, \not{k}_{(0)} \gamma_5 + F_3\, \bar{\not{k}}_{(\|)} \gamma_5 + F_4\, \epsilon_{\alpha\beta\gamma\mu} k_1^\alpha k_2^\beta k_3^\gamma \gamma^\mu + \frac{\sqrt{k_3^2}}{4(m_b + m_u)} F_t \gamma_5\,. \tag{6.24}$$

The momentum k_3 is almost time-like ($k_3^2 = m_\pi^2 \simeq 0$) and $k_{(0)}, k_{(\|)}$ are (space-like) vectors orthogonal to k_3 and built from $k_{1,2,3}$. We find that in the leading order $B^+ \to \pi^+\pi^-\pi^+$ amplitude only the time-like form factor F_t contributes (see Sec. 6.5). Its definition coincides with [57]. Note that for similar arguments as in the case of the 2π-LCDA the $F^{B\to\pi\pi}$ form factor for the doubly-charged $(\pi^+\pi^+)$-system is zero.

In order to be able to make a quantitative prediction, we can relate time-like form factor F_t to the 2π-LCDAs via a light-cone sum rule [69]

$$F_t(\zeta, s_{12}) = \frac{m_b^2}{\sqrt{2}\hat{f}_B m_\pi} \int_{u_0}^1 \frac{dz}{z}\, \exp\left[\frac{(1 + s_{12}\bar{z})m_B^2}{M^2} - \frac{m_b^2}{zM^2}\right]\, \Phi_\|(z, \zeta, s_{12})\,. \tag{6.25}$$

Here, $\hat{f}_B$ is the B-meson decay constant extracted from a corresponding sum-rule, which is correlated to the Borel parameter M and to the threshold parameter u_0. These three parameters must be determined simultaneously with the condition that the physical decay constant and form factor are independent of M and u_0. We remark that Eq. (6.25) is a preliminary result. More details will be presented in the forthcoming publication [69]. While we do not attempt to perform a full error analysis here, we note that the values $\hat{f}_B \simeq 0.316$, $u_0 \simeq 0.6$ and $M^2 \simeq 10\ \text{GeV}^2$ satisfy this correlation approximately. F_t can be further decomposed into an isoscalar and isovector component

$$F_t = F_t^0 + F_t^1\,. \tag{6.26}$$

The convolution with $\Phi_\|^0$ in the sum-rule for F_t^0 is in general not zero because the integrand is not even in z. As we do not know the asymptotic limit for $\Phi_\|^0$ in terms of known form factors (see Sec. 6.3.1) we will neglect this contribution in the numerical analysis later but note that this will not affect the final conclusions in Sec. 6.6. For the isovector component we take $\Phi_\|^1$ in the asymptotic limit, given by Eq. (6.22), and obtain

$$F_t^{\mathbf{1}}(\zeta, s_{12}) = \frac{3\sqrt{2}m_b^2(2\zeta - 1)F_\pi(s_{12})}{\hat{f}_B m_\pi} \int_{u_0}^1 du\ \bar{u}\ \exp\left[\frac{(1 + s_{12}\bar{u})m_B^2}{M^2} - \frac{m_b^2}{uM^2}\right]\,. \tag{6.27}$$

With Eqs. (6.18), (6.19), (6.24) and (6.27) we have finally specified the nonperturbative inputs that are needed in the evaluation of the leading order in Λ_{QCD}/m_B and α_s amplitude in Region II of the Dalitz plot (see Sec. 6.5). We proceed with the calculation of the amplitude in the central region of the Dalitz plot.

6.4. The Central Region of the Dalitz Plot

We have argued in Sec. 6.2 that for a very heavy B meson, the central region of the Dalitz plot (Region I) is dominant since the width of the edges scales as m_R/m_B. The condition $m_B^2 s_{ij} \gg \Lambda_{\rm QCD}^2$ is satisfied in most of the Dalitz plot and hence the resonances pile up at the edges. The amplitude is expected to factorize according to Eq. (6.13) which we again display here

$$\begin{aligned}\langle \pi^+\pi^-\pi^+|\mathcal{O}_i|B\rangle_{s_{ij}\sim 1/3} &= T^I \otimes F^{B\to\pi^+} \otimes \Phi_{\pi^-} \otimes \Phi_{\pi^+} + T^I \otimes F^{B\to\pi^-} \otimes \Phi_{\pi^+} \otimes \Phi_{\pi^+} \\ &+ T^{II} \otimes \Phi_B \otimes \Phi_{\pi^+} \otimes \Phi_{\pi^-} \otimes \Phi_{\pi^+} \ . \end{aligned} \tag{6.28}$$

We calculate the hard scattering kernels to leading order in the strong coupling α_s. While the study of α_s^2 corrections[7] is beyond the scope of this analysis, we expect these to be about $\sim 10\%$ relative to the leading color-allowed amplitude, similar to the case of $B \to \pi\pi$ (see e.g. [182]). Below, we present the construction of the leading order Feynman diagrams that contribute to the kernel T^I. We will see that T^{II} only receives corrections which are proportional to α_s^2.

6.4.1. Leading Order Feynman Diagrams

We consider the following product of three fermion lines

$$\left[(\bar q_n)^a_\alpha\,(\Gamma_1)^{ab}_{\alpha\beta}\,b^b_\beta\right]\,\left[(\bar q_j)^c_\gamma\,(\Gamma_2)^{cd}_{\gamma\delta}\,(q_i)^d_\delta\right]\,\left[\bar q^e_\sigma\,(\Gamma_3)^{ef}_{\sigma\tau}\,q^f_\tau\right]\ , \tag{6.29}$$

where the Latin and the Greek letters denote the colour and the spinor indices, respectively. The $(\Gamma_k)^{ab}_{\alpha\beta}$, $k=1,2,3$, can be further decomposed into a Dirac part $(\Gamma_k)_{\alpha\beta}$ where Γ_k is an arbitrary Dirac matrix, and a colour part $\mathcal{C}^{ab}$ that will be addressed later. The $q\bar q$ pair is produced by a gluon that couples to one of the other two fermion lines $[\bar q_n\,\Gamma_1\,b]$ or $[\bar q_i\,\Gamma_2\,q_j]$. The two quarks contribute to the leading-Fock states of two different pions which have a large invariant mass of order m_B. Hence, the gluon as well must have virtuality of order m_B. Considering that there are four possibilities for attaching the gluon to these two lines we have to modify the latter according to one of the following expressions

$$\begin{aligned}&\left[(\bar q_n)^a_\alpha\,(\times)^{aa'}_{\alpha\alpha'}\,(\Gamma_1)^{a'b}_{\alpha'\beta}\,b^b_\beta\right]\ , \quad \left[(\bar q_n)^a_\alpha\,(\Gamma_1)^{ab'}_{\alpha\beta'}\,(\times)^{b'b}_{\beta'\beta}\,b^b_\beta\right]\ , \\ &\left[(\bar q_j)^c_\gamma\,(\times)^{cc'}_{\gamma\gamma'}\,(\Gamma_2)^{c'd}_{\gamma'\delta}\,(q_i)^d_\delta\right]\ , \quad \left[(\bar q_j)^c_\gamma\,(\Gamma_2)^{cd'}_{\gamma\delta'}\,(\times)^{d'd}_{\delta'\delta}\,(q_i)^d_\delta\right]\ . \end{aligned} \tag{6.30}$$

Here, the cross marks the additional Dirac matrices stemming from the gluon insertion. A schematic visualization is given in Fig. 6.6. Note that diagrams where the gluon interaction involves the spectator quark are kinematically forbidden at leading order since the momentum of the spectator quark in the B meson is of order $\Lambda_{\rm QCD}$ and thus, cannot decay into two particles with momentum of order m_B. Hence, we do not obtain a contribution to T^{II} in Eq. (6.28) to leading order[8] in α_s. Next, the fermion lines have to be contracted

[7] The leading order corrections are already proportional to α_s as two of the gluons contributing to the leading-Fock states of the three pions must be produced in gluon-quark-pair production.

[8] Contributions to T^{II} arise at order α_s^2, when there is e.g. an additional hard gluon interacting with the spectator quark.

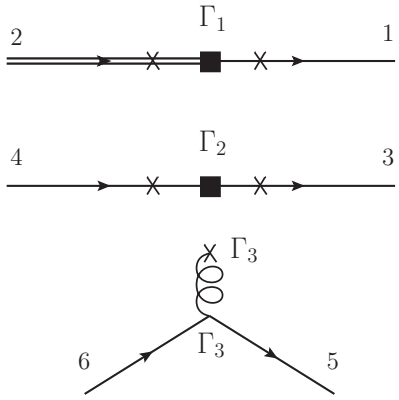

Figure 6.6. – Construction of the LO Feynman diagrams. $(1,2)$, $(3,4)$ and $(5,6)$ represent the fermion lines $(\bar{q}_n \Gamma_1 b)$, $(\bar{q}_i \Gamma_2 q_j)$ and $(\bar{q} \Gamma_3 q)$, respectively. The crosses on the fermion lines mark the four possibilities where the hard gluon from the $q\bar{q}$ pair $(5,6)$ can couple to.

to form bilinears. We assign numbers to each spinor and denote the trivial contraction $[\bar{q}_n \, \Gamma_1 \, b] \; [\bar{q}_j \, \Gamma_2 \, q_i] \; [\bar{q} \, \Gamma_3 \, q]$ - including the corresponding replacement (6.30) - by the number pairs $(1,2)\,(3,4)\,(5,6)$. Note that each of the pairs $(1,2)\,(3,4)\,(5,6)$ has to be a colour singlet and the corresponding colour octet contribution vanishes. Other combinations can be obtained by once or twice applying Fierz identities

$$[\bar{q}_1 A q_2] \; [\bar{q}_3 B q_4] = \frac{1}{4} \sum_m \left[\bar{q}_1 \Gamma^{(m)} \, q_4\right] \; \left[\bar{q}_3 B \Gamma_{(m)} A q_2\right] \; , \tag{6.31}$$

where $\Gamma^{(m)} = \{\mathbf{1},\, \gamma_5,\, \gamma^\rho \,, i\gamma^\rho \gamma_5,\, \sigma^{\rho\tau}/\sqrt{2}\}$ and A, B are arbitrary Dirac matrices and the $q_1, \ldots, q_4$ arbitrary spinors. There are six possibilities for contracting the fermion lines (6.29). Together with the four choices for the gluon attachment, we end up with a set of 24 different diagrams.

The three bilinears are mapped to a $B \to \pi$ form factor and to two single-pion LCDAs Φ_π (cf. Sec. 1.1.1), schematically

$$(a,2) \to F^{B\to\pi} \,, \quad (b,4) \to \Phi_\pi \,, \quad (c,6) \to \Phi_\pi \,, \tag{6.32}$$

where a, b, c is a permutation of the numbers 1, 3, 5. In the center of the Dalitz plot the momentum transfer to the three pions is large, thus for the $B \to \pi$ form factors defined in Eq. (1.4) we find the large-recoil relation [53]

$$F_+^{B\to\pi} = \frac{m_B}{2E_\pi} F_0^{B\to\pi} \,, \tag{6.33}$$

where E_π is the energy of the of the pion. We further use the asymptotic form of the LCDA[9] given in Eq. (1.6). From the weak Hamiltonian (1.11) we have $q_n = u$ in the current-current and $q_n = d$ in the penguin transitions. Moreover, $\Gamma_{1,2} = \{\gamma^\mu, \gamma^\mu\gamma_5\}$ and

[9]We assume that the asymptotic form has the same endpoint behaviour as Φ_π at the scale $\mu \sim m_B$ as argued in [27].

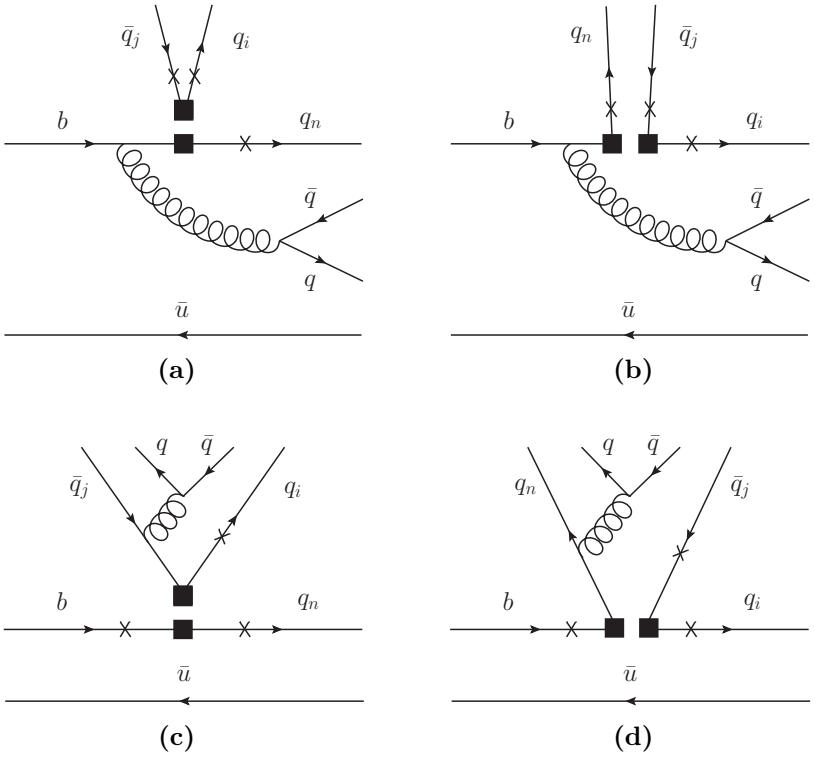

Figure 6.7. – Leading order Feynman diagrams for the decays $B^+ \to \pi^+\pi^-\pi^+$. The crosses mark all possible insertions of the gluon propagator creating the $\bar{q}q$ quark-antiquark pair.

$\mathcal{C}^{ab}\mathcal{C}^{cd} = \{\delta^{ab}\delta^{cd}, (T^B)^{ab}(T^B)^{cd}\}$, where T^B is a generator of $SU(3)$ colour gauge group. $(\Gamma_3)^{ef}_{\sigma\tau}$ is stemming from the $q\bar{q}$ production of a gluon and therefore, Γ_3 is an arbitrary Dirac matrix γ_α and $\mathcal{C}^{ef} = (T^A)^{ef}$. We find that all eight combinations where the spinors $(5, 6)$ form a pion render zero as in the projection on the leading-twist LCDA given in Eq. (1.7) only contributions involving the axial vector survive. Finally, we are left with the 16 Feynman diagrams shown in Fig. 6.7 that contribute to the leading order decay amplitude. The results for the diagrams are presented in the App. F.

6.4.2. Differential Decay Rate

We find that all diagrams (a)-(d) in Fig. (6.7) yield non-vanishing contributions to the hard scattering kernels. Moreover, the convolutions of the latter with the two single-pion LCDAs in Eq. (6.28) are free of endpoint divergences, which is a necessary but not sufficient condition for factorization to apply (see Sec. 1.1.1). Note that this is a nontrivial statement already at leading order since, in contrast to two-body decays, at this order the hard scattering kernels $T_i^I(u, v)$ depend on the momentum fractions u and v of the two pions.

We have further computed the differential decay rate $d^2\Gamma/(ds_{++}\, ds_{+-})$ by using Eq. (6.5). We do not display the full result here as it is not very illuminating but rather comment on some interesting features. First of all, moving from the central point $s_{++} = s_{+-} = 1/3$ (Region I) toward the edge $s_{++} \sim 0$ (Region IIa), we find that the rate remains regular, that

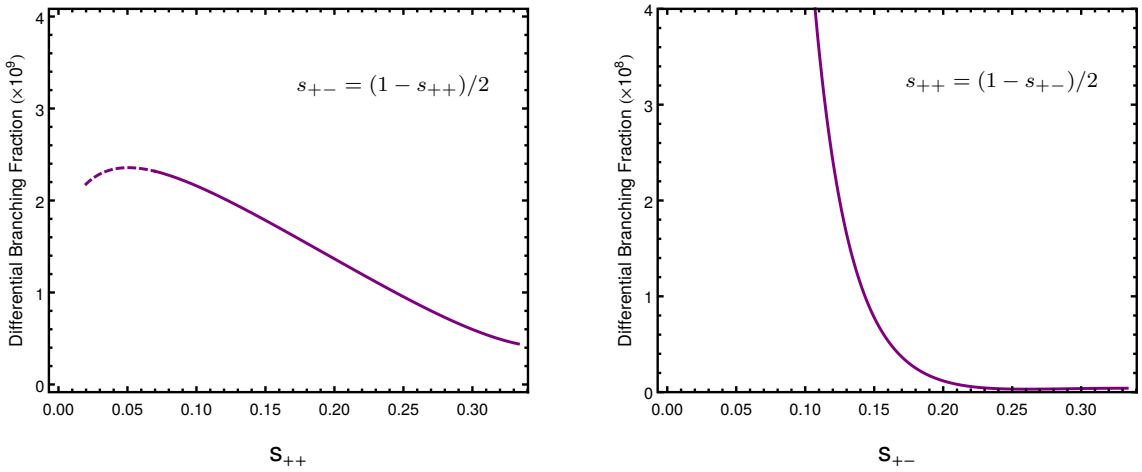

Figure 6.8. – Differential decay rate when extrapolated from the center region of the Dalitz plot towards the collinear edges. The extrapolation to small s_{++} remains regular, while the limit to small s_{+-} diverges. See text for details.

is, it approaches a finite limit as $s_{++} \to 0$. This can be seen explicitly in the calculation, with no propagator becoming soft as $s_{++} \to 0$. More precisely, moving away from the center along the line $s_{+-} = (1 - s_{++})/2$, we find

$$\left.\frac{d\Gamma}{ds_{++}\, ds_{+-}}\right|_{\substack{s_{++} \to 0 \\ s_{+-} \sim 1/2}} \sim \Gamma_0 \; F_+^{B\to\pi}(m_B^2/2)^2 \tag{6.34}$$

up to a coefficient of order one, with

$$\Gamma_0 = \frac{G_F^2 \alpha_s^2(m_B) f_\pi^4 m_B |V_{ub}V_{ud}^*|^2}{32\pi} \; . \tag{6.35}$$

In Fig. 6.8 (left panel) we show the exact dependence of the rate as a function of s_{++}, along this direction in the Dalitz plane. This regular behavior does not depend on how we approach the $s_{++} = 0$ edge.

The situation is very different if we consider the behavior of $d^2\Gamma/(ds_{++}\, ds_{+-})$ as s_{+-} gets small (towards Region IIb). We consider now the direction along the line $s_{++} = (1 - s_{+-})/2$. In this region the rate behaves as,

$$\left.\frac{d\Gamma}{ds_{++}\, ds_{+-}}\right|_{\substack{s_{+-} \to 0 \\ s_{++} \sim 1/2}} \sim \frac{1}{s_{+-}^2}\Gamma_0 \; F_+^{B\to\pi}(m_B^2/2)^2 \; + \text{ regular terms as } s_{+-} \to 0 \tag{6.36}$$

rendering the rate non-integrable. One may interpret this behaviour as an indication that the edge of the Dalitz plot with small s_{+-} is populated by hadronic resonances. In this region the three-body decay effectively becomes a quasi two-body decay, and the amplitude has to be described by generalized form factors and distribution amplitudes. We proceed with the discussion of the edges of the Dalitz plot.

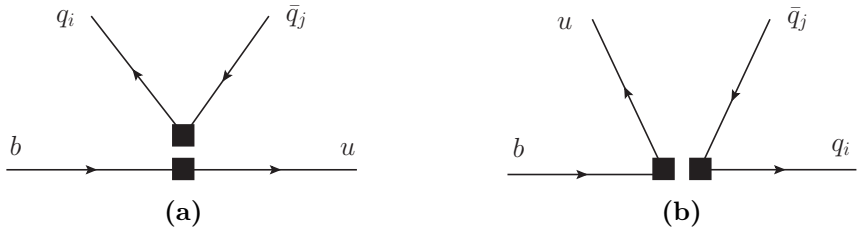

Figure 6.9. – Leading contributions to the hard kernels given in Eq. 6.11. Here, we have omitted the spectator quark of the B meson.

6.5. The Collinear Regions of the Dalitz Plot

We consider the collinear Regions IIa and IIb of the Dalitz plot in which we expect factorization to apply according to Eq. (6.11), which is given here again

$$\langle \pi^i\pi^j\pi^k|\mathcal{Q}_a|B\rangle_{s_{ij}\ll 1} = T^I \otimes F^{B\to\pi^k} \otimes \Phi_{\pi^i\pi^j} + T^I \otimes F^{B\to\pi^i\pi^j} \otimes \Phi_{\pi^k} + T^{II} \otimes \Phi_B \otimes \Phi_{\pi^k} \otimes \Phi_{\pi^i\pi^j} \ . \tag{6.37}$$

The $B \to \pi\pi$ form factor and the 2π-LCDA have been defined in Sec. 6.3. At leading order the contributions to the hard scattering kernels T^I are given by the Feynman diagrams depicted in Fig. 6.9, contributions to T^{II} only arise at order α_s. The computation of the Feynman diagrams in Fig. 6.9 is trivial and we see that the hard kernels do not depend on the momentum fractions of the single- or 2π-LCDAs.

Moreover, we find that in the contribution involving $F^{B\to\pi\pi}$ in Eq. (6.37) the only relevant form factor is the time-like form factor F_t defined in Eq. (6.24). To see this, we consider that the Dirac structure of the hard kernel T^I is given by $T^I \sim \Gamma \otimes \Gamma'$, where we have $\Gamma, \Gamma' \in \{\gamma^\mu, \gamma^\mu\gamma_5\}$ from the effective operators. The convolution of $F^{B\to\pi\pi}(s_{12})$ with the pion LCDA Φ_π is proportional to $\mathrm{tr}[F^{B\to\pi\pi}\Gamma]\mathrm{tr}[\not{k}_3\gamma_5\Gamma']$. To leading order, only $\Gamma' = \gamma^\mu\gamma_5$ contributes, and by orthogonality, the form factor trace is only non-zero for the time-like component of the axial form factor F_t.

Considering the term with the 2π-LCDA and the $B \to \pi$ form factor in Eq. (6.37) we find that it receives only contribution from the vector 2π-LCDA $\Phi_\parallel$ defined in Eq. (6.16). The reason is the simple Dirac structure of the leading order hard scattering kernel $T^I \sim \Gamma \otimes \Gamma'$ with $\Gamma, \Gamma' \in \{\gamma^\mu, \gamma^\mu\gamma_5\}$. We further employ the large-recoil relation Eq. (6.33) for the $B \to \pi$ form factor since the pion that recoils against the two collinear pions (which are described by the 2π-LCDA) has large energy.

Altogether, we obtain the following expression for the leading order amplitude in the Region IIb[10]

$$\mathcal{A}|_{s_{+-}\ll 1} = \frac{G_F}{\sqrt{2}}\big[f_\pi m_\pi(a_1{-}a_4)\cdot F_t(\zeta, s_{+-}){+}m_B^2(a_2{+}a_4)(2\zeta{-}1)\cdot F_0^{B\to\pi}(s_{+-})\cdot F_\pi(s_{+-})\big] \ . \tag{6.38}$$

[10]For the collinear Region IIa we have $\mathcal{A}|_{s_{++}\ll 1} = 0$ as anticipated in Sec. 6.3.

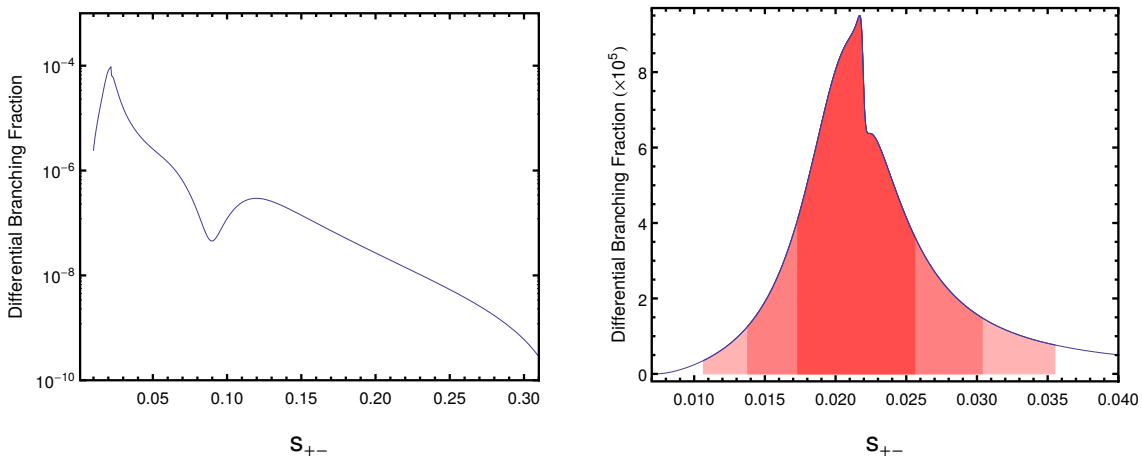

Figure 6.10. – Differential decay rate obtained from the description in terms of two-pion distributions for small s_{+-}. Left: extrapolation to $s_{+-} \sim 1/3$, with the $\rho''(1700)$ apparent, and the $\rho - \omega - \rho'$ peak, in logarithmic scale. Right: Zoom to resonant contribution from the $\rho(770)$ and $\omega(782)$.

The parameters a_i are combinations of the Wilson coefficients $a_{1,2} = V_{ub}^* V_{ud}(C_{2,1} + C_{1,2}/N_c)$ and $a_{3,4} = V_{tb}^* V_{td}(C_{3,4} + C_{4,3}/N_c)$. The isovector contribution of F_t can be related to F_π by the QCD sum rule (6.27). Note that to this order all the convolution integrals are trivial. Hard kernels are known already at NNLO from studies of two-body decays [45, 47, 48, 94, 183–185], but the convolutions with two-pion distributions still need to be worked out, in particular the contribution of $\Phi_\perp$. This is beyond the scope of this work. The conclusions derived here at this order of approximation should nevertheless remain valid.

A qualitative difference of three-body decays in this kinematic regime with respect to two-body decays is that the nonperturbative input is much richer in terms of QCD effects. In particular, F_π contains resonance and rescattering contributions, including an imaginary part from non-perturbative dynamics. In contrast, in two-body decays the imaginary parts that determine the strong rescattering phases are, at the leading power, of perturbative origin [28][11]. This has also implications for the determination of CP asymmetries. Most of the information on $F_\pi(s)$ can be obtained from data (see Fig. 6.5), allowing for a data-driven model-independent interpretation of three-body Dalitz plots, at least within the accuracy of factorization theorems.

As a simple application of this result, we estimate the branching fraction $BR(B^+ \to \rho\pi^+)$ by integrating the differential decay rate (see Eq. (6.5)) in a window around the ρ resonance which is the dominant resonance in the $(\pi^+\pi^-)$-system:

$$\widehat{BR}(B^+ \to \rho\pi^+) \equiv \int_0^1 ds_{++} \int_{s_\rho^-}^{s_\rho^+} ds_{+-} \frac{\tau_B \, d\Gamma}{ds_{++} ds_{+-}} = \int_0^1 ds_{++} \int_{s_\rho^-}^{s_\rho^+} ds_{+-} \frac{\tau_B \, m_B |\mathcal{A}|^2}{32(2\pi)^3} \,, \quad (6.39)$$

where $s_\rho^\pm = (m_\rho \pm n\Gamma_\rho)^2/m_B^2$ with n specifying the window size in units of the ρ-meson

[11] The physical picture behind the perturbative origin of the strong rescattering phases is the hard gluon exchange between the two final-state mesons [26].

width. We find[12]:

$$\widehat{BR}(B^+ \to \rho\pi^+) \simeq 2.4 \cdot 10^{-6} \quad \text{for} \quad n = 1\,, \tag{6.40}$$
$$\widehat{BR}(B^+ \to \rho\pi^+) \simeq 3.0 \cdot 10^{-6} \quad \text{for} \quad n = 2\,, \tag{6.41}$$
$$\widehat{BR}(B^+ \to \rho\pi^+) \simeq 3.2 \cdot 10^{-6} \quad \text{for} \quad n = 3\,, \tag{6.42}$$
$$\widehat{BR}(B^+ \to \rho\pi^+) \simeq 3.3 \cdot 10^{-6} \quad \text{for} \quad n = 4\,. \tag{6.43}$$

Note that extending the window size beyond $m_\rho \pm 4\Gamma_\rho$ does not modify the result very much, as the resonant ρ contribution dominates the full decay rate (see Fig. 6.10). Comparing these numbers to the experimental value [158]

$$BR(B^+ \to \rho\pi^+)^{\rm exp} = (8.3 \pm 1.2) \cdot 10^{-6}\,, \tag{6.44}$$

we see that the result is in the right ballpark. However, $\widehat{BR}$ is an object different from the $B \to \rho\pi$ branching fraction as given in [158], and can be measured experimentally in a direct and model-independent manner, without the need to extract the ρ from the full distribution[13]. A this point we must emphasize that this is still a very crude estimate and a more careful study would need to be performed to really test the data.

6.6. Reconstructing the Dalitz Plot

So far we have used two different factorization formulas for Region I and Region II. Region I has been described using the conventional QCD factorization in terms of single pion states (which we will call QCDF_I hereafter), while Region II has been described in terms of hadronic input describing two-pion states with small invariant mass (called QCDF_II hereon). To get the full Dalitz distribution one needs to match the result from the central region with the one of the edges. To this end, we assume that there is an intermediate region between the edge ($s_{+-}^{\rm low} \equiv s \simeq 0$) and the center ($s_{+-}^{\rm low} \equiv s \simeq s_{+-}^{\rm high} \simeq 1/3$) where both descriptions apply. This region corresponds to $\Lambda^2_{\rm QCD}/m_B^2 \ll s \ll 1/3$, and it certainly exists, if m_B is large enough. We will investigate below, whether this happens for physical B-meson masses.

In this intermediate region, one might use QCDF_II (see Sec. 6.5) to write the amplitude in terms of two-pion states, then take the perturbative limit for the 2π-LCDAs and $B \to \pi\pi$ form factors and finally compare the result with the factorized QCDF_I amplitude of Sec. 6.4. The idea is, that for $s \gg \Lambda^2_{\rm QCD}/m_B^2$, we have (schematically)[14]

$$\Phi_{\pi\pi} \;\; \to \;\; f_\pi^2 \int du\, dv\, T_\phi(u,v)\, \phi_\pi(u)\, \phi_\pi(v)\;, \tag{6.45}$$

[12] The neglected power and α_s corrections to Eq. 6.38 are formally of the order 10% and 20%, respectively.

[13] Usually a parametrization of the ρ and ω mesons is fitted to the experimental line shape of F_π (higher resonances such as ρ' and ρ'' may be included in the fit). From this fit the masses and widths of the resonances can be extracted, which however depends on the parametrization.

[14] The dots in Eq. (6.46) account for "factorizable" contributions proportional to the B-meson light-cone distribution, corresponding to neglected contributions in Sec. 6.4.

Center ($\mathrm{QCDF_I}$)	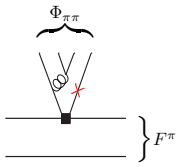	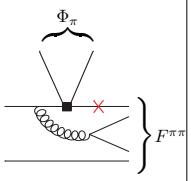	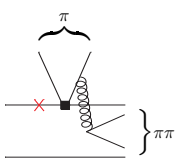	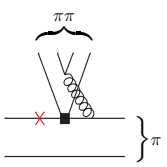	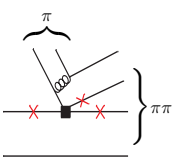	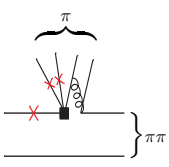
Edge ($\mathrm{QCDF_{II}}$)	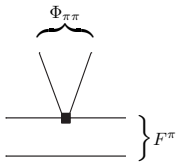	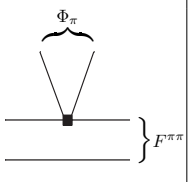	"Non-factorizable" Power-suppressed	"Non-factorizable" Power-suppressed	6-quark operator Power-suppressed	6-quark operator Power-suppressed

Figure 6.11. – Diagrammatic correspondence between the different contributions at the center ($\mathrm{QCDF_I}$) and the edge ($\mathrm{QCDF_{II}}$) of the Dalitz plot. The black square denotes the different weak interaction vertices. Crosses mark the alternative insertions of the gluon. One- and two-pion distributions are denoted by Φ_π and $\Phi_{\pi\pi}$ respectively, while F^π and $F^{\pi\pi}$ denote $B \to \pi$ and $B \to \pi\pi$ form factors. The last four contributions are leading at the center but power-suppressed at the edge.

$$F^{B\to\pi\pi} \quad \to \quad f_\pi \, F^{B\to\pi}(0) \int du \, T_F(u,v) \, \phi_\pi(u) + \cdots \, . \tag{6.46}$$

Taking this limit for the leading power contribution in $\mathrm{QCDF_{II}}$, we expect to fully recover some of the contributions obtained using $\mathrm{QCDF_I}$.

In Fig. 6.11 we show the correspondence between the different contributions to the amplitude in this intermediate region, either in $\mathrm{QCDF_I}$ or $\mathrm{QCDF_{II}}$. The first column shows the contributions from two-pion distribution amplitudes. In $\mathrm{QCDF_{II}}$ (lower diagram), this is a leading-power contribution proportional to the 2π-LCDA, $\Phi_{\pi\pi}$. As the invariant mass of the two pions in this intermediate region is also large, the two pions can be factorized according to Eq. (6.45). The production of two pions with large invariant mass requires a hard gluon, as shown in by the diagram at the top (corresponding to $\mathrm{QCDF_I}$). A similar argument goes through for the $B \to \pi\pi$ contribution, shown in the second column. The contribution in $\mathrm{QCDF_I}$ (where the two pions are assumed to have large invariant mass) requires a hard gluon (top diagram), and can be obtained from the contribution in $\mathrm{QCDF_{II}}$ (bottom diagram) by factorization of $F^{B\to\pi\pi}$ according to Eq. (6.46). We have checked analytically that by applying Eq. (6.46) to the part proportional to $F^{B\to\pi\pi}$ in Eq. (6.37) we recover the corresponding results in Sec. 6.4. Similar, by using Eq. 6.45 the contribution proportional to $\Phi_{\pi\pi}$ in Eq. (6.37) is expected to factorizate reproducing the corresponding results in Sec. 6.4 [172].

However, some contributions in $\mathrm{QCDF_I}$ correspond to contributions in $\mathrm{QCDF_{II}}$ that are power suppressed, and do not arise from the perturbative limit of leading power contributions in $\mathrm{QCDF_{II}}$. These are shown in the last four columns in Fig. 6.11. Again, the contributions in $\mathrm{QCDF_I}$ ($s \gg \Lambda_{\mathrm{QCD}}/m_B$) require a hard gluon. Columns 3 and 4 show the cases in which this gluon becomes collinear (in the $[\pi\pi]$ direction) as $s \to 0$. They are termed "non-

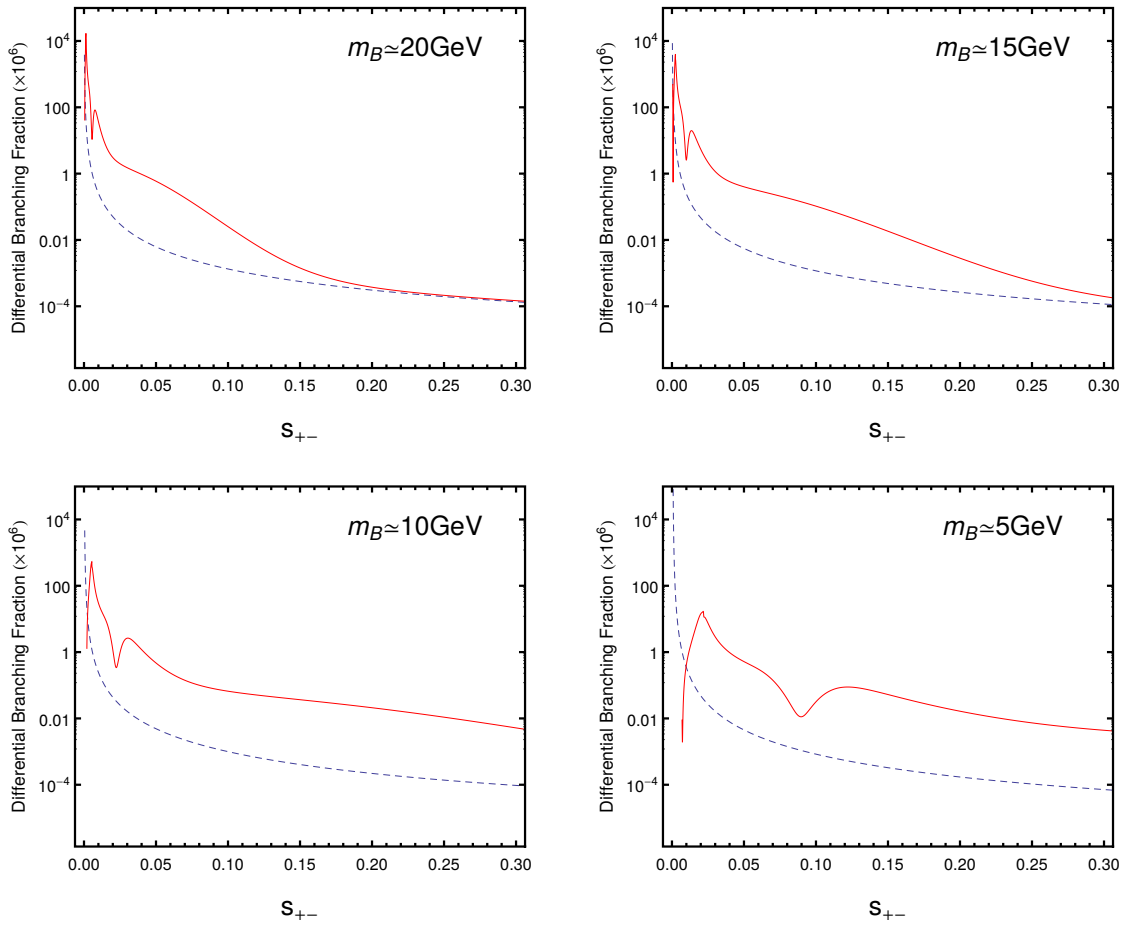

Figure 6.12. – Contributions from 2π-LCDAs to the $B^+ \to \pi^+\pi^-\pi^+$ differential branching fraction, for $s_{++} = (1 - s_{+-})/3$: Full contribution (solid) and perturbative contribution (dashed). A perturbative region exists for large s_{+-} in the heavy-quark limit, but probably not for physical values of the b-quark mass.

factorizable" since the gluon connects the two different collinear sectors. As $s \to 0$, the quark propagator remains hard, which represents a power suppression with respect to the leading contributions. Columns 5 and 6 show the cases in which the gluon remains hard for all $s < 1/3$. For $s \to 0$, these match onto 6-quark operators that are again power-suppressed with respect to the leading contributions. There is therefore a one-to-one diagrammatic correspondence between QCDF_I and QCDF_II, but this correspondence does not respect the power counting.

We note at this point that in the center, since all invariant masses are large and of order m_B^2, there are always two hard propagators, leading to an amplitude that is power suppressed with respect to the amplitude in the edge. In addition, the perturbative nature of the hard gluon exchange leads to an $\alpha_s(m_B)$ suppression at the center, which is not present at the edge, where the gluon becomes soft. All in all, the amplitude at the center is expected to be both power- and α_s-suppressed with respect to the amplitude at the edge.

While the previous considerations imply that formally there must be a good matching

between both regions, the question is whether this happens in practice for physical B-meson masses. To this end we focus on the 2π-LCDA contribution shown in the first column in Fig. 6.11. This contribution arises from the second term in Eq. (6.38). We find that, in the limit of large $(m_B^2 s_{+-})$, this amplitude reproduces the corresponding contribution obtained from the QCDF_I calculation in Sec. 6.4 [15]. The particular values of s for which this matching occurs depends on the value of m_B^2. In Fig. 6.12 we show the results of both calculations for different values of m_B. We see that for $m_B \sim 20$ GeV there is enough phase space to reach a perturbative regime in the central region of the Dalitz plot. However, the phase space gets reduced considerably when m_B is decreased to its physical value, where there seems to be no perturbative regime.

Similar conclusions are expected for the $B \to \pi\pi$ form-factor contribution in the second column in Fig. 6.11. Adding the rest of the central-region contributions to the perturbative side, we will get a mismatch at large $(m_B^2 s_{+-})$ of the order of the perturbative contribution itself, which is expected to be of the same order as neglected power corrections to the QCDF_II calculation in the perturbative limit. This corresponds to the contributions in the last four columns in Fig. 6.11. Since we anyway do not expect the two-pion system to factorize into single-pion distributions as early as $m_B^2 s_{+-} \sim 8\ \text{GeV}^2$, we can conclude that the QCDF_I calculation of Sec. 6.4 might not be relevant in any region of the Dalitz plot.

We summarize that the amplitude in the Dalitz plot can be described in certain regions of the phase space by applying factorization theorems. In the central region of the Dalitz plot the amplitude factorizes into a $B \to \pi$ form factor and/or single-meson LCDAs. For the description of the edges of the Dalitz plot generalized non-perturbative inputs in form of 2π-LCDAs and $B \to \pi\pi$ form factors are needed. We have evaluated the amplitude in the central region of the Dalitz plot and have found that the convolution integrals with the LCDAs are finite. We remark that although this is not a proof of factorization, it is a mandatory condition for factorization to apply. Moreover, we have evaluated the amplitude in the edge of the Dalitz plot and have integrated the corresponding differential decay rate in a window around the ρ resonance. This rough estimate of the branching ratio is in the right ballpark of the experimental result. Finally, we have analyzed the prospects of a merging of the descriptions in both regions in an intermediate kinematical regime. We find that the perturbative regime described by the QCDF_I calculation seems only kinematically allowed for B-meson masses several times larger that the physical value.

[15] This happens by construction, since we force the function $F_\pi(s)$ to satisfy the perturbative limit asymptotically for large $s\, m_B^2$. This is in fact the only information we have on $F_\pi(s)$ at large energies, since data reaches only up to ~ 3 GeV. For our purposes, the relevant observation is that data shows that the perturbative regime might lie beyond 3 GeV.

Chapter 7

Conclusion and Outlook

Hadronic decays of B mesons yield a broad spectrum of observables for testing the CKM sector of the Standard Model. The theory description of many of these observables from non-leptonic two-body decays is based on QCD factorization (QCDF), which is a model-independent framework that exploits the structure of a decay amplitude in the heavy-mass limit. A genuine QCD-based description of non-leptonic three-body decays on the other hand is still not yet available. In this thesis we have considered two applications of QCDF.

In the first part, we have calculated the vertex corrections to the colour-allowed tree topology of the decays $\bar{B}^0 \to D^{(*)+}\pi^-$ and $\bar{B}^0 \to D^{(*)+}\rho^-$ to NNLO accuracy. The calculation has been performed by applying the Laporta algorithm for the reduction of the several thousand scalar two-loop two-scale integrals to master integrals. For the evaluation of the master integrals we have used a new approach and have obtained analytical results for them in a canonical basis. The final result for the perturbative contribution a_1 (defined in Sec. (5.2)) to NNLO accuracy reads

$$\begin{aligned} a_1(DL) &= (1.071^{+0.011}_{-0.013} + 0.044i^{+0.022i}_{-0.014i}) + (0.003^{+0.003}_{-0.002} - 0.007i^{+0.002i}_{-0.003i})\alpha_2^L \,, \\ a_1(D^*L) &= (1.071^{+0.012}_{-0.013} + 0.033i^{+0.017i}_{-0.010i}) + (0.000^{+0.001}_{-0.000} - 0.009i^{+0.003i}_{-0.004i})\alpha_2^L \,, \end{aligned} \tag{7.1}$$

where α_2^L is the second Gegenbauer moment of the light meson L, which is π or ρ. Within the given uncertainties we can thus confirm the quasi-universality of a_1 also at NNLO accuracy. We have calculated the $B \to D^{(*)}L$ branching ratios and find a tension of 2-3 σ with respect to the corresponding experimental values, whose central values are about $20-30\%$ smaller. Moreover, we have performed factorization tests to see how well these decay channels are described in QCDF. The preliminary results for experimental ratios of non-leptonic to semi-leptonic decay rates that directly probe the magnitude of a_1 turn out to favour a central value $|a_1| \simeq 0.94$, with errors in the individual channels at the 2-10%-level. This number is smaller than the quasi-universal value $|a_1| \simeq 1.07 \pm 0.01$ from the NNLO results in Eq. (7.1). Power corrections which rise to 10-20% could account for this differences in a_1 and also the deviations of the calculated and experimental BRs. Moreover, as data points towards a quasi-universality of a_1 and all central values for the NNLO BRs are about $20-30\%$ larger

than the experimental BRs one could suspect a common mechanism that pushes the power correction in the same direction. This would be also supported by the good agreement of the experimental and theoretical values for the ratios of the non-leptonic decay rates as similar-sized power corrections could cancel in the ratios. We will update the numbers for the experimentally extracted values of a_1 in a forthcoming publication [E]. Moreover, the results for the hard scattering kernels also apply in the evaluation of the NNLO corrections to the colour-allowed tree topologies of the decays $\bar{B}^0 \to D^{(*)+}K^{(*)-}$ or baryonic decays like $\Lambda_b^0 \to \Lambda_c^+\pi^-$. We will determine the values of a_1 for these decays and include the results in the factorization tests.

Finally, it should be noted that the two-loop correction will most probably be the final word on the perturbative side of the factorization formula (1) since the perturbative series is expected to be well-behaved and should therefore not be subject of unexpected large corrections. As the precision on the form factor and Gegenbauer moments of the LCDA is expected to improve, a comparison to experimental data will allow one to estimate the size of power corrections more precisely. The uncertainties of the experimental values for the branching ratios are currently at the 5%-level for the decays $\bar{B}^0 \to D^{(*)+}\pi^-$ and below the 20%-level for the decays $\bar{B}^0 \to D^{(*)+}\rho^-$ and $\bar{B}^0 \to D^{(*)+}K^{(*)-}$ [158].

In the second part of this thesis, we have provided a description of non-leptonic three-body B decays in the framework of QCDF using the decay $B^+ \to \pi^+\pi^-\pi^+$ as an example. We have divided the Dalitz plot in several regions which have special kinematic configurations. Based on the factorization properties of non-leptonic two-body decays we have employed different descriptions in the central region and in the edges of the Dalitz plot. Whereas the central region can be described by conventional form factors and LCDAs, generalized $B \to \pi\pi$ form factors and two-pion distribution amplitudes are also needed for the description of the edges of the Dalitz plot. We have evaluated the transition amplitudes in the different regions to leading power in Λ/m_b and leading order in the strong coupling. Moreover, assuming that these two regions are well described by the respective factorization formulae, we have tried a merging of both descriptions in an intermediate kinematical regime. We have seen that some of the contributions at the center correspond, in the heavy-quark limit, to the expression for the amplitude at the edge with factorized $B \to \pi\pi$ form factors and 2π-LCDAs. Therefore, a parametrization of these nonperturbative objects that is consistent with their perturbative regime leads automatically to a well behaved limit of the result at the edge when extrapolated to the center. However, it seems that the perturbative regime is only kinematically allowed for b-quark masses several times larger that the physical value.

It seems promising to continue the study of non-leptonic three-body decays as the NLO and even NNLO hard scattering kernels are already known from non-leptonic two-body decays. However, for a more precise study a better knowledge of the $B \to 2\pi$ form factor and the 2-pion LCDAs and improved sum rule calculations are indispensable. From the theoretical point decays like $B_s^0 \to D_s^-\pi^+\pi^0$ are also interesting, as factorization is assumed to be considerably simpler. On the other hand, decays involving kaons in the final states such as $B^+ \to K^+\pi^-\pi^+$, which have already been measured at the B-factories and the LHC, provide another avenue to study CP violation (see e.g. [171, 186]). Our descriptions also apply to these decays. However, for a further study, knowledge about πK (KK) form factors and πK and 2-K distribution amplitudes is required. The former can be obtained from semi-leptonic

B decays (e.g. [187]) whereas the latter can be probed in τ decays (e.g. [188]).

Finally, we remark that three-body decays with their large phase space have the potential of studying factorization and hadronic effects in B decays in different kinematic regions and may provide a deeper understanding of the nature of power corrections in the framework of QCDF.

Appendix

Appendix A

Laporta Reduction of a Sample Feynman Diagram

We present the Laporta reduction of the two-loop Feynman diagram 14a) given in Fig. 2.4 by using FIRE [101, 102]. There arises a subtlety which all diagrams of the topology 14 have in common and which will be explained below.

The topology of diagram 14a) is depicted in Fig. A.1. q_i $(i = 1, \ldots 4)$ and $k_{1,2}$ are the external and loop momenta, respectively. The momenta of the internal lines can be parametrized arbitrarily. A particular choice for the propagators is given in the following list

$$\{(k_2 - q_3 - q)^2 - m_b^2,\, (k_1 - k_2 + uq)^2,\, (k_1 - (1-u)q)^2,\, k_1^2,\, k_2^2,\, (k_1 + uq)^2\}\,, \tag{A.1}$$

where we have substituted $q_1 = uq$, $q_2 = (1-u)q$ and $q_4 = -q_3 - q$. Four of those are fermion propagators (the propagators 1-3 and 6 in the list (A.1)). Hence, there can appear tensor integrals which, at most, carry four Lorentz indices. One can easily see that after the PV decomposition (see Sec. 3.1) there may show up the following seven scalar products in the numerator of the integrals (3.9): k_1^2, k_2^2, $(k_1 \cdot k_2)$, $(q \cdot k_1)$ and $(q_3 \cdot k_2)$ can be expressed by one of the propagators of the list (A.1) however, for reducing $(q_3 \cdot k_1)$ and $(q \cdot k_2)$ we have to introduce two new propagators. We find $(k_2 - uq)^2$ and $(q_3 + k_1)^2 - m_c^2$ to be a suitable choice. Thus the topology 14a) can be fully described by the set of integrals

$$\begin{aligned} &F(a_1, a_2, a_3, a_4, a_5, a_6, a_7, a_8) = \\ &\int \frac{d^d k}{(2\pi)^d} \frac{1}{[(k_2 - q_3 - q)^2 - m_b^2]^{a_1}\ [(k_1 - k_2 + uq)^2]^{a_2}\ [(k_1 - (1-u)q)^2]^{a_3}\ [k_1^2]^{a_4}} \\ &\qquad \frac{1}{[k_2^2]^{a_5}\,[(q_3 + k_1)^2 - m_c^2]^{a_6}\ [(k_2 - uq)^2]^{a_7}\ [(k_1 + uq)^2]^{a_8}}\,, \end{aligned} \tag{A.2}$$

where the a_i are some integer powers. In the following we perform the reduction of integrals of type (A.2) with a particular choice of indices to master integrals by applying FIRE. First, the packages FIRE_3.5.0.m and IBP.m, which can be obtained from [189], have to be loaded. We then enter the commands `Internal` and `External`, which specify the internal and the linearly independent external momenta, respectively:

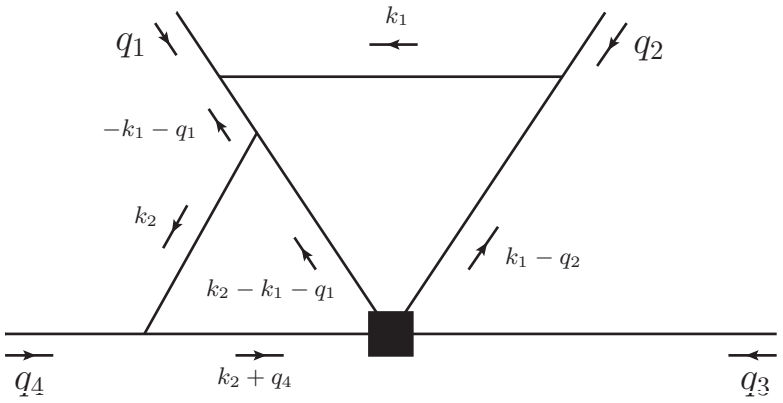

Figure A.1. – Topology of diagram 14a): The external momenta are $q_1 = uq$, $q_2 = (1-u)q$, q_3 and q_4 with $q = -q_3 - q_4$ and the loop momenta are k_1 and k_2. The momentum flow in the internal lines is given for a concrete choice.

```
Internal = {k1, k2};
External = {q, q3};
```

Note that the choice for the external momenta is not unique. We use the parametrization (A.2) for the propagators which are initiated by the command

```
(* original list Propagators *)
Propagators = {(k2 - q3 - q)^2 - mb^2,(k1 - k2 + u q)^2,(k1 - (1 - u) q)^2,
   k1^2,k2^2,(q3 + k1)^2 - mc^2,(k2 - u q)^2,(k1 + u q)^2};
```

The routine

```
PrepareIBP[ ];
```

prepares the corresponding IBPs which later are automatically generated. However, for the case at hand an error message appears:

```
Out[ ] =  Linearly dependant propagators. Perform reduction first.
```

The reason for this is the following: Two of the eight propagators are linearly dependent, which are $(k_1 - (1-u)q)^2$ and $(k_1 + uq)^2$. Therefore the reduction of the scalar product $(q \cdot k_1)$ is not unique since it either can be expressed in terms of $(k_1 - (1-u)q)^2$, $(k_1 + uq)^2$ or a linear combination of both. The routine for preparing the IBPs cannot handle linearly dependent propagators and does not further proceed. Since we do not want to perform a reduction of the propagators as suggested by the error message, we use a workaround to this problem [190]. First, we consider only seven linearly independent propagators, here $(k_1 + uq)^2$ is left out:

```
(* new list Propagators *)
Propagators = {(k2 - q3 - q)^2 - mb^2,(k1 - k2 + u q)^2,(k1 - (1 - u) q)^2,
   k1^2,k2^2,(q3 + k1)^2 - mc^2,(k2 - u q)^2};
PrepareIBP[ ];
```

MMA proceeds by preparing the IBPs for the seven propagators:

```
Out[ ]= Prepared
```

We then specify the on-shell conditions for the external momenta:

```
reprs = {q^2 -> 0,q3^2 -> mc^2,q q3 -> (mb^2 - mc^2)/2};
```

For generating all IBPs we also have to take into account the propagator $(k_1 + uq)^2$ that does not appear in the new list `Propagators`. Therefore, using the definition (3.22) we manually evaluate IBP$(k_1, k_1 - k_2 + uq)$, IBP$(k_1, k_1 - (1-u)q)$, IBP(k_1, k_1), IBP$(k_1, k_1 + uq)$ and IBP$(k_1, k_1 + q_3)$, reducing the scalar product $(q \cdot k)$ either to the third propagator of the original list `Propagators`, $(k_1 - (1-u)q)^2$, or to the new eighth propagator $(k_1 + uq)^2$. This yields ten IBP relations. We will denote the IBPs where $(q \cdot k)$ has been reduced to the third and the eighth propagator by IBP3 and IBP8, respectively, i.e. IBP3$(k_1, \dots)$ and IBP8$(k_1, \dots)$. The remaining four IBPs that contain the derivation with respect to k_2, which are IBP(k_2, k_2), IBP$(k_2, k_2 - q_3 - q)$, IBP$(k_2, k_2 - k_1 - uq)$ and IBP$(k_2, k_2 - uq)$, can be generated automatically by means of the command `IBP[k2,...]`. The reason for this lies in the notation of the IBPs in FIRE created by the command `IBP`:

- A propagator that is reduced (raised) by one is described by `Ym[i]` (`Y[i]`), where `i` marks its position in the list `Propagators`. The `a[i]` denote the a_i as given in (A.2).
- Propagators which do not receive any change do not appear.

Hence, from the new list `Propagators` all IBP$(k_2, ...)$ can be created automatically by using the command `IBP`. The manually derived IBPs have to be converted to the internal form of the `IBP` command. Finally, we can generate all IBPs by entering[1]

```
startinglist = {IBP[k2, k2],IBP[k2, k2 - q3 - q],IBP[k2, k2 - k1 - u q],
   IBP[k2, k2 - u q],IBP3[k1, k1 - k2 + u q],IBP3[k1, k1 - (1 - u) q],
   IBP3[k1, k1],IBP3[k1, k1 + u q],IBP3[k1, k1 + q3],
   IBP8[k1, k1 - k2 + u q],IBP8[k1, k1 - (1 - u) q],IBP8[k1, k1],
   IBP8([k1, k1 + u q],IBP8[k1, k1 + q3]}/.reprs;
```

Next, we have to specify the topologies for which (A.2) vanishes. We find that for the case at hand all topologies where the first propagator is raised to a negative integer or is absent, render zero since the resulting integrals are scaleless. This information can be feed into FIRE by using the command:

```
RESTRICTIONS = {{-1, 0, 0, 0, 0, 0, 0, 0}};
```

[1]The relations IBP3(..) and IMP8(...) have to be generated manually. The explicit code for these IBPs is not given here as it is rather lengthy and not illuminating.

The zeros denote any arbitrary integers whereas the -1 represents a non-positive entry or zero. As optional input the symmetries of the integral can be provided. However, we do not find any for diagram 14a).

Considering Eq. (3.23) we find that for the case at hand there are $2(2+2) = 8$ independent IBP relations. However, by the command `startinglist` 14 IBPs are generated and thus not all will be independent. In order for FIRE to work properly the following command has to be added:

```
LeeIdeas = False;
```

This option has to be used in case that the IBPs do not form a Lie algebra (or one does not know if the IBPs form one). Otherwise there might remain additional master integrals after the reduction [190][2]. Finally, FIRE can be run by adding the two commands

```
Prepare[ ];
Out[ ] = Dimension set to 8
Out[ ] = No symmetries
Burn[ ];
```

Integrals are automatically reduced by calling `F[{...}]`. For instance the command

```
F[{1,1,0,1,0,0,0,1}]
```

yields the following linear combination of master integrals, which are denoted by G({...})

$$\begin{aligned}\mathrm{F}(\{1,1,0,1,0,0,0,1\}) = &-\frac{6(d-2)\left(m_b^2u-m_b^2-m_c^2u\right)\mathrm{G}(\{1,1,-1,1,0,0,0,0\})}{(d-4)(u-1)u^2(m_b-m_c)^3(m_b+m_c)^3}\\ &+\frac{(5dm_b^2u-4dm_b^2-5dm_c^2u-12m_b^2u+10m_b^2+12m_c^2u)\,\mathrm{G}(\{1,1,0,1,0,0,0,0\})}{(d-4)u^2(m_b-m_c)^2(m_b+m_c)^2}\\ &-\frac{(3d-8)\mathrm{G}(\{1,1,0,0,0,0,0,1\})}{2(d-4)u(m_b-m_c)(m_b+m_c)}\,. \end{aligned} \tag{A.3}$$

We express the master integral with entry -1 in terms of a master integral with a douply-dotted propagator. For instance $\mathrm{G}(\{1,1,-1,1,0,0,0,0\})$ can be extracted from the following equation

$$\begin{aligned}\mathrm{F}(\{2,1,0,1,0,0,0,0\}) = &\frac{3(d-2)\left(m_b^2u-m_b^2-m_c^2u\right)\mathrm{G}(\{1,1,-1,1,0,0,0,0\})}{m_b^2(u-1)u(m_b-m_c)^2(m_b+m_c)^2}\\ &-\frac{(dm_b^2u-2dm_b^2-dm_c^2u-2m_b^2u+5m_b^2+2m_c^2u)\,\mathrm{G}(\{1,1,0,1,0,0,0,0\})}{m_b^2u(m_b-m_c)(m_b+m_c)}\,. \end{aligned} \tag{A.4}$$

Note that the package Sbases.m [192] turned out to be a useful addition to decrease the evaluation time. It can be used to obtain master integrals in certain (sub)topologies (sectors) by constructing so-called sector-bases (or s-bases). In the remaining sectors the master integrals are found by applying the Laporta reduction. The command `BuildAll`

[2]By default LeeIdeas is set to true since one knows that the IBPs define a Lie Algebra [191].

automatically tries to build such bases. It has to be provided directly before applying `Burn`. By construction master integrals cannot arise in topologies where the newly added propagators have positive indices, in the case at hand that are the sixth and the seventh propagator. Therefore, we apply for instance the following command:

```
BuildAll[{0, 0, 0, 0, 0, 0, -1, 0}]
```

The zeros stand for arbitrary integers whereas the entry -1 states that there is no master integral that has a positive entry on the seventh line. We do not display the output here as it is rather lengthy, but only note that bases have been build in 35 sectors. For more details on the s-bases approach and the definition of a sector see [105, 106].

Appendix B

Reduction of the γ-matrix Algebra to Operators

We consider the various Dirac γ-matrices contracted with the tensorial structures resulting from the PV decomposition (see Sec. 3.4) and reduce them to a set of known operators. The reduction consists of two parts, which are described below: First, we modify the Dirac strings and the corresponding spinors by using Mathematica to obtain rather simple patterns and then, we express the later in terms of operators that have the same Dirac structure as the SCET operators (2.18)-(2.23) but with spinors defined in QCD. The explicit matching onto the SCET operators is subject of Sec. 2.2. Finally, we present two examples for the reduction.

B.1. Part I: Simplification by a Mathematica Routine

We describe the Mathematica routine that we have created in order to simplify the Dirac γ-strings consisting of γ-matrices contracted with the tensorial structures from the PV decomposition (see Sec. 3.4). For the reduction we use the following conditions and relations:

- The external momenta are on-shell, i.e.

$$q_4^2 = m_b^2\,, \quad q_3^2 = m_c^2\,, \quad q^2 = 0\,. \tag{B.1}$$

- As a result of the on-shell conditions the equations of motion (eom) for the spinors can be applied[1]. Since we consider u and d as massless we do not distinguish their flavour anymore but denote them by $\mathbf{q}$ (not to be confused with the momentum q of the light meson). The eom then read

$$\begin{aligned} \not{q}_4\, b(q_4) &= m_b\, b(q_4)\,, & \bar{c}(-q_3)\,\not{q}_3 &= -m_c\,\bar{c}(-q_3)\,, \\ \not{q}\,\mathbf{q}(-q_1) &= 0\,, & \bar{\mathbf{q}}(-q_2)\not{q} &= 0\,. \end{aligned} \tag{B.2}$$

[1]We shall remember that all momenta are taken to be incoming.

- The Dirac matrices obey the Clifford algebra

$$\{\gamma^\mu, \gamma^\nu\} = 2g^{\mu\nu}\,. \tag{B.3}$$

We remark that throughout the reduction, all Lorentz indices are first contracted before any further change is made. The routine then is constructed as follows.

Preparation

Before starting the reduction we prepare each string such that it has the following form

$$\left[\bar{\mathbf{q}}(-q_1)\,\Gamma_l\,\mathbf{q}(-q_2)\right]\left[\bar{c}(-q_3)\,\Gamma_h\,b(q_4)\right] \equiv \Gamma_l \otimes \Gamma_h\,. \tag{B.4}$$

The $\Gamma_{l,h}$ are products of an arbitrary number of γ-matrices, contracted amongst each other or with q^μ, q_3^μ, q_4^μ. They explicitly contain the projectors $P_{L(R)} = (1 \mp \gamma_5)/2$. Note, that all Lorentz indices are contracted. There also are strings where all γ-matrices can be contracted among themselves and the momenta $\not{q}, \not{q}_3, \not{q}_4$ can appear more that once in $\Gamma_{l,h}$. The former kind of gamma strings will not get modified by the following four reduction steps and thus one can immediatelly skip to part II of the process (see Sec. B.2).

In the following we write the products defined in Eq. (B.4) in the schematic form

$$\Gamma_l \otimes \Gamma_h = \{\gamma^{a_1}, \ldots, \gamma^{a_m}, \not{q}, \not{q}_3, \not{q}_4\} \otimes \{\gamma_{a_1}, \ldots, \gamma_{a_n}, \not{q}, \not{q}_3, \not{q}_4\}\,, \tag{B.5}$$

where the γ-matrices and the slashed momenta might have an arbitrary ordering and the Lorentz indices $n, m \in \mathbf{N}$.

First Step

The first step includes the elimination of equal momenta appearing twice or three times on the quark lines Γ_l and Γ_h (cf. Eq. (B.5)) and the removal of the momenta $q_{3,4}$ and q in Γ_h and Γ_l, respectively. Afterwards the strings have the following form

$$\Gamma_l \otimes \Gamma_h = \{\gamma^{a_1}, \ldots, \gamma^{a_n}, \not{q}_3, \not{q}_4\} \otimes \{\gamma_{a_1}, \ldots, \gamma_{a_n}, \not{q}\}\,, \tag{B.6}$$

where $q_{3,4}$ and q appear only once. We execute this step as follows: First, the Clifford algebra is used to exchange the Dirac matrices in order to bring two identical momenta next to each other. Applying the on-shell conditions Eq. (B.1) we can substitute these two momenta by their mass squared. Next, we commute the momenta to their corresponding spinors in order to exploit the eom (B.2). As a consequence there again may appear γ-strings with two identical momenta on one quark line. If so we apply the above mentioned changes as often as necessary such that all γ-strings match the form given in Eq. (B.6).

Second Step

The next step aims at obtaining strings of the following structure

$$\Gamma_l \otimes \Gamma_h = \{\gamma^{a_1}, \ldots, \gamma^{a_m}, \not{q}_3\} \otimes \{\gamma_{a_1}, \ldots, \gamma_{a_n}\}\,, \tag{B.7}$$

where q_3 can appear even more that once on Γ_l. To achieve this, we make use of the conservation of momenta and in Eq. (B.6) we substitute $q \to -\not{q}_3 - \not{q}_4$ and $q_4 \to -\not{q} - \not{q}_3$ on Γ_h and Γ_l, respectively. Next, exploiting the Clifford algebra we commute the momenta such that we can apply the corresponding eom. In this process there again may appear γ-strings of the form (B.6). If so this step has to be repeated until all γ-strings have the structure given in Eq. (B.7).

Third Step

This step applies to γ-strings (B.7) that contain the momentum q_3 more that once. By using the Clifford algebra we bring the two q_3 together and can eliminate them. In this process, there might show up γ-strings with q_3 on the heavy quark line and we commute this momentum to the left in order to apply the eom. This might again lead to γ-strings containing more the one momentum q_3 (cf. Eq. (B.7)). Thus, we repeat this step as often as necessary to arrive at Dirac strings of the form

$$\Gamma_l \otimes \Gamma_h = \{\gamma^{a_1}, \ldots, \gamma^{a_m}, \not{q}_3\} \otimes \{\gamma_{a_1}, \ldots, \gamma_{a_n}\}\,, \tag{B.8}$$

where q_3 only appears once.

Forth Step

The remaining task is to order the Dirac strings (B.8) such that the momentum q_3 is located on the left hand end on Γ_l

$$\Gamma_l \otimes \Gamma_h = \not{q}_3\{\gamma^{a_1}, \ldots, \gamma^{a_m}\} \otimes \{\gamma_{a_1}, \ldots, \gamma_{a_n}\}\,. \tag{B.9}$$

In order to obtain this structure we use the Clifford algebra and in Eq. (B.8) commute the momentum to the correct location. This will introduce γ-strings with an additional momentum q_3 on the heavy quark line which can be eliminated using the eom. Again, strings of the form (B.8) may appear and thus, iterations of this step might be necessary to reduce all γ-strings to the structure given in Eq. (B.9).

After having applied these four steps we are left with structures of the form (B.9) and strings where all γ-matrices are contracted among themselves. At last, we get rid of all γ-matrices that are contracted on the same quark line by exploiting the Clifford algebra and then, we replace the remaining scalar products using the on-shell conditions Eq. (B.1) and also $q \cdot q_4 = 1/2(m_c^2 - m_b^2)$, $q \cdot q_3 = 1/2(m_b^2 - m_c^2)$ and $q_3 \cdot q_4 = -1/2(m_b^2 + m_c^2)$.

B.2. Part II: Reduction to Known Operators

We consider the two γ-strings obtained from the previous reduction

$$\left[\bar{\mathbf{q}}(-q_1)\, 2P_{L(R)}\, \not{q}_3\{\gamma^{a_1} \ldots \gamma^{a_m}\}\, \mathbf{q}(-q_2)\right] \left[\bar{c}(-q_3)\, 2P_L\, \{\gamma_{a_1} \ldots \gamma_{a_n}\}\, b(q_4)\right], \tag{B.10}$$

$$\left[\bar{\mathbf{q}}(-q_1)\, 2P_{L(R)}\, \{\gamma^{a_1} \ldots \gamma^{a_n}\}\, \mathbf{q}(-q_2)\right] \left[\bar{c}(-q_3)\, 2P_L\, \{\gamma_{a_1} \ldots \gamma_{a_n}\}\, b(q_4)\right]. \tag{B.11}$$

Below, we describe the transformation of these strings into the operators

$$\mathcal{O}_1^{QCD} = \left[\bar{\mathbf{q}}\,\frac{\not{n}_-}{2}(2P_L)\mathbf{q}\right]\ \left[\bar{c}\,\not{n}_+(2P_L)b\right]\,, \tag{B.12}$$

$$\mathcal{O}_2^{QCD} = \left[\bar{\mathbf{q}}\,\frac{\not{n}_-}{2}(2P_L)\gamma_\perp^\alpha\gamma_\perp^\beta\mathbf{q}\right]\ \left[\bar{c}\,\not{n}_+(2P_L)\gamma_{\perp,\beta}\gamma_{\perp,\alpha}b\right]\,, \tag{B.13}$$

$$\mathcal{O}_3^{QCD} = \left[\bar{\mathbf{q}}\,\frac{\not{n}_-}{2}(2P_L)\gamma_\perp^\alpha\gamma_\perp^\beta\gamma_\perp^\gamma\gamma_\perp^\delta\mathbf{q}\right]\ \left[\bar{c}\,\not{n}_+(2P_L)\gamma_{\perp,\delta}\gamma_{\perp,\gamma}\gamma_{\perp,\beta}\gamma_{\perp,\alpha}\right]\,, \tag{B.14}$$

and

$$\mathcal{O}_1^{\prime QCD} = \left[\bar{\mathbf{q}}\,\frac{\not{n}_-}{2}(2P_L)\mathbf{q}\right]\ \left[\bar{c}\,\not{n}_+(2P_R)b\right]\,, \tag{B.15}$$

$$\mathcal{O}_2^{\prime QCD} = \left[\bar{\mathbf{q}}\,\frac{\not{n}_-}{2}(2P_L)\gamma_\perp^\alpha\gamma_\perp^\beta\mathbf{q}\right]\ \left[\bar{c}\,\not{n}_+(2P_R)\gamma_{\perp,\alpha}\gamma_{\perp,\beta}b\right]\,, \tag{B.16}$$

$$\mathcal{O}_3^{\prime QCD} = \left[\bar{\mathbf{q}}\,\frac{\not{n}_-}{2}(2P_L)\gamma_\perp^\alpha\gamma_\perp^\beta\gamma_\perp^\gamma\gamma_\perp^\delta\mathbf{q}\right]\ \left[\bar{c}\,\not{n}_+(2P_R)\gamma_{\perp,\alpha}\gamma_{\perp,\beta}\gamma_{\perp,\gamma}\gamma_{\perp,\delta}b\right]\,. \tag{B.17}$$

Note that this set of operators matches the definition of the SCET operators Eqs. (2.18)-(2.23) except that the fields are defined in full QCD.

We start by expressing $q_{3,4}$ and q in terms of the two light-like vectors $n_\pm$ and the time-like vector v, defined in Sec. 2.1.1. Working in the B meson rest frame and using momentum conservation $q_4 = -q_3 - q$ we obtain

$$q = \frac{m_c^2 - m_b^2}{2m_b}n_+\,, \tag{B.18}$$

$$q_3 = -\frac{m_b}{2}n_- - \frac{m_c^2}{2m_b}n_+\,, \tag{B.19}$$

$$q_4 = m_b\,v\,. \tag{B.20}$$

The eom (B.2) then take the following form[2]

$$\bar{\mathbf{q}}(-q_1)\not{n}_+ = 0\,, \qquad \not{n}_+\mathbf{q}(-q_2) = 0\,, \tag{B.21}$$

$$\not{v}b(q_4) = b(q_4)\,. \tag{B.22}$$

It is convenient to first modify the strings (B.10) and (B.11) such that they take the form

$$\left[\bar{\mathbf{q}}\,\not{n}_- P_L\,\{\gamma^{a_1},\ldots,\gamma^{a_n}\}\,\mathbf{q}\right]\ \left[\bar{c}\,\not{n}_+ P_{L(R)}\{\gamma_{a_1},\ldots,\gamma_{a_n}\}\,b\right]\,. \tag{B.23}$$

One can easily verify that in the case at hand $n = 0, 2, 4$, which altogether yields 54 different γ-strings. Note that exploiting the Clifford algebra, strings with different permutations of the γ-matrices can easily be related to a certain combination, preferable the one given by

[2]We do not display the corresponding eom for q_3 since we will not use them.

the operators (B.12)-(B.17). This combination can then be expressed in terms of the latter by replacing all γ_μ by the decomposition (2.3), which for γ_μ takes the form

$$\gamma^\mu = \gamma_\perp^\mu + \frac{n_-^\mu}{2}\not{n}_+ + \frac{n_+^\mu}{2}\not{n}_- \,, \tag{B.24}$$

and using the relations

$$\begin{aligned} \{\gamma_\perp^\mu, \not{n}_\pm\} = 0 \,, \qquad \{\gamma_\perp^\mu, \gamma_5\} = 0 \,, \qquad \gamma_\perp^\mu \gamma_{\perp\mu} = d-2 \,, \\ \gamma_\perp \cdot n_\pm = 0 \,, \qquad \{\gamma_\perp^\mu, \gamma_\perp^\nu\} = 2g^{\mu\nu} - n_+^\mu n_-^\nu - n_-^\mu n_+^\mu \,. \end{aligned} \tag{B.25}$$

It remains to describe the reduction of the γ-strings (B.10) and (B.11) to the form given in Eq. (B.23). We find that, while simplifying strings of the form (B.10), we also encounter γ-strings with the structure (B.11). Thus, we start reducing the former and substitute q_3 by n_+ and n_- using Eq. (B.19). The term with n_+ vanishes due to the eom (B.21) we and obtain

$$\not{n}_- P_L \{\gamma^{a_1}, \ldots, \gamma^{a_n}\} \otimes P_{L(R)} \{\gamma_{a_1} \ldots \gamma_{a_m}\} \,. \tag{B.26}$$

Next, we introduce the momentum q_3 on the heavy quark line by applying the reverse eom (B.2) and then replace q_3 by n_+ and v (cf. (B.19) and $n_- = 2v - n_+$). The contribution with n_+ already has the desired structure given in Eq. (B.23) and thus, we do not further consider it. The remaining γ-strings have the form

$$\not{n}_- P_L \{\gamma^{a_1}, \ldots, \gamma^{a_n}\} \otimes \not{v} P_{L(R)} \{\gamma_{a_1} \ldots \gamma_{a_m}\} \,. \tag{B.27}$$

The further reduction consists of the following building blocks:

1) We consider γ-strings of the form

$$\not{n}_- P_L \{\gamma^{a_1}, \ldots, \gamma^{a_n}\} \otimes P_{L(R)} \{\gamma_{a_1}, \ldots, \gamma_{a_m}, \not{v}\} \,, \tag{B.28}$$

and commute v on the heavy quark line to the right in order to apply the eom (B.22). From this we encounter strings that have the form given in Eq. (B.26) which, thus, need not to be further modified[3]. In addition, γ-strings show up with v on the light quark line. In those we substitute $v = 1/2\,(n_- + n_+)$ and proceed following (2) and (4), respectively.

2) We further simplify γ-strings

$$\not{n}_- P_L \{\gamma^{a_1}, \ldots, \gamma^{a_n}, \not{n}_-\} \otimes P_{L(R)} \{\gamma_{a_1}, \ldots, \gamma_{a_m}\} \,, \tag{B.29}$$

where there appear two n_- on the light quark line. We commute them together by using the Clifford algebra and apply $\not{n}_-^2 = 0$. This will lead to γ-strings that involve n_- on the heavy quark line (see (3)).

[3]Note that γ-strings with different chiralities can mix. In order to reduce those, a system of coupled equations has to be solved (see App B.3).

3) Next, we deal with strings which have the following pattern

$$\not{n}_- P_L \{\gamma^{a_1}, \ldots, \gamma^{a_n}\} \otimes P_{L(R)} \{\gamma_{a_1}, \ldots, \gamma_{a_m}, \not{n}_-\} \tag{B.30}$$

and substitute $n_- = 2v - n_+$ on the heavy quark line. We are done, if we arrive at $\mathcal{O}_1^{(\prime)\mathrm{QCD}}$ or at structures $\not{n}_- P_L \otimes P_{L(R)} \not{v} = \not{n}_- P_L \otimes P_{L(R)}$, which can easily be related to the operators $\mathcal{O}_1^{(\prime)\mathrm{QCD}}$. Otherwise, the terms involving v are reduced following (1). The γ-strings including n_+ are pursued in (5).

4) We consider γ-strings which take the form

$$\not{n}_- P_L \{\gamma^{a_1}, \ldots, \gamma^{a_n}, \not{n}_+\} \otimes P_{L(R)} \{\gamma_{a_1}, \ldots, \gamma_{a_m}\}\,. \tag{B.31}$$

Using the Clifford algebra we commute n_+ either to the right or to the left in order to exploit the eom (B.21). While doing so, there will appear γ-strings with n_+ on the heavy quark line (see (5)) and eventually also strings of the form (B.11) (see (6)). In order to avoid the appearance of the latter strings, n_+ should be commuted to the right.

5) There arise strings of the form

$$\not{n}_- P_L \{\gamma^{a_1}, \ldots, \gamma^{a_n}\} \otimes P_{L(R)} \{\gamma_{a_1}, \ldots, \gamma_{a_m}, \not{n}_+\}\,. \tag{B.32}$$

We are done if they already have the same structure given in Eq. (B.23). Otherwise n_+ must be shifted in order to obtain the correct position. In this process there will appear γ-strings with n_+ on the light quark line. For their reduction follow (4).

6) We also may encounter strings of the form (B.11). In order to reduce those, we insert the identity

$$1 = \frac{\not{n}_+ \not{n}_-}{4} + \frac{\not{n}_- \not{n}_+}{4} \tag{B.33}$$

on light quark line next to left spinor. The first term vanishes due to eom (B.21) and we are left with γ-strings

$$\not{n}_- \not{n}_+ P_L \{\gamma^{a_1}, \ldots, \gamma^{a_n}\} \otimes P_{L(R)} \{\gamma_{a_1}, \ldots, \gamma_{a_n}\}\,. \tag{B.34}$$

To further simplify them we follow (4) but commute $\not{n}_+$ to the right in order to not go back to the starting point.

For the reduction of strings of the form (B.27), we start with (1). Depending on the explicit structures of the γ-strings, not all might be needed and we finally arrive at strings that have the desired structure given in Eq. (B.23).

Below, we present to examples of the reduction γ-strings of the forms (B.10) and (B.11) to the operator basis.

B.3. Examples for the Reduction

After applying our Mathematica routine the γ-strings take the forms (B.10) and (B.11). Here, we give two examples for the reduction of such strings to the set of operators given in Eqs. (B.12)-(B.17). In this procedure we will encounter the following γ-strings

$$\mathcal{S}_{L(R)} = \left[\bar{\mathbf{q}}\, \not{n}_- P_L \gamma^\alpha \gamma^\mu \mathbf{q}\right] \left[\bar{c}\, \not{n}_+ P_{L(R)} \gamma_\mu \gamma_\alpha b\right] \equiv \not{n}_- P_L \gamma^\alpha \gamma^\mu \otimes \not{n}_+ P_{L(R)} \gamma_\mu \gamma_\alpha \,, \tag{B.35}$$

which have to be related to the operators O_1 – O_3'. We first consider $\mathcal{S}_L$ and replace γ_μ by the decomposition (B.24). Due to Eq. (B.25) and $n_\pm^2 = 0$ most of the terms cancel and with $n_+ \cdot n_- = 2$ we find

$$\mathcal{S}_L = \not{n}_- P_L \gamma^\alpha \gamma_\perp^\mu \otimes \not{n}_+ P_L \gamma_{\perp\mu} \gamma_\alpha + \frac{1}{2} \not{n}_- P_L \gamma^\alpha \not{n}_- \otimes \not{n}_+ P_L \not{n}_+ \gamma_\alpha \,. \tag{B.36}$$

The first term matches the definition of the operator $\mathcal{O}_2^{QCD}$ (cf. (2.19)). Using $P_L \not{n}_+ = \not{n}_+ P_R$ and $n_+^2 = 0$ the second term vanishes and thus, the result is given by

$$\mathcal{S}_L = \frac{1}{2} \mathcal{O}_2^{QCD} \,. \tag{B.37}$$

Next, we consider the Dirac structure $\mathcal{S}_R$. Before substituting γ_μ by the light-cone decomposition, we interchange the ordering of the γ-matrices in order to match the operators with the primed indices (B.15)- (B.17)

$$\mathcal{S}_R = -\not{n}_- P_L \gamma^\alpha \gamma^\mu \otimes \not{n}_+ P_R \gamma_\alpha \gamma_\mu + 2d\, \not{n}_- P_L \otimes \not{n}_+ P_R \,. \tag{B.38}$$

The second term can already be expressed in terms of $\mathcal{O}_1^{\prime QCD}$ and in the first term, we proceed similarly as in the reduction of $\mathcal{S}_L$. We obtain

$$\mathcal{S}_R = -\frac{1}{2} \mathcal{O}_2^{\prime QCD} + (d-2) \mathcal{O}_1^{\prime QCD} \,. \tag{B.39}$$

Example 1

We consider the Dirac structure

$$\mathcal{K}_{L(R)} = \left[\bar{\mathbf{q}}\, \not{q}_3 P_L \gamma^\alpha \gamma^\mu \mathbf{q}\right] \left[\bar{c}\, P_{L(R)} \gamma_\mu \gamma_\alpha b\right] \tag{B.40}$$

and reduce it to the set of operators Eqs. (B.12)-(B.17). As first step, q_3 is replaced by n_+ and n_- using Eq. (B.19). Taking into account the eom (B.21) the contribution involving n_+ vanishes and we obtain

$$\mathcal{K}_{L(R)} = -\frac{m_b}{2} \left[\bar{\mathbf{q}}\, \not{n}_- P_L \gamma^\alpha \gamma^\mu \mathbf{q}\right] \left[\bar{c}\, P_{L(R)} \gamma_\mu \gamma_\alpha b\right] \,. \tag{B.41}$$

In the following we omit the prefactor $-m_b/2$ and use the abbreviations

$$\tilde{\mathcal{K}}_{L(R)} \equiv \left[\bar{\mathbf{q}}\, \not{n}_- P_L \gamma^\alpha \gamma^\mu \mathbf{q}\right] \left[\bar{c}\, P_{L(R)} \gamma_\mu \gamma_\alpha b\right] \equiv \not{n}_- P_L \gamma^\alpha \gamma^\mu \otimes P_{L(R)} \gamma_\mu \gamma_\alpha \,. \tag{B.42}$$

Next, we focus on $\tilde{\mathcal{K}}_L$ and introduce the momentum q_3 on the heavy quark line by applying the eom (B.2)

$$\tilde{\mathcal{K}}_L = -\frac{1}{m_c} \not{n}_- P_L \gamma^\alpha \gamma^\mu \otimes \not{q}_3 P_L \gamma_\mu \gamma_\alpha \ . \tag{B.43}$$

Then, q_3 is further substituted by n_+ and v (cf. (B.19) and $n_- = 2v - n_+$). The resulting expression reads:

$$\tilde{\mathcal{K}}_L = \frac{m_c^2 - m_b^2}{4 m_b m_c} \not{n}_- P_L \gamma^\alpha \gamma^\mu \otimes \not{n}_+ P_L \gamma_\mu \gamma_\alpha + \frac{m_b}{m_c} \not{n}_- P_L \gamma^\alpha \gamma^\mu \otimes P_R \not{v} \gamma_\mu \gamma_\alpha \ . \tag{B.44}$$

The Dirac structure of the first term can be expressed in terms of $\mathcal{O}_2^{\text{QCD}}$ (cf. Eq. (B.37)). In the second term we commute v to the right by using the Clifford algebra (B.3) which yields two additional terms

$$\begin{aligned} \tilde{\mathcal{K}}_L = \frac{m_c^2 - m_b^2}{4 m_b m_c} \mathcal{O}_2^{\text{QCD}} + \frac{m_b}{m_c} \not{n}_- P_L \gamma^\alpha \gamma^\mu \otimes P_R \gamma_\mu \gamma_\alpha \not{v} + \frac{2 m_b}{m_c} P_R \not{n}_- \gamma^\alpha \not{v} \otimes P_R \gamma_\alpha \\ - \frac{2 m_b}{m_c} P_R \not{n}_- \not{v} \gamma^\mu \otimes P_R \gamma_\mu \ , \end{aligned} \tag{B.45}$$

where we have used $\not{n}_- P_L = P_R \not{n}_-$. Due to $\not{v} b(q_4) = b(q_4)$ the Dirac structure of the second term matches $\tilde{\mathcal{K}}_R$. In the other two terms we replace $v = (n_+ + n_-)/2$. The contribution of n_+ in the third and n_- in the last term yield zero due to the eom (B.21) and $n_-^2 = 0$, respectively, and we find

$$\tilde{\mathcal{K}}_L = \frac{m_c^2 - m_b^2}{4 m_b m_c} \mathcal{O}_2^{\text{QCD}} + \frac{m_b}{m_c} \tilde{\mathcal{K}}_R + \frac{m_b}{m_c} P_R \not{n}_- \gamma^\alpha \not{n}_- \otimes P_R \gamma_\alpha - \frac{m_b}{m_c} P_R \not{n}_- \not{n}_+ \gamma^\mu \otimes P_R \gamma_\mu \ . \tag{B.46}$$

We then move n_- to the left in the third term in order to apply $n_-^2 = 0$, and in the last term we commute n_+ to the right to use the eom (B.21)

$$\tilde{\mathcal{K}}_L = \frac{m_c^2 - m_b^2}{4 m_b m_c} \mathcal{O}_2^{\text{QCD}} + \frac{m_b}{m_c} \tilde{\mathcal{K}}_R + \frac{2 m_b}{m_c} P_R \not{n}_- \otimes P_R \not{n}_- - \frac{2 m_b}{m_c} P_R \not{n}_- \otimes P_R \not{n}_+ \ . \tag{B.47}$$

In third term we substitute $n_- = 2v - n_+$ on the heavy quark line and apply the eom (B.22) to remove v. The contribution with n_+ matches the definition of O_1^{QCD}. Moreover, the last term can be written as O_1^{QCD} and with $P_R \not{n}_- \otimes P_R = \frac{1}{4} O_1^{\text{QCD}} + \frac{m_c}{4 m_b} O_1^{\prime \text{QCD}}$[4] we obtain

$$\tilde{\mathcal{K}}_L = \frac{m_c^2 - m_b^2}{4 m_b m_c} \mathcal{O}_2^{\text{QCD}} + \frac{m_b}{m_c} \tilde{\mathcal{K}}_R + \mathcal{O}_1^{\prime \text{QCD}} - \frac{m_b}{m_c} \mathcal{O}_1^{\text{QCD}} \ . \tag{B.48}$$

Similar, we find that $\tilde{\mathcal{K}}_R$ mixes with $\tilde{\mathcal{K}}_L$[5] and using Eq. (B.39) and $P_R \not{n}_- \otimes P_L = \frac{m_c}{4 m_b} O_1^{\text{QCD}} + 2(d-2) O_1^{\prime \text{QCD}}$ the corresponding expression can be derived:

$$\tilde{\mathcal{K}}_R = \frac{-m_c^2 + m_b^2}{4 m_b m_c} \mathcal{O}_2^{\prime \text{QCD}} + \frac{m_c}{m_b} \tilde{\mathcal{K}}_L + \left[\frac{m_c^2 - m_b^2}{4 m_b m_c} 2(d-2) - \frac{m_b}{m_c} \right] \mathcal{O}_1^{\prime \text{QCD}} + \mathcal{O}_1^{\text{QCD}} \ , \tag{B.49}$$

[4] This relation can be easily derived following the same lines as the example presented here.

[5] Note that in the operators with the primed indices, the ordering of the Dirac matrices on the heavy quark line is reversed.

where d denotes the spacetime dimension. From Eqs. (B.48) and (B.49) the expressions for $\tilde{\mathcal{K}}_{L(R)}$ in terms of the operators (B.12)- (B.17) can be extracted

$$\tilde{\mathcal{K}}_L = \frac{d}{2}\mathcal{O}_1^{\prime\mathrm{QCD}} - \frac{1}{4}\mathcal{O}_2^{\prime\mathrm{QCD}} + \frac{m_c}{4m_b}\mathcal{O}_2^{\mathrm{QCD}} \,, \tag{B.50}$$

$$\tilde{\mathcal{K}}_R = \frac{1}{2}\frac{m_c}{m_b}(d-2)\mathcal{O}_1^{\prime\mathrm{QCD}} - \frac{1}{4}\frac{m_c}{m_b}\mathcal{O}_2^{\prime\mathrm{QCD}} + \mathcal{O}_1^{\mathrm{QCD}} + \frac{1}{4}\mathcal{O}_2^{\mathrm{QCD}} \,, \tag{B.51}$$

which then multiplied by $-m_b/2$ yield the results for $\mathcal{K}_{L(R)}$.

Example 2

As second example we perform the reduction of the following operators

$$\mathcal{R}_{L(R)} = \left[\bar{\mathbf{q}}\, P_R\gamma^\mu\gamma^\alpha\gamma^\beta\mathbf{q}\right]\left[\bar{c}\, P_{L(R)}\gamma_\mu\gamma_\alpha\gamma_\beta b\right] \equiv P_R\gamma^\mu\gamma^\alpha\gamma^\beta \otimes P_{L(R)}\gamma_\mu\gamma_\alpha\gamma_\beta, \tag{B.52}$$

which have the Dirac structures of the form (B.11). First, we consider $\mathcal{R}_L$ and insert the identity (B.33) on the l.h.s. of the light quark line:

$$\mathcal{R}_L = \frac{1}{4}(\not{n}_+\not{n}_- + \not{n}_-\not{n}_+)P_L\gamma^\mu\gamma^\alpha\gamma^\beta \otimes P_L\gamma_\mu\gamma_\alpha\gamma_\beta \,. \tag{B.53}$$

The first term in the sum vanishes as a result of the eom (B.21). Next, we commute n_+ to the right and again applying the E.o.M (B.21) we obtain

$$\mathcal{R}_L = \frac{1}{2}\left(P_R\not{n}_-\gamma^\alpha\gamma^\beta \otimes P_L\not{n}_+\gamma_\alpha\gamma_\beta - P_R\not{n}_-\gamma^\alpha\gamma^\beta \otimes P_L\gamma_\alpha\not{n}_+\gamma_\beta + P_R\not{n}_-\gamma^\alpha\gamma^\beta \otimes P_L\gamma_\alpha\gamma_\beta\not{n}_-\right) \,. \tag{B.54}$$

The first term can be related to $\mathcal{O}_2^{\prime\mathrm{QCD}}$, as given in Eq. (B.39). The γ-matrices in the second and third term can be commuted such that they match the structure of $\mathcal{O}_2^{\prime\mathrm{QCD}}$ as well and after a few simplifications the final result takes the form

$$\mathcal{R}_L = \mathcal{O}_1^{\prime\mathrm{QCD}} + \frac{3}{4}\mathcal{O}_2^{\prime\mathrm{QCD}} \,. \tag{B.55}$$

In an analogue calculation and by means Eq. (B.37) one finds

$$\mathcal{R}_R = \frac{1}{4}(-8+6d)\mathcal{O}_1^{\mathrm{QCD}} - \frac{3}{4}\mathcal{O}_2^{\mathrm{QCD}} \,. \tag{B.56}$$

Appendix C

Results for the Master Integrals

We show the results for master integrals given in Fig. 4.1. The calculation was performed using the techniques presented in Chap. 4 and the integration measure $\int d^dk/(2\pi)^d$. In order to facilitate the presentation of the results we write the master integrals as

$$\tilde{M} = -\frac{M}{(m_b^2)^{d-n} S_\Gamma^2}\,, \tag{C.1}$$

with an integer n that denotes the sum of all propagator powers, such that the integral $\tilde{M}$ is dimensionless and S_Γ defined as

$$S_\Gamma = \frac{1}{(4\pi)^{d/2}\Gamma(1-\epsilon)}\,. \tag{C.2}$$

The results for mass-flipped integrals can be obtained by letting $z_c \to 1/z_c$, keeping in mind that the analytic continuation is done via $z_c \to z_c - i\eta$, with infinitesimal $\eta > 0$. We remind that for the master integrals $M_{13,14,15}$ we have found a closed representation in terms of hypergeometric functions. $M_{4,5,19}$ were calculated by solving differential equations and for $M_{1-3,6-12,16-18,20-23}$ a MB representation was found. For the master integrals in the canonical basis and the corresponding results we refer to [C].

The analytic results for $M_{4,5,19}$ are only displayed up to $\mathcal{O}(\epsilon)$ since the expressions of $\mathcal{O}(\epsilon^2)$ are rather lengthy. The latter can be derived from the corresponding differential equations and the boundary conditions given in Sec. 4.4 (see also App. D.3 for the evaluation of $M_{4,5}$). For $M_{1-3,6-12,16-18,20-22}$ a MB representation was derived with AMBRE.m. We don't present the results for the integrals M_{20-22}. Their MB representation contains highly oscillating integrands which could not be evaluated by MB.m. Here, we rely on the corresponding analytic results obtained in the canonical basis which we numerically cross-checked by the sector decomposition method implemented in SecDec (see also Sec. 4.6). We present the MB representations for the remaining integrals before having performed the analytic continuation to $\epsilon \to 0$ and state the real parts of the Barnes parameters which fix the contours in the complex plain. The analytic continuation can be performed using MB.m and the expressions

for the master integral can be derived up to an arbitrary order in ϵ. Note that for two integrals, namely M_1 and M_{10}, an additional regulator δ has to be introduced in order to fix the contours. One power of a certain propagator then is shifted by the regulator and subsequently $\delta \to 0$. In the resulting expression, which is independent of δ, the analytic continuation $\epsilon \to 0$ can be performed:

$$\begin{aligned}\tilde{M}_1 = &\int_{-i\infty-\frac{9}{32}}^{i\infty-\frac{9}{32}} \frac{dz_1}{2\pi i} \int_{-i\infty-\frac{3}{256}}^{i\infty-\frac{3}{256}} \frac{dz_2}{2\pi i} \int_{-i\infty-\frac{7}{16}}^{i\infty-\frac{7}{16}} \frac{dz_3}{2\pi i} \int_{-i\infty-\frac{1}{2}}^{i\infty-\frac{1}{2}} \frac{dz_4}{2\pi i} \int_{-i\infty-\frac{1}{8}}^{i\infty-\frac{1}{8}} \frac{dz_5}{2\pi i} \\ &\times \frac{(-1)^{\delta+5}}{\Gamma(\delta+2)} \left(m_b^2\right)^{-\delta} u^{z_3+z_4} (-1-i\eta)^{z_3+z_5} z_c^{-\delta-2\epsilon-1-z_3-z_5} \frac{\Gamma(1-\epsilon)^2}{\Gamma(2-2\epsilon)} \Gamma(z_1+1) \\ &\times \frac{\Gamma(-z_2)\Gamma(-z_3)\Gamma(-z_4)\Gamma(-z_5)}{\Gamma(-2\epsilon+z_1-\delta+1)\Gamma(-\epsilon-z_2-\delta)} \Gamma(-2\epsilon-z_1+1)\Gamma(\epsilon+z_1)\Gamma(z_3+z_4+1) \\ &\times \Gamma(-\epsilon+z_1-z_2+1)\Gamma(-\epsilon+z_2-\delta)\Gamma(-\epsilon-z_2-z_3-z_4-\delta-1) \\ &\times \Gamma(\epsilon-z_1+z_2+z_3+z_4+z_5+\delta+1) \end{aligned} \tag{C.3}$$

with $\epsilon = \frac{11}{32}$, where we have introduced a regulator δ in the dotted propagator (this expression can now be savely expanded in δ and is finite for $\delta \to 0$),

$$\begin{aligned}\tilde{M}_2 = &\int_{-i\infty-\frac{13}{16}}^{i\infty-\frac{13}{16}} \frac{dz_1}{2\pi i} \int_{-i\infty-\frac{1}{2}}^{i\infty-\frac{1}{2}} \frac{dz_2}{2\pi i} \int_{-i\infty-\frac{1}{16}}^{i\infty-\frac{1}{16}} \frac{dz_3}{2\pi i} \int_{-i\infty-\frac{23}{32}}^{i\infty-\frac{23}{32}} \frac{dz_4}{2\pi i} \int_{-i\infty-\frac{1}{8}}^{i\infty-\frac{1}{8}} \frac{dz_5}{2\pi i} \\ &\times -u^{z_3+z_4} (-1-i\eta)^{-\epsilon-1+z_1-2z_2-z_3-2z_5} z_c^{-\epsilon-1+z_1-2z_2-z_3-2z_5} \frac{\Gamma(1-\epsilon)^2}{\Gamma(2-2\epsilon)} \Gamma(-\epsilon+z_2+1) \\ &\times \frac{\Gamma(-z_2)\Gamma(-z_3)\Gamma(-z_4)\Gamma(-z_5)}{\Gamma(-\epsilon-z_2+1)\Gamma(-2\epsilon+z_1-z_2-z_5+1)} \Gamma(z_3+z_4+2)\Gamma(z_1-z_2-z_5+1) \\ &\times \Gamma(-\epsilon+z_1-2z_2-z_5)\Gamma(\epsilon+z_1-z_2-z_5)\Gamma(-2\epsilon-z_1+z_2+z_5+1) \\ &\times \Gamma(-\epsilon-z_2-z_3-z_4-1)\Gamma(\epsilon-z_1+2z_2+z_3+z_4+2z_5+1) \end{aligned} \tag{C.4}$$

with $\epsilon = \frac{1}{4}$,

$$\begin{aligned}\tilde{M}_3 = &\int_{-i\infty-\frac{3}{16}}^{i\infty-\frac{3}{16}} \frac{dz_1}{2\pi i} \int_{-i\infty-\frac{1}{32}}^{i\infty-\frac{1}{32}} \frac{dz_2}{2\pi i} \int_{-i\infty-\frac{1}{2}}^{i\infty-\frac{1}{2}} \frac{dz_3}{2\pi i} \int_{-i\infty-\frac{1}{4}}^{i\infty-\frac{1}{4}} \frac{dz_4}{2\pi i} \int_{-i\infty-\frac{1}{8}}^{i\infty-\frac{1}{8}} \frac{dz_5}{2\pi i} \\ &\times -u^{z_3+z_4} (-1-i\eta)^{-2\epsilon-1-z_1-z_3} z_c^{-2\epsilon-1-z_1-z_3} \frac{\Gamma(1-\epsilon)^2}{\Gamma(1-2\epsilon)} \Gamma(-\epsilon+z_2+1)\Gamma(z_3+z_4+1) \\ &\times \frac{\Gamma(-z_2)\Gamma(-z_3)\Gamma(-z_4)\Gamma(-z_5)\Gamma(-z_1+z_2+z_5)}{\Gamma(-\epsilon-z_2+1)\Gamma(-3\epsilon-z_1+z_2+z_5+1)} \Gamma(-2\epsilon-z_1+z_5)\Gamma(-\epsilon-z_2-z_3-z_4) \\ &\times \Gamma(-\epsilon+z_1-z_2-z_5+1)\Gamma(-\epsilon-z_1+z_2+z_5)\Gamma(2\epsilon+z_1+z_3+z_4+1) \end{aligned} \tag{C.5}$$

with $\epsilon = 0$,

$$\tilde{M}_4 = \frac{1}{2\boldsymbol{\epsilon^2}} + \frac{5}{2\boldsymbol{\epsilon}} - \frac{1}{6(z_c-1)} \big[6z_c \ln(1-z_c) \ln^2(z_c) + 6z_c \ln(1-z_c) \ln(z_c)$$

$$
\begin{aligned}
&- 12\ln(1-z_c)\ln(z_c) + 6z_c\mathrm{Li}_2(1-z_c)\ln(z_c) + 6z_c\mathrm{Li}_2(z_c)\ln(z_c) \\
&- 6\mathrm{Li}_2(z_c)\ln(z_c) - 57z_c - 6\mathrm{Li}_2(1-z_c) + 6z_c\mathrm{Li}_2(z_c) - 12\mathrm{Li}_2(z_c) + 12\mathrm{Li}_3(z_c) \\
&- 12\zeta_3 + \pi^2 + 57\big] \\
&+ \boldsymbol{\epsilon}\,\frac{1}{240(z_c-1)}\big[240H_{3,0}(z_c) + 240H_{2,0,0}(z_c) + 1440H_{2,1,0}(z_c) + 240\mathrm{Li}_2(z_c)^2 \\
&+ 1200z_c\mathrm{Li}_2(z_c) - 1200\mathrm{Li}_2(z_c) + 480z_c\mathrm{Li}_3(1-z_c) - 480\mathrm{Li}_3(1-z_c) + 240z_c\mathrm{Li}_3(z_c) \\
&- H_{2,0,0}(z_c)\mathrm{Li}_3(z_c) - 240\mathrm{Li}_2(1-z_c)\ln^2(z_c) - 480\mathrm{Li}_2(z_c)\ln^2(z_c) \\
&+ 240z_c\mathrm{Li}_2(1-z_c)\ln(z_c) + 480\mathrm{Li}_2(1-z_c)\ln(1-z_c)\ln(z_c) - 240\mathrm{Li}_2(1-z_c)\ln(z_c) \\
&+ 960\mathrm{Li}_2(z_c)\ln(1-z_c)\ln(z_c) + 240\mathrm{Li}_2(z_c)\ln(z_c) + 480\mathrm{Li}_3(z_c)\ln(z_c) \\
&- 960z_c\mathrm{Li}_2(1-z_c)\ln(1-z_c) + 960\mathrm{Li}_2(1-z_c)\ln(1-z_c) - 960z_c\mathrm{Li}_2(z_c)\ln(1-z_c) \\
&+ 960\mathrm{Li}_2(z_c)\ln(1-z_c) - 960\mathrm{Li}_3(z_c)\ln(1-z_c) - 960S_{2,2}(z_c) - 240z_c\zeta_3 - 720\zeta_3\ln(z_c) \\
&+ 960\zeta_3\ln(1-z_c) + 7800z_c - 40z_c\ln^3(z_c) - 240\ln(1-z_c)\ln^3(z_c) + 40\ln^3(z_c) \\
&+ 480\ln^2(1-z_c)\ln^2(z_c) + 600z_c\ln^2(z_c) + 120z_c\ln(1-z_c)\ln^2(z_c) \\
&- 120\ln(1-z_c)\ln^2(z_c) + 60\pi^2\ln^2(z_c) - 600\ln^2(z_c) - 960z_c\ln^2(1-z_c)\ln(z_c) \\
&+ 960\ln^2(1-z_c)\ln(z_c) - 120\pi^2 z_c\ln(z_c) - 4560z_c\ln(z_c) + 1200z_c\ln(1-z_c)\ln(z_c) \\
&- 160\pi^2\ln(1-z_c)\ln(z_c) - 1200\ln(1-z_c)\ln(z_c) + 80\pi^2\ln(z_c) + 3215\ln(z_c) \\
&+ 160\pi^2 z_c\ln(1-z_c) - 160\pi^2\ln(1-z_c) + 740\psi^{(2)}(3)\ln(z_c) - 160\psi^{(2)}(2)\ln(z_c) \\
&- 100\psi^{(2)}(1)\ln(z_c) + 720\zeta_3 + 16\pi^4 - 7800\big] + \mathcal{O}(\boldsymbol{\epsilon^2})\ ,
\end{aligned}
\tag{C.6}
$$

where $S_{2,2}$ is a Nielson polylogarithm,

$$
\begin{aligned}
\tilde{M}_5 = &\frac{-2\mathrm{Li}_3(z_c) + \mathrm{Li}_2(z_c)\log(z_c) + 2\zeta_3}{z_c-1} \\
&+ \boldsymbol{\epsilon}\,\frac{1}{180(z_c-1)}\big[-720\zeta_3 H_-(\sqrt{z_c}) + 120\pi^2 H_{-,0}(\sqrt{z_c}) - 4320H_{0,0,-,0}(\sqrt{z_c}) \\
&- 7200H_{0,-,0,0}(\sqrt{z_c}) - 1440H_{0,-,0,-}(\sqrt{z_c}) - 720H_{0,-,-,0}(\sqrt{z_c}) - 1440H_{-,0,-,0}(\sqrt{z_c}) \\
&- 1440\log(1-z_c)H_{0,-,0}(\sqrt{z_c}) + 1440\log(z_c)H_{0,-,0}(\sqrt{z_c}) - 720H_{0,+,+,0}(\sqrt{z_c}) \\
&- 720\zeta(3)\log(1-z_c) + 7\pi^4\big] + \mathcal{O}(\boldsymbol{\epsilon^2})\ ,
\end{aligned}
\tag{C.7}
$$

$$
\begin{aligned}
\tilde{M}_6 = &\int_{-i\infty-\frac{309}{512}}^{i\infty-\frac{309}{512}}\frac{dz_1}{2\pi i}\int_{-i\infty-\frac{317}{512}}^{i\infty-\frac{317}{512}}\frac{dz_2}{2\pi i}\int_{-i\infty-\frac{1}{4}}^{i\infty-\frac{1}{4}}\frac{dz_3}{2\pi i}\int_{-i\infty-\frac{1}{256}}^{i\infty-\frac{1}{256}}\frac{dz_4}{2\pi i}\int_{-i\infty-\frac{1}{4}}^{i\infty-\frac{1}{4}}\frac{dz_5}{2\pi i}\int_{-i\infty-\frac{1}{16}}^{i\infty-\frac{1}{16}}\frac{dz_6}{2\pi i} \\
&\times\int_{-i\infty-\frac{1}{32}}^{i\infty-\frac{1}{32}}\frac{dz_7}{2\pi i}\,u^{z_4+z_5+z_6+z_7}\,(-1-i\eta)^{z_4}\,z_c^{z_3+z_5+z_7}\frac{\Gamma(1-\epsilon)^2\Gamma(-z_1)\Gamma(z_2+1)}{\Gamma(-2\epsilon)\Gamma(-3\epsilon-z_1)\Gamma(-\epsilon+z_2+1)} \\
&\times\Gamma(-z_3)\Gamma(-z_4)\Gamma(-z_5)\Gamma(-z_6)\Gamma(-z_7)\Gamma(-\epsilon-z_1-1)\Gamma(z_6+z_7+1)\Gamma(-\epsilon+z_1-z_2) \\
&\times\Gamma(-z_2+z_4+z_5)\Gamma(z_3+z_4+z_5+1)\Gamma(-\epsilon+z_2-z_3-z_4-z_5) \\
&\times\Gamma(-3\epsilon-z_1+z_2-z_4-z_5-z_6-z_7-1)\Gamma(2\epsilon+z_1+z_3+z_4+z_5+z_6+z_7+2)
\end{aligned}
\tag{C.8}
$$

with $\epsilon = -\frac{51}{128}$,

$$\begin{aligned}\tilde{M}_7 = &\int_{-i\infty-\frac{309}{512}}^{i\infty-\frac{309}{512}} \frac{dz_1}{2\pi i} \int_{-i\infty-\frac{317}{512}}^{i\infty-\frac{317}{512}} \frac{dz_2}{2\pi i} \int_{-i\infty-\frac{1}{4}}^{i\infty-\frac{1}{4}} \frac{dz_3}{2\pi i} \int_{-i\infty-\frac{1}{256}}^{i\infty-\frac{1}{256}} \frac{dz_4}{2\pi i} \int_{-i\infty-\frac{1}{4}}^{i\infty-\frac{1}{4}} \frac{dz_5}{2\pi i} \int_{-i\infty-\frac{1}{16}}^{i\infty-\frac{1}{16}} \frac{dz_6}{2\pi i} \\ &\times \int_{-i\infty-\frac{1}{32}}^{i\infty-\frac{1}{32}} \frac{dz_7}{2\pi i}\, u^{z_4+z_5+z_6+z_7} (-1-i\eta)^{z_5+z_6} \frac{z_c^{-2\epsilon-2-z_3-z_4}\Gamma(1-\epsilon)^2\Gamma(z_2+1)}{\Gamma(-2\epsilon)\Gamma(-3\epsilon-z_1)\Gamma(-\epsilon+z_2+1)} \\ &\times \Gamma(-z_1)\Gamma(-z_3)\Gamma(-z_4)\Gamma(-z_5)\Gamma(-z_6)\Gamma(-z_7)\Gamma(-\epsilon-z_1-1)\Gamma(z_6+z_7+1) \\ &\times \Gamma(-\epsilon+z_1-z_2)\Gamma(-z_2+z_4+z_5)\Gamma(z_3+z_4+z_5+1)\Gamma(-\epsilon+z_2-z_3-z_4-z_5) \\ &\times \Gamma(-3\epsilon-z_1+z_2-z_4-z_5-z_6-\mathrm{z}7-1)\Gamma(2\epsilon+z_1+z_3+z_4+z_5+z_6+z_7+2)\end{aligned} \tag{C.9}$$

with $\epsilon = -\frac{51}{128}$,

$$\begin{aligned}\tilde{M}_8 = &\int_{-i\infty-\frac{1}{4}}^{i\infty-\frac{1}{4}} \frac{dz_1}{2\pi i} \int_{-i\infty-\frac{1}{32}}^{i\infty-\frac{1}{32}} \frac{dz_2}{2\pi i} \int_{-i\infty-\frac{1}{8}}^{i\infty-\frac{1}{8}} \frac{dz_3}{2\pi i} \int_{-i\infty-\frac{1}{2}}^{i\infty-\frac{1}{2}} \frac{dz_4}{2\pi i} \int_{-i\infty-\frac{1}{16}}^{i\infty-\frac{1}{16}} \frac{dz_5}{2\pi i} \\ &\times -u^{z_3+z_4} (-1-i\eta)^{z_3} z_c^{-2\epsilon-1-z_2-z_3-z_5} \frac{\Gamma(1-\epsilon)^2}{\Gamma(1-2\epsilon)} \frac{\Gamma(-z_1)\Gamma(-z_2)\Gamma(-z_3)\Gamma(-z_4)\Gamma(-z_5)}{\Gamma(-3\epsilon-z_1+1)\Gamma(-\epsilon+z_2+z_5+1)} \\ &\times \Gamma(-\epsilon-z_1)\Gamma(-\epsilon+z_1+1)\Gamma(-\epsilon-z_2)\Gamma(2z_2+z_5+1)\Gamma(z_3+z_4+1) \\ &\times \Gamma(-3\epsilon-z_1-z_3-z_4)\Gamma(2\epsilon+z_1+z_2+z_3+z_4+z_5+1)\end{aligned} \tag{C.10}$$

with $\epsilon = \frac{1}{128}$,

$$\begin{aligned}\tilde{M}_9 = &\int_{-i\infty-\frac{1}{16}}^{i\infty-\frac{1}{16}} \frac{dz_1}{2\pi i} \int_{-i\infty-\frac{3}{128}}^{i\infty-\frac{3}{128}} \frac{dz_2}{2\pi i} \int_{-i\infty-\frac{1}{2}}^{i\infty-\frac{1}{2}} \frac{dz_3}{2\pi i} \int_{-i\infty-\frac{3}{32}}^{i\infty-\frac{3}{32}} \frac{dz_4}{2\pi i} \int_{-i\infty-\frac{3}{64}}^{i\infty-\frac{3}{64}} \frac{dz_5}{2\pi i} \\ &\times -u^{z_3+z_4} (-1-i\eta)^{z_3} z_c^{-2\epsilon-1-z_2-z_3-z_5} \frac{\Gamma(1-\epsilon)^2}{\Gamma(1-2\epsilon)} \frac{\Gamma(-z_1)\Gamma(-z_2)\Gamma(-z_3)\Gamma(-z_4)\Gamma(-z_5)}{\Gamma(-3\epsilon-z_1+1)\Gamma(-\epsilon+z_2+z_5+1)} \\ &\times \Gamma(-\epsilon-z_1+1)\Gamma(z_1-\epsilon)\Gamma(-\epsilon-z_2)\Gamma(2z_2+z_5+1)\Gamma(z_3+z_4+1) \\ &\times \Gamma(-3\epsilon-z_1-z_3-z_4)\Gamma(2\epsilon+z_1+z_2+z_3+z_4+z_5+1)\end{aligned} \tag{C.11}$$

with $\epsilon = -\frac{1}{8}$,

$$\begin{aligned}\tilde{M}_{10} = &\int_{-i\infty-\frac{3}{16}}^{i\infty-\frac{3}{16}} \frac{dz_1}{2\pi i} \int_{-i\infty-\frac{1}{8}}^{i\infty-\frac{1}{8}} \frac{dz_2}{2\pi i} \int_{-i\infty-\frac{3}{32}}^{i\infty-\frac{3}{32}} \frac{dz_3}{2\pi i} \int_{-i\infty-\frac{21}{32}}^{i\infty-\frac{21}{32}} \frac{dz_4}{2\pi i} \\ &\times \frac{(-1)^{\delta+5}}{\Gamma(\delta+1)} \left(m_b^2\right)^{-\delta} (-1-i\eta)^{z_3} u^{z_3+z_4} z_c^{z_2+z_4} \frac{\Gamma(1-\epsilon)^2}{\Gamma(-\epsilon)} \Gamma(-z_1)\Gamma(-z_2)\Gamma(-z_3)\Gamma(-z_4) \\ &\times \frac{\Gamma(-\epsilon-z_1+1)\Gamma(z_3+z_4+2)}{\Gamma(-2\epsilon-\delta+2)\Gamma(-3\epsilon-z_1-\delta+1)} \Gamma(-\epsilon+z_1-\delta+1)\Gamma(z_2+z_3+z_4+1) \\ &\times \Gamma(-\epsilon-z_2-z_3-z_4-1)\Gamma(-3\epsilon-z_1-z_3-z_4-\delta-1) \\ &\times \Gamma(2\epsilon+z_1+z_2+z_3+z_4+\delta+1)\end{aligned} \tag{C.12}$$

with $\delta = \frac{5}{8}$ and $\epsilon = -\frac{1}{4}$, where δ is the regulator of the undotted massless propagator,

$$\begin{aligned}\tilde{M}_{11} = &\int_{-i\infty-\frac{1}{16}}^{i\infty-\frac{1}{16}} \frac{dz_1}{2\pi i} \int_{-i\infty-\frac{1}{2}}^{i\infty-\frac{1}{2}} \frac{dz_2}{2\pi i} \int_{-i\infty-\frac{1}{4}}^{i\infty-\frac{1}{4}} \frac{dz_3}{2\pi i} \int_{-i\infty-\frac{1}{8}}^{i\infty-\frac{1}{8}} \frac{dz_4}{2\pi i} \\ &\times -(u)^{z_3+z_4} (-1-i\eta)^{z_3} z_c^{z_2+z_4} \frac{\Gamma(1-\epsilon)}{\Gamma(1-2\epsilon)} \frac{\Gamma(z_3+z_4+1)}{\Gamma(-3\epsilon-z_1+1)} \Gamma(-z_1)\Gamma(-z_2)\Gamma(-z_3)\Gamma(-z_4) \\ &\times \Gamma(-\epsilon-z_1)\Gamma(-\epsilon+z_1+1)\Gamma(z_2+z_3+z_4+1)\Gamma(-3\epsilon-z_1-z_3-z_4) \\ &\times \Gamma(-\epsilon-z_2-z_3-z_4)\Gamma(2\epsilon+z_1+z_2+z_3+z_4+1) \end{aligned} \tag{C.13}$$

with $\epsilon = \frac{1}{64}$,

$$\begin{aligned}\tilde{M}_{12} = &\int_{-i\infty-\frac{1}{16}}^{i\infty-\frac{1}{16}} \frac{dz_1}{2\pi i} \int_{-i\infty-\frac{25}{48}}^{i\infty-\frac{25}{48}} \frac{dz_2}{2\pi i} \int_{-i\infty-\frac{1}{4}}^{i\infty-\frac{1}{4}} \frac{dz_3}{2\pi i} \int_{-i\infty-\frac{1}{2}}^{i\infty-\frac{1}{2}} \frac{dz_4}{2\pi i} \\ &\times -u^{z_3+z_4} (-1-i\eta)^{z_3} z_c^{z_2+z_4} \frac{\Gamma(1-\epsilon)}{\Gamma(2-2\epsilon)} \frac{\Gamma(z_3+z_4+1)}{\Gamma(-3\epsilon-z_1+1)} \Gamma(-z_1)\Gamma(-z_2)\Gamma(-z_3)\Gamma(-z_4) \\ &\times \Gamma(-\epsilon-z_1+1)\Gamma(-\epsilon+z_1+1)\Gamma(z_2+z_3+z_4+2)\Gamma(-3\epsilon-z_1-z_3-z_4) \\ &\times \Gamma(-\epsilon-z_2-z_3-z_4-1)\Gamma(2\epsilon+z_1+z_2+z_3+z_4+1) \end{aligned} \tag{C.14}$$

with $\epsilon = \frac{3}{16}$,

$$\tilde{M}_{13} = -\Gamma(\epsilon)\frac{\Gamma^2(1-\epsilon)}{1-\epsilon}\Gamma(-1+\epsilon)\, z_c^{1-\epsilon}\, {}_2F_1(1,\epsilon,-\epsilon+2,1-u(1-z_c)-i\eta)\,, \tag{C.15}$$

$$\begin{aligned}\tilde{M}_{14} = &\Gamma^2(\epsilon)\frac{\Gamma^2(1-\epsilon)}{(1-\epsilon)^2}\, z_c^{-\epsilon}\, {}_2F_1(1,\epsilon,-\epsilon+2,1-u(1-z_c)-i\eta) \\ &\times\ {}_2F_1(1,\epsilon,-\epsilon+2,1-\bar{u}(1-z_c^{-1})+i\eta)\,, \end{aligned} \tag{C.16}$$

$$\tilde{M}_{15} = \frac{\Gamma^2(1-\epsilon)\Gamma^2(\epsilon)}{(\epsilon-1)(2\epsilon-1)}\, {}_2F_1(\epsilon,2\epsilon-1;2\epsilon;1-z_c+i\eta)\ , \tag{C.17}$$

$$\tilde{M}_{16} = -\int_{-i\infty-\frac{1}{4}}^{i\infty-\frac{1}{4}} \frac{dz_2}{2\pi i} (-1-i\eta)^{z_2} z_c^{z_2} \Gamma(1-\epsilon)^4 \frac{\Gamma(-z_2)\Gamma(\epsilon+z_2)\Gamma(2\epsilon+z_2-1)}{\Gamma(-\epsilon+z_2+2)} \tag{C.18}$$

with $\epsilon = \frac{3}{4}$,

$$\tilde{M}_{17} = \int_{-i\infty-\frac{1}{4}}^{i\infty-\frac{1}{4}} \frac{dz_2}{2\pi i} (-1-i\eta)^{z_2} z_c^{z_2} \Gamma(1-\epsilon)^4 \frac{\Gamma(-z_2)\Gamma(\epsilon+z_2)\Gamma(2\epsilon+z_2)}{\Gamma(-\epsilon+z_2+2)} \tag{C.19}$$

with $\epsilon = \frac{1}{2}$,

$$\tilde{M}_{18} = \int_{-i\infty-\frac{1}{8}}^{i\infty-\frac{1}{8}} \frac{dz_2}{2\pi i} \int_{-i\infty-\frac{5}{32}}^{i\infty-\frac{5}{32}} \frac{dz_3}{2\pi i} \int_{-i\infty-\frac{7}{512}}^{i\infty-\frac{7}{512}} \frac{dz_5}{2\pi i} \int_{-i\infty-\frac{7}{64}}^{i\infty-\frac{7}{64}} \frac{dz_7}{2\pi i} \int_{-i\infty-\frac{7}{128}}^{i\infty-\frac{7}{128}} \frac{dz_8}{2\pi i} \int_{-i\infty-\frac{7}{256}}^{i\infty-\frac{7}{256}} \frac{dz_9}{2\pi i}$$

$$\times (-1)\, u^{z_7+z_8}(-1-i\eta)^{z_8} z_c^{-2\epsilon-1-z_2-z_3-z_5-z_7-z_9} \frac{\Gamma(1-\epsilon)^2}{\Gamma(1-2\epsilon)}\Gamma(z_2-\epsilon)\Gamma(z_7+z_8+1)$$
$$\times \frac{\Gamma(-z_2)\Gamma(-z_3)\Gamma(-z_5)\Gamma(z_5+1)\Gamma(-z_7)\Gamma(-z_8)\Gamma(-z_9)\Gamma(-\epsilon-z_2+1)}{\Gamma(-3\epsilon-z_2+1)\Gamma(-\epsilon+z_3+z_5+z_9+1)\Gamma(z_5+z_7+z_8+z_9+2)}$$
$$\times \Gamma(z_7+z_8+z_9+1)\Gamma(-3\epsilon-z_2-z_7-z_8)\Gamma(-2\epsilon-z_2-z_3-z_7-z_8)$$
$$\times \Gamma(2\epsilon+z_2+z_3+z_5+z_7+z_8+z_9+1)\Gamma(\epsilon+z_2+2z_3+z_5+z_7+z_8+z_9+1) \tag{C.20}$$

with $\epsilon = -\frac{1}{4}$,

$$\begin{aligned}
\tilde{M}_{19} = {} & \frac{1}{2\boldsymbol{\epsilon^2}} + \frac{5-2\ln(z_c)}{2\boldsymbol{\epsilon}} + \frac{1}{6(z_c-1)}\big[-6z_c\mathrm{Li}_2(1-z_c)+6\mathrm{Li}_2(1-z_c)-12\mathrm{Li}_3(z_c) \\
& +6\mathrm{Li}_2(1-z_c)\ln(z_c)+12\mathrm{Li}_2(z_c)\ln(z_c)+\pi^2 z_c+57z_c+3z_c\ln^2(z_c) \\
& +6\ln(1-z_c)\ln^2(z_c)-3\ln^2(z_c)-30z_c\ln(z_c)-2\pi^2\ln(z_c)+30\ln(z_c)+12\zeta_3-\pi^2-57\big] \\
& +\boldsymbol{\epsilon}\,\frac{1}{240(z_c-1)}\big[240H_{3,0}(z_c)+240H_{2,0,0}(z_c)+1440H_{2,1,0}(z_c)+240\mathrm{Li}_2(z_c)^2 \\
& +1200z_c\mathrm{Li}_2(z_c)-1200\mathrm{Li}_2(z_c)+480z_c\mathrm{Li}_3(1-z_c)-480\mathrm{Li}_3(1-z_c)+240z_c\mathrm{Li}_3(z_c) \\
& -720\mathrm{Li}_3(z_c)-240\mathrm{Li}_2(1-z_c)\ln^2(z_c)-480\mathrm{Li}_2(z_c)\ln^2(z_c)+240z_c\mathrm{Li}_2(1-z_c)\ln(z_c) \\
& +480\mathrm{Li}_2(1-z_c)\ln(1-z_c)\ln(z_c)-240\mathrm{Li}_2(1-z_c)\ln(z_c)+960\mathrm{Li}_2(z_c)\ln(1-z_c)\ln(z_c) \\
& +240\mathrm{Li}_2(z_c)\ln(z_c)+480\mathrm{Li}_3(z_c)\ln(z_c)-960z_c\mathrm{Li}_2(1-z_c)\ln(1-z_c) \\
& +960\mathrm{Li}_2(1-z_c)\ln(1-z_c)-960z_c\mathrm{Li}_2(z_c)\ln(1-z_c)+960\mathrm{Li}_2(z_c)\ln(1-z_c) \\
& -960\mathrm{Li}_3(z_c)\ln(1-z_c)-960S_{2,2}(z_c)-240z_c\zeta_3-720\zeta_3\ln(z_c) \\
& +960\zeta_3\ln(1-z_c)+7800z_c-40z_c\ln^3(z_c)-240\ln(1-z_c)\ln^3(z_c)+40\ln^3(z_c) \\
& +480\ln^2(1-z_c)\ln^2(z_c)+600z_c\ln^2(z_c)+120z_c\ln(1-z_c)\ln^2(z_c) \\
& -120\ln(1-z_c)\ln^2(z_c)+60\pi^2\ln^2(z_c)-600\ln^2(z_c)-960z_c\ln^2(1-z_c)\ln(z_c) \\
& +960\ln^2(1-z_c)\ln(z_c)-120\pi^2 z_c\ln(z_c)-4560z_c\ln(z_c)+1200z_c\ln(1-z_c)\ln(z_c) \\
& -160\pi^2\ln(1-z_c)\ln(z_c)-1200\ln(1-z_c)\ln(z_c)+80\pi^2\ln(z_c)+3215\ln(z_c) \\
& +160\pi^2 z_c\ln(1-z_c)-160\pi^2\ln(1-z_c)+740\psi^{(2)}(3)\ln(z_c)-160\psi^{(2)}(2)\ln(z_c) \\
& -100\psi^{(2)}(1)\ln(z_c)+H_{2,0,0}(z_c)\zeta_3+16\pi^4-7800\big]+\mathcal{O}(\boldsymbol{\epsilon^2})\,,
\end{aligned} \tag{C.21}$$

$$\begin{aligned}
\tilde{M}_{23} = {} & \frac{\Gamma^4(1-\epsilon)}{\Gamma(2-2\epsilon)}\frac{1}{\Gamma(-3\epsilon+2)}\frac{1}{(2\pi i)^2}\int_{-i\infty-\frac{3}{16}}^{i\infty-\frac{3}{16}} dz_1 \int_{-i\infty-\frac{1}{16}}^{i\infty-\frac{1}{16}} dz_2\, \bar{u}^{z_2} u^{z_1-z_2}(1-z_c)^{z_1}\frac{\Gamma(\epsilon+z_2)}{\Gamma(1+\epsilon+z_2)} \\
& \times \Gamma(-4\epsilon+1-z_1)\Gamma(1+\epsilon+z_1)\Gamma(-z_1+z_2)\Gamma(2\epsilon+z_1)\Gamma(-z_2)
\end{aligned} \tag{C.22}$$

with $\epsilon = -\frac{1}{8}$.

Appendix D

Examples of Evaluating Master Integrals

We present the explicit evaluation of a selection of master integrals by applying the methods presented in Chap. 4. The results for the other integrals are obtained in a similar manner.

D.1. Hypergeometric Functions: M_{15}

The master integral M_{15} depicted in Fig. D.1 is evaluated by using Feynman parameters and hypergeometric functions. With the parametrization of the momenta as shown in Fig. D.1 the integral is given by the following expression

$$\int \frac{d^dk_1}{(2\pi)^d} \int \frac{d^dk_2}{(2\pi)^d} \frac{1}{[(q_4-k_2)^2-m_b^2+i\eta]\ [(q_3+k_1)^2-m_c^2+i\eta]\ [(k_2-k_1)^2+i\eta]}\,, \tag{D.1}$$

where $\eta > 0$ denotes the location of the poles in the complex plane. In the following, we consider the second and the third propagator of (D.1), since those are the only ones that depend on the integration momentum k_1. By introducing a Feynman parameter x according to (E.6) we find

$$\begin{aligned}\int \frac{d^dk_1}{(2\pi)^d} &\frac{1}{[(q_3+k_1)^2-m_c^2+i\eta]\ [(k_2-k_1)^2+i\eta]} \\ &= \int \frac{d^dk_1}{(2\pi)^d} \int_0^1 dx \frac{1}{[x(q_3+k_1)^2-xm_c^2+(1-x)(k_2-k_1)^2+i\eta]^2}\,.\end{aligned} \tag{D.2}$$

In order to perform the integration over k_1, we simplify and rearrange the denominator and arrive at the following expression

$$\int \frac{d^dk_1}{(2\pi)^d} \int_0^1 dx \frac{1}{[(k_1+xq_3-\bar{x}k_2)^2-A^2+i\eta]^2}\,, \tag{D.3}$$

where $A^2 = m_c^2x^2 - x\bar{x}k_2^2 - 2x\bar{x}q_3k_2$ and $\bar{x} = (1-x)$. Since A^2 is independent of k_1, we shift the integration variable $k_1 \to k_1 + xq_3 - \bar{x}k_2$ according to (E.1). By applying (E.2) the

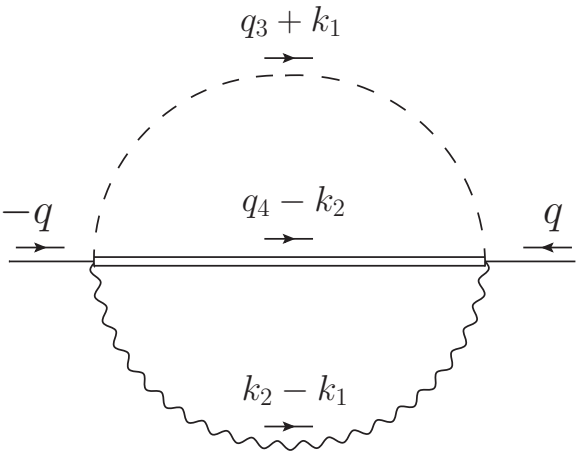

Figure D.1. – M_{15} with a specific choice of the momentum flow of the inner lines. k_1 and k_2 are loop momenta and $q = -q_3 - q_4$ is the external momentum.

integration over k_1 can be performed and we obtain

$$\frac{i}{(4\pi)^{\frac{d}{2}}}\Gamma(2-\tfrac{d}{2})\int_0^1 dx \frac{x^{-2+\frac{d}{2}}}{\left[\tilde{A}^2 - i\eta\right]^{2-\frac{d}{2}}}\,, \tag{D.4}$$

where $\tilde{A}^2 = A^2/x$. Note that in (D.4) the denominator has a small imaginary part with a negative sign. In order to trace the location of the poles in the complex plane in the further calculation, we take out a factor (-1) of the denominator in (D.4) by applying Eq. (E.5) such that the sign of the imaginary part becomes positive.

We then combine the result with the first propagator in (D.1) by introducing a second Feynman parameter y and after some simplifications we obtain the following expression for the master integral

$$\begin{aligned} M_{15} = \frac{i}{(4\pi)^{\frac{d}{2}}}(-1)^{2-\frac{d}{2}}\,\Gamma(3-\tfrac{d}{2})\int_0^1 dx \int_0^1 dy\, y^{1-\frac{d}{2}} x^{-2+\frac{d}{2}}(1-xy)^{-3+\frac{d}{2}} \\ \times \int \frac{d^dk_2}{(2\pi)^d}\left[\left(k_2 + \frac{y\bar{x}q_3 - \bar{y}q_4}{1-xy}\right)^2 - B^2 + i\eta\right]^{-3+\frac{d}{2}} \end{aligned} \tag{D.5}$$

with $B^2 = (\bar{y}m_b^2 + ym_c^2)/(1-xy)$. By means of a suitable shift $k_2 \to k_2 + (y\bar{x}q_3 - \bar{y}q_4)/(1-xy)$ the integration over k_2 can be performed by applying (E.2) and the simplified result reads

$$M_{15} = \frac{1}{(4\pi)^d}\Gamma(3-d)\big(m_b^2\big)^{-3+d}\int_0^1 dx\int_0^1 dy\,\frac{y^{1-\frac{d}{2}}x^{-2+\frac{d}{2}}(1-xy)^{-\frac{d}{2}}}{[1-y(1-z_c+i\eta)]^{3-d}}\,, \tag{D.6}$$

with $z_c = m_c^2/m_b^2$. Substituting $d = 4-2\epsilon$ the integration over x can easily be performed by using

$$\int_0^1 dx \frac{x^{-\epsilon}}{(1-xy)^{2-\epsilon}} = -\frac{(1-y)^{-1+\epsilon}}{-1+\epsilon} \tag{D.7}$$

and we obtain the following expression

$$M_{15} = -S_\Gamma^2 \left(m_b^2\right)^{1-2\epsilon} \frac{\Gamma(-1+2\epsilon)\Gamma^2(1-\epsilon)}{(-1+\epsilon)} \int_0^1 dy \, \frac{y^{-1+\epsilon}\bar{y}^{-1+\epsilon}}{\left[1-y(1-z_c+i\eta)\right]^{-1+2\epsilon}}$$
$$= -\frac{1}{(4\pi)^d} m_b^{-2\epsilon+1} \frac{\Gamma(-1+2\epsilon)}{-1+\epsilon} \frac{\Gamma(\epsilon)^2}{\Gamma(2\epsilon)} \, {}_2F_1(\epsilon, -1+2\epsilon, 2\epsilon; 1-z_c+i\eta) \,. \tag{D.8}$$

Here, we have used the definition of the hypergeometric function (4.3) to obtain the second line and S_Γ is given in Eq. (C.2). Eq. (D.8) can be expanded in ϵ up to the desired order by applying the MMA package HypExp.m. We find that the leading pole is $1/\epsilon^2$.

Note that the choice of first contracting the propagators that contain k_1 was arbitrary. The final result does not change if we first perform the contraction of the propagators involving k_2[1]. However, a certain choice which is not always obvious in the beginning can simplify the evaluation.

D.2. MB Representations: $M_{23}^{\leftrightarrow}$ and M_{18}

We present two examples of calculating master integrals by using MB representations. First, the mass flipped master integral $M_{23}^{\leftrightarrow}$ is evaluated by manually introducing MB representations in the calculation. In the second example we use AMBRE.m to derive a MB representation for the master integral M_{18} and state the input to be provided for the routine. Then, we take one specific term and simplify it by applying the techniques presented in Sec. E.2.

D.2.1. "Manual" Evaluation of $M_{23}^{\leftrightarrow}$

The mass flipped master integral $M_{23}^{\leftrightarrow}$ shown in Fig. D.2 is evaluated by applying Feynman parameters and by introducing MB representations. Using the choice of momenta given in Fig. D.2, $M_{23}^{\leftrightarrow}$ takes the following form

$$M_{23}^{\leftrightarrow} = \int \frac{d^dk_1}{(2\pi)^d} \int \frac{d^dk_2}{(2\pi)^d} \frac{1}{\left[(q_3+q_1+k_1)^2-m_c^2\right] \, k_1^2 \, (q_2-k_2)^2 \, (k_2-k_1)^2} \,, \tag{D.9}$$

where we tacitly assume the "$+i\eta$"–description to be included in the propagators. The first steps of the calculation are performed analogously to the evaluation of M_{15}. We start with the propagators three and four of (D.9) and combine them by introducing a Feynman parameter x. After some simplifications and a suitable shift of the loop momentum k_2 the integration over the latter can be performed as well as the integration over x for $d = 4-2\epsilon$, which only yields Gamma functions. The result then is combined with the second propagator of (D.9) by introducing another Feynman parameter x. Since both terms are massless and differ only by light-like momenta the resulting expression simplifies to a large extent and combined with the first propagator in (D.9) – by introducing a new Feynman parameter y – yields $M_{23}^{\leftrightarrow}$. Applying a suitable shift $k_1 \to k_1 + yq_3 + yq_1 - 2x\bar{y}q_2$ ($\bar{y} = 1-y$) we are able

[1]The explicit form of the result may deviate from Eq. (D.8) though.

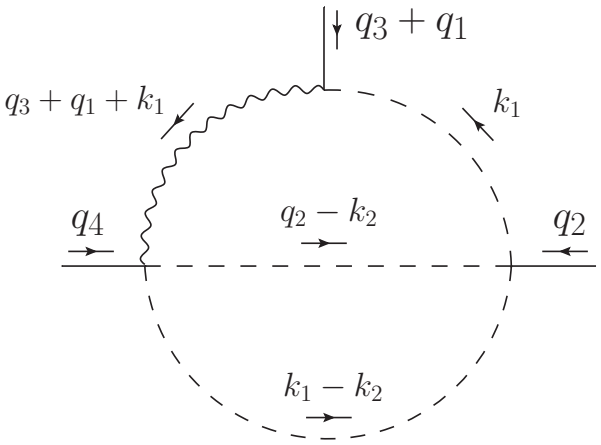

Figure D.2. – $M_{23}^{\leftrightarrow}$ with an arbitrary choice of parametrization. $q_1 \dots q_4$ denote the external and k_1 and k_2 are the loop momenta.

to perform the integration over this loop momentum. After some simplifications and setting $d = 4 - 2\epsilon$ we find

$$M_{23}^{\leftrightarrow} = -\, S_\Gamma^2 \left(m_b^2\right)^{-2\epsilon} A \int_0^1 dx\, x^{-1+\epsilon} \int_0^1 dy\, \bar{y}^\epsilon y^{-2\epsilon} \left[(1-y)(u+\bar{u}x)\left(\frac{1}{z_c}-1\right) - y + i\eta\right]^{-2\epsilon}, \tag{D.10}$$

with $z_c = m_c^2/m_b^2$, $A = z_c^{-2\epsilon}\Gamma(2\epsilon)\Gamma(1-\epsilon)^4/\Gamma(2-2\epsilon)$ and S_Γ defined in Eq. (C.2). It is not possible to perform the integration over x or y analytically. Therefore, we introduce two Barnes parameters z_1 and z_2 according to (4.4) such that[2]

$$\begin{aligned} M_{23}^{\leftrightarrow} = &- \frac{S_\Gamma^2}{\Gamma(2\epsilon)} \frac{\left(m_b^2\right)^{-2\epsilon}}{(2\pi i)^2} A \int_0^1 dx\, x^{-1+\epsilon} \int_0^1 dy\, \bar{y}^\epsilon y^{-2\epsilon} \int_{c-i\infty}^{c+i\infty} dz_1 \left[(1-y)\left(\frac{1}{z_c}-1\right)\right]^{z_1} y^{-2\epsilon-z_1} \\ &\times (-1+i\eta)^{-2\epsilon-z_1}\, \Gamma(2\epsilon+z_1) \int_{c'-i\infty}^{c'+i\infty} dz_2 (\bar{u}x)^{z_2} u^{z_1-z_2} \Gamma(-z_1+z_2)\Gamma(-z_2)\,, \end{aligned} \tag{D.11}$$

Now, the terms involving the integrations over x and y are separated. These integrations can be performed analytically yielding products of Gamma functions. The final result is given by

$$\begin{aligned} M_{23}^{\leftrightarrow} = &- S_\Gamma^2 \left(m_b^2\right)^{-2\epsilon} \frac{\Gamma(1-\epsilon)^4}{\Gamma(2-2\epsilon)} z_c^{-2\epsilon} \frac{1}{(2\pi i)^2} \frac{1}{\Gamma(-3\epsilon+2)} \int_{c-i\infty}^{c+i\infty} dz_1 \int_{c'-i\infty}^{c'+i\infty} dz_2 \left(\frac{1}{z_c}-1\right)^{z_1} \\ &\times (-1+i\eta)^{-2\epsilon-z_1}\, \Gamma(2\epsilon+z_1)\Gamma(-4\epsilon-z_1+1)\Gamma(\epsilon+z_1+1) \\ &\times \bar{u}^{z_2} u^{z_1-z_2} \Gamma(-z_1+z_2)\Gamma(-z_2) \frac{\Gamma(z_2+\epsilon)}{\Gamma(z_2+\epsilon+1)}\,. \end{aligned} \tag{D.12}$$

[2]The integration constants c and c' are chosen such that right and left poles are separated (see Sec. 4.3 for details).

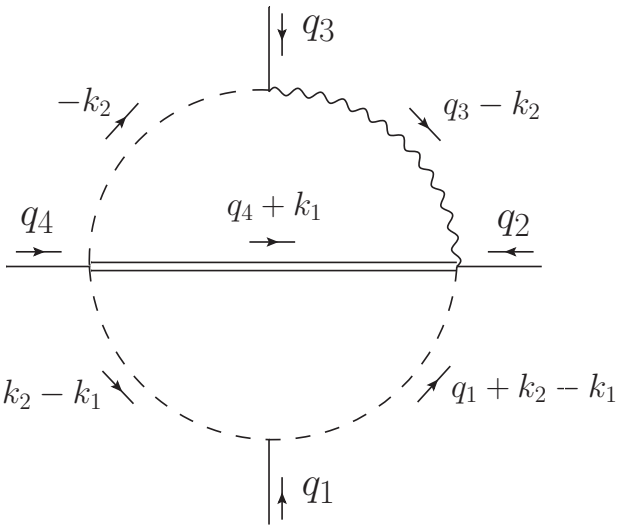

Figure D.3. – Master integral M_{18} for an arbitrary parametrization of the momentum flow. k_1 and k_2 are the loop and $q_1 \ldots q_4$ the external momenta.

D.2.2. Evaluation of M_{18} by Using AMBRE.m

We evaluate M_{18} by deriving a MB representation with AMBRE.m and further simplifying it by applying the first and second Barnes lemma and Cauchy's residue theorem. Here, only a part of the calculation is presented.

The master integral M_{18} is depicted in Fig. D.3 with some concrete choice of the inner momentum flow. For using AMBRE.m the following input has to be provided: the propagators with the choice shown in Fig. D.3, the invariants and the information which loop momentum is to be integrated first, here we take k_1. Feeding the input into the AMBRE.m routine, we find that ten Barnes integrations are introduced. Further commands automatically check the applicability of the first and second Barnes lemma. In the case at hand, four Barnes integrations can be performed and we arrive at a six dimensional MB representation for M_{18}. Next, we apply MB.m to find a suitable contour and perform the analytical continuation $\epsilon \to 0$. The final expression is given by two MB representations, a six and a five dimensional one. The latter reads

$$\begin{aligned} M_{18}^{(5)} = & \int_{-i\infty-5/32}^{i\infty-5/32} \frac{dz_3}{2\pi i} \int_{-i\infty-7/512}^{i\infty-7/512} \frac{dz_5}{2\pi i} \int_{-i\infty-7/64}^{i\infty-7/64} \frac{dz_7}{2\pi i} \int_{-i\infty-7/128}^{i\infty-7/128} \frac{dz_8}{2\pi i} \int_{-i\infty-7/256}^{i\infty-7/256} \frac{dz_9}{2\pi i} \\ & \times \frac{-(u)^{z_7+z_8} z_c^{-1-3\epsilon-z_3-z_5-z_7-z_9} (-1-i\eta)^{z_8}}{\Gamma(1-4\epsilon)\Gamma(1-\epsilon+z_3+z_5+z_9)\Gamma(2+z_5+z_7+z_8+z_9)} \Gamma(1-\epsilon)^2\Gamma(-\epsilon) \\ & \times \Gamma(-z_3)\Gamma(-z_5)\Gamma(1+z_5)\Gamma(-z_7)\Gamma(-4\epsilon-z_7-z_8)\Gamma(-3\epsilon-z_3-z_7-z_8)\Gamma(-z_8) \\ & \times \Gamma(1+z_7+z_8)\Gamma(-z_9)\Gamma(1+z_7+z_8+z_9)\Gamma(1+3\epsilon+z_3+z_5+z_7+z_8+z_9) \\ & \times \Gamma(1+2\epsilon+2z_3+z_5+z_7+z_8+z_9)\,. \end{aligned} \tag{D.13}$$

The real parts in the integration borders fix the contours, which are straight lines parallel to the imaginary axis. As the contours are not unique the real parts are chosen such that a better convergence of the integral is achieved. Introducing a new variable s by performing a

shift $z_9 \to s - z_5$ we are able to apply the first Barnes lemma (E.10) for integration over z_5. In order not to change the contours the real part of this new variable is fixed $\mathrm{Re}(s) = -\frac{21}{512}$. We introduce another new variable r according to $z_8 \to r - z_7$ with real part $\mathrm{Re}(r) = -\frac{21}{128}$. The complete dependence on z_7 then is given by the following expression

$$\int_{c-i\infty}^{c+i\infty} dz_7\, \Gamma(-r+z_7)\Gamma(-z_7) f(z_7)\,, \tag{D.14}$$

where $f(z_7) = (-1-i\eta)^{-z_7} z_c^{-z_7}$ is an analytic function and $\mathrm{Re}(r) < c < 0$. Eq. (D.14) has exactly the form of Eq. (E.8). Hence, we can perform the integration by applying Cauchy's residue theorem. Considering the above discussions about contours we find that in the case at hand no deformation and no shift is needed. The contour at $\mathrm{Re}(z_7) = -\frac{7}{64}$ separates the left and the right poles and the limit $\epsilon \to 0$ obviously is safe. Thus, we close the contour to the right and sum up all residues inside the region. The integral (D.14) is then given by the sum

$$\begin{aligned}\sum_{z_7=0}^{\infty} \mathrm{Res}\big[\Gamma(-r+z_7)\Gamma(-z_7)f(z_7)\big] &= 2\pi i \sum_{n=0}^{\infty} (-1)^n \frac{1}{\Gamma(n+1)} \Gamma(-r+n)(-1-i\eta)^{-n} z_c^{-n} \\ &= 2\pi i \left(1 + \frac{1}{(-1-i\eta)z_c}\right)^r \Gamma(-r)\,. \end{aligned} \tag{D.15}$$

A final shift $s \to w - z_3$ with real part $\mathrm{Re}(w) = -\frac{101}{512}$ allows one to perform the integration over z_3 by applying the first Barnes lemma. We arrive at the following two dimensional MB representation in r and w

$$\begin{aligned} M_{18}^{(5)} = -\frac{\Gamma(1-\epsilon)\Gamma(-\epsilon)}{\Gamma(1-4\epsilon)} \int_{-i\infty-\frac{21}{128}}^{i\infty-\frac{21}{128}} dr \int_{-i\infty-\frac{101}{512}}^{i\infty-\frac{101}{512}} dw\, u^r \big(1+(-1-i\eta)z_c\big)^r z_c^{-1-3\epsilon-r-w} \Gamma(2+r) \\ \times \Gamma(-4\epsilon-r)\Gamma(-r)\Gamma(1+r)^2 \Gamma(-3\epsilon-r-w)\Gamma(-w)\Gamma(1+2\epsilon+r+w) \\ \times \Gamma(1+3\epsilon+r+w)\,. \end{aligned} \tag{D.16}$$

The six dimensional representation can be simplified in a similar way. Note that in the derivation of the MB representation we have taken out a factor $-S_\Gamma^2 \cdot (m_b^2)^{-1-2\epsilon}$, with S_Γ defined in Eq. (C.2). Thus, (D.16) has to be multiplied by this prefactor. The final result can be expanded up to the desired power in ϵ and can then be evaluated by applying MB.m.

D.3. Differential Equations: M_4 and M_5

The master integrals M_4 and M_5 are evaluated by applying the method of differential equations. Both M_4 and M_5 depend on the scale z_c and on ϵ, but not on the momentum fraction u, thus, we can construct two differential equations according to Eq. (4.32). Applying the Laporta algorithm all integrals are written in terms of master integrals and we obtain the

following expressions for the two differential equations ($d = 4 - 2\epsilon$)

$$\frac{d}{dz_c}$$ 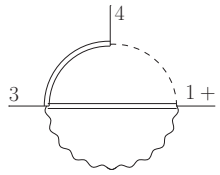 $$= \frac{dz_c - 3d - 4z_c + 10}{2(z_c-1)z_c}$$ 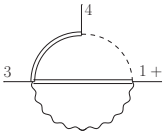 $$- \frac{m_b}{z_c}$$ 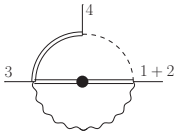

$$- \frac{1+3z_c}{(-1+z_c)^2}$$ 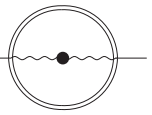 $$+ \frac{(-2+d)(1+z_c)}{2(-1+z_c)^2 z_c m_b}$$ 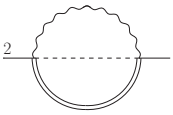

$$+ \frac{-8+3d}{2(-1+z_c)^2 m_b}$$ 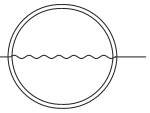

$$- \frac{(-2+d)^2(1+2z_c)}{4(-3+d)(-1+z_c)^2 z_c m_b^2}$$, (D.17)

$$\frac{d}{dz_c}$$ 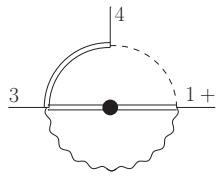 $$= \frac{d-z_c-4}{(z_c-1)z_c}$$ 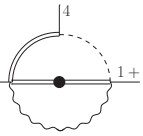 $$- \frac{(-4+d)(-10+3d)}{2(-1+z_c)z_c m_b}$$ 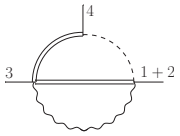

$$- \frac{(-11+3d)(1+z_c)}{2(-1+z_c)^2 m_b}$$ 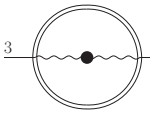 $$+ \frac{(-4+d)(-2+d)}{2(-1+z_c)^2 z_c m_b^2}$$ 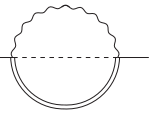

$$+ \frac{(-11+3d)(-8+3d)}{8(-1+z_c)^2 m_b^2}$$ 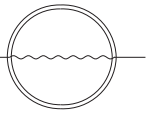 $$+ \frac{(-2+d)^2}{8(-1+z_c)^2 z_c m_b^3}$$ 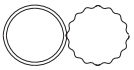

$$- \frac{(-2+d)^2(-16+4d-17z_c+5d\,z_c)}{16(-3+d)(-1+z_c)^2 z_c m_b^3}$$ 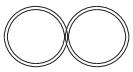 . (D.18)

Here, the labels 1 to 4 in the figures of the master integrals denote the incoming momenta $q_1, \ldots, q_4$. In the following we use primed indices for all quantities involved in the differential equation for M_5. We can read off $D(z_c, d) = \frac{dz_c-3d-4z_c+10}{2(z_c-1)z_c}$ and $D'(z_c, d) = \frac{d-z_c-4}{(z_c-1)z_c}$ for the

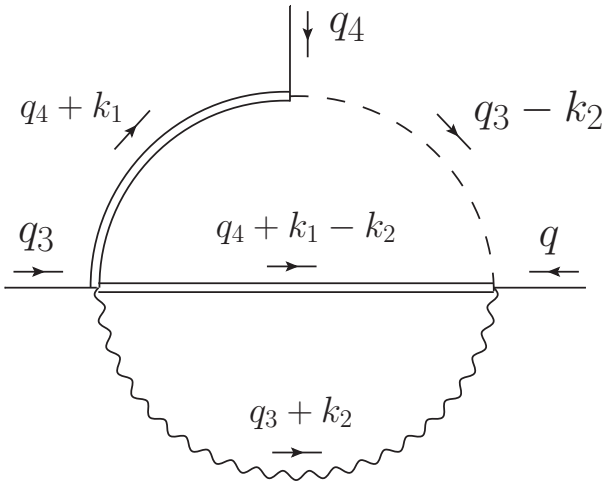

Figure D.4. – The topology of the master integrals M_4 and M_5 with a specify choice of momentum flow. k_1 and k_2 are the loop and q, q_3 and q_4 are the external momenta with $q = -q_3 - q_4$.

coefficients in front of M_4 and M_5, respectively. Hence, the integrated functions $\mathcal{D}(z_c, d)$ read

$$\mathcal{D}(z_c, d) = \frac{1}{2}\left[(3d-10)\log(z_c) - 2(d-3)\log(1-z_c)\right] , \tag{D.19}$$

$$\mathcal{D}'(z_c, d) = (d-5)\log(1-z_c) - (d-4)\log(z_c) . \tag{D.20}$$

All master integrals on the r.h.s. of Eq. (D.17) and (D.18) which are subtopologies of M_4 and M_5 are assumed to be known. However, we find that M_5 appears in the differential equation of M_4 and vice versa and therefore, we obtain a coupled system of equations. Taking a closer look at the differential equation for M_5 we find that M_4 appears alongside a factor $(d-4) \sim \epsilon$. Hence, the differential equations decouple order-by-order in ϵ. We take the lowest order in ϵ coefficients of M_4 and M_5 from applying Ambre.m (see Sec. 4.3.2) we find

$$M_4 = -(m_b^2)^{-2\epsilon} S_\Gamma^2 \left[\frac{1}{2\epsilon^2} + \frac{5}{2\epsilon} + O(\epsilon^0)\right] , \tag{D.21}$$

$$M_5 = O(\epsilon^0) , \tag{D.22}$$

with S_Γ defined Eq. (C.2). Both finite parts in ϵ contain non-trivial Barnes parameters. Inserting (D.21) and (D.22) in the differential equation for M_5 (D.18), we apply (4.34) and then expand the resulting expression in ϵ up to the finite order. After performing the integration over z_c in (4.35) the master integral is given by the following expression

$$M_5(z_c, \epsilon) = \left(f'(z_c, \epsilon) + \mathcal{C}'\right) \exp\left[\mathcal{D}'(z_c, \epsilon)\right] \tag{D.23}$$

with

$$f'(z_c, \epsilon) = -(m_b^2)^{-2\epsilon-1} S_\Gamma^2 \left[-\log(z_c)\mathrm{Li}_2(z_c) + 2\mathrm{Li}_3(z_c)\right] . \tag{D.24}$$

The unknown integration constant $\mathcal{C}'$ remains to be calculated according to the boundary condition (4.37). Looking at the explicit expression for $\mathcal{D}'$ given in (D.20) we see that there is an artificial logarithmic divergence at $z_c = 1$, which in the exponential in Eq. (D.23) becomes a simple power divergence. As stated above the master integrals are analytic for $z_c > 0$ and hence this divergence has to be artificial. We remove it by choosing $\mathcal{C}' = -f'(1,\epsilon)$ and obtain the following result for the finite part of M_5

$$M_5(z_c,\epsilon) = -(m_b^2)^{-2\epsilon-1} S_\Gamma^2 \left[\frac{-2\mathrm{Li}_3(z_c) + \mathrm{Li}_2(z_c)\log(z_c) + 2\zeta_3}{z_c - 1} + O(\epsilon) \right]. \tag{D.25}$$

Inserting this result back in the differential equation for M_5 yields zero, which provides a good check of the calculation.

Next, we consider the differential equation for M_4 and plug in (D.21) and (D.25) on the r.h.s. Following exactly the above mentioned steps for evaluating the finite part of M_5 we find a logarithmic divergence at $z_c = 1$ in (D.19) which can be removed by applying the boundary condition (4.37). The expression for M_4 up the finite part then reads

$$\begin{aligned} M_4(z_c,\epsilon) = -(m_b^2)^{-2\epsilon} S_\Gamma^2 \Big\{ & \frac{1}{2\epsilon^2} + \frac{5}{2\epsilon} - \frac{1}{6(z_c-1)} \big[-6\mathrm{Li}_2(1-z_c) + 6z_c\mathrm{Li}_2(z_c) - 12\mathrm{Li}_2(z_c) \\ & + 12\mathrm{Li}_3(z_c) + 6z_c\mathrm{Li}_2(1-z_c)\log(z_c) + 6z_c\mathrm{Li}_2(z_c)\log(z_c) - 6\mathrm{Li}_2(z_c)\log(z_c) \\ & - 57z_c + 6z_c\log(1-z_c)\log^2(z_c) + 6z_c\log(1-z_c)\log(z_c) \\ & - 12\log(1-z_c)\log(z_c) - 12\zeta_3 + \pi^2 + 57 \big] + O(\epsilon) \Big\}. \end{aligned} \tag{D.26}$$

We go back to the differential equation for M_5 in order to evaluate the $O(\epsilon)$ part of M_5 and then to the differential equation for M_4 for the $O(\epsilon)$ part of M_4. This can be repeated, until we have evaluated the master integrals up to the desired orders in ϵ.

Note, that beginning at $O(\epsilon)$ there is a subtlety in evaluating M_5. In the $O(\epsilon)$ differential equation there only appear HPLs with argument $\sqrt{z_c}$, since the results for the lower line master integrals at higher orders in ϵ contain those HPLs. The MMA package HPL.m can only perform integrations of HPLs with argument t with are multiplied by the weights $f_{1,0,-1}$ and $f_{+,-}$ (see Sec. 4.4.1 for the definition of $f_{1,0,-1}$ and $f_{+,-}$). Therefore we substitute $t = \sqrt{z_c}$ and consider a modified differential equation in this new variable

$$\frac{1}{2t}\frac{dM_5}{dt} = \left.\frac{dM_5}{dz_c}\right|_{z_c=t^2}. \tag{D.27}$$

An analogous change of variables is done for the differential equation for M_4. By using these new differential equations we obtain the higher $O(\epsilon)$ results for the master integrals following the above described procedure. The results for M_4 and M_5 up to $\mathcal{O}(\epsilon)$ are displayed in App. C. Note, that one can also express them in terms of the new variable t, however the result remains more compact, if we chose not to do so.

D.4. Canonical Basis: M_6 and M_7

We present the calculation of the master integrals M_6 and M_7 by solving differential equations in a canonical basis [107]. In the differential equation of M_6 and M_7 there appear ten integrals

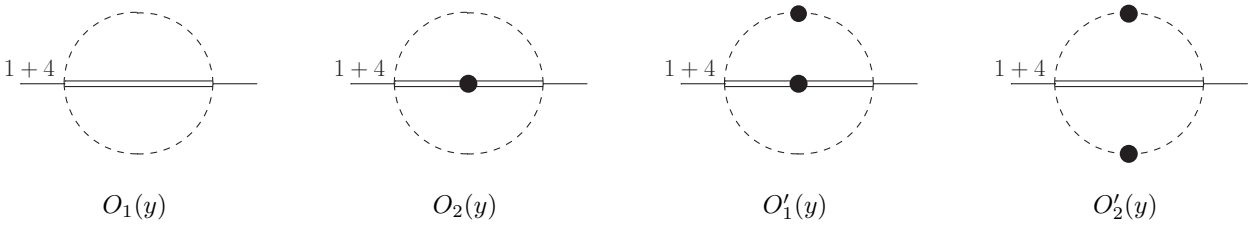

Figure D.5. – Master integrals in different bases with $y = 1-u(1-z_c)$: 1−4 denote the incoming external momenta $q_1, \ldots, q_4$. The double and curly line represent a propagator with mass m_b and m_c, respectively, and the dashed line denotes a massless one. The dot on a line indicates a squared propagator.

with fewer lines, which are $M_{8,9}$, $M_{8,9}^{\leftrightarrow}$, M_{15} and five master integrals with three or less lines (which are known from previous calculations). In order to close the system of differential equations these lower line master integrals have to be converted to the canonical basis as well, which is then given by $\vec{C} = (C_1, \ldots C_{12})$. The basis is obtained by searching for suitable linear combinations of master integrals which yield pure functions (see Sec. 4.5.2). As an example for finding such a linear combination consider a basis of the two master integrals O_1 and O_2 depicted in Fig. D.5 which arise in the Laporta reduction of several master integrals of the set of two-loop integrals shown in Figs. 2.4 and 2.5. They are subtopologies of M_6 and M_7 and are known from previous calculations. Their analytic expressions up to finite order in ϵ read

$$O_1(y) = -(m_b^2)^{-2\epsilon+1} S_\Gamma^2 \Big\{ \frac{1}{2\epsilon^2} + \frac{1}{\epsilon}\left(\frac{3}{2} - \frac{y}{4}\right) - G_{0,1}(y) - \frac{13y}{8} + \frac{1}{2} y G_1(y) - \frac{G_1(y)}{2y} + \frac{\pi^2}{3} + 3 \Big\}, \tag{D.28a}$$

$$O_2(y) = -(m_b^2)^{-2\epsilon} S_\Gamma^2 \Big\{ \frac{1}{2\epsilon^2} + \frac{1}{2\epsilon} - G_{0,1}(y) - \frac{G_1(y)}{y} + G_1(y) + \frac{\pi^2}{3} - \frac{1}{2} \Big\}, \tag{D.28b}$$

with $y = 1 - u(1 - z_c)$ and S_Γ defined Eq. (C.2). Both integrals contain algebraic factors and moreover, the terms in the finite parts have different weights. However, neither O_1 and O_2 nor any linear combination yield pure functions. We consider a different basis and find that the doubly-dotted integrals O_1' and O_2' defined in Fig. D.5 are a good choice[3]. Their analytic expressions can be easily obtained from Eqs. (D.28a) and (D.28b) by applying the Laporta algorithm and up to $\mathcal{O}(\epsilon^0)$ are given by

$$O_1'(y) = -(m_b^2)^{-2\epsilon-1} S_\Gamma^2 \left(-\frac{G_1(y)}{y\epsilon} + \frac{4G_{0,0}(y) - G_{0,1}(y)}{y} \right), \tag{D.29a}$$

$$O_2'(y) = -(m_b^2)^{-2\epsilon-1} S_\Gamma^2 \Bigg(\frac{1}{(y-1)\epsilon^2} - \frac{2(y+1)G_1(y)}{(y-1)y\epsilon} + \frac{2\left[12(y+1)G_{0,0}(y) + \pi^2 y - (6y+3)G_{0,1}(y)\right]}{3(y-1)y} \Bigg). \tag{D.29b}$$

[3] O_1' and O_2' are equal to the integrals I_8 and I_9 in Fig. D.6.

The individual integrals are not pure but the following linear combinations yield pure functions

$$C_8 \equiv \epsilon^2\, y\, O_1' = -(m_b^2)^{-2\epsilon+1} S_\Gamma^2 \left\{ -\epsilon\, G_1(y) + \epsilon^2 \left[4G_{0,0}(y) - G_{0,1}(y)\right] + \mathcal{O}(\epsilon^3)\right\}, \tag{D.30a}$$

$$C_9 \equiv \epsilon^2\, (y-1)\, (O_2' + 2O_1') = -(m_b^2)^{-2\epsilon+1} S_\Gamma^2 \Big\{ 1 - 4\epsilon\, G_1(y) + \epsilon^2 \left(16G_{0,0}(y) - 4G_{0,1}(y) + \frac{2}{3}\pi^2 \right) + \mathcal{O}(\epsilon^3) \Big\}. \tag{D.30b}$$

Note that the master integrals have to be evaluated to $\mathcal{O}(\epsilon^4)$ since the two-loop amplitude contains poles up to $1/\epsilon^4$ stemming from the infrared and ultraviolet regions. We find that C_8 and C_9 are pure functions to $\mathcal{O}(\epsilon^4)$ and the corresponding differential equations in z_c given in Eq. (4.50) and in u given in Eq. (4.51) factorize the kinematics from the space-time dependence

$$\frac{d}{dz_c} \begin{pmatrix} C_8 \\ C_9 \end{pmatrix} = \epsilon \begin{pmatrix} \frac{y-1}{y(z_c-1)} & \frac{1}{z_c-1} \\ \frac{6(1-y)}{y(z_c-1)} & \frac{4}{1-z_c} \end{pmatrix} \begin{pmatrix} C_8 \\ C_9 \end{pmatrix}, \tag{D.31}$$

$$\frac{d}{du} \begin{pmatrix} C_8 \\ C_9 \end{pmatrix} = \epsilon \begin{pmatrix} \frac{z_c-1}{y} & \frac{z_c-1}{y-1} \\ \frac{6(1-z_c)}{y} & \frac{4(1-z_c)}{y-1} \end{pmatrix} \begin{pmatrix} C_8 \\ C_9 \end{pmatrix}. \tag{D.32}$$

Hence, instead of O_1 and O_2 we take C_8 and C_9 in the canonical basis as new master integrals. The procedure for finding pure linear combinations of the remaining master integrals is similar. Finally, we obtain the following expressions for the master integrals C_{1-12} in terms of the integrals I_{1-12} defined in figure D.6 ($\bar{x} = 1 - x$):

$$C_1(u, z_c) = \epsilon^3\, u\bar{z}_c\, I_1(u, z_c), \tag{D.33}$$

$$C_2(u, z_c) = \epsilon^3\, u(z_c - 1) z_c\, I_2(u, z_c), \tag{D.34}$$

$$C_3(u, z_c) = \epsilon^3\, \bar{u}\bar{z}_c\, I_3(u, z_c), \tag{D.35}$$

$$C_4(u, z_c) = \epsilon^3\, \bar{u}\bar{z}_c\, I_4(u, z_c), \tag{D.36}$$

$$C_5(u, z_c) = \epsilon^3\, \bar{u}(z_c - 1)\, I_5(u, z_c), \tag{D.37}$$

$$C_6(u, z_c) = \epsilon^3\, \bar{u}(z_c - 1)\, I_6(u, z_c), \tag{D.38}$$

$$C_7(z_c) = \epsilon\, (1 - \epsilon)\bar{z}_c\, I_7(z_c), \tag{D.39}$$

$$C_8(u, z_c) = \epsilon^2\, (\bar{u} + u z_c)\, I_8(u, z_c), \tag{D.40}$$

$$C_9(u, z_c) = \epsilon^2\, u\bar{z}_c \Big(I_9(u, z_c) + 2I_8(u, z_c) \Big), \tag{D.41}$$

$$C_{10}(u, z_c) = \epsilon^2\, (u + \bar{u} z_c)\, I_{10}(u, z_c), \tag{D.42}$$

$$C_{11}(u, z_c) = \epsilon^2\, u(z_c - 1) \Big(I_{11}(u, z_c) + 2I_{10}(u, z_c) \Big), \tag{D.43}$$

$$C_{12}(z_c) = \epsilon^2\, I_{12}(z_c). \tag{D.44}$$

The explicit differential equations for the C_i take the canonical form given in Eqs. (4.52) and (4.53) and we obtain the following expression for $\tilde{A}$

$$\tilde{A} = \begin{pmatrix}
-4L_1 - L_4 & 3L_3 - 3L_4 & -2L_2 - \frac{L_3}{2} - \frac{L_4}{2} + L_6 & -L_2 + \frac{L_3}{2} - L_4 + \frac{L_6}{2} & L_2 + \frac{L_3}{2} - \frac{L_4}{2} \\
-3L_4 & -4L_1 - L_3 - L_4 & L_2 - \frac{L_4}{2} & -L_2 - L_4 & -2L_2 - \frac{L_4}{2} + L_5 \\
0 & 0 & 2L_2 - L_3 + 2L_4 - 2L_6 & L_3 - L_6 & 0 \\
0 & 0 & -2L_1 - 2L_4 + 2L_6 & -4L_1 + 2L_2 - 2L_4 + L_6 & 0 \\
0 & 0 & 0 & 0 & 2L_2 - L_3 + 2L_4 - 2L_5 \\
0 & 0 & 0 & 0 & -2L_1 - 2L_4 + 2L_5 \\
0 & 0 & 0 & 0 & 0 \\
0 & 0 & 0 & 0 & 0 \\
0 & 0 & 0 & 0 & 0 \\
0 & 0 & 0 & 0 & 0 \\
0 & 0 & 0 & 0 & 0 \\
0 & 0 & 0 & 0 & 0
\end{pmatrix}$$

$$\begin{pmatrix}
-L_2 + L_3 - L_4 & \frac{L_3}{4} - \frac{L_6}{4} & 0 & \frac{L_3}{4} - \frac{L_4}{4} & \frac{3L_6}{2} - \frac{3L_3}{2} & -\frac{L_3}{2} + \frac{L_4}{4} + \frac{L_6}{4} & \frac{L_6}{4} - \frac{L_3}{4} \\
-L_2 - L_4 + \frac{L_5}{2} & \frac{L_5}{4} & \frac{3L_5}{2} & \frac{L_4}{4} + \frac{L_5}{4} & 0 & -\frac{L_4}{4} & \frac{L_5}{4} \\
0 & \frac{L_6}{2} & 0 & 0 & -2L_6 & -\frac{L_6}{2} & -\frac{L_6}{2} \\
0 & L_1 - \frac{L_6}{2} & 0 & 0 & L_6 & \frac{L_6}{2} & \frac{L_6}{2} \\
-L_5 & \frac{L_3}{2} - \frac{L_5}{2} & 2L_3 - 2L_5 & \frac{L_3}{2} - \frac{L_5}{2} & 0 & 0 & \frac{L_3}{2} - \frac{L_5}{2} \\
-4L_1 + 2L_2 - L_3 - 2L_4 + L_5 & -L_1 - \frac{L_3}{2} + \frac{L_5}{2} & L_5 - L_3 & \frac{L_5}{2} - \frac{L_3}{2} & 0 & 0 & \frac{L_5}{2} - \frac{L_3}{2} \\
0 & -2L_4 & 0 & 0 & 0 & 0 & L_3 \\
0 & 0 & L_5 & L_1 + L_4 & 0 & 0 & 0 \\
0 & 0 & -6L_5 & -4L_1 - 4L_4 & 0 & 0 & 0 \\
0 & 0 & 0 & 0 & L_6 - 3L_3 & L_1 - L_3 + L_4 & 0 \\
0 & 0 & 0 & 0 & 6L_3 - 6L_6 & -4L_1 + 2L_3 - 4L_4 & 0 \\
0 & 0 & 0 & 0 & 0 & 0 & -L_3
\end{pmatrix}. \tag{D.45}$$

$L_{1,\ldots 6}$ are logarithms which only linearly depend on the arguments u and z_c

$$\begin{aligned}
L_1 &= \ln(u)\,, & L_4 &= \ln(1 - z_c)\,, \\
L_2 &= \ln(1 - u)\,, & L_5 &= \ln(1 - u(1 - z_c))\,, \\
L_3 &= \ln(z_c)\,, & L_6 &= \ln(z + u(1 - z_c))\,.
\end{aligned} \tag{D.46}$$

By using the scaling relation (4.45) we can change the arguments of the Goncharov polylogarithms. As mentioned above, u is a good choice for the Goncharov polylogarithms that depend on this scale since this will simplify the convolution with the pion LCDA. Then we find that the weights are either integer $(0, \pm 1)$ or one of the following z_c-dependent expressions

$$a_1 = \frac{1}{1 - z_c}\,, \qquad a_2 = \frac{z_c}{z_c - 1}\,. \tag{D.47}$$

Products of Goncharov polylogarithms of the same argument are expanded by means of the Hopf algebra.

For details of solving the differential equations we refer to the example in the "traditional" basis in Sec. D.3. Here, we will only specify the various boundary conditions. C_7 and C_{12} both are independent of u and vanish at $z_c = 1$. $C_{3,4}$ and $C_{5,6}$ vanish at $u = 1$. For $C_{1,2,8,9,10,11}$ we haven't found a specific kinematic point where they vanish. Thus, we have evaluated $C_{8,9}$ for $(u_0, z_{c_0}) = (1, 0)$ and $C_{10,11}$ for $(u_0, z_{c_0}) = (1, 1/2)$. A difficulty arises when solving the

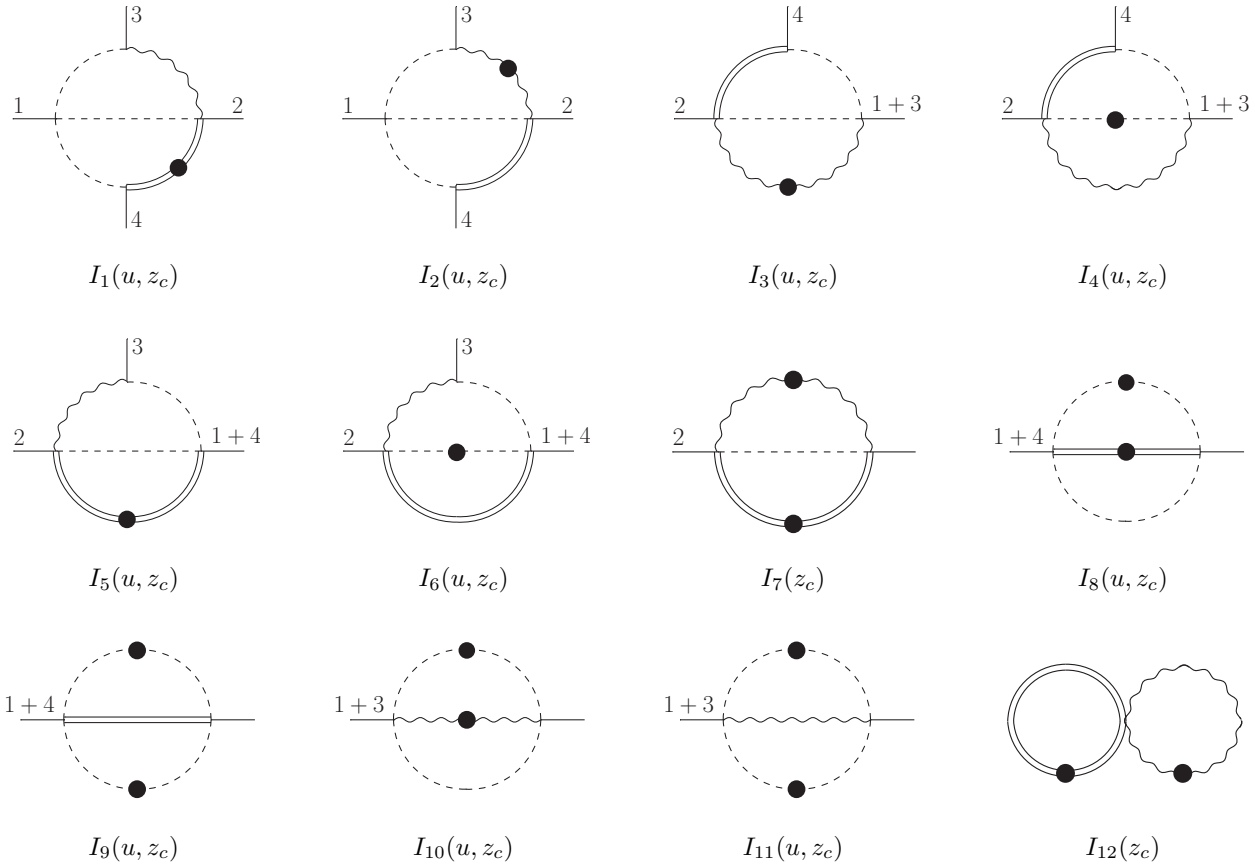

Figure D.6. – Set of basic integrals needed in the construction of the pure master integrals $C_{1,2}$: $1 - 4$ denote the incoming external momenta $q_1, \ldots, q_4$. The double and curly line represent a propagator with mass m_b and m_c, respectively, and the dashed line denotes a massless one. The dot on a line indicates a squared propagator.

differential equation for $C_{1,2}$ with respect to z_c. We encounter Goncharov polylogarithms with non-trivial dependence on z_c in the weights, e.g. $G_{1,a_2}(u_0)$. The integration over z_c cannot easily be performed by rescaling the weights using Eq. (4.45) and applying Eq. (4.39). As an alternative to integrating the differential equation with respect to z_c one can obtain the function $C(u_0, z_c)$ from MB representations (see [C]).

Appendix E

Useful Identities and Definitions for Evaluating Integrals

We present some useful identities and definitions which apply in the calculation of Feynman diagrams or can be used to reduce the dimensionality of a given Mellin Barnes representation (see Sec. 4.3).

E.1. Identities for Calculating Feynman Diagrams

We provide some useful identities and definitions for calculating Feynman diagrams. Most of the relations given here can be found in [193].

The following type of integrals are invariant under a linear shift of the integration variable

$$\int \frac{d^dk}{(2\pi)^d} \frac{\{f(k),1\}}{[(p-k)^2-\Delta+i\eta]^n} = \int \frac{d^dk}{(2\pi)^d} \frac{\{f(p+k),1\}}{[k^2-\Delta+i\eta]^n} \,, \tag{E.1}$$

where $f(k)$ is some function of k and Δ is independent of k. The momentum p is usually a linear combination of external momenta and $\eta > 0$ (infinitesimal) and $n \in \mathbb{R}$. After this shift, the integration over k can be performed by applying one of the following identitites

$$\int \frac{d^dk}{(2\pi)^d} \frac{1}{(k^2-\Delta+i\eta)^n} = \frac{i(-1)^{-n}}{(4\pi)^{d/2}} \frac{\Gamma(n-\frac{d}{2})}{\Gamma(n)} (\Delta - i\eta)^{-n+\frac{d}{2}} \,, \tag{E.2}$$

$$\int \frac{d^dk}{(2\pi)^d} \frac{k^2}{(k^2-\Delta+i\eta)^n} = \frac{i(-1)^{-n+1}}{(4\pi)^{d/2}} \frac{d}{2} \frac{\Gamma(n-\frac{d}{2}-1)}{\Gamma(n)} (\Delta - i\eta)^{-n+\frac{d}{2}-1} \,, \tag{E.3}$$

$$\int \frac{d^dk}{(2\pi)^d} \frac{(k^2)^2}{(k^2-\Delta+i\eta)^n} = \frac{i(-1)^{-n+2}}{(4\pi)^{d/2}} \frac{d(d+2)}{4} \frac{\Gamma(n-\frac{d}{2}-2)}{\Gamma(n)} (\Delta - i\eta)^{-n+\frac{d}{2}-2} \,. \tag{E.4}$$

We further find

$$\frac{1}{(-\Delta \pm i\eta)^n} = \frac{(-1)^{\mp n}}{(\Delta \mp i\eta)^n} \,. \tag{E.5}$$

There are other identities like the Feynman parameters and the Beta functions. The former can be used to express the product of propagators with a sum by introducing additional integrations

$$\frac{1}{E_1^{\alpha_1}\dots E_n^{\alpha_n}} = \frac{\Gamma(\alpha_1+\dots+\alpha_n)}{\Gamma(\alpha_1)\dots\Gamma(\alpha_n)} \int_0^1 dx_1\dots dx_n \frac{\delta(1-\sum_i x_i) x_1^{\alpha_1-1}\dots x_n^{\alpha_n-1}}{[x_1E_1+\dots+x_nE_n]^{\sum_i \alpha_i}}\,. \tag{E.6}$$

Some of the integrations over the Feynman parameters may be performed (at a later stage of the calculation) by using the definition of the Beta function

$$B(\alpha,\beta) = \int_0^1 dx\, x^{\alpha-1}(1-x)^{\beta-1} = \frac{\Gamma(\alpha)\Gamma(\beta)}{\Gamma(\alpha+\beta)}\,, \quad \mathrm{Re}(\alpha,\beta)>0\,. \tag{E.7}$$

E.2. Cauchy's Residue Theorem and Barnes Lemmas

Mellin Barnes (MB) representations have been discussed in Sec. 4.3. Here, we present methods that apply in the reduction of the dimensionality of a given MB representation.

The integration over a Barnes parameter z can be performed by means of Cauchy's residue theorem, if z only appears linearly in two Gamma functions with opposite sign and all other dependence on z is given by an analytic function $f(z)$

$$\int_{c-i\infty}^{c+i\infty} \frac{dz}{2\pi i}\,\Gamma(z+a)\Gamma(-z+b)f(z) = \sum_{n=0}^{\infty} \mathrm{Res}\big[\Gamma(n+a+b)\Gamma(-n)f(n+b)\big]\,. \tag{E.8}$$

The integration contour is parallel to the imaginary axis and c is chosen such that $\Gamma(\dots\mp z)$ has poles on the right/left of the contour. For $f(z)=x^z$, x being an arbitrary z-independent variable, which is often realized in the calculations of the master integrals, and $\mathrm{Re}(a+b)>0$, we find

$$\int_{c-i\infty}^{c+i\infty} \frac{dz}{2\pi i}\,\Gamma(z+a)\Gamma(-z+b)\,x^z = x^b(1+x)^{-a-b}\,\Gamma(a+b)\,. \tag{E.9}$$

Moreover, if applicable, Barnes integrations can be performed by the first and second Barnes lemma, which read

$$\int_{c-i\infty}^{c+i\infty} dz\,\Gamma(a+z)\Gamma(b+z)\Gamma(c-z)\Gamma(d-z) = \frac{\Gamma(a+c)\Gamma(a+d)\Gamma(b+c)\Gamma(b+d)}{\Gamma(a+b+c+d)}\,, \tag{E.10}$$

$$\int_{c-i\infty}^{c+i\infty} dz\,\frac{\Gamma(a+z)\Gamma(b+z)\Gamma(c+z)\Gamma(d-z)\Gamma(e-z)}{\Gamma(a+b+c+d+e+z)} = \frac{\Gamma(a+d)\Gamma(a+e)\Gamma(b+d)\Gamma(b+e)\Gamma(c+d)\Gamma(c+e)}{\Gamma(a+b+d+e)\Gamma(a+c+d+e)\Gamma(b+c+d+e)}\,. \tag{E.11}$$

The integration contours are fixed such that $\Gamma(\dots\mp z)$ are right/left poles. There are also modified versions of the Barnes lemmas, some even involving Polygamma functions

$$\psi^{(0)} = \frac{d}{dz}\ln\Gamma\,, \tag{E.12}$$

$$\psi^{(n)} = \frac{d}{dz}\psi^{(n-1)}\,, \quad n > 0 \text{ integer}\,. \tag{E.13}$$

A copious list of these integrals can be found in [116].

The above mentioned simplifications apply for integrals in d dimensions as well as for integrals which already have been expanded in a series in ϵ. It is advisable to perform as many integrations as possible before expanding the integrand since this often reduces the effort to a large extent. After the expansion, the Barnes lemmas or Eq. (E.8) may still apply for the lower order ϵ terms. In some cases these simplifications are only possible after suitable shifts of MB variables.

Appendix F

Results for the Feynman Diagrams in the Central Region of the Dalitz Plot

We present the results for the leading order Feynman diagrams depicted in Fig. 6.7 including the contributions of the form factors and the LCDAs. We find that only the combinations $V-V$ or $A-A$ yield non-vanishing contributions, where V (A) denotes the vector (axial) current. The momentum fraction of the LCDA that involves the spinor $\bar{q}_j$ ($\bar{q}$) is denoted by u (v). The gluon can be attached to the different quark lines and we assign numbers 1-4 to the insertions of the gluon on the b, q_n, q_i or $\bar{q}_j$ quark line, respectively. The results from the colour singlet and colour octet operators are marked by the superscripts "0" and "8", respectively. E.g. $(A^0_{V\otimes V})_{a1}$ denotes the result of diagram (a) of the vector-vector contribution of the colour singlet operator with gluon insertion on the b quark line.

$$
\begin{aligned}
(A^0_{V\otimes V})_{a1} &= 0\,,\\
(A^8_{V\otimes V})_{a1} &= 0\,,\\
(A^0_{A\otimes A})_{a1} &= 2\alpha_s\pi\frac{(1+u)C_F}{u(2+u)N_c}f_\pi^2F_+^{B\to\pi}(m_B^2/3)\Phi_\pi(u)\Phi_\pi(v)\,,\\
(A^8_{A\otimes A})_{a1} &= 0\,,\\
(A^0_{V\otimes V})_{a2} &= 0\,,\\
(A^8_{V\otimes V})_{a2} &= 0\,,\\
(A^0_{A\otimes A})_{a2} &= 2\alpha_s\pi\frac{C_F}{uN_c}f_\pi^2F_+^{B\to\pi}(m_B^2/3)\Phi_\pi(u)\Phi_\pi(v)\,,\\
(A^8_{A\otimes A})_{a2} &= 0\,,\\
(A^0_{V\otimes V})_{a3} &= 0\,,\\
(A^8_{V\otimes V})_{a3} &= -\alpha_s\pi\frac{(-1+u)C_F}{2N_c^2u(-1+u(-2+v)+v))}f_\pi^2F_+^{B\to\pi}(m_B^2/3)\Phi_\pi(u)\Phi_\pi(v)\,,\\
(A^0_{A\otimes A})_{a3} &= 0\,,
\end{aligned}
$$

$$
\begin{aligned}
(A^8_{A\otimes A})_{a3} &= \alpha_s\pi\frac{(3+u-2v)C_F}{2u(-1+u(-2+v)+v)N_c^2}f_\pi^2F_+^{B\to\pi}(m_B^2/3)\Phi_\pi(u)\Phi_\pi(v)\,,\\
(A^0_{V\otimes V})_{a4} &= 0\,,\\
(A^8_{V\otimes V})_{a4} &= \alpha_s\pi\frac{(-1+u)C_F}{2N_c^2u(u+v+uv)}f_\pi^2F_+^{B\to\pi}(m_B^2/3)\Phi_\pi(u)\Phi_\pi(v)\,,\\
(A^0_{A\otimes A})_{a4} &= 0\,,\\
(A^8_{A\otimes A})_{a4} &= \alpha_s\pi\frac{(1+u+2v)C_F}{2N_c^2u(u+v+uv)}f_\pi^2F_+^{B\to\pi}(m_B^2/3)\Phi_\pi(u)\Phi_\pi(v)\,,\\
(A^0_{V\otimes V})_{b1} &= -\alpha_s\pi\frac{(1+u)C_F}{N_c^2u(2+u)}f_\pi^2F_+^{B\to\pi}(m_B^2/3)\Phi_\pi(u)\Phi_\pi(v)\,,\\
(A^8_{V\otimes V})_{b1} &= -\alpha_s\pi\frac{(1+u)C_F^2}{N_c^2u(2+u)}f_\pi^2F_+^{B\to\pi}(m_B^2/3)\Phi_\pi(u)\Phi_\pi(v)\,,\\
(A^0_{A\otimes A})_{b1} &= -\alpha_s\pi\frac{(1+u)C_F}{N_c^2u(2+u)}f_\pi^2F_+^{B\to\pi}(m_B^2/3)\Phi_\pi(u)\Phi_\pi(v)\,,\\
(A^8_{A\otimes A})_{b1} &= -\alpha_s\pi\frac{(1+u)C_F^2}{N_c^2u(2+u)}f_\pi^2F_+^{B\to\pi}(m_B^2/3)\Phi_\pi(u)\Phi_\pi(v)\,,\\
(A^0_{V\otimes V})_{b2} &= -\alpha_s\pi\frac{C_F}{N_c^2u}f_\pi^2F_+^{B\to\pi}(m_B^2/3)\Phi_\pi(u)\Phi_\pi(v)\,,\\
(A^8_{V\otimes V})_{b2} &= -\alpha_s\pi\frac{C_F^2}{N_c^2u}f_\pi^2F_+^{B\to\pi}(m_B^2/3)\Phi_\pi(u)\Phi_\pi(v)\,,\\
(A^0_{A\otimes A})_{b2} &= -\alpha_s\pi\frac{C_F}{N_c^2u}f_\pi^2F_+^{B\to\pi}(m_B^2/3)\Phi_\pi(u)\Phi_\pi(v)\,,\\
(A^8_{A\otimes A})_{b2} &= -\alpha_s\pi\frac{C_F^2}{N_c^2u}f_\pi^2F_+^{B\to\pi}(m_B^2/3)\Phi_\pi(u)\Phi_\pi(v)\,,\\
(A^0_{V\otimes V})_{b3} &= \alpha_s\pi\frac{(-2+v)C_F}{N_c^2u(-1+u(-2+v)+v)}f_\pi^2F_+^{B\to\pi}(m_B^2/3)\Phi_\pi(u)\Phi_\pi(v)\,,\\
(A^8_{V\otimes V})_{b3} &= -\alpha_s\pi\frac{(-2+v)C_F}{2N_c^3u(-1+u(-2+v)+v)}f_\pi^2F_+^{B\to\pi}(m_B^2/3)\Phi_\pi(u)\Phi_\pi(v)\,,\\
(A^0_{A\otimes A})_{b3} &= \alpha_s\pi\frac{(-2+v)C_F}{N_c^2u(-1+u(-2+v)+v)}f_\pi^2F_+^{B\to\pi}(m_B^2/3)\Phi_\pi(u)\Phi_\pi(v)\,,\\
(A^8_{A\otimes A})_{b3} &= -\alpha_s\pi\frac{(-2+v)C_F}{2N_c^3u(-1+u(-2+v)+v)}f_\pi^2F_+^{B\to\pi}(m_B^2/3)\Phi_\pi(u)\Phi_\pi(v)\,,\\
(A^0_{V\otimes V})_{b4} &= -\alpha_s\pi\frac{(u+v)C_F}{N_c^2u(u+v+uv)}f_\pi^2F_+^{B\to\pi}(m_B^2/3)\Phi_\pi(u)\Phi_\pi(v)\,,\\
(A^8_{V\otimes V})_{b4} &= \alpha_s\pi\frac{(u+v)C_F}{2N_c^3u(u+v+uv}f_\pi^2F_+^{B\to\pi}(m_B^2/3)\Phi_\pi(u)\Phi_\pi(v)\,,\\
(A^0_{A\otimes A})_{b4} &= -\alpha_s\pi\frac{(u+v)C_F}{N_c^2u(u+v+uv)}f_\pi^2F_+^{B\to\pi}(m_B^2/3)\Phi_\pi(u)\Phi_\pi(v)\,,
\end{aligned}
$$

$$(A^8_{A\otimes A})_{b4} = \alpha_s\pi\frac{(u+v)C_F}{2N_c^3u(u+v+uv)}f_\pi^2F_+^{B\to\pi}(m_B^2/3)\Phi_\pi(u)\Phi_\pi(v)\,,$$
$$(A^0_{V\otimes V})_{c1} = 0\,,$$
$$(A^8_{V\otimes V})_{c1} = \alpha_s\pi\frac{(-1+u-v)C_F}{2N_c^2u(-1+v)(2+u-2v+uv)}f_\pi^2F_+^{B\to\pi}(m_B^2/3)\Phi_\pi(u)\Phi_\pi(v)\,,$$
$$(A^0_{A\otimes A})_{c1} = 0\,,$$
$$(A^8_{A\otimes A})_{c1} = \alpha_s\pi\frac{(-1+u+v)C_F}{2N_c^2u(-1+v)(2+u-2v+uv)}f_\pi^2F_+^{B\to\pi}(m_B^2/3)\Phi_\pi(u)\Phi_\pi(v)\,,$$
$$(A^0_{V\otimes V})_{c2} = 0\,,$$
$$(A^8_{V\otimes V})_{c2} = -\alpha_s\pi\frac{(3+u-v)C_F}{2N_c^2u(-1+v)(-1+u(-2+v)+v))}f_\pi^2F_+^{B\to\pi}(m_B^2/3)\Phi_\pi(u)\Phi_\pi(v)\,,$$
$$(A^0_{A\otimes A})_{c2} = 0\,,$$
$$(A^8_{A\otimes A})_{c2} = \alpha_s\pi\frac{(-1+u+v)C_F}{2N_c^2u(-1+v)(-1+u(-2+v)+v)}f_\pi^2F_+^{B\to\pi}(m_B^2/3)\Phi_\pi(u)\Phi_\pi(v)\,,$$
$$(A^0_{V\otimes V})_{c3} = 2\alpha_s\pi C_FN_cu(-1+v)f_\pi^2F_+^{B\to\pi}(m_B^2/3)\Phi_\pi(u)\Phi_\pi(v)\,,$$
$$(A^8_{V\otimes V})_{c3} = 0\,,$$
$$(A^0_{A\otimes A})_{c3} = 0\,,$$
$$(A^8_{A\otimes A})_{c3} = 0\,,$$
$$(A^0_{V\otimes V})_{c4} = -2\alpha_s\pi\frac{C_F}{N_cu(-1+v)}f_\pi^2F_+^{B\to\pi}(m_B^2/3)\Phi_\pi(u)\Phi_\pi(v)\,,$$
$$(A^8_{V\otimes V})_{c4} = 0\,,$$
$$(A^0_{A\otimes A})_{c4} = 0\,,$$
$$(A^8_{A\otimes A})_{c4} = 0\,,$$
$$(A^0_{V\otimes V})_{d1} = -\alpha_s\pi\frac{(-1+u)C_F}{N_c^2u(-1+v)(2+u-2v+uv)}f_\pi^2F_+^{B\to\pi}(m_B^2/3)\Phi_\pi(u)\Phi_\pi(v)\,,$$
$$(A^8_{V\otimes V})_{d1} = \alpha_s\pi\frac{(-1+u)C_F}{2N_c^3u(-1+v)(2+u-2v+uv)}f_\pi^2F_+^{B\to\pi}(m_B^2/3)\Phi_\pi(u)\Phi_\pi(v)\,,$$
$$(A^0_{A\otimes A})_{d1} = -\alpha_s\pi\frac{(-1+u)C_F}{N_c^2u(-1+v)(2+u-2v+uv)}f_\pi^2F_+^{B\to\pi}(m_B^2/3)\Phi_\pi(u)\Phi_\pi(v)\,,$$
$$(A^8_{A\otimes A})_{d1} = \alpha_s\pi\frac{(-1+u)C_F}{2N_c^3u(-1+v)(2+u-2v+uv)}f_\pi^2F_+^{B\to\pi}(m_B^2/3)\Phi_\pi(u)\Phi_\pi(v)\,,$$
$$(A^0_{V\otimes V})_{d2} = \alpha_s\pi\frac{C_F}{N_c^2u(-1+v)}f_\pi^2F_+^{B\to\pi}(m_B^2/3)\Phi_\pi(u)\Phi_\pi(v)\,,$$
$$(A^8_{V\otimes V})_{d2} = \alpha_s\pi\frac{C_F^2}{N_c^2u(-1+v)}f_\pi^2F_+^{B\to\pi}(m_B^2/3)\Phi_\pi(u)\Phi_\pi(v)\,,$$
$$(A^0_{A\otimes A})_{d2} = \alpha_s\pi\frac{C_F}{N_c^2u(-1+v)}f_\pi^2F_+^{B\to\pi}(m_B^2/3)\Phi_\pi(u)\Phi_\pi(v)\,,$$

$$(A^8_{A\otimes A})_{d2} = \alpha_s\pi\frac{C_F^2}{N_c^2 u(-1+v)} f_\pi^2 F_+^{B\to\pi}(m_B^2/3)\Phi_\pi(u)\Phi_\pi(v)\,,$$

$$(A^0_{V\otimes V})_{d3} = -\alpha_s\pi\frac{(-2+v)C_F}{N_c^2 u(-1+v)(-1+u(-2+v)+v)} f_\pi^2 F_+^{B\to\pi}(m_B^2/3)\Phi_\pi(u)\Phi_\pi(v)\,,$$

$$(A^8_{V\otimes V})_{d3} = \alpha_s\pi\frac{(-2+v)C_F}{2N_c^3 u(-1+v)(-1+u(-2+v)+v)} f_\pi^2 F_+^{B\to\pi}(m_B^2/3)\Phi_\pi(u)\Phi_\pi(v)\,,$$

$$(A^0_{A\otimes A})_{d3} = -\alpha_s\pi\frac{(-2+v)C_F}{N_c^2 u(-1+v)(-1+u(-2+v)+v)} f_\pi^2 F_+^{B\to\pi}(m_B^2/3)\Phi_\pi(u)\Phi_\pi(v)\,,$$

$$(A^8_{A\otimes A})_{d3} = \alpha_s\pi\frac{(-2+v)C_F}{2N_c^3 u(-1+v)(-1+u(-2+v)+v)} f_\pi^2 F_+^{B\to\pi}(m_B^2/3)\Phi_\pi(u)\Phi_\pi(v)\,,$$

$$(A^0_{V\otimes V})_{d4} = \alpha_s\pi\frac{C_F}{(u-uv)N_c^2} f_\pi^2 F_+^{B\to\pi}(m_B^2/3)\Phi_\pi(u)\Phi_\pi(v)\,,$$

$$(A^8_{V\otimes V})_{d4} = \alpha_s\pi\frac{C_F^2}{(u-uv)N_c^2} f_\pi^2 F_+^{B\to\pi}(m_B^2/3)\Phi_\pi(u)\Phi_\pi(v)\,,$$

$$(A^0_{A\otimes A})_{d4} = \alpha_s\pi\frac{C_F}{(u-uv)N_c^2} f_\pi^2 F_+^{B\to\pi}(m_B^2/3)\Phi_\pi(u)\Phi_\pi(v)\,,$$

$$(A^8_{A\otimes A})_{d4} = \alpha_s\pi\frac{C_F^2}{(u-uv)N_c^2} f_\pi^2 F_+^{B\to\pi}(m_B^2/3)\Phi_\pi(u)\Phi_\pi(v)\,.$$

Bibliography

[1] G. Aad et al. Observation of a new particle in the search for the Standard Model Higgs boson with the ATLAS detector at the LHC. *Phys.Lett.*, B716:1–29, 2012.

[2] S. Chatrchyan et al. Observation of a new boson at a mass of 125 GeV with the CMS experiment at the LHC. *Phys.Lett.*, B716:30–61, 2012.

[3] G. Aad et al. Evidence for the spin-0 nature of the Higgs boson using ATLAS data. *Phys.Lett.*, B726:120–144, 2013.

[4] V. Khachatryan et al. Constraints on the spin-parity and anomalous HVV couplings of the Higgs boson in proton collisions at 7 and 8 TeV. 2014.

[5] T.D. Lee and C-N Yang. Question of Parity Conservation in Weak Interactions. *Phys.Rev.*, 104:254–258, 1956.

[6] C.S. Wu, E. Ambler, R.W. Hayward, D.D. Hoppes, and R.P. Hudson. Experimental Test of Parity Conservation in Beta Decay. *Phys.Rev.*, 105:1413–1414, 1957.

[7] J.H. Christenson, J.W. Cronin, V.L. Fitch, and R. Turlay. Evidence for the 2π Decay of the K_2^0 Meson. *Phys.Rev.Lett.*, 13:138–140, 1964.

[8] F. Abe et al. Observation of top quark production in $\bar{p}p$ collisions. *Phys.Rev.Lett.*, 74:2626–2631, 1995.

[9] N. Cabibbo. Unitary Symmetry and Leptonic Decays. *Phys.Rev.Lett.*, 10:531–533, 1963.

[10] M. Kobayashi and T. Maskawa. CP Violation in the Renormalizable Theory of Weak Interaction. *Prog.Theor.Phys.*, 49:652–657, 1973.

[11] I. I.Y. Bigi and A.I. Sanda. Notes on the Observability of CP Violations in B Decays. *Nucl.Phys.*, B193:85, 1981.

[12] A. E. Snyder and H. R. Quinn. Measuring CP asymmetry in $B \to \rho\pi$ decays without ambiguities. *Phys.Rev.*, D48:2139–2144, 1993.

[13] Y. Grossman, Z. Ligeti, and A. Soffer. Measuring γ in $B^{\pm} \to K^{\pm}(KK^*)(D)$ decays. *Phys.Rev.*, D67:071301, 2003.

[14] Y. Amhis et al. Averages of b-hadron, c-hadron, and τ-lepton properties as of summer 2014. 2014.

[15] L. Dong. Dalitz Plot Analyses of $B^- \to D^+\pi^-\pi^-$, $B^+ \to \pi^+\pi^-\pi^+$ and $D^+_{(s)} \to \pi^+\pi^-\pi^+$ at BABAR. 2009.

[16] R. Aaij et al. Measurement of CP violation in the phase space of $B^{\pm} \to K^+K^-\pi^{\pm}$ and $B^{\pm} \to \pi^+\pi^-\pi^{\pm}$ decays. *Phys.Rev.Lett.*, 112(1):011801, 2014.

[17] T. S. Miyashita. BaBar Results For Alpha: Measurement of CP-Violating Asymmetries in $B^0 \to (\rho\pi)^0$ Using a Time-Dependent Dalitz Plot Analysis. 2013.

[18] I. Nasteva. Studies of charmless B decays including CP violation effects. 2013.

[19] R. Aaij et al. Measurements of CP violation in the three-body phase space of charmless $B^{\pm}$ decays. *Phys.Rev.*, D90:112004, 2014.

[20] J.P. Lees et al. Evidence for CP violation in $B^+ \to K^*(892)^+\pi^0$ from a Dalitz plot analysis of $B^+ \to K^0_S\pi^+\pi^0$ decays. 2015.

[21] A. et al. Aaij. Letter of Intent for the LHCb Upgrate . `http://cds.cern.ch/record/1333091`, 2011.

[22] T. Aushev, W. Bartel, A. Bondar, J. Brodzicka, T.E. Browder, et al. Physics at Super B Factory. 2010.

[23] M. Bauer, B. Stech, and M. Wirbel. Exclusive Nonleptonic Decays of D, $D_{(s)}$, and B Mesons. *Z.Phys.*, C34:103, 1987.

[24] D. Zeppenfeld. $SU(3)$ Relations for B Meson Decays. *Z.Phys.*, C8:77, 1981.

[25] Y.-Y. Keum, H.-N. Li, and A.I. Sanda. Fat penguins and imaginary penguins in perturbative QCD. *Phys.Lett.*, B504:6–14, 2001.

[26] M. Beneke, G. Buchalla, M. Neubert, and C. T. Sachrajda. QCD factorization for $B \to \pi\pi$ decays: Strong phases and CP violation in the heavy quark limit. *Phys.Rev.Lett.*, 83:1914–1917, 1999.

[27] M. Beneke, G. Buchalla, M. Neubert, and C. T. Sachrajda. QCD factorization for exclusive, nonleptonic B meson decays: General arguments and the case of heavy light final states. *Nucl.Phys.*, B591:313–418, 2000.

[28] M. Beneke, G. Buchalla, M. Neubert, and C. T. Sachrajda. QCD factorization in $B \to \pi K$, $\pi\pi$ decays and extraction of Wolfenstein parameters. *Nucl.Phys.*, B606:245–321, 2001.

[29] R.M. Sternheimer and S.J. Lindenbaum. Extension of the Isobaric Nucleon Model for Pion Production in Pion-Nucleon, Nucleon-Nucleon, and Antinucleon-Nucleon Interactions. *Phys.Rev.*, 123:333–376, 1961.

[30] D. Herndon, P. Soding, and R.J. Cashmore. A generalized isobar model formalism. *Phys.Rev.*, D11:3165, 1975.

[31] S.U. Chung, J. Brose, R. Hackmann, E. Klempt, S. Spanier, et al. Partial wave analysis in K matrix formalism. *Annalen Phys.*, 4:404–430, 1995.

[32] A. Garmash et al. Dalitz analysis of the three-body charmless decays $B^+ \to K^+\pi^+\pi^-$ and $B^+ \to K^+K^+K^-$. *Phys.Rev.*, D71:092003, 2005.

[33] N. R.-L. Lorier, M. Imbeault, and D. London. Diagrammatic Analysis of Charmless Three-Body B Decays. *Phys.Rev.*, D84:034040, 2011.

[34] M. Imbeault and D. London. $SU(3)$ Breaking in Charmless B Decays. *Phys.Rev.*, D84:056002, 2011.

[35] C.-K. Chua, W.-S. Hou, S.-Y. Shiau, and S.-Y. Tsai. Evidence for factorization in three-body $\bar{B} \to D^{(*)}K^-K^0$ decays. *Phys.Rev.*, D67:034012, 2003.

[36] H.-Y. Cheng, C.-K. Chua, and A. Soni. CP-violating asymmetries in B^0 decays to $K^+K^-K^0_{S(L)}$ and $K^0_S K_S K^0_{S(L)}$. *Phys.Rev.*, D72:094003, 2005.

[37] H.-Y. Cheng, C.-K. Chua, and A. Soni. Charmless three-body decays of B mesons. *Phys.Rev.*, D76:094006, 2007.

[38] C.-H. Chen and H.-N. Li. Three body nonleptonic B decays in perturbative QCD. *Phys.Lett.*, B561:258–265, 2003.

[39] W.-F. Wang, H.-C. Hu, H.-N. Li, and C.-D. Lu. Direct CP asymmetries of three-body B decays in perturbative QCD. *Phys.Rev.*, D89:074031, 2014.

[40] S. Descotes-Genon and C. T. Sachrajda. Sudakov effects in $B \to \pi l\nu(l)$ form-factors. *Nucl.Phys.*, B625:239–278, 2002.

[41] F. Feng, J.P. Ma, and Q. Wang. Inconsistences of the k_T-Factorization in Exclusive B-Meson Decays. 2009.

[42] I. Bediaga, I.I. Bigi, A. Gomes, G. Guerrer, J. Miranda, et al. On a CP anisotropy measurement in the Dalitz plot. *Phys.Rev.*, D80:096006, 2009.

[43] I. Bediaga, J. Miranda, A.C. dos Reis, I.I. Bigi, A. Gomes, et al. Second Generation of 'Miranda Procedure' for CP Violation in Dalitz Studies of B (D, τ) Decays. *Phys.Rev.*, D86:036005, 2012.

[44] M. Beneke and M. Neubert. QCD factorization for $B \to PP$ and $B \to PV$ decays. *Nucl.Phys.*, B675:333–415, 2003.

[45] G. Bell. NNLO vertex corrections in charmless hadronic B decays: Imaginary part. *Nucl.Phys.*, B795:1–26, 2008.

[46] G. Bell. NNLO vertex corrections in charmless hadronic B decays: Real part. *Nucl.Phys.*, B822:172–200, 2009.

[47] M. Beneke, T. Huber, and X.-Q. Li. NNLO vertex corrections to non-leptonic B decays: Tree amplitudes. *Nucl.Phys.*, B832:109–151, 2010.

[48] G. Bell and T. Huber. Master integrals for the two-loop penguin contribution in non-leptonic B-decays. *JHEP*, 1412:129, 2014.

[49] R. Fleischer, N. Serra, and N. Tuning. Tests of Factorization and $SU(3)$ Relations in B Decays into Heavy-Light Final States. *Phys.Rev.*, D83:014017, 2011.

[50] A.V. Efremov and A.V. Radyushkin. Factorization and Asymptotical Behavior of Pion Form-Factor in QCD. *Phys.Lett.*, B94:245–250, 1980.

[51] G. P. Lepage and S. J. Brodsky. Exclusive Processes in Perturbative Quantum Chromodynamics. *Phys.Rev.*, D22:2157, 1980.

[52] H. Georgi. An Effective Field Theory for Heavy Quarks at Low-energies. *Phys.Lett.*, B240:447–450, 1990.

[53] M. Beneke and T. Feldmann. Symmetry breaking corrections to heavy to light B meson form-factors at large recoil. *Nucl.Phys.*, B592:3–34, 2001.

[54] K. G. Wilson. Confinement of Quarks. *Phys.Rev.*, D10:2445–2459, 1974.

[55] M. A. Shifman, A.I. Vainshtein, and V. I. Zakharov. QCD and Resonance Physics. Sum Rules. *Nucl.Phys.*, B147:385–447, 1979.

[56] G. Bell, T. Feldmann, Y.-M. Wang, and M. W Y Yip. Light-Cone Distribution Amplitudes for Heavy-Quark Hadrons. *JHEP*, 11:191, 2013.

[57] S. Faller, T. Feldmann, A. Khodjamirian, T. Mannel, and D. van Dyk. Disentangling the Decay Observables in $B^- \to \pi^+\pi^-\ell^-\bar{\nu}_\ell$. *Phys.Rev.*, D89(1):014015, 2014.

[58] J. H. Kuhn and A. Santamaria. Tau decays to pions. *Z.Phys.*, C48:445–452, 1990.

[59] M. Diehl, T. Gousset, B. Pire, and O. Teryaev. Probing partonic structure in $\gamma^*\gamma \to \pi\pi$ near threshold. *Phys.Rev.Lett.*, 81:1782–1785, 1998.

[60] M. V. Polyakov. Hard exclusive electroproduction of two pions and their resonances. *Nucl.Phys.*, B555:231, 1999.

[61] M. Diehl. Generalized parton distributions. *Proc.Int.Sch.Phys.Fermi*, 180:81–105, 2012.

[62] M. Diehl. Generalized parton distributions. *Phys.Rept.*, 388:41–277, 2003.

[63] M. Fujikawa et al. High-Statistics Study of the $\tau \to \pi^-\pi^0\nu(\tau)$ Decay. *Phys. Rev.*, D78:072006, 2008.

[64] D. R. Boito, R. Escribano, and M. Jamin. $K\pi$ vector form-factor, dispersive constraints and $\tau \to \nu(\tau)K\pi$ decays. *Eur. Phys. J.*, C59:821–829, 2009.

[65] B. Aubert et al. Precise measurement of the $e^+e^- \to \pi^+\pi^-(\gamma)$ cross section with the Initial State Radiation method at BABAR. *Phys. Rev. Lett.*, 103:231801, 2009.

[66] F. Ambrosino et al. Measurement of $\sigma(e^+e^- \to \pi^+\pi^-)$ from threshold to $0.85\,\mathrm{GeV}^2$ using Initial State Radiation with the KLOE detector. *Phys.Lett.*, B700:102–110, 2011.

[67] C. Hanhart. A New Parameterization for the Pion Vector Form Factor. *Phys. Lett.*, B715:170–177, 2012.

[68] D. Gomez Dumm and P. Roig. Dispersive representation of the pion vector form factor in $\tau \to \pi\pi\nu_\tau$ decays. *Eur.Phys.J.*, C73(8):2528, 2013.

[69] C. Hambrock and A. Khodjamirian. In preparation.

[70] Feldmann T. Boeer, P. and D. van Dyk. In preparation.

[71] C.-H. V. Chang and H.-N. Li. Three - scale factorization theorem and effective field theory. *Phys.Rev.*, D55:5577–5580, 1997.

[72] T.-W. Yeh and H.-N. Li. Factorization theorems, effective field theory, and nonleptonic heavy meson decays. *Phys.Rev.*, D56:1615–1631, 1997.

[73] Y.Y. Keum, H.-N. Li, and A.I. Sanda. Penguin enhancement and $B \to K\pi$ decays in perturbative QCD. *Phys.Rev.*, D63:054008, 2001.

[74] H.-N. Li, S. Mishima, and A.I. Sanda. Resolution to the $B \to \pi K$ puzzle. *Phys.Rev.*, D72:114005, 2005.

[75] H.-N. Li and S. Mishima. Implication of the $B \to \rho\rho$ data on the $B \to \pi\pi$ puzzle. *Phys.Rev.*, D73:114014, 2006.

[76] M. J. Savage and M. B. Wise. $SU(3)$ Predictions for Nonleptonic B Meson Decays. *Phys.Rev.*, D39:3346, 1989.

[77] M. Gronau and D. London. Isospin analysis of CP asymmetries in B decays. *Phys.Rev.Lett.*, 65:3381–3384, 1990.

[78] R. Fleischer. New strategies to extract Beta and γ from $B_d \to \pi^+\pi^-$ and $B_S \to K^+K^-$. *Phys.Lett.*, B459:306–320, 1999.

[79] M. Gronau, J. L. Rosner, and D. London. Weak coupling phase from decays of charged B mesons to πK and $\pi\pi$. *Phys.Rev.Lett.*, 73:21–24, 1994.

[80] A. Soni and D. A. Suprun. Determination of γ from Charmless $B \to M_1 M_2$ Decays Using U-Spin. *Phys.Rev.*, D75:054006, 2007.

[81] M. Nagashima, A. Szynkman, and D. London. U-spin tests of the standard model and new physics. *Mod.Phys.Lett.*, A23:1175–1185, 2008.

[82] G. Buchalla, A. J. Buras, and M. E. Lautenbacher. Weak decays beyond leading logarithms. *Rev.Mod.Phys.*, 68:1125–1144, 1996.

[83] K. G. Chetyrkin, M. Misiak, and M. Munz. Weak radiative B meson decay beyond leading logarithms. *Phys.Lett.*, B400:206–219, 1997.

[84] M. Gorbahn and U. Haisch. Effective Hamiltonian for non-leptonic $|\Delta F| = 1$ decays at NNLO in QCD. *Nucl.Phys.*, B713:291–332, 2005.

[85] T. Huber, E. Lunghi, M. Misiak, and D. Wyler. Electromagnetic logarithms in anti-$B \to X_{(s)} l^+ l^-$. *Nucl. Phys.*, B740:105–137, 2006.

[86] C. W. Bauer, S. Fleming, and M. E. Luke. Summing Sudakov logarithms in $B \to X(s\gamma)$ in effective field theory. *Phys.Rev.*, D63:014006, 2000.

[87] C. W. Bauer, S. Fleming, D. Pirjol, and I. W. Stewart. An Effective field theory for collinear and soft gluons: Heavy to light decays. *Phys.Rev.*, D63:114020, 2001.

[88] C. W. Bauer, D. Pirjol, and I. W. Stewart. Soft collinear factorization in effective field theory. *Phys.Rev.*, D65:054022, 2002.

[89] B. O. Lange. Soft-collinear factorization and Sudakov resummation of heavy meson decay amplitudes with effective field theories. 2004.

[90] T. Becher, A. Broggio, and A. Ferroglia. Introduction to Soft-Collinear Effective Theory. 2014.

[91] For a review see M. Neubert. Heavy quark symmetry. *Phys.Rept.*, 245:259–396, 1994.

[92] N. Isgur and M. B. Wise. Weak Decays of Heavy Mesons in the Static Quark Approximation. *Phys. Lett.*, B232:113–117, 1989.

[93] N. Isgur and M. B. Wise. Weak transition form factors between heavy mesons. *Phys. Lett.*, B237:527–530, 1990.

[94] M. Beneke and S. Jager. Spectator scattering at NLO in non-leptonic b decays: Tree amplitudes. *Nucl.Phys.*, B751:160–185, 2006.

[95] G. Passarino and M.J.G. Veltman. One Loop Corrections for e^+e^- Annihilation Into $\mu^+\mu^-$ in the Weinberg Model. *Nucl.Phys.*, B160:151, 1979.

[96] S. Laporta and E. Remiddi. The Analytical value of the electron $(g-2)$ at order α^3 in QED. *Phys.Lett.*, B379:283–291, 1996.

[97] S. Laporta. High precision calculation of multiloop Feynman integrals by difference equations. *Int.J.Mod.Phys.*, A15:5087–5159, 2000.

[98] K.G. Chetyrkin and F.V. Tkachov. Integration by Parts: The Algorithm to Calculate beta Functions in 4 Loops. *Nucl.Phys.*, B192:159–204, 1981.

[99] J.C. Collins. Renormalization: An Introduction to Renormalization, the Renormalization Group and the Operator-Product Expansion. Cambridge University Press, 1984.

[100] C. Anastasiou and A. Lazopoulos. Automatic integral reduction for higher order perturbative calculations. *JHEP*, 0407:046, 2004.

[101] A.V. Smirnov. Algorithm FIRE – Feynman Integral REduction. *JHEP*, 0810:107, 2008.

[102] A. V. Smirnov. FIRE5: a C++ implementation of Feynman Integral REduction. 2014.

[103] C. Studerus. Reduze-Feynman Integral Reduction in C++. *Comput. Phys. Commun.*, 181:1293–1300, 2010.

[104] A. V. Smirnov and V. A. Smirnov. Applying Grobner bases to solve reduction problems for Feynman integrals. *JHEP*, 01:001, 2006.

[105] A. V. Smirnov and V. A. Smirnov. S-bases as a tool to solve reduction problems for Feynman integrals. *Nucl. Phys. Proc. Suppl.*, 160:80–84, 2006.

[106] A. V. Smirnov and V. A. Smirnov. On the reduction of Feynman integrals to master integrals. *PoS*, ACAT2007:085, 2007.

[107] J. M. Henn. Multiloop integrals in dimensional regularization made simple. *Phys.Rev.Lett.*, 110(25):251601, 2013.

[108] H. Bateman. Higher transcendental functions. MC Graw-Hill Book Company, 1955.

[109] T. Huber and D. Maitre. HypExp: A Mathematica package for expanding hypergeometric functions around integer-valued parameters. *Comput.Phys.Commun.*, 175:122–144, 2006.

[110] M. Czakon. Automatized analytic continuation of Mellin-Barnes integrals. *Comput.Phys.Commun.*, 175:559–571, 2006.

[111] M.C. Bergere and Y.-M. P. Lam. Asymptotic expansion of Feynman amplitudes. Part 1: The convergent case. *Commun.Math.Phys.*, 39:1, 1974.

[112] Ussyukina. *Teor. Mat. Fiz.*, 22:300, 1975.

[113] E.E. Boos and A. I. Davydychev. A Method of evaluating massive Feynman integrals. *Theor.Math.Phys.*, 89:1052–1063, 1991.

[114] V. A. Smirnov. Analytical result for dimensionally regularized massless on shell double box. *Phys.Lett.*, B460:397–404, 1999.

[115] J.B. Tausk. Nonplanar massless two loop Feynman diagrams with four on-shell legs. *Phys.Lett.*, B469:225–234, 1999.

[116] V.A. Smirnov. Feynman Integral Calculus. Springer, 2006.

[117] J. Gluza, K. Kajda, and T. Riemann. AMBRE: A Mathematica package for the construction of Mellin-Barnes representations for Feynman integrals. *Comput.Phys.Commun.*, 177:879–893, 2007.

[118] A.V. Kotikov. Differential equations method: New technique for massive Feynman diagrams calculation. *Phys.Lett.*, B254:158–164, 1991.

[119] E. Remiddi. Differential equations for Feynman graph amplitudes. *Nuovo Cim.*, A110:1435–1452, 1997.

[120] T. Gehrmann and E. Remiddi. Differential equations for two loop four point functions. *Nucl.Phys.*, B580:485–518, 2000.

[121] T. Gehrmann and E. Remiddi. Two loop master integrals for $\gamma^* \to 3$ jets: The Planar topologies. *Nucl.Phys.*, B601:248–286, 2001.

[122] T. Gehrmann and E. Remiddi. Two loop master integrals for $\gamma^* \to 3$ jets: The Nonplanar topologies. *Nucl.Phys.*, B601:287–317, 2001.

[123] M. Argeri and P. Mastrolia. Feynman Diagrams and Differential Equations. *Int.J.Mod.Phys.*, A22:4375–4436, 2007.

[124] E. Remiddi and J.A.M. Vermaseren. Harmonic polylogarithms. *Int.J.Mod.Phys.*, A15:725–754, 2000.

[125] D Maitre. HPL, a mathematica implementation of the harmonic polylogarithms. *Comput.Phys.Commun.*, 174:222–240, 2006.

[126] D. Maitre. Extension of HPL to complex arguments. *Comput.Phys.Commun.*, 183:846, 2012.

[127] L. Lewin. Polylogarithms and associated functions. Elsevier (North Holland), New York, London and Amsterdam, 1981.

[128] N. Nielsen. Nova Acta Leopoldina. (Halle) 90 (1909) 123, 1909.

[129] A. B. Goncharov. Multiple polylogarithms, cyclotomy and modular complexes. *Math.Res.Lett.*, 5:497–516, 1998.

[130] J. M. Henn, A. V. Smirnov, and V. A. Smirnov. Analytic results for planar three-loop four-point integrals from a Knizhnik-Zamolodchikov equation. *JHEP*, 1307:128, 2013.

[131] J. M. Henn and V. A. Smirnov. Analytic results for two-loop master integrals for Bhabha scattering I. *JHEP*, 1311:041, 2013.

[132] J. M. Henn, A. V. Smirnov, and V. A. Smirnov. Evaluating single-scale and/or non-planar diagrams by differential equations. *JHEP*, 1403:088, 2014.

[133] M. Argeri, S. Di Vita, P. Mastrolia, E. Mirabella, J. Schlenk, et al. Magnus and Dyson Series for Master Integrals. *JHEP*, 1403:082, 2014.

[134] J. M. Henn, K. Melnikov, and V. A. Smirnov. Two-loop planar master integrals for the production of off-shell vector bosons in hadron collisions. *JHEP*, 1405:090, 2014.

[135] T. Gehrmann, A. von Manteuffel, L. Tancredi, and E. Weihs. The two-loop master integrals for $q\overline{q} \to VV$. *JHEP*, 1406:032, 2014.

[136] F. Caola, J. M. Henn, K. Melnikov, and V. A. Smirnov. Non-planar master integrals for the production of two off-shell vector bosons in collisions of massless partons. *JHEP*, 1409:043, 2014.

[137] S. Di Vita, P. Mastrolia, U. Schubert, and V. Yundin. Three-loop master integrals for ladder-box diagrams with one massive leg. *JHEP*, 1409:148, 2014.

[138] A. von Manteuffel, R. M. Schabinger, and H. X. Zhu. The two-loop soft function for heavy quark pair production at future linear colliders. 2014.

[139] M. Hoschele, J. Hoff, and T. Ueda. Adequate bases of phase space master integrals for gg $\to$ h at NNLO and beyond. *JHEP*, 1409:116, 2014.

[140] H. X. Zhu. On the calculation of soft phase space integral. *JHEP*, 1502:155, 2015.

[141] N. Arkani-Hamed, J. L. Bourjaily, F. Cachazo, and J. Trnka. Local Integrals for Planar Scattering Amplitudes. *JHEP*, 1206:125, 2012.

[142] F. Cachazo. Sharpening The Leading Singularity. 2008.

[143] N. Arkani-Hamed, J. L. Bourjaily, F. Cachazo, A. B. Goncharov, A. Postnikov, et al. Scattering Amplitudes and the Positive Grassmannian. 2012.

[144] L. Tancredi. Integration by parts identities in integer numbers of dimensions. A criterion for decoupling systems of differential equations. 2015.

[145] J. Vollinga and S. Weinzierl. Numerical evaluation of multiple polylogarithms. *Comput.Phys.Commun.*, 167:177, 2005.

[146] J. Carter and G. Heinrich. SecDec: A general program for sector decomposition. *Comput.Phys.Commun.*, 182:1566–1581, 2011.

[147] A. Grozin. Lectures on QED and QCD. 2005.

[148] P. Gambino, M. Gorbahn, and U. Haisch. Anomalous dimension matrix for radiative and rare semileptonic B decays up to three loops. *Nucl.Phys.*, B673:238–262, 2003.

[149] M. Beneke and D. Yang. Heavy-to-light B meson form-factors at large recoil energy: Spectator-scattering corrections. *Nucl.Phys.*, B736:34–81, 2006.

[150] Private communication with M. Beneke.

[151] K. G. Chetyrkin, B. A. Kniehl, and M. Steinhauser. Decoupling relations to $O(\alpha_s^3)$ and their connection to low-energy theorems. *Nucl. Phys.*, B510:61–87, 1998.

[152] D. Mueller. Conformal constraints and the evolution of the nonsinglet meson distribution amplitude. *Phys. Rev.*, D49:2525–2535, 1994.

[153] S. V. Mikhailov and A. V. Radyushkin. Evolution Kernels in QCD: Two Loop Calculation in Feynman Gauge. *Nucl. Phys.*, B254:89, 1985.

[154] D. Mueller. The Evolution of the pion distribution amplitude in next-to-leading-order. *Phys. Rev.*, D51:3855–3864, 1995.

[155] V. M. Braun et al. Moments of pseudoscalar meson distribution amplitudes from the lattice. *Phys. Rev.*, D74:074501, 2006.

[156] R. Arthur, P. A. Boyle, D. Brommel, M. A. Donnellan, J. M. Flynn, A. Juttner, T. D. Rae, and C. T. C. Sachrajda. Lattice Results for Low Moments of Light Meson Distribution Amplitudes. *Phys. Rev.*, D83:074505, 2011.

[157] M. Dimou, J. Lyon, and R. Zwicky. Exclusive Chromomagnetism in heavy-to-light FCNCs. *Phys. Rev.*, D87(7):074008, 2013.

[158] K. A. Olive et al. Review of Particle Physics. *Chin. Phys.*, C38:090001, 2014.

[159] I. Caprini, L. Lellouch, and M. Neubert. Dispersive bounds on the shape of $\bar{B} \to D^{(*)}$ lepton anti-neutrino form-factors. *Nucl. Phys.*, B530:153–181, 1998.

[160] Y. Sakaki and H. Tanaka. Constraints on the charged scalar effects using the forward-backward asymmetry on $B^- \to D^{(*)}\tau\bar{\nu}_\tau$. *Phys. Rev.*, D87(5):054002, 2013.

[161] R. Dutta, A. Bhol, and Anjan K. Giri. Effective theory approach to new physics in b u and b c leptonic and semileptonic decays. *Phys. Rev.*, D88(11):114023, 2013.

[162] S. Fajfer, J. F. Kamenik, and I. Nisandzic. On the $B \to D^*\tau\bar{\nu}_\tau$ Sensitivity to New Physics. *Phys. Rev.*, D85:094025, 2012.

[163] J. D. Bjorken. Topics in B Physics. *Nucl. Phys. Proc. Suppl.*, 11:325–341, 1989.

[164] M. Neubert and B. Stech. Nonleptonic weak decays of B mesons. *Adv. Ser. Direct. High Energy Phys.*, 15:294–344, 1998.

[165] M. Beneke. Talk given at the Three-Body Charmless B Decays Workshop, Paris, France, 1-3 Feb 2006.

[166] I. Stewart. Talk given at the Three-Body Charmless B Decays Workshop, Paris, France, 1-3 Feb 2006.

[167] J. at al. (Particle Data Group) Beringer. *Phys.Rev.*, D86:010001, 2012.

[168] R. H. Dalitz. On the Analysis of τ-Meson Data and the Nature of the τ-Meson. *Phil. Mag.*, 44:1068.

[169] E. Fabri. A study of τ-meson decay. *Il Nuovo Cimento*, 11:479.

[170] A.J. Bevan et al. The Physics of the B Factories. *Eur.Phys.J.*, C74(11):3026, 2014.

[171] B. Aubert et al. Dalitz Plot Analysis of the Decay $B^0(\bar{B}^0) \to K^{\pm}\pi^{\mp}\pi^0$. *Phys.Rev.*, D78:052005, 2008.

[172] M. Diehl, T. Feldmann, P. Kroll, and C. Vogt. The Perturbative limit of the two pion light cone distribution amplitude. *Phys.Rev.*, D61:074029, 2000.

[173] G. P. Lepage and S. J. Brodsky. Exclusive Processes in Quantum Chromodynamics: Evolution Equations for Hadronic Wave Functions and the Form-Factors of Mesons. *Phys. Lett.*, B87:359–365, 1979.

[174] J.P. Lees et al. Precise Measurement of the $e^+e^- \to \pi^+\pi^-(\gamma)$ Cross Section with the Initial-State Radiation Method at BABAR. *Phys.Rev.*, D86:032013, 2012.

[175] O. Shekhovtsova, T. Przedzinski, P. Roig, and Z. Was. Resonance chiral Lagrangian currents and τ decay Monte Carlo. *Phys.Rev.*, D86:113008, 2012.

[176] R.R. Akhmetshin et al. Reanalysis of hadronic cross-section measurements at CMD-2. *Phys.Lett.*, B578:285–289, 2004.

[177] R.R. Akhmetshin et al. High-statistics measurement of the pion form factor in the rho-meson energy range with the CMD-2 detector. *Phys.Lett.*, B648:28–38, 2007.

[178] M.N. Achasov, K.I. Beloborodov, A.V. Berdyugin, A.G. Bogdanchikov, A.V. Bozhenok, et al. Update of the $e^+e^- \to \pi^+\pi^-$ cross-section measured by SND detector in the energy region 400 MeV $< \sqrt{s} <$ 1000 MeV. *J.Exp.Theor.Phys.*, 103:380–384, 2006.

[179] A. Aloisio et al. Measurement of sigma($e^+e^- \to \pi^+\pi^-\gamma$) and extraction of sigma($e^+e^- \to \pi^+\pi^-$) below 1-GeV with the KLOE detector. *Phys.Lett.*, B606:12–24, 2005.

[180] F. Ambrosino et al. Measurement of $\sigma(e^+e^- \to \pi^+\pi^-\gamma(\gamma)$ and the dipion contribution to the muon anomaly with the KLOE detector. *Phys.Lett.*, B670:285–291, 2009.

[181] V.P. Druzhinin, S.I. Eidelman, S.I. Serednyakov, and E.P. Solodov. Hadron Production via e+e- Collisions with Initial State Radiation. *Rev.Mod.Phys.*, 83:1545, 2011.

[182] M. Beneke. Soft-collinear factorization in B decays. *Nucl.Part.Phys.Proc.*, 261-262:311–337, 2015.

[183] N. Kivel. Radiative corrections to hard spectator scattering in $B \to \pi\pi$ decays. *JHEP*, 0705:019, 2007.

[184] M. Beneke and S. Jager. Spectator scattering at NLO in non-leptonic B decays: Leading penguin amplitudes. *Nucl.Phys.*, B768:51–84, 2007.

[185] V. Pilipp. Hard spectator interactions in $B \to \pi\pi$ at order α_s^2. *Nucl.Phys.*, B794:154–188, 2008.

[186] R Aaij et al. Measurement of CP violation in the phase space of $B^\pm \to K^\pm\pi^+\pi^-$ and $B^\pm \to K^\pm K^+ K^-$ decays. *Phys. Rev. Lett.*, 111:101801, 2013.

[187] D. Das, G. Hiller, M. Jung, and A. Shires. The $\overline{B} \to \overline{K}\pi\ell\ell$ and $\overline{B}_s \to \overline{K}K\ell\ell$ distributions at low hadronic recoil. *JHEP*, 09:109, 2014.

[188] D. R. Boito, R. Escribano, and M. Jamin. $K\pi$ vector form factor constrained by $\tau \to K\pi\nu_\tau$ and K_{l3} decays. *JHEP*, 09:031, 2010.

[189] `http://www.ttp.kit.edu/~asmirnov/`.

[190] Private communication with A.V. Smirnov.

[191] R. N. Lee. Group structure of the integration-by-part identities and its application to the reduction of multiloop integrals. *JHEP*, 07:031, 2008.

[192] A.V. Smirnov. An Algorithm to construct Grobner bases for solving integration by parts relations. *JHEP*, 0604:026, 2006.

[193] M.E. Peskin and D.V. Schroeder. *An Introduction to Quantum Field Theory*. Advanced book classics. Addison-Wesley Publishing Company, 1995.

Publications and Proceedings

[A] S. Kränkl and A. Manashov, Two-loop renormalization of three-quark operators in QCD, *Phys. Lett.* B703, (2011) 519-523.

[B] T. Huber and S. Kränkl, Towards NNLO corrections in $B \to D\pi$, 17th International Moscow School of Physics and 42nd ITEP Winter School of Physics Moscow, Russia, February 11-18, arXiv:1405.5911, (2014)

[C] T. Huber and S. Kränkl, Two-loop master integrals for non-leptonic heavy-to-heavy decays, *JHEP* 1504, (2015) 140.

[D] S. Kränkl, M. Mannel, J. Virto, Three-Body Non-Leptonic B Decays and QCD Factorization, *Nucl. Phys.* B899, (2015) 247-264.

[E] T. Huber, S. Kränkl and Xin-Qiang Li, In Preparation

Acknowledgements

Zum Abschluss möchte ich allen danken, ohne deren Unterstützung diese Arbeit nicht möglich gewesen wäre.

Ich bedanke mich bei Prof. Dr. Mannel, der mir im Rahmen der Doktorarbeit die Möglichkeit gegeben hat, das spannende Gebiet der Teilchenphysik weiterzuverfolgen. Mein besonderer Dank gilt Tobias Huber für die hervoragende Betreuung während dieser Zeit. Er hat nicht nur sein Wissen mit mir geteilt, sondern war auch stets zur Stelle um meine Fragen zu beantworten.

Desweiteren möchte ich mich bei Javier Virto für die vielen anregenden Diskussionen und die gute Zusammenarbeit bedanken. Mein Dank geht zudem an Björn Lange für viele hilfreiche Anregungen und an Prof. Dr. Feldmann für die wertvollen Diskussionen besonders in der frühen Phase der Arbeit. Auch bedanke ich mich bei der Deutschen Forschungsgemeinschaft (DFG) für die finanzielle Unterstützung im Rahmen der Forschergruppe FOR 1873 (QFET).

Ich bedanke mich auch bei allen, die viel Zeit in die Korrektur bzw. das Ausdrucken meiner Arbeit investiert haben: Dirk Seidel, Björn Lange, Javier Virto, Sven Faller, Danny van Dyk, Florian Hartmann, Robin Brüser und ganz besonders Johannes Heinonen, der das ganze Manuskript gelesen hat. Auch möchte ich meinen Kommilitonen, Kollegen und WG Mitbewohnern danken. Meine Zeit in Siegen werde ich immer in guter Erinnerung behalten.

Ein besonderer Dank geht zuletzt auch an meine Eltern, meine Schwester, meinen Freund Philipp und Katharina Umminger für die Unterstützung während dieser Zeit.